CALIX[4]ARENE-BASED SYNTHETIC NANOTUBES

by

VOLTAIRE GUANLAO ORGANO

Presented to the Faculty of the Graduate School of

The University of Texas at Arlington in Partial Fulfillment

of the Requirements

for the Degree of

DOCTOR OF PHILOSOPHY

THE UNIVERSITY OF TEXAS AT ARLINGTON

December 2006

ACKNOWLEDGEMENTS

I would like to acknowledge the people who were instrumental to the success of this work:

Dr. Dmitry M. Rudkevich, my supervisor and mentor, for motivating and challenging me to always give my best, and for introducing me to the exciting field of supramolecular chemistry and calixarenes.

The members of my research committee: Drs. Frederick M. MacDonnell, Edward Bellion, Carl J. Lovely, Martin Pomerantz and Kevin A. Schug for their valuable comments and suggestions to improve this work.

Dr. H. V. Rasika Dias for his expertise in analyzing the crystal structures of our compounds.

Drs. Grigory Zyryanov, Alexander Leontiev, and Valentina Sgarlata for sharing their knowledge and technical skills in organic synthesis and molecular recognition.

Other members of the Rudkevich group: Dr. Vaclav Stastny, Dr. Yanlong Kang, Dr. Heng Xu, Farhood Firouzbakht, Albert Wong, Hexiang Zhang, Anas Saleh, and Eranda Wanigasekara, for their friendship and support and for making my research experience memorable.

Sa aking pamilya na patuloy na nagmamahal, at higit sa lahat, sa Panginoong Diyos na nagbigay buhay, gabay at biyaya.

Maraming salamat sa inyong lahat!

November 28, 2006

ABSTRACT

CALIX[4]ARENE-BASED SYNTHETIC NANOTUBES

Publication No. _____

Voltaire Guanlao Organo, PhD.

The University of Texas at Arlington, 2006

Supervising Professor: Dr. Dmitry M. Rudkevich

Nanoscale science and technology represents a tremendous opportunity to gain unprecedented insight into the unique phenomena that exists at the nanometer scale, and to use that knowledge to develop materials and devices with novel characteristics. This dissertation explores the unique properties of calix[4]arene-based synthetic nanotubes, the process of filling and characteristics of materials confined in one dimension.

Chapter 1 provides an overview of recently developed nanoscale materials, particularly single-walled carbon nanotubes and their ability to encapsulate materials in a one-dimensional configuration. Molecules inside carbon nanotubes are reported to

exhibit structural and dynamic properties that are not observed in the bulk. Approaches are also discussed towards synthetic nanotubes as a supplement to carbon nanotubes.

Chapter 2 deals with calix[4]arenes as building blocks for constructing nanotubes. Multiple calix[4]arenes in the 1,3-alternate conformation are covalently connected to build robust synthetic nanotubes using conventional organic chemistry protocols. The dimensions of the nanotubes are controlled precisely and easily. They effectively pack into infinite tubular bundles in the solid state.

In Chapter 3, the calix[4]arene-based nanotubes are filled with multiple NO^+ guests. They exhibit typical properties of calix[4]arene-NO^+ complexes as evidenced by UV-vis, ^1H NMR and FTIR spectroscopy. The stoichiometry of the complexes reveals the encapsulation of one NO^+ guest per calixarene cavity. NO^+ guests are entrapped deep inside the nanotube tunnel and experience strong electron donor-acceptor interactions.

In Chapter 4, the dynamics of the filling material inside calix[4]arene nanotubes are discussed. The tunnel of the nanotube allows the NO^+ guests to freely rotate along the N-O axis and also tumble within the cavity at room temperature. Though the filled nanotube is stable, it allows the release and re-entry of guests within its hollow structure. NO^+ can be transferred to and from another host such as 18-crown-6. The guest exchange and dynamics are monitored by conventional spectroscopic techniques.

TABLE OF CONTENTS

LIST OF ILLUSTRATIONS

LIST OF SCHEMES

CHAPTER 1

INTRODUCTION

1.1 Importance of Nanoscale Science and Technology

Nanoscale science and technology (NS&T) is a rapidly developing field. It deals with the design, construction, and utilization of functional materials, devices and systems in the range of about 1 to 100 nanometers (nm).[1] Such materials are of great interest because they display properties significantly different from those displayed by either atoms or bulk materials.[2] The capability to manipulate matter at this scale can therefore lead to novel and improved characteristics and behavior of materials.

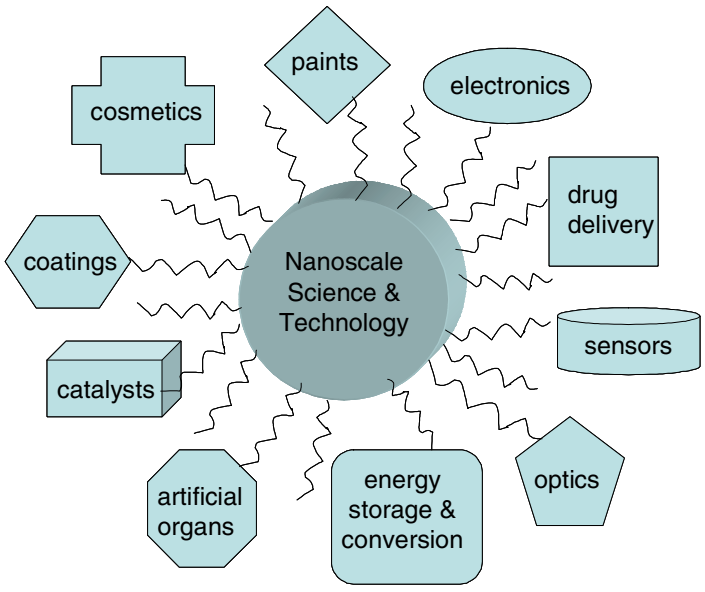

Figure 1. Current and potential applications of nanoscale science and technology.[1]

Applications of NS&T span across the fields of science, engineering, technology and medicine (Figure 1). Early applications of nanoscale materials involve nanoscale powders like titanium dioxide and zinc oxide used by the cosmetics industry for facial creams and sunscreen lotions.[1] Titanium dioxide powders are also used in paints to improve its reflective properties; and in wear-resistant coatings.[3] Nanoparticles are widely used in the electronics industry for the manufacture of integrated circuit chips and hard disks.[4] In the biomedical field, nano-sized structures called liposomes have been synthesized for improved delivery of therapeutic agents, while others have developed fluorescent nanoparticles to detect tumor cells, or infectious and genetic diseases.[5] Further developing technologies in NS&T involve more efficient catalysts for industrial processes and waste treatment,[6] sensors for chemical and biological hazard detection, and environmental monitoring,[7] fuel cells,[8] and improved materials for implants and artificial organs.[9]

In the United States, the potential impact of NS&T on economics has led to the establishment of the National Nanotechnology Initiative (NNI), which aims to accelerate the discovery, development, and deployment of nanotechnology. Financial support for nanotechnology research and development has now reached over $5 billion since its inception in 2001.[2] This tremendous support is an indication of the growing interest in advancement of this multi-disciplinary field.

Indeed, the ability to understand and control matter on the nanoscale can open new opportunities for technological and commercial development.

1.2 Nanotubes

Among the nanostructured materials being studied extensively are nanotubes. In Nature, hollow tubular structures perform diverse functions such as selective transport of molecules and ions across membranes, and catalysis.[10] These biological structures have inspired researchers to construct nanotubes for sensing, transport, catalysis, storage, and other applications.[10-12] Another goal of constructing nanotubes, which goes beyond mimicking biological functions, is to confine materials in a quasi-one dimensional system which may lead to novel properties.[13]

1.2.1 Carbon Nanotubes

Carbon nanotubes can be thought to consist of graphitic sheets which have been rolled up into a cylindrical shape. Since their discovery by Iijima[14] and by Bethune et al.[15] in 1993, there has been a large interest in the study of single-walled carbon nanotubes (SWNTs), particularly in filling them with foreign guests. Aside from the discovery or preparation of novel materials, the interest in SWNTs lies in the peculiar properties that can be expected from the nanometer dimensions associated with the filling process. As mentioned earlier, physical features can be drastically modified for nanoscale materials. This is especially true for SWNTs, which have inner hollow cavities with diameters ranging from 1 to 20 nm.[16] Their narrow channel forces the filling materials to adopt a one-dimensional morphology. In this case, SWNTs can either serve as molds or composite materials for preparing nanoscale wires, transistors and sensors. SWNTs can also serve as containers for nano-sized catalysts. In this instance, the inert carbon sheath protects the catalyst from the components of a catalytic

process. Upon oxidation, the carbon is removed and the catalyst becomes activated.[17] Similarly, SWNTs can also be used to encapsulate important gases like hydrogen for fuel storage.[18]

1.2.1.1. Molecules Inside Single-Walled Carbon Nanotubes

For potential applications, it is valuable to gain insight on the structural and dynamic behavior of guests encapsulated in carbon nanotubes. The first reported molecule inside SWNTs was the buckminster fullerene C_{60} (Figure 2).[19] These so-called peapods formed spontaneously as by-products during the post-synthesis of the nanotubes. The structural and dynamic behavior of C_{60} in SWNTs has been analyzed by high-resolution transmission electron microscopy (HRTEM).[20] It was found that the interfullerene spacing, dictated by the van der Waals interaction, is about 3% shorter in nanotubes than in bulk crystals (1.004 nm). This suggests that fullerenes experience compression inside nanotubes as a result of encapsulation. Also, depending on the internal diameter of the nanotubes, several packing arrangements were found possible for C_{60} inside nanotubes, none of which exist in the bulk.

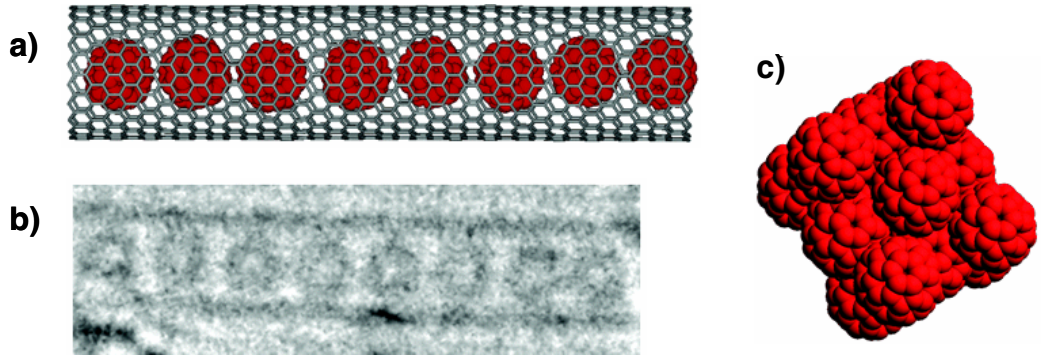

Figure 2. SWNTs filled with fullerenes. (a) structural representation, (b) HRTEM micrograph image, (c) structural representation of a C_{60} crystal.[19]

Studies carried out with SWNTs filled with an ellipsoidal fullerene, C_{70}, revealed two different orientations inside the nanotube with intermolecular spacing of 1.00 and 1.10 nm for the transverse and longitudinal orientations, respectively (Figure 3a-b).[20] In narrower 1.36 nm nanotubes, the elongated fullerenes adopt exclusively a longitudinal orientation to minimize van der Waals repulsion with the interior of the nanotubes; while in wider 1.49 nm nanotubes, the molecules are oriented in a transverse fashion to maximize the van der Waals attractive forces. These observations suggest that fullerene-nanotube interactions have greater influence than fullerene-fullerene interactions on the molecular orientations in these systems. On the other hand, a phase transition, rather than change in orientation, was observed for C_{60} peapods as a consequence of nanotube diameter (Figure 3c-d). Below 1.45 nm nanotube diameter, the C_{60} molecules form a linear array, while above which they form a zigzag phase. Again, the fullerene-nanotube interaction seems to be the dominant interaction for this phase transition.

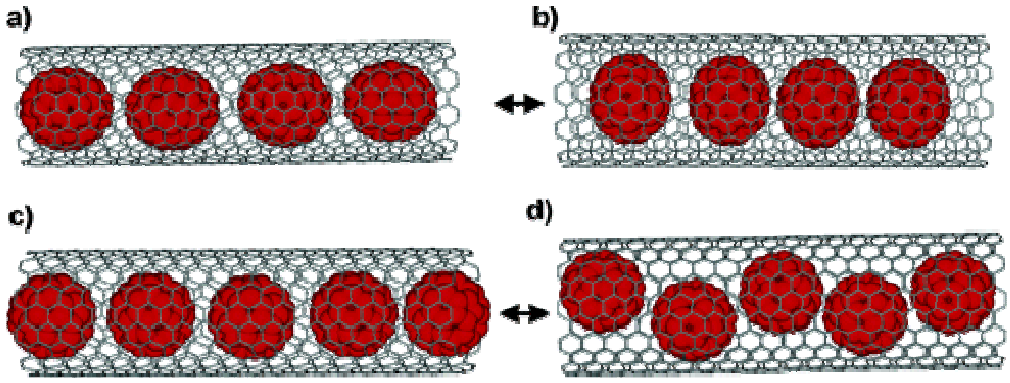

Figure 3. Molecular orientations of fullerenes inside SWNTs. (a) longitudinal and (b) transverse orientation of C_{70}, (c) straight chain packing and (d) zig-zag packing of C_{60}.[20]

Another interesting behavior is observed for endohedral metallofullerenes inside SWNTs (Figure 4).[21] Endohedral metallofullerenes are molecules containing one or more metal atoms inside the fullerene cage, denoted here as $X@C_n$ (where X is an atom and C_n is the fullerene cage). These molecules possess electric dipole moments resulting from the interaction of the incarcerated metal atom with the cage. The effect of dipole interactions on molecular orientation inside nanotubes was studied with $Ce@C_{82}$ molecules. HRTEM images show that the metallofullerenes tend to align their dipole moments along the nanotube axis and maximize dipole-dipole interactions with neighboring molecules. Such an alignment is not observed in the bulk crystal or in solutions of $Ce@C_{82}$ where the molecules freely rotate at room temperature.

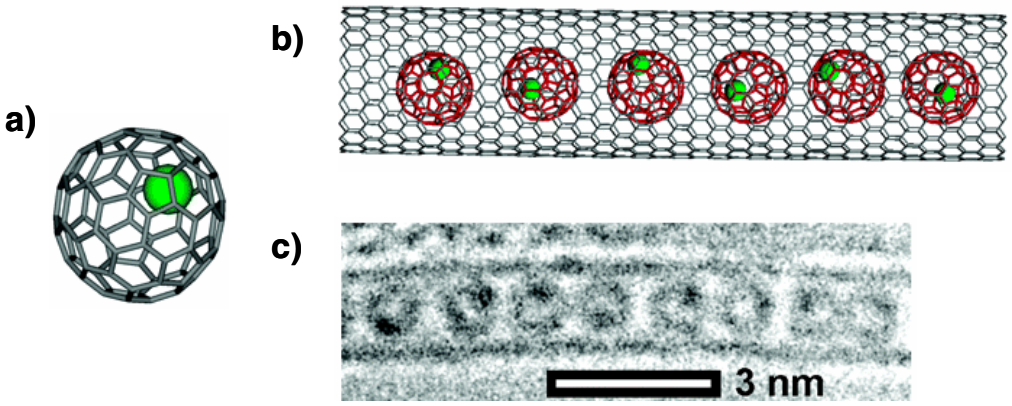

Figure 4. Endohedral metallofullerenes inside SWNTs. Structural diagram of (a) $Ce@C_{82}$, (b) $Ce@C_{82}$ inside SWNTs, (c) HRTEM micrograph of $Ce@C_{82}$ in SWNTs.[21]

Non-fullerene molecules inside SWNTs have been investigated as well. These molecules have also shown to exhibit peculiar properties. For example, octasiloxane ($Si_8H_8O_{12}$), a cube-shaped molecule with an H-atom pointing outwards from each

corner of the cube, was inserted in SWNTs with diameters of 1.4 - 1.5 nm and analyzed by IR spectroscopy (Figure 5).[22] Since the H atoms can have direct contact with the nanotube surface, the stretching vibrations of Si – H bonds were used to probe the interaction between the octasiloxane and the nanotube. The vibrational frequency of the Si – H bond, which normally appears as a sharp band at $\nu = 2277\ cm^{-1}$ in CCl_4 solution, was found broadened and red-shifted by about $\Delta\nu = -15\ cm^{-1}$. This is in contrast to a $\Delta\nu = +17\ cm^{-1}$ shift in Si – H absorption band observed for octasiloxane in solid state. This observation suggests that the Si – H bonds elongate as a result of dispersion forces acting between $Si_8H_8O_{12}$ and the nanotube.

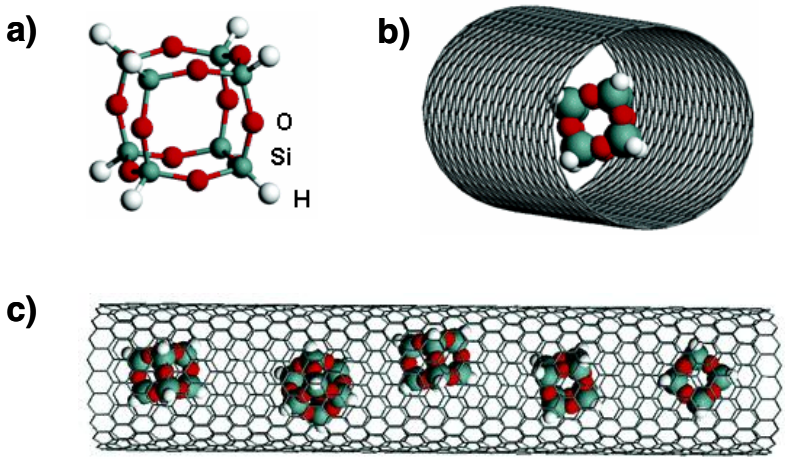

Figure 5. Octasiloxane in SWNTs. Structural representations of (a) $Si_8H_8O_{12}$, (b)-(c) $Si_8H_8O_{12}$ inside SWNTs.[22]

On the other hand, inserting $Si_8H_8O_{12}$ in narrower nanotubes (diameters of 0.8-1.2 nm) resulted in a red shift of the Si – H vibrational frequency by only $\Delta\nu = -6\ cm^{-1}$. This indicates that, in addition to van der Waals dispersive forces, the molecules in

narrower nanotubes experience greater compression than in wider nanotubes. Such a compression would shorten the Si – H bonds and effectively compensate for the elongation due to the dispersion interactions and thus suppress the observed red shift of the ν(Si-H) band.

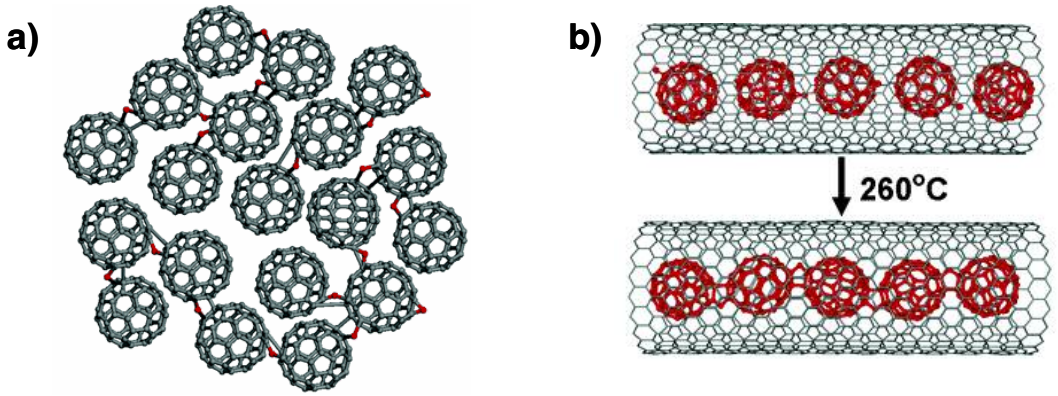

Figure 6. Polymerization of fullerene epoxide in (a) solid state and (b) inside SWNTs.[23]

The encapsulation effect has also been demonstrated in the polymerization of fullerene epoxide, $C_{60}O$ confined inside SWNTs.[23] Fullerene epoxide is stable at room temperature. Above 200°C, the strained epoxide ring opens up, forming a reactive intermediate, and reacts with carbon-carbon double bonds to form a furan ring. Polymerization of $C_{60}O$ in the solid state produces tangled, branched, three-dimensional polymers (Figure 6a). On the other hand, $C_{60}O$ inside SWNTs result in linear, unbranched polymers. The $C_{60}O$ molecules bond to each other in a head-to-tail fashion, indicating that the molecules were aligned in the same direction during reaction (Figure 6b).

The confinement of water molecules inside carbon nanotubes has been studied by vibrational spectroscopy.[24] In an infinite ice crystal each water molecule is tetrahedrally coordinated, donating and accepting two hydrogen atoms simultaneously to form a hydrogen-bonded network. This arrangement is disrupted in agglomerates of crystalline water in finite sizes, resulting in a variety of shapes for small water clusters with different types of OH groups ranging from bulk-like to free OH groups. The diversity of the OH groups can be detected by vibrational spectroscopy.

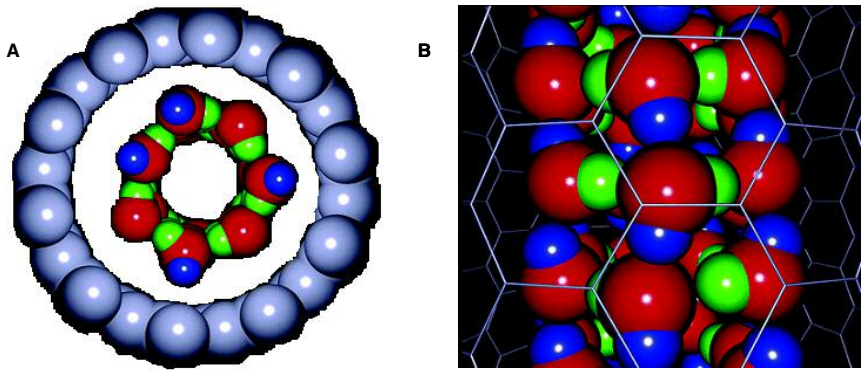

Figure 7. Snapshot from a molecular simulation of water inside a SWNT forming heptagon rings. (A) End view and (B) side view. (Red = oxygen, blue = hydrogens involved in inter-ring H-bonding, green = hydrogens involved in intra-ring H-bonding.[24]

It was found that H_2O molecules confined inside SWNTs form stacked ring structures that involve hydrogen bonds of two types, as illustrated in Figure 7. Hydrogen bonds formed within the ring structure exhibit frequencies similar to bulk H_2O (ν(OH) = ~3400-3450 cm^{-1}) while hydrogen bonds formed between neighboring rings exhibit a distinct OH stretching frequency. The infrared mode at ν = 3693 cm^{-1} assigned to the "free" OH groups dangling at the surface of amorphous ice disappears

when water diffuses inside the nanotube, and an OH vibration mode at ν = 3507 cm^{-1} was observed in addition to associated OH features in the ν = 3000-3450 cm^{-1} region. The observed infrared mode at ν = 3507 cm^{-1} is assigned to vibrations of the inter-ring OH groups, and believed to be a direct result of the confinement of H_2O molecules in SWNTs.

1.2.1.2. Experimental Difficulties Associated with Carbon Nanotubes

In spite of a number of publications devoted to the study and use of carbon nanotubes, there are several difficulties associated with them. One of the primary challenges encountered involves purity. SWNTs are usually prepared by dissolving carbon in a transition metal nanoparticle melt then subjecting the mixture to high temperature.[25] This process produces carbon nanotubes contaminated with metal catalysts, amorphous carbon and non-SWNT carbon particles. Several purification methods have been introduced and these usually involve filtration to remove large graphite particles, treatment with concentrated acid or oxidants to destroy the catalysts, and chromatography.[26] However, these methods are usually difficult to scale up in order to obtain large volumes of sample. Moreover, treating the sample under strong oxidizing conditions tends to destroy the sample.

The synthesis of carbon nanotubes normally produces closed structures which prevent access to its interior.[27] Chemical treatment is therefore required to open the end caps to access the interior of the nanotube. This is usually done using strong oxidizing agents. Again, this procedure can damage the nanotubes and introduce several defect sites on its walls.

Another limitation that hampers the practical use of SWNTs is the lack of solubility and the difficulty of manipulation in any solvent. They can be dispersed in some solvents by sonication but only temporarily. To address this issue, functional groups are introduced on the surface of the carbon nanotubes; typically by taking advantage of defect sites created by oxidation treatment.[28,29]

Finally, the investigation involving filled SWNTs and understanding its mechanism is non-trivial.[16,30,31] The use of nano-probe spectroscopic methods on isolated, single SWNTs is required to conduct accurate measurements, and ascertain whether foreign guests are encapsulated in the tube and not intercalated between tubes. Methods such as high-resolution transmission electron miscroscopy (HRTEM), Raman spectroscopy or electron energy loss spectroscopy (EELS) have to be used for accurate characterization.[32]

These challenges should therefore be addressed before SWNTs can have viable applications. In the meantime, researchers have also considered looking for other means to construct nanotubes.

1.2.2 Synthetic Nanotubes

Aside from carbon, inorganic and organic systems have been introduced to synthesize nanotubes. Although inorganic systems benefit from the majority of elements in the periodic table, organic systems take advantage of its inherent power of synthetic molecular and supramolecular chemistry.[33] Organic synthesis also provides greater structural variation and control over the diameter and length of the tube. These features are important for studying guest dynamics and in the design for potential

storing chambers and catalytic vessels. Thus, the development of a design which is analogous to carbon nanotubes may hold promise in understanding the principles of supramolecular chemistry, particularly multiple guest encapsulation, chemical dynamics and information storage/processing.

1.2.2.1 Self-assembled Synthetic Nanotubes

A novel class of self-assembling nanotubes has been introduced by Ghadiri and co-workers.[10] These are based on cyclic peptide molecules consisting of even numbered alternating D- and L-amino acids. They showed that these molecules self-assemble via hydrogen bonding into nanotubes (Scheme 1).

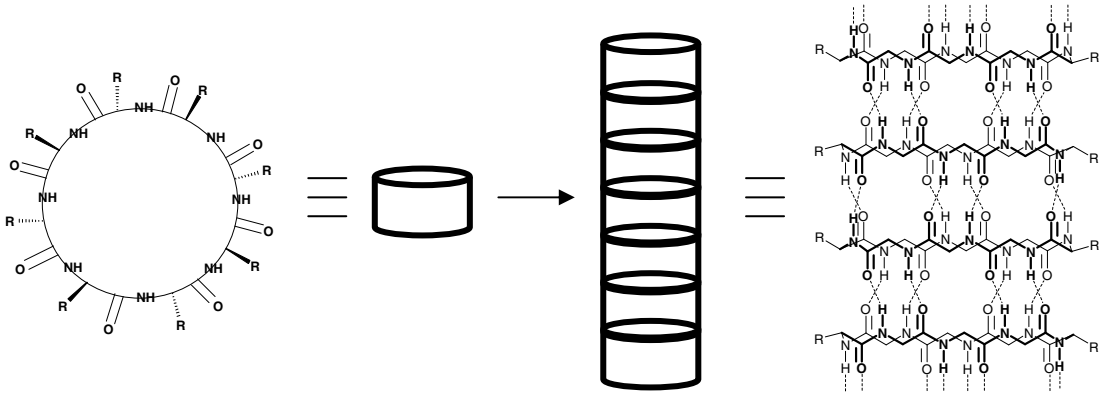

Scheme 1. Schematic diagram of nanotube self-assembly from cyclic D, L-peptides.[10]

An interesting feature of this peptide nanotube is the ease with which the external surface properties and the internal diameter of the tube may be altered by changing the appropriate amino acid side chains and the size of the peptide ring, respectively. For example, they have shown that with appropriate hydrophobic side

chains, these cyclic peptides partition into nonpolar lipid bilayers and self-assemble to form artificial transmembrane ion channels. Similar systems have also been utilized as biosensors for detection of ions and small organic molecules. On the other hand, Gazit and Reches[34] used a cyclic phenylalanine structural motif to build nanotubes and encapsulate silver ions in solution. Reduction of the ionic silver within the tubes, followed by degradation of the peptide backbone, resulted in the formation of silver nanowires.

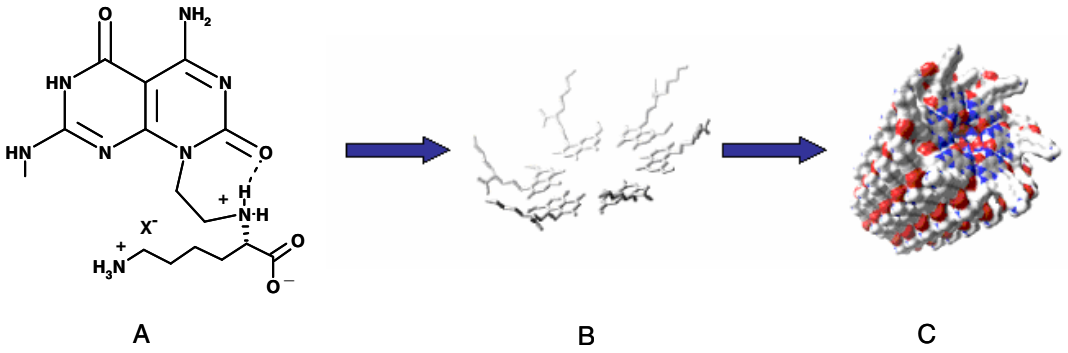

Scheme 2. Self-assembly of rosette nanotubes. (A) bicyclic base system (B) Molecular model of the rosette structure (C) Molecular model of the proposed nanotube.[35]

Another self-assembled nanotube was reported by Fenniri et al.[36] The design is based on a heteroaromatic bicyclic base motif. These molecules self-assemble into discrete nanotubular structures in water. With the unique feature of forming Watson-Crick type H-bonding arrays, plus its hydrophobic character, the bicyclic system undergoes a hierarchical self-assembly to form six-membered rosettes. Several stacks of these rosettes then organize together to grow hollow tubular structures with an open

channel 1.1 nm across and several micrometers long (Scheme 2). Varying the functional groups introduced to the bicyclic motif modifies the surface properties of the nanotubes, and consequently influences its structure, stability and functionality.[33,35]

Another design introduced by Matile and co-workers[37] was based on rigid-rod β-barrels. These artificial β-barrels are synthesized by coupling the N-termini of short peptide strands with the carboxylic acids along the scaffold of octa(*p*-phenylene)s. Self-assembly of the octa(*p*-phenylene)-peptide conjugate results in the formation of the rigid-rod β-barrels via hydrogen bonding (Scheme 3). The barrels then serve as synthetic ion channels or pores when affixed in planar or spherical lipid bilayers.

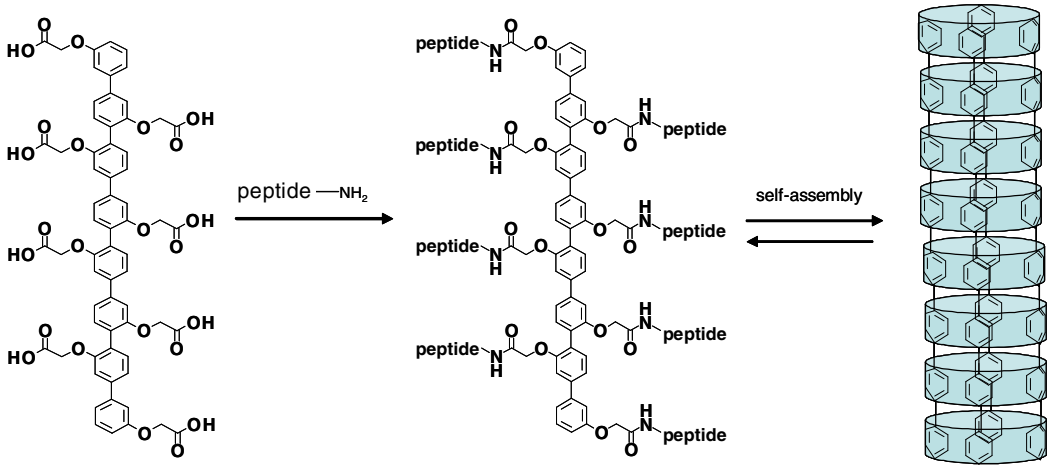

Scheme 3. Formation of rigid-rod β-barrels from octa(*p*-phenylene)s. Arrows between octa(*p*-phenylene) staves indicate β-sheets (N → C).[37]

The design allows molecules to interact with the barrel either at the external surface or at the pore. Interaction of molecules with the external residues causes an increase in barrel-membrane interaction which leads to the activation or opening of the pore. On the other hand, interactions of molecules that pass through the pore across a

bilayer membrane may result to pore-closing or blockage. Recognition of guests is usually measured by taking advantage of the synthetic pores' intrinsic fluorescent property. A broad spectrum of recognized guests already studied range from small inorganic ions to higher aromatics such as fullerenes and calixarenes to polypeptides, polysaccharides and DNA.[11]

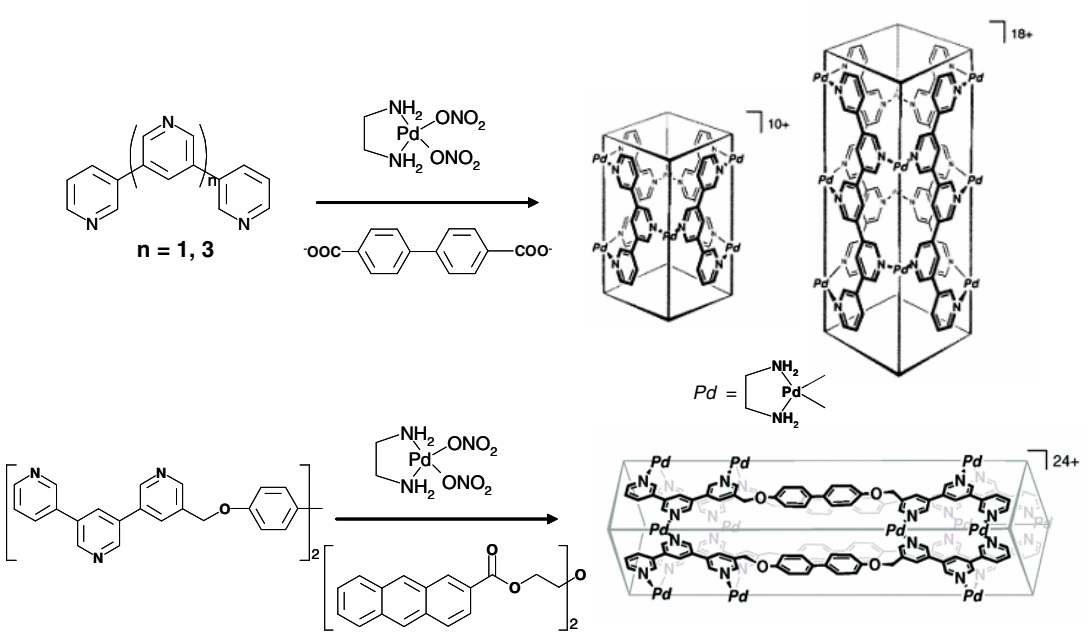

Scheme 4. Self-assembled nanotubes through metal coordination.[38,39]

A novel approach to self-assembled nanotubes was also reported by Fujita and co-workers.[38] Their approach was based on metal coordination. They found that oligo(3,5-pyridine)s self-assemble into tubular structures with the aid of rod-like molecules acting as templates (Scheme 4). The oligomeric ligand, which takes on a planar conformation due to the dipole-dipole repulsion between pyridine nuclei, is linked together through coordination with Pd(II) building blocks. This process,

however, only occurs in the presence of a template molecule which interacts strongly with the pyridine moieties through π-π interactions. Thus, when the template molecules are removed, the nanotube collapses into oligomers. However, when the ligand was extended using a biphenyl linker, the longer nanotube formed becomes more stable even after removal of the template molecule.[39]

1.2.2.2 Covalent Strategy

Synthetic nanotubes constructed through self-assembly have shown promise as sensors, catalysts, ion channels, metal wire scaffolds, and drug delivery vehicles.[40] However, these nanotubes are controlled by non-covalent interactions and are thus, only stable under specific conditions. For example, hydrogen-bond-driven self-assemblies like peptide and rosette nanotubes are sensitive to pH and solvent because the protonation states of amino acid residues influence the strength of intermolecular hydrogen bonding.[35,40] Another example was presented earlier involving coordination nanotubes by Fujita and co-workers in which the nanotubes are only stable in the presence of a template molecule.[38] Thus, to stabilize the nanotubes without sacrificing structure and functionality, researchers have introduced the covalent approach.

The combined strategy involving non-covalent interaction and covalent bonding has been demonstrated by Harada and co-workers.[41] Using threaded α-cyclodextrins (CD) as precursors, they successfully constructed the first reported synthetic nanotube.

α-CDs are cyclic oligomers of glucose which contain a cylindrical cavity of approximately 0.7 nm in depth and 0.45 nm in diameter. They were found to complex with poly(ethylene glycol) very efficiently, forming a chain of threaded CD complexes

called polyrotaxanes. Bulky stoppers ($NH(C_6H_3)(NO_2)_2$ groups) were introduced at the ends of the chain, keeping CD molecules in close contact with each other and preventing their dissociation. Upon treatment with epichlorohydrin in aqueous base, the CD hydroxyl groups formed covalent bonds with neighboring units (Scheme 5). Adding a large excess of base then cleaved the stopper groups and subsequently released the CD-based nanotubes in solution.

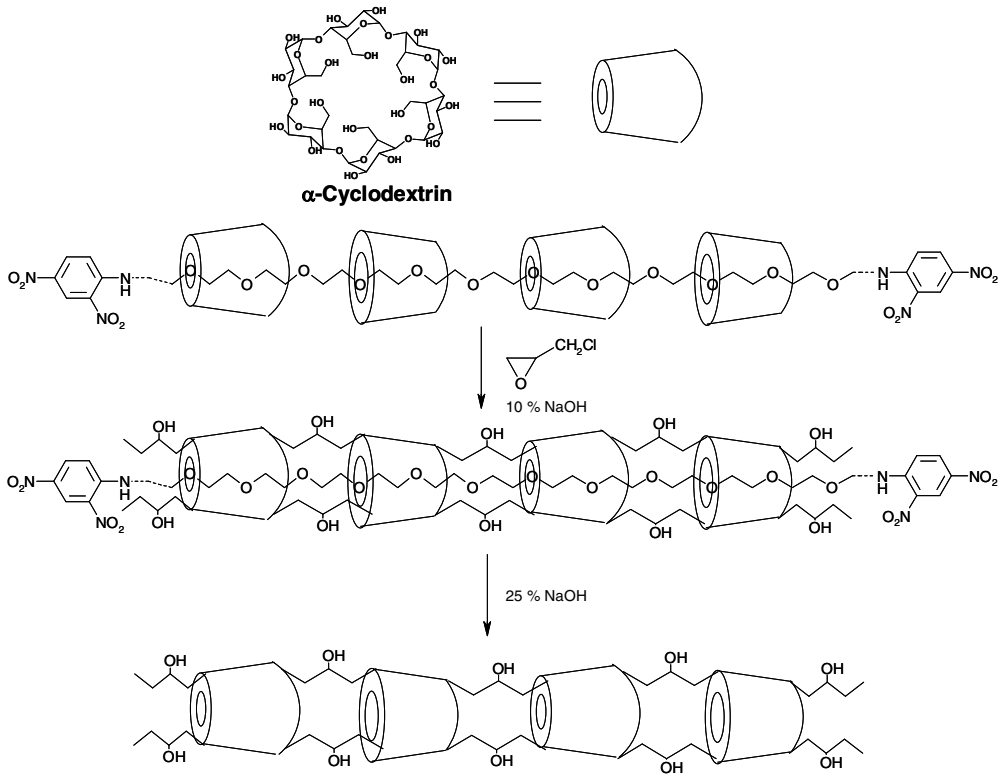

Scheme 5. Preparation of synthetic nanotube from α-cyclodextrins.[41]

The CD nanotubes were reported to encapsulate I_3^- ions from a pale yellow solution of potassium iodide with iodine ($KI-I_2$), resulting in a deep red colored solution. This color change was not observed with monomeric α-CDs nor with

randomly cross-linked α-CDs; thus, possibly indicating the presence of linearly arranged I_3^- ions inside the nanotube.

Biesalski and co-workers[42] introduced a polymer hybrid version of the cyclic peptide nanotube (Scheme 6). The octameric cyclic peptides with alternating D- and L-configurations were modified with bromoisobutyramide initiators attached on the lysine side chains. Once the nanotubes are formed, these were reacted with N-isopropylacrylamide monomer and subjected to atom-transfer radical polymerization (ATRP) reaction. This technique allowed the polymer to grow a homogeneous shell around the cylindrical peptide core.

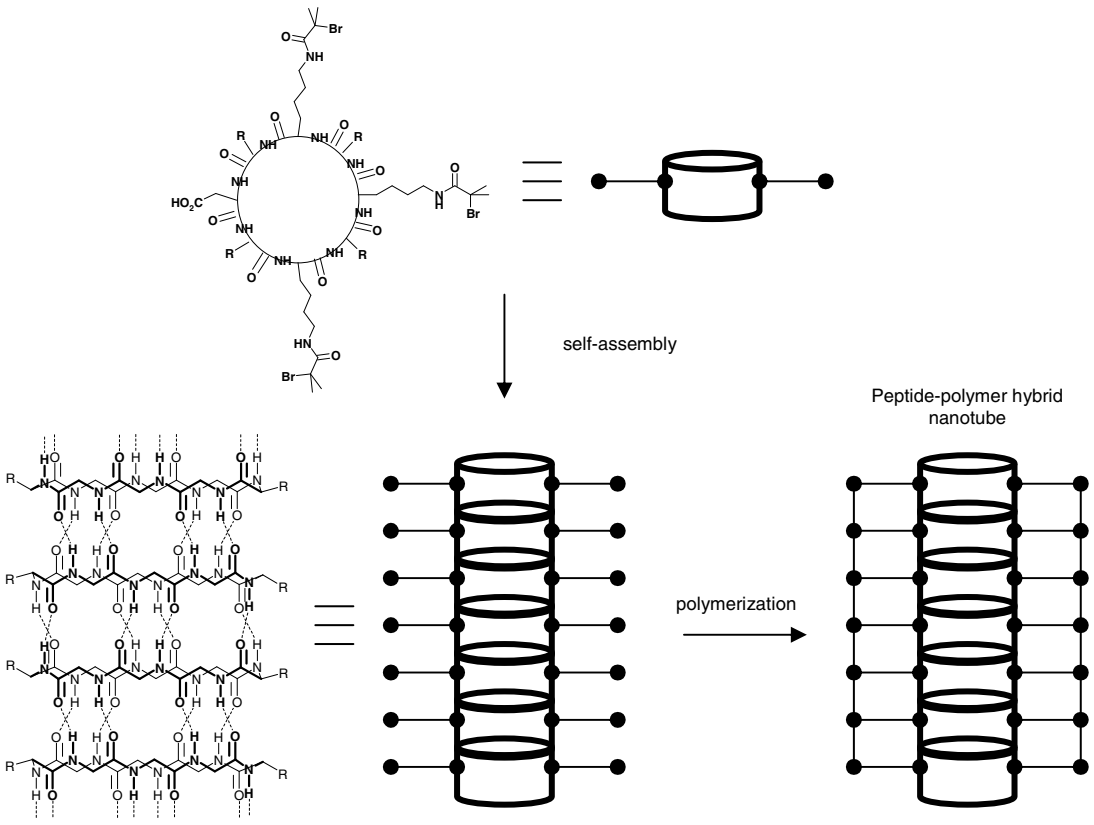

Scheme 6. Schematic outline of the synthesis of peptide-polymer hybrid nanotubes.[42]

Hetch and co-workers[43] generated organic nanotubes from intramolecularly crosslinked, helically folded polymers. They synthesized amphiphilic poly(*m*-phenyleneethynylene)s that bear cinnamate groups to serve as backbone. In polar solvents, non-covalent interactions such as π-π stacking of the aromatic units and solvophobic interactions allow the polymer strand to fold itself into a helical conformation. Such conformation brings reactive groups in proximity for effective cross-linking via [2+2] photodimerization, producing rigid organic nanotubes (Scheme 7). The helix-coil transition can be monitored using UV-vis absorption and fluorescence spectroscopies. However, the degree of cross-linking was only estimated to be about 20-30%.

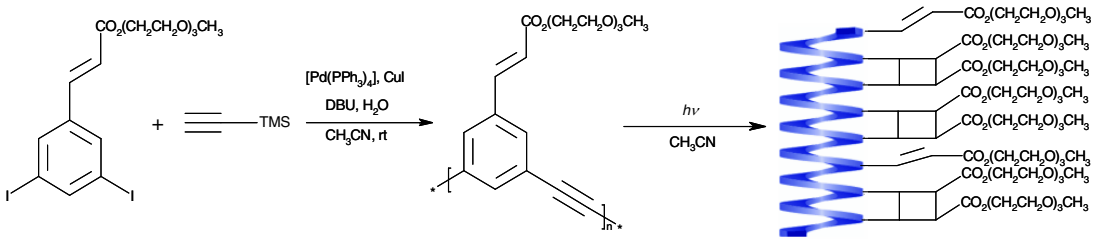

Scheme 7. Synthesis of crosslinked amphiphilic poly(*m*-phenyleneethynylene).[44]

Another covalent design was introduced by Zimmerman and co-workers.[45] They incorporated porphyrins and dendrimers in constructing nanostructures. In this case, the porphyrin assembly serves as a core-shell for molding dendrimers around it (Scheme 8). Porphyrin dendrimers containing multiple alkene end groups were first synthesized then complexed with tin (IV). The metalloporphyrin dendrimers were bridged together, forming stacks of the dendrimers. The peripheral alkene groups were then subjected to

ring-closing metathesis (RCM) to generate the nanotubes. Finally, in order to form hollow structures, the porphyrin moiety was removed at the dendron-porphyrin linkages by transesterification reaction. With this strategy, the thickness of the tube wall is determined by the generation of the dendron, and the inner diameter can be controlled by an appropriate sized core. Functionality of the outer and inner surfaces of the tube can also be modified by linking desired reactive groups. However, there is no significant control over the length of the tube. Also, more information is required to determine whether the hollow structure collapses or remains open upon removal of the porphyrin core.

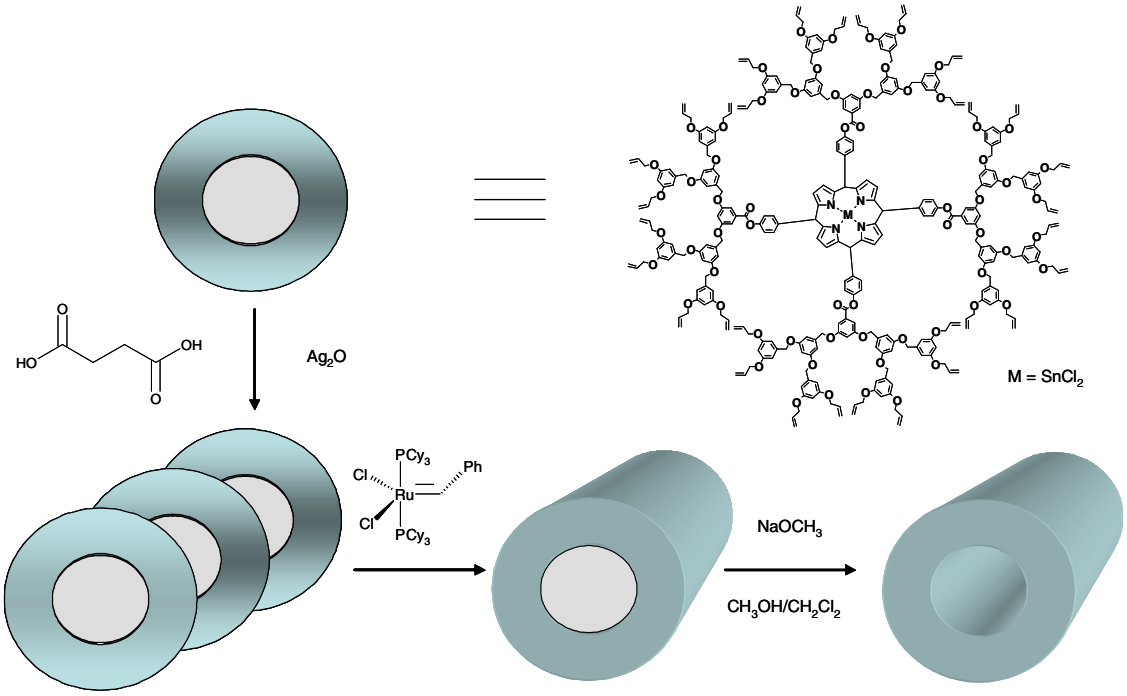

Scheme 8. Synthesis of nanotubes from porphyrin dendrimers.[45]

1.3. Summary

In summary, the fast-growing field of nanoscale science and technology has led to important discoveries and potential applications. One such discovery is carbon nanotubes; particularly, single-walled carbon nanotubes. These nanotubes have a unique structure with the ability to encapsulate materials in a one-dimensional configuration. Such a property has motivated researchers to investigate the effect of confinement to the filling materials. Several reports have shown that molecules inside carbon nanotubes exhibit structural and dynamic properties that are not observed in the bulk. However, carbon nanotubes suffer from the high cost of processing, low purity and homogeneity, poor solubility, and lack of simple methodologies for accurate measurements. Alternatively, synthetic nanotubes offer simplicity and convenience in construction, processing and analysis. Several approaches to synthetic nanotubes which utilize covalent and non-covalent interactions have been developed. Still, there are limitations to their design and their ability to encapsulate materials remains a challenge. An improved design with improved encapsulation properties is needed to overcome these drawbacks and further add to our understanding of confined materials at nanoscale dimensions.

CHAPTER 2

CALIX[4]ARENE-BASED SYNTHETIC NANOTUBES

2.1 Calix[4]arenes

Calix[n]arenes are a popular class of macrocycles formed from the condensation of a *p*-substituted phenol with formaldehyde. The "n" refers to the number of phenolic residues in the calixarene. The descriptive name "calixarene" was coined by Gutsche because the bowl-shaped conformation of the cyclic tetramer resembles a Greek vase called a *calix crater*.[46]

Calixarenes are characterized by an upper rim, a lower rim and a central annulus (Figure 8). The selective functionalization at the upper and/or lower rim makes calixarenes extremely versatile host frameworks for cations, anions and neutral molecules.[46-49]

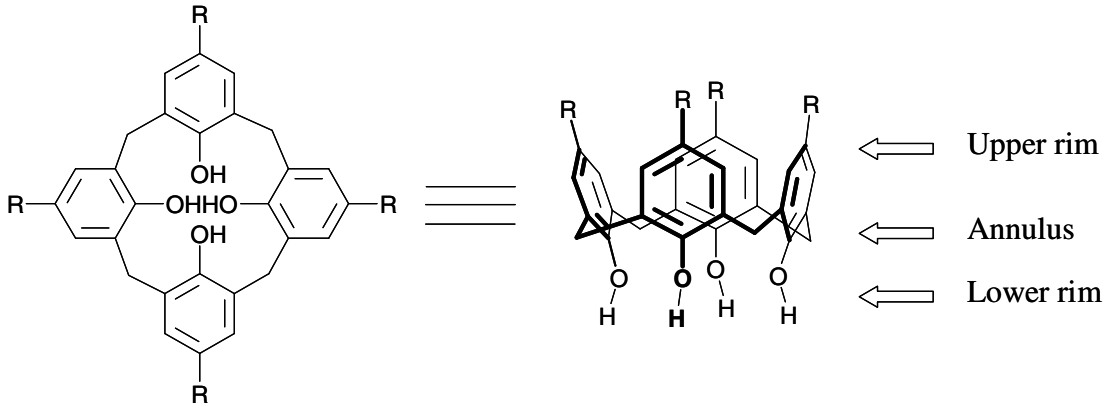

Figure 8. Representation of calix[4]arenes.

Calix[4]arenes adopt four possible conformations, namely *cone*, *partial cone*, *1,2-alternate* and *1,3-alternate*. These conformations can be described based on the projections of the aryl groups, either upward ("u") or downward ("d"), relative to the annulus. Thus, "u,u,u,u," is designated for *cone*; "u,u,u,d" for *partial cone*; "u,u,d,d" for *1,2-alternate*; and "u,d,u,d" for *1,3-alternate*, as illustrated in Figure 9.[46]

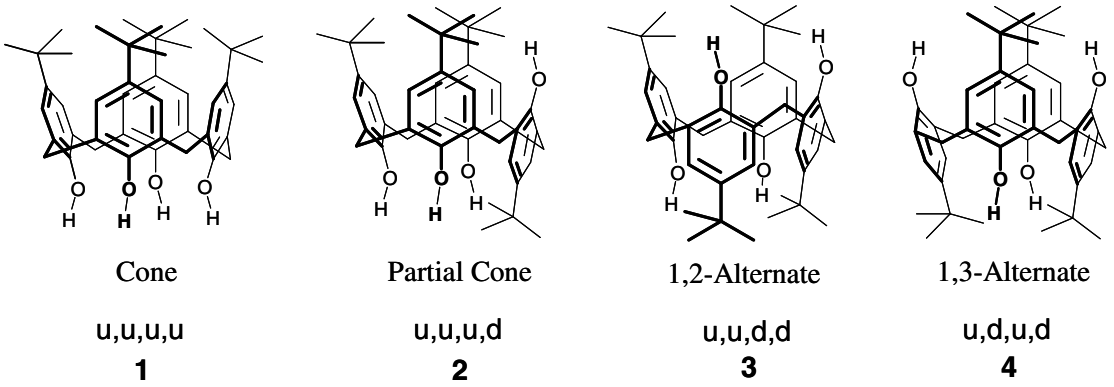

Figure 9. Conformations of calix[4]arenes.

The four conformations can be identified through their ^{1}H and ^{13}C NMR spectra.[50] The NMR patterns of the bridging methylene groups are very useful in distinguishing three out of the four conformations (Figure 10). The ^{1}H NMR spectrum of *cone* calix[4]arenes with the same substituents at each *para* position shows a pair of doublets (at ~ 3.1 ppm and 4.0 ppm) for the methylene bridges below the coalescence temperature, while a singlet (at ~3.5 ppm) is observed for the *1,3-alternate* conformer. Both pair of doublets and singlet are present in *partial cone* and *1,2-alternate* conformations. Although the less common *1,2-alternate* conformation shows a similar

pattern to the *partial cone*, the two conformations can be distinguished by the number and multiplicity of proton signals in the aromatic region of the spectrum. The conformations also exhibit distinguishing patterns in the ^{13}C NMR spectrum. De Mendoza and co-workers[51] have shown that the bridge methylene carbon resonance is near 31 ppm when two adjacent aryl groups are in the *syn* orientation, and near 37 ppm when they are in the *anti* orientation.

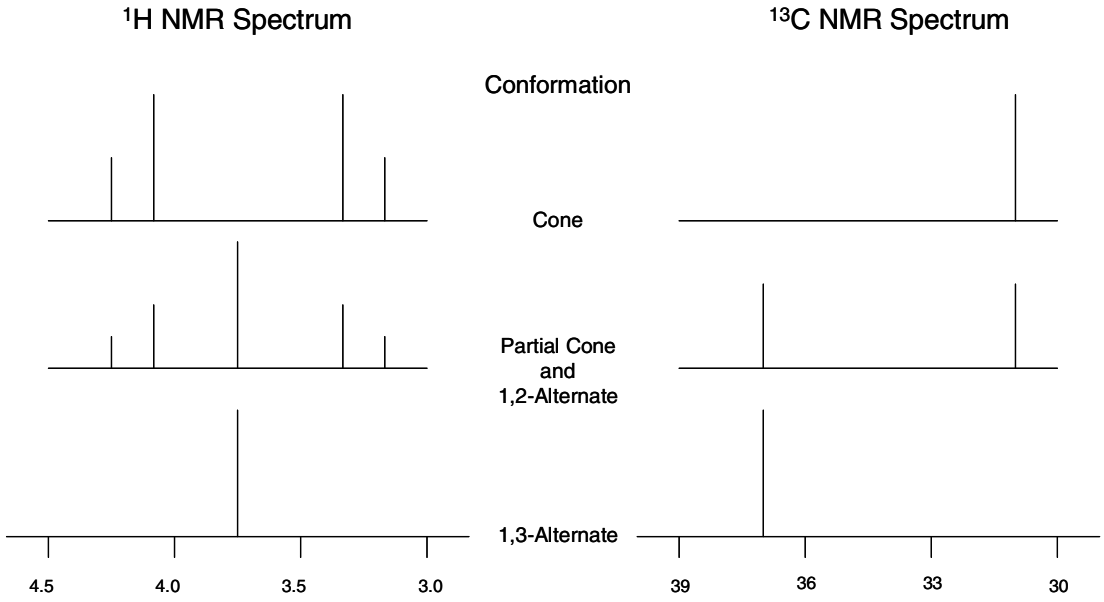

Figure 10. Patterns of signals in ^{1}H and ^{13}C NMR of four calix[4]arene conformers.

Among the conformers, calix[4]arenes in the *1,3-alternate* conformation have several interesting structural features. They have two metal-binding sites at the edges of the calix[4]arene cavity. The binding sites are composed of two "hard" phenolic oxygens and two "soft" π-basic benzene rings. These two binding sites, defined by two cofacial pairs of aromatic rings that are oriented orthogonally along the cavity axis, are

linked together to form a cylindrical π-basic benzene tunnel. X-ray studies reveal that this tunnel is ~5-6 Å in diameter.[52,53] These unique structural features are reflected by their metal-binding properties. For example, *1,3-alternate* calix[4]arenes can form 1:1 complexes with metal cations like K^+ and Ag^+.[54] Moreover, in a 1:1 complex, the metal cation vibrates between the metal-binding sites through the π-basic tunnel (Figure 11).[55]

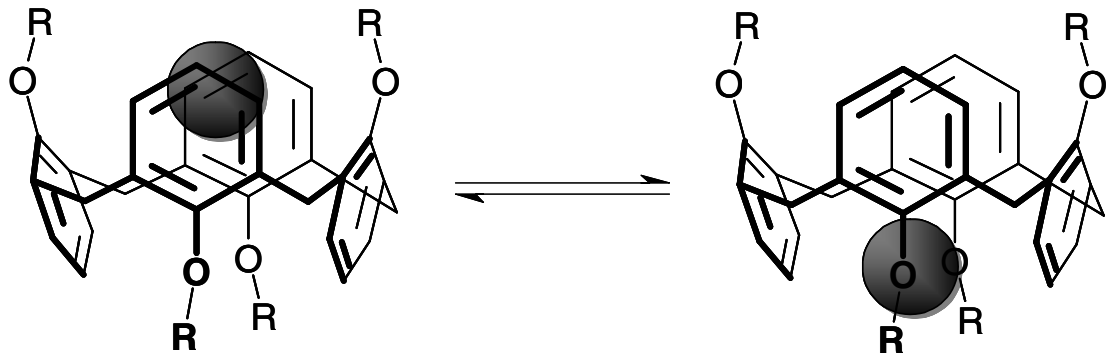

Figure 11. Metal-tunneling through a π-basic tube of *1,3-alternate* calix[4]arene.

These characteristics of the *1,3-alternate* calix[4]arene have led to the construction of synthetic nanotubes based on this motif which can serve as metal cation receptors or artificial ion channels.

2.2 Early Calixarene-based Nanotubes

Calix[4]arene-based nanotubes or calix[4]tubes were first introduced by Shinkai and co-workers.[56,57] Taking a cue from the dynamic behavior of small metal cation complexes with *1,3-alternate* calix[4]arenes, they connected several calixarenes to form

nanotubes **5**-**7b** (Figure 12). Conceptually, nanotubes **5**-**7b** would allow metal cations to tunnel through its π-basic interior.

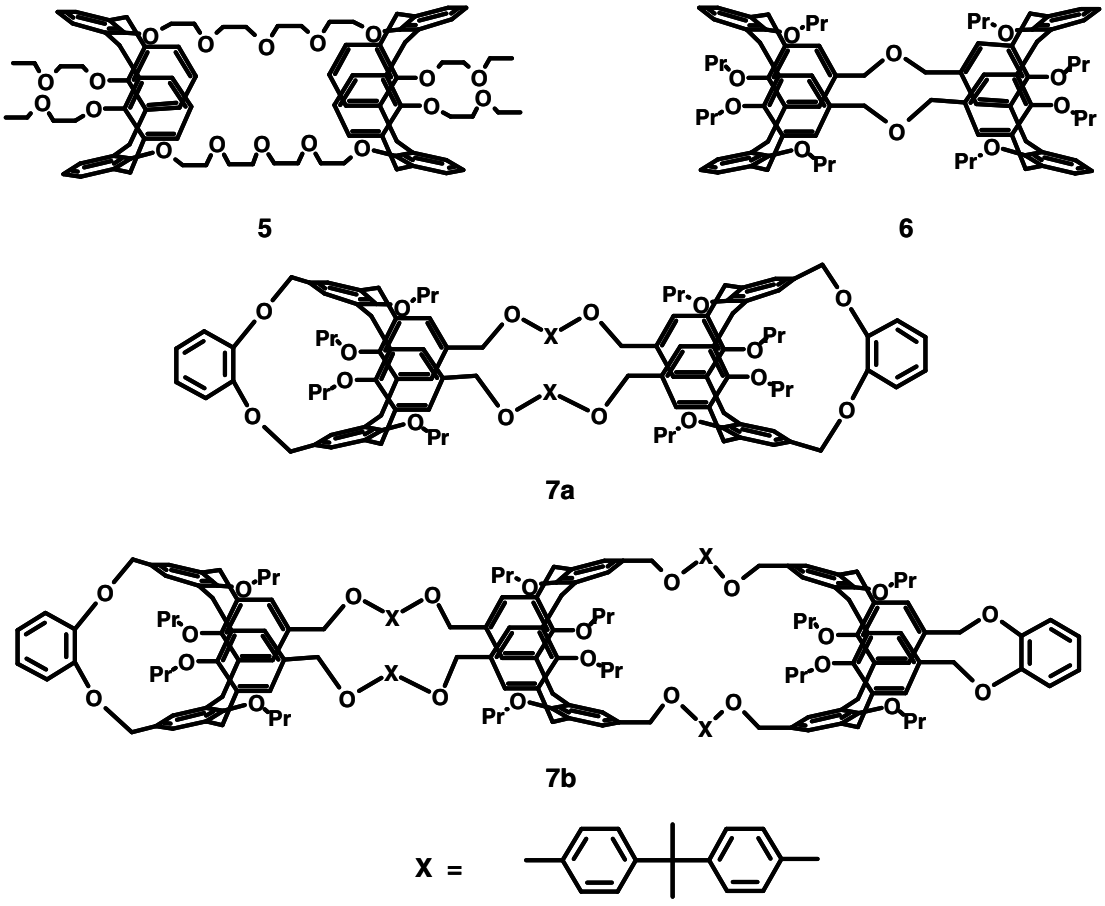

Figure 12. Shinkai's calix[4]arene nanotubes.[57]

Complexation experiments with $AgCF_3SO_3$ has revealed the presence of a 1:1 Ag^+ ion complex with calix[4]tube **5**. Analysis of the ^1H NMR spectrum of the complex suggests that the Ag^+ ion is delocalized between two calixarenes. The authors proposed that the metal cation oscillates between metal-binding sites in calix[4]tubes in two possible modes: intracalixarene metal-tunneling and intercalixarene metal-hopping

(Figure 13). This dynamic behavior, however, was not observed in the complexation with calix[4]tube **6**; instead, a mixture of free tube **6** and 1:2 tube-Ag^+ complex was found in the ^1H NMR spectum. It was suggested that the *p*-substituents used to connect the two calixarenes interfered with the cation-π interaction, thus, suppressing the metal tunneling. In this case, the Ag^+ ions were said to be localized at the edges of the tube, interacting with the calixarene phenyl groups and the propyloxy-oxygen groups through cation-π and electrostatic O-Ag^+ interactions, respectively.

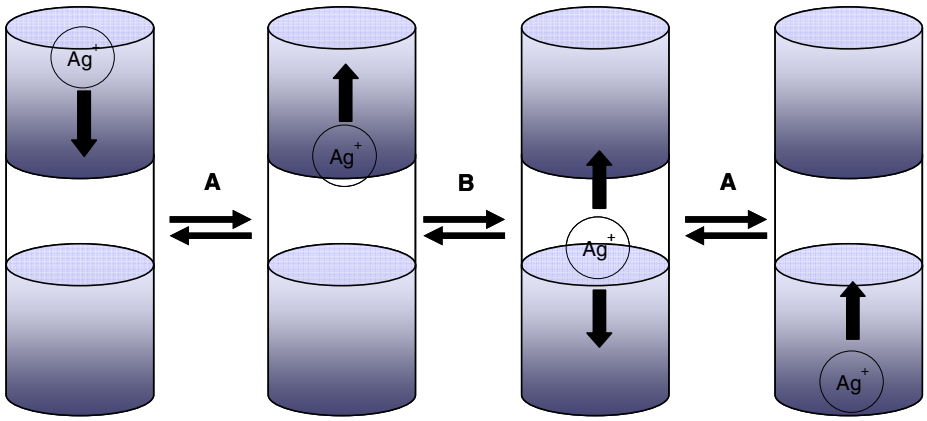

Figure 13. Intracalixarene metal-tunneling (A) and intercalixarene metal-hopping (B). [57]

Similarly, there was no evidence of metal-tunneling in the complexation studies with calix[4]tube **7a** (no report of the same experiment with **7b**). A 1:1 mixture of **7a** and AgO_3SCF_3 yielded three different species: free **7a**, **7a**•Ag^+ and **7a**•$(Ag^+)_2$ in a 1:2:1 ratio. This result implies that Ag^+ is bound to **7a** according to probability. Moreover, the lack of metal-tunneling was suspected to be the result of several structural features of **7a**. These are: the para-substitution of phenyl groups in the calixarene units; the

increased distance between two calixarene units relative to other structures; and the non-ionophoric bridges connecting the calixarene units.

Kim et al.[58] reported similar multiply-connected *1,3-alternate* calix[4]arenes (Figure 14). However, the terminal calixarene units were capped with crown ethers (calix[4]crowns). Similar to Shinkai, metal ion shuttling was not observed, and metal ions were only bound at the end-calixcrown "stoppers."[59] X-ray crystal structure of the biscalix[4]crown **8** with K^+ ions revealed that electrostatic interactions between the oxygen donor atoms of the crown ether ring and the metal cation plays a major role for entrapping the metal ion while the cation-π interaction plays a minor role.

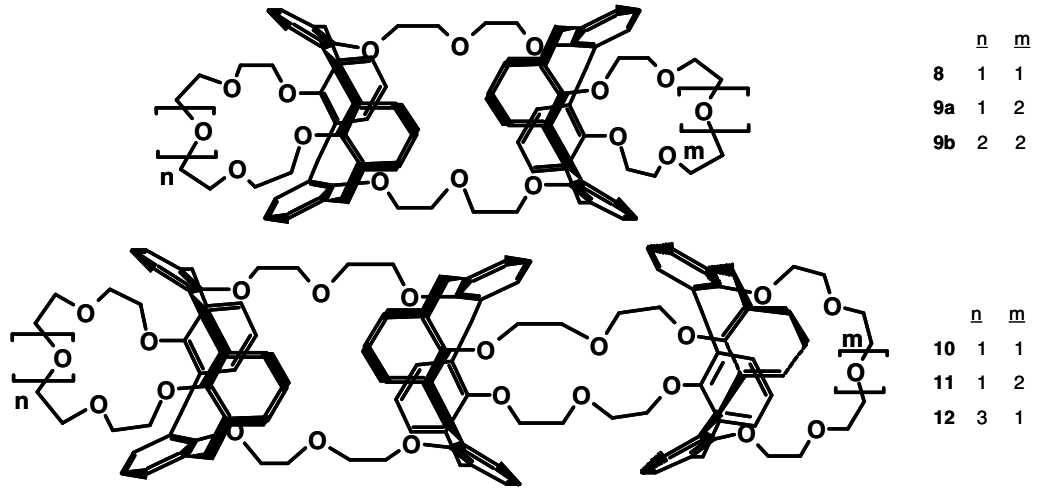

Figure 14. Kim and Vicens' synthetic nanotubes.[58]

Our group recently found cation-π complexes with calix[4]arenes which feature unique stabilities. These are based on interactions between calix[4]arenes and nitrosonium (NO^+) cations.

2.3 Towards A Novel Design for Synthetic Nanotubes

Our laboratory recently discovered that simple calix[4]arenes, for example **13**, reversibly interact with NO_2/N_2O_4 and entrap the highly reactive NO^+ cation within their π-electron rich interiors (Scheme 9).[60,61] Molecular modeling suggested that the *1,3-alternate* calix[4]arene has a sufficiently wide cavity to accommodate one NO^+ guest.

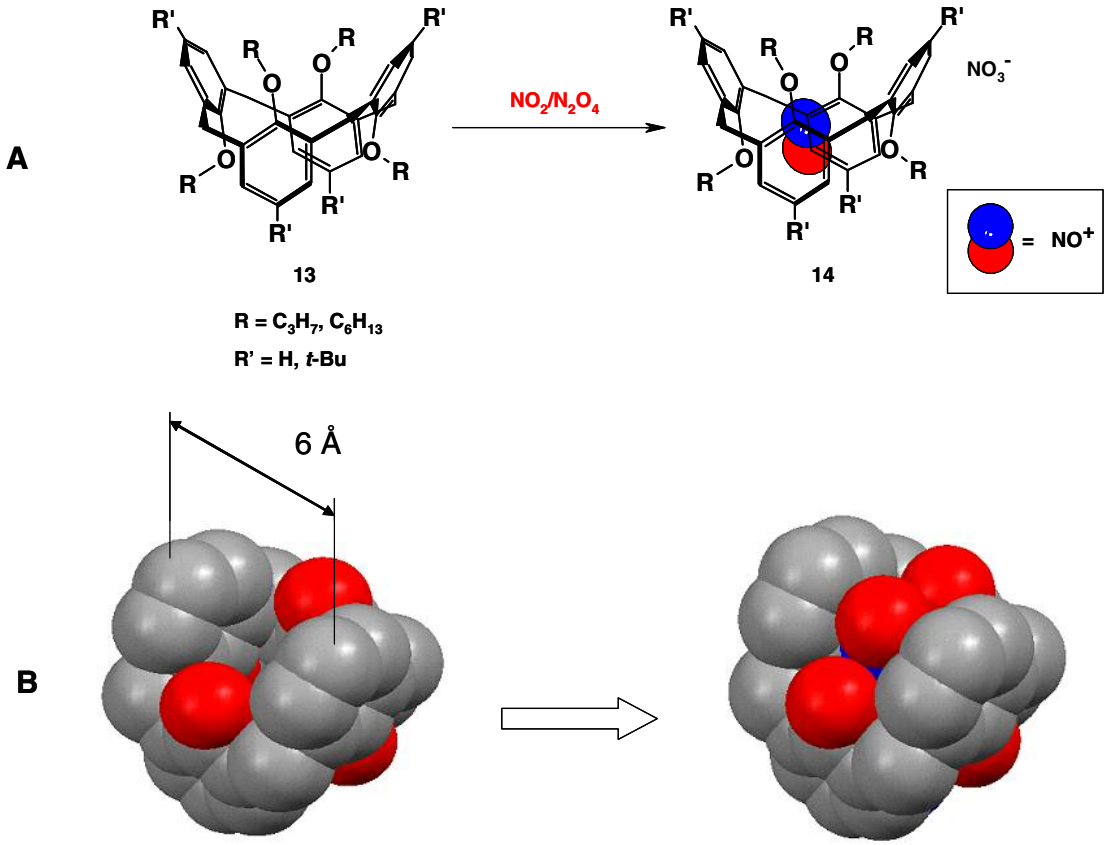

Scheme 9. Formation of calix[4]arene-NO^+ complex.[61] (A) Reaction of NO_2/ N_2O_4 with **13**. (B) Molecular model representations of **13** and **14** (hydrogens and counter ions are omitted for clarity).

NO^+ is generated from N_2O_4, which is known to disproportionate to $NO^+NO_3^-$. When NO_2/N_2O_4 gas is bubbled through a $CHCl_3$ solution of **13**, a deep purple solution was produced instantly. This is in striking contrast to the colorless solution of **13** and a pale yellow solution of NO_2/N_2O_4 in $CHCl_3$. Upon complexation, the UV-vis absorption spectrum changed accordingly, with the appearance of a broad band at λ_{max} = 512 nm. This observation is attributed to a strong charge-transfer process between the electron-deficient NO^+ species and the π-electron rich calixarene cavity, in which the NO^+ species is sandwiched between two aromatic rings.[62-64]

The host-guest dynamics of the NO^+ complexes can also be studied using ^1H NMR. The ^1H NMR spectrum of complex **14** exhibited new sets of signals compared to empty calixarene **13** (Figure 15). The aromatic proton signals of empty **13** were seen as a doublet and a triplet, 2:1, at 6.92 and 6.68 ppm, respectively (J = 7.5 Hz). In the NO^+ complex **14**, these signals were transformed into a triplet and a doublet, 1:2, at 7.17 and 7.08 ppm, respectively (J = 7.5 Hz). The methylene bridge CH_2 and OCH_2 protons of **13** were seen as a singlet and a triplet, 1:1, at 3.62 and 3.54 ppm (J = 7.5 Hz), respectively; whereas, in complex **14**, these were transformed into a triplet and a singlet, 1:1, at 3.87 and 3.60 ppm, respectively (J = 7.5 Hz). These results show that aside from the NO^+-aromatic interaction, the NO^+ guest also interacts with the phenolic oxygens through ion-dipole interactions.

The stepwise addition of NO_2/N_2O_4 or commercially available $NO^+SbF_6^-$ salt in $CHCl_3$ solution reveals both free **13** and complex **14**, indicating that the NO^+ exchange

in and out of the calixarene cavity is slow on the NMR time scale. This observation is typical for host-guest complexes with high association constants (K_{assoc} >>10^6 M^{-1}).

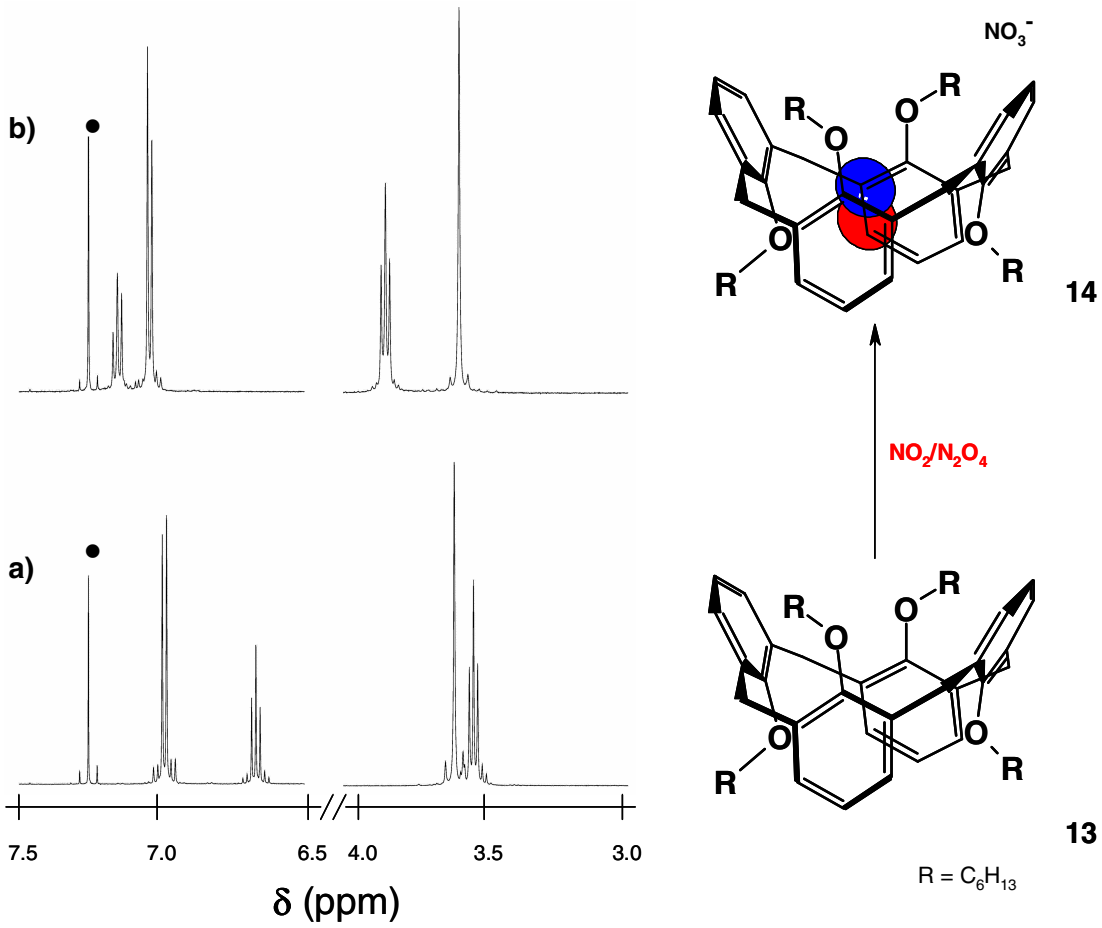

Figure 15. Portions of the ^{1}H NMR spectra (500 MHz, $CDCl_3$, 295 K) of (a) calix[4]arene **13**, and (b) nitrosonium complex **14**.[61]

The complexes formed are very stable and can be stored in the absence of moisture for several weeks, both in $CHCl_3$ solution and in the solid state. On the other hand, the complexation process is reversible, and the NO^+ guest can leave the calixarene

cavity. Addition of H_2O or methanol to the freshly prepared $CHCl_3$ solution of complex **14** resulted in the complete removal of NO^+ and the recovery of calixarene **13**.

2.3.1. Design of Calix[4]tubes

Taking advantage of the unique chemistry between calixarenes and NO^+ species, in principle calix[4]arene tubes can now be constructed and filled. In order to accomplish this, the calix[4]arenes should be rigidly connected from both sides of their rims, with at least two symmetrical bridging units. This is possible for a *1,3- alternate* conformation. The *1,3-alternate* calix[4]arenes are connected via their phenolic oxygens through two diethylene glycol bridges. Based on molecular models, the bridge length is optimal, providing a relatively rigid tubular structure with narrow gaps between calixarene modules. By our calculations, the calix[4]arene units are separated by about 9 Å, and the nanotubes have dimensions of about 6 Å in diameter and 15, 25, 35, and 45 Å in length for calix[4]tubes **15**-**18**, respectively (Figure 16).

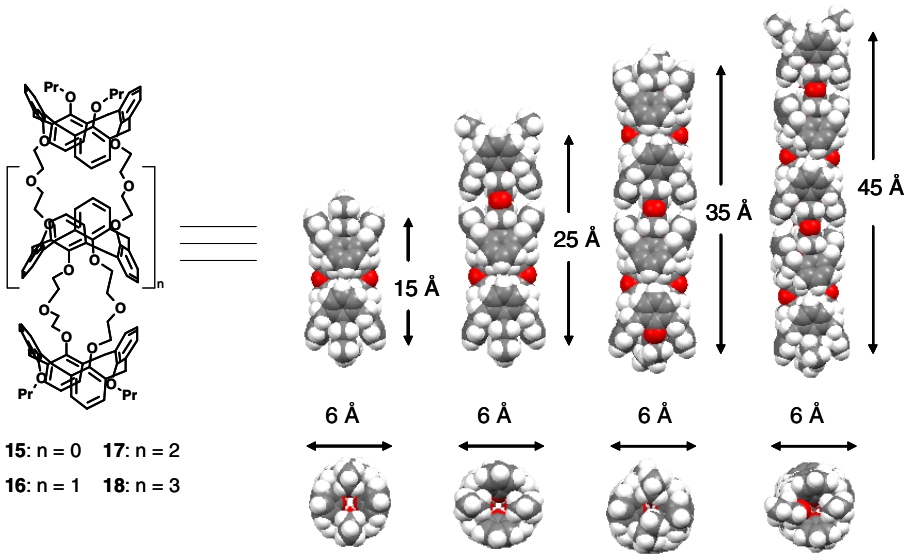

Figure 16. MacroModel 7.1 (Amber* Force Field) space-filling representation of nanotubular structures **15**-**18** (side and top views).

2.3.2. Synthesis of Calix[4]tubes

The synthesis of calix[4]tubes **15**-**18** is based on a straightforward modular strategy which incorporates reliable Williamson-type alkylation of alcohols. To immobilize the calix[4]arenes in the four conformations (cone, partial cone, 1,2-alternate, and 1,3-alternate), substituents bulkier than the ethyl group must be introduced into the four phenolic groups.[65] The conformation in which the calix[4]arene is fixed upon derivatization depends on the reaction temperature, the solvent, the base, the *para*-substituents of the calixarene, and the reactivity of the electrophile.[66] A general method has been developed for the preparation of tetra-*O*-alkylated calix[4]arenes in the *1,3-alternate* conformation.[67] *1,3-alternate* calix[4]arenes can be obtained selectively either by alkylating the four phenolic groups of unsubstituted calix[4]arenes or by alkylating the two remaining phenolic groups of diametrically di-*O*-alkylated calix[4]arenes, using $CsCO_3$ as base. The Cs^+ has been viewed to act as template metal cation in this transformation because of the high affinity of *1,3-alternate* calix[4]arene derivatives with Cs^+ ion.[66]

Bis-calix[4]tube **15** was synthesized via coupling of diol **22**[68] with ditosylate **23**[69] according to Scheme 10. The first important procedure involved here is the reaction of **20**[70] with 2-(*tert*-butyldimethylsiloxy)ethanol-*p*-toluenesulfonate in the presence of $CsCO_3$ to yield 1,3-alternate-**21**. After desilylation, diol **22** was tosylated to form **23**. The second important procedure is the connection of 1,3-alternate-**22** and **23** in the presence of NaH to produce tube **15** in 55% yield.

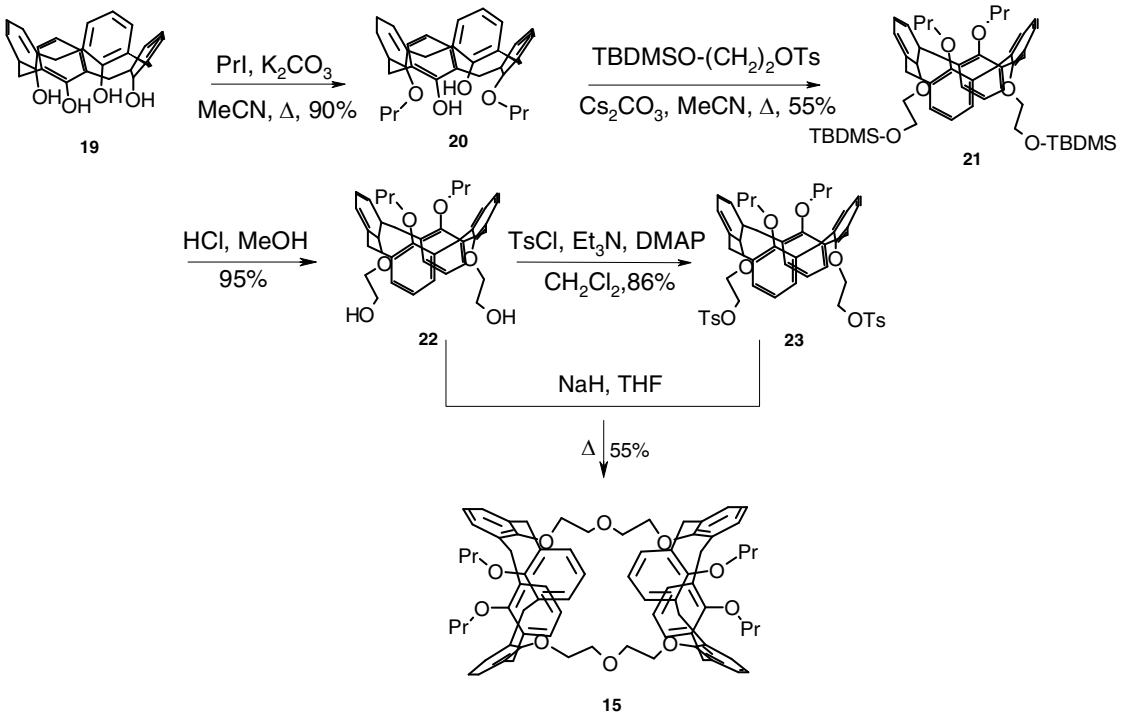

Scheme 10. Synthesis of bis-calix[4]tube **15**.

The trimeric tube **16** was synthesized according to Scheme 11. The key step in the synthesis is the formation of **26**[71] which serves as the central calixarene unit of the tube. Treatment of the parent calix[4]arene **19** with ethyl bromoacetate in the presence of Cs_2CO_3 afforded **24**[72] in one step. Reduction of **24**, followed by tosylation produced calix[4]arene **26**. Finally, **26** was reacted with 2 equivalents of diol **22** in the presence of NaH to form trimeric tube **16** in 70% yield.

Tube **17**, which contains four calixarenes, was prepared by reaction of biscalixarene diol **27** with derived from it ditosylate **28** in 64% yield (NaH, K_2CO_3, THF). Finally, reaction of two equivalents of diol **27** with tetratosylate **26** under the

same conditions afforded pentameric nanotube **18** in remarkable 82% yield (Scheme 12).

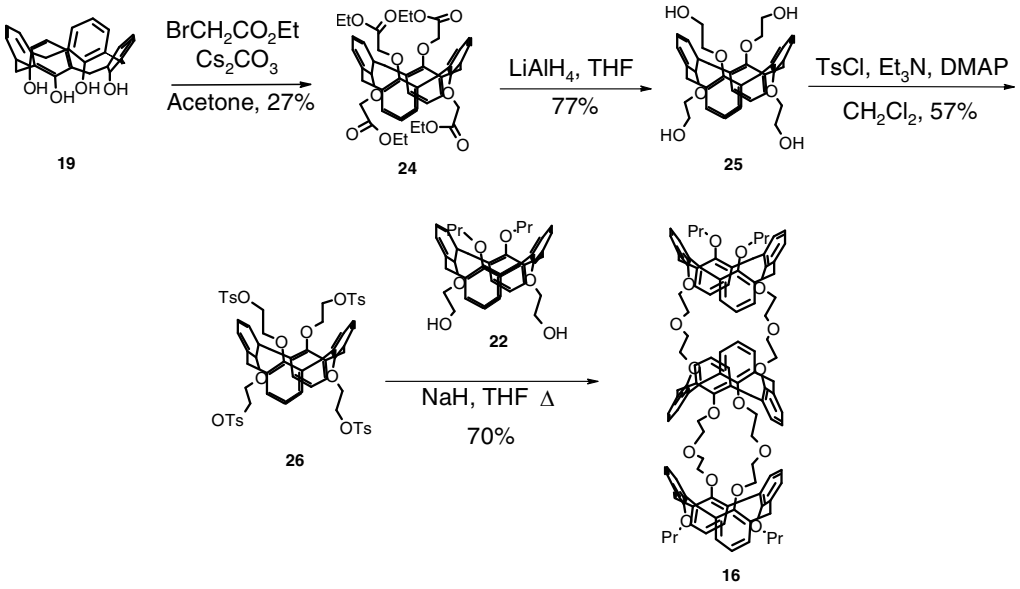

Scheme 11. Synthesis of tris-calix[4]tube **16**.

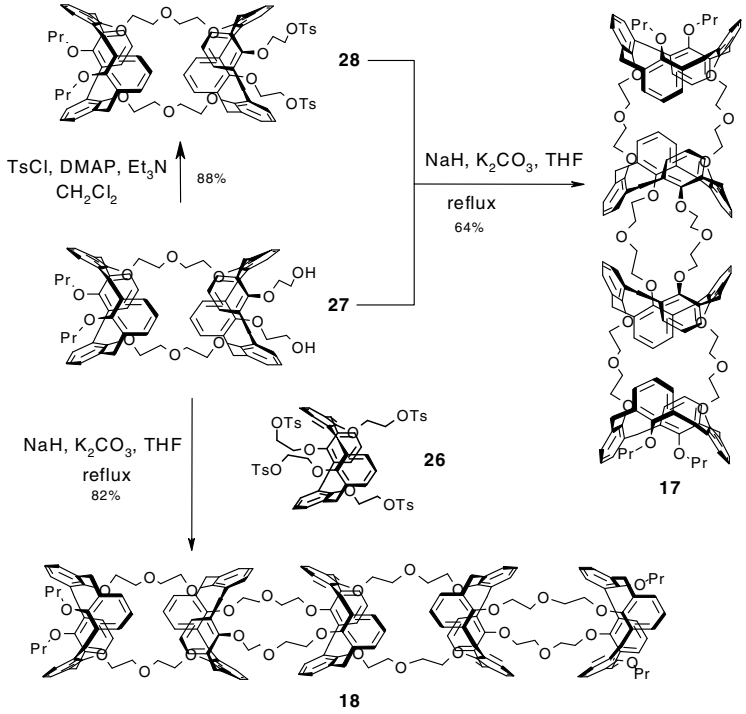

Scheme 12. Synthesis of calix[4]tubes **17** and **18** from precursors **27** and **28**.

Syntheses of precursors for tubes **17** and **18** were based on conventional calixarene transformations (Scheme 13). Calix[4]arene **29** was obtained by alkylation of the parent calix[4]arene **19**[73] with 2-(benzyloxy)ethanol *p*-toluene sulfonate and K_2CO_3 in hot MeCN in 62% yield. It was further alkylated with 2-(*tert*-butyldimethylsiloxy)ethanol-*p*-toluenesulfonate and Cs_2CO_3 in DMF with the formation of 1,3-alternate calix[4]arene **30**. Removal of the protecting group resulted in calixarene **31**. This was coupled to ditosylate **23** in THF in the presence of NaH as a base. This afforded a tubular biscalixarene **32** in 56%, which was subsequently debenzylated (H_2, Pd/C, AcOH, THF) to give derivative **27** in 82% yield. This was smoothly (86%) converted into ditosylate **28** by using *p*-toluenesulfonyl chloride, Et_3N and 4-(dimethylamino)-pyridine (DMAP) in CH_2Cl_2.

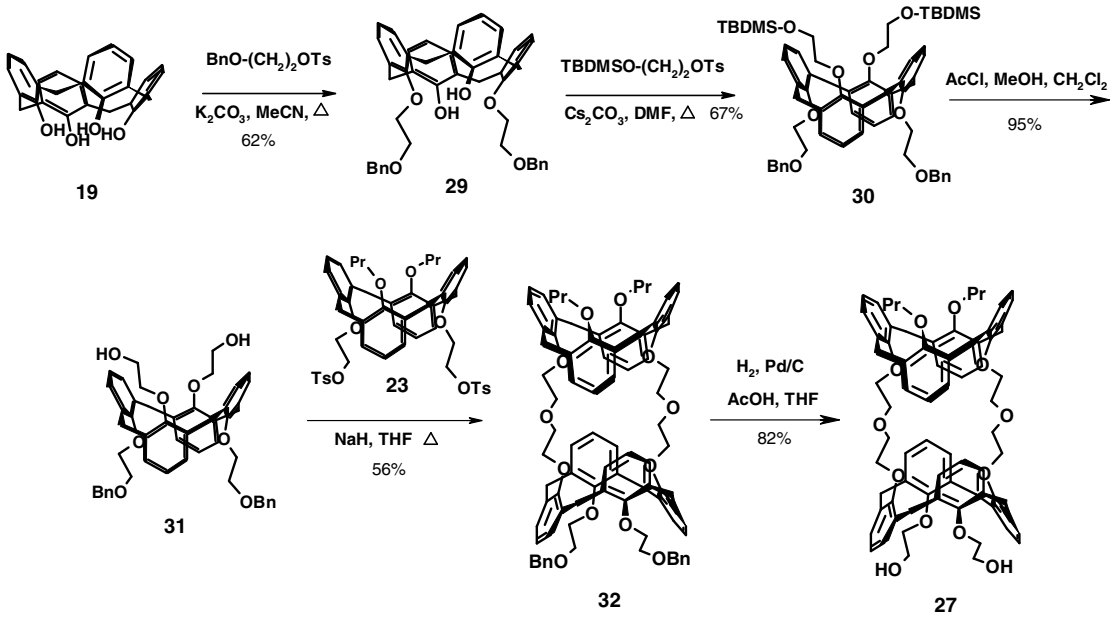

Scheme 13. Synthesis of calix[4]arene precursor **27**.

2.3.3 X-ray Analysis of Calix[4]tubes[74]

Single crystals of calix[4]arene **31** suitable for x-ray analysis were obtained by slow evaporation of CH_2Cl_2-CH_3OH (96:4) solution. The x-ray crystal structure of the compound revealed the calix[4]arene adopted the *1,3-alternate* conformation (Figure 17). The diameter of the calixarene cavity was measured to be 6 Å in diameter, which is typical for the *1,3-alternate* conformation.[52,53]

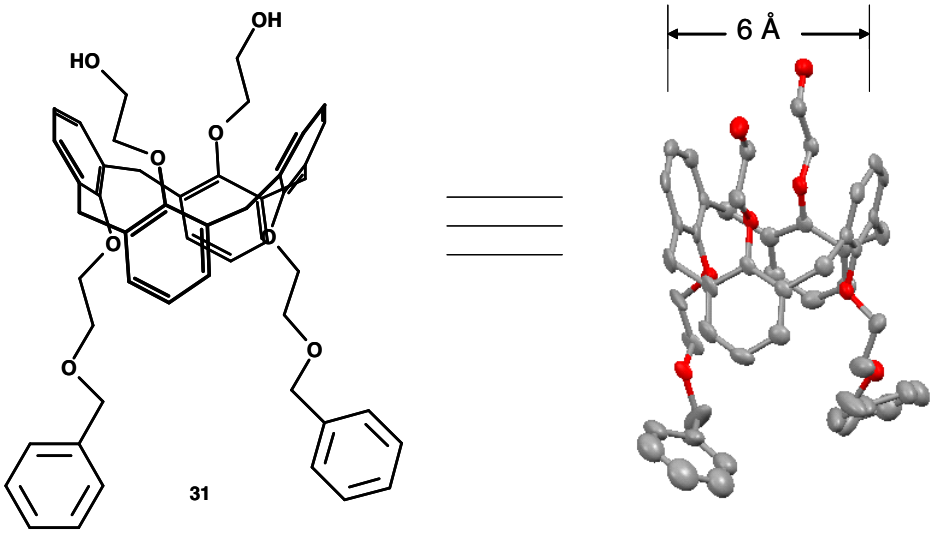

Figure 17. X-ray crystal structure of calix[4]arene **31**. Hydrogens are omitted for clarity.

Unequivocal evidence of multiply-connected *1,3-alternate* calix[4]arenes was provided by x-ray crystallographic structures of calix[4]tubes **15** and **16**. Single crystals of calix[4]tubes **15** and **16** were grown by slow diffusion of CH_3OH in $CHCl_3$ solution at room temperature. X-ray analysis of the crystals revealed *1,3-alternate* calix[4]arenes rigidly linked with diethylene glycol bridges to form hollow cylinders with diameters cavities of approximately 6 Å and lengths of 17 and 26 Å, respectively (Figure 18). The

inner tunnels are defined by two cofacial pairs of aromatic rings oriented orthogonally along the cavity axis.

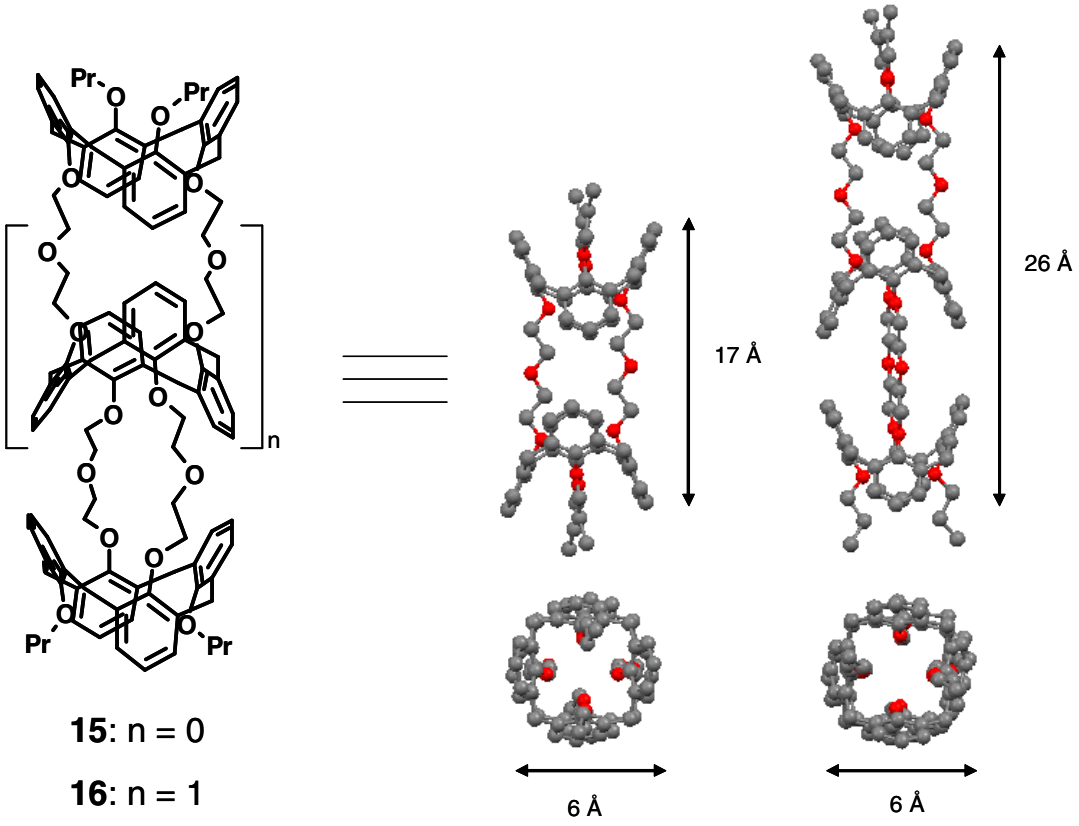

Figure 18. X-ray crystal structures of calix[4]tubes **15** and **16** (side and top views; O = red, C = gray). Hydrogen atoms are omitted for clarity.

Crystal packing of nanotube **15** shows alternating rows of molecules oriented diagonally in two directions (Figure 19). The nanotubes in a row are parallel to each other and are separated by about 4 Å. They also stack together, though slightly distorted, to form a long cylindrical tunnel. The intermolecular distance between stacked nanotubes is about 12 Å. The solvent molecules occupy the vacant spaces between the tubes.

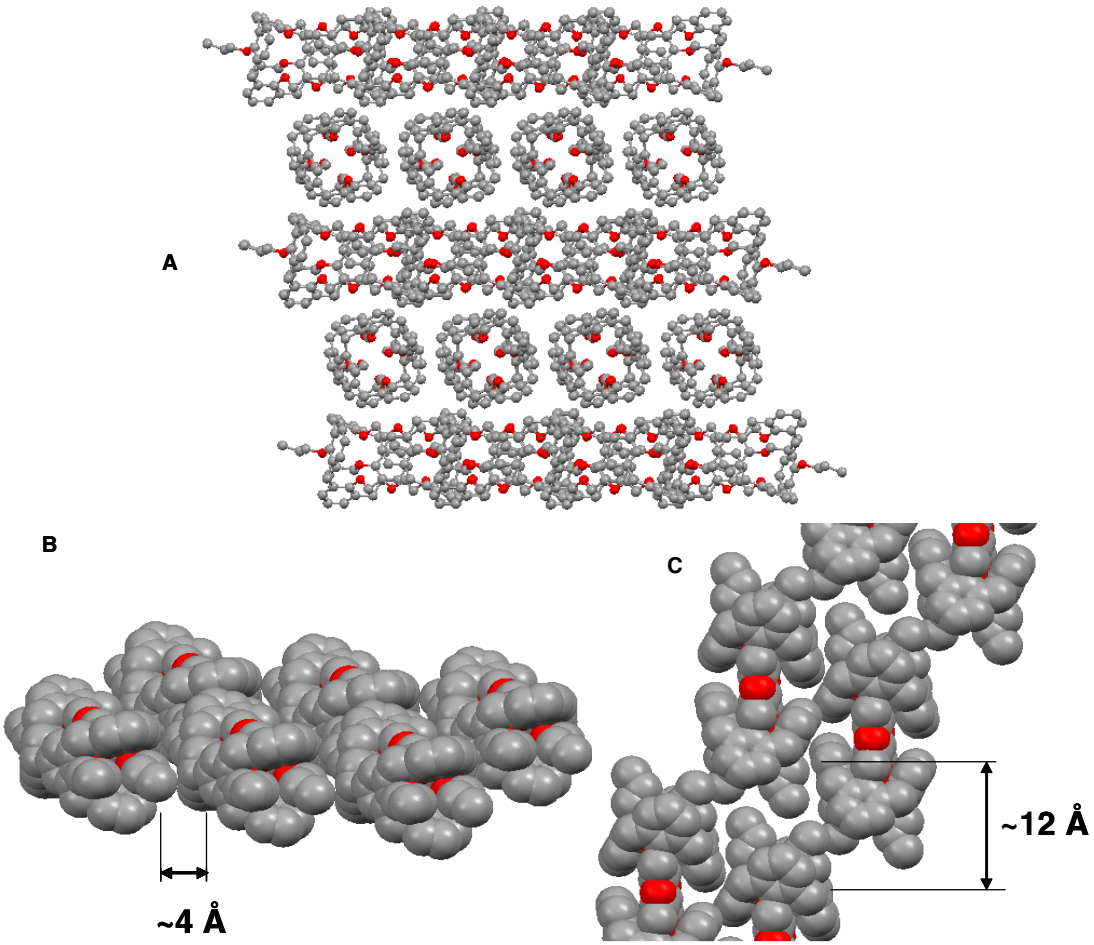

Figure 19. Crystal packing structure of nanotube **15**. (A) Two orientations of alternating rows of nanotubes. (B) Parallel nanotubes in a row. (C) Side view of stacked nanotubes. Solvent molecules and hydrogen atoms are omitted for clarity.

Surprisingly, a more organized packing is observed for nanotube **16**. The nanotubes are packed head-to-tail in straight rows with solvent molecules occupying the vacant spaces between the tubes. The crystal packing also shows a particularly appealing supramolecular structure with the neighboring nanocylinders aligned parallel to each other (Figure 20). In each nanocylinder, molecules are twisted by 90° relative to each other, and the Ar-O-Pr propyl groups effectively occupy the voids between the

adjacent molecules. The intermolecular distance between two neighboring tubes in the nanocylinder is around 10 Å, while the calixarene units within the tube are separated from each other by about 9 Å. With this arrangement, the nanotubes stack efficiently to form long, infinite cylinders. The unique linear nanostructures maximize the intermolecular van der Waals interactions in the crystal through the overall shape simplification. This supramolecular order is not observed in shorter nanotube **15**, and hence may have been influenced by the tube length.

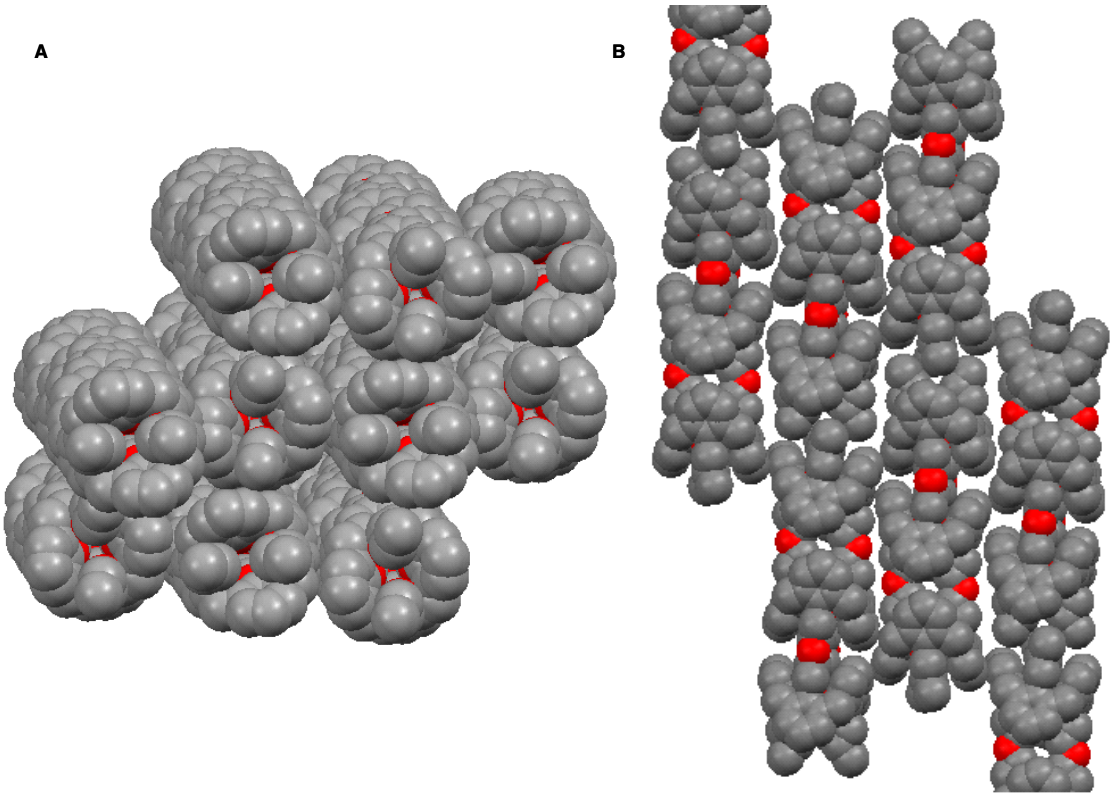

Figure 20. Nanotube bundles. (A) Angular and (B) side views of the crystal packing of nanotube **16** into infinite nanocylinders and the parallel stacking of neighboring nanotubes. Solvent molecules and hydrogen atoms are omitted for clarity.

2.4 Conclusions

Multiple calix[4]arenes in the 1,3-alternate conformation can be covalently connected to build robust synthetic nanotubes by conventional organic protocols. The length of the nanotubes can be controlled precisely and easily. Longer tubes can effectively pack into infinite tubular bundles in the solid state. Conceptually, these nanotubes can be filled with guests by applying the unique chemistry between calix[4]arenes and nitrosonium cations (NO^+).

CHAPTER 3

FILLING OF NANOTUBES

3.1 Encapsulation Studies

Monitoring entrapped guests inside SWNTs requires a combination of various spectroscopic and microscopic techniques. Especially important are high resolution TEM and FTIR spectroscopy as they allow the study of the location of trapped molecules and their molecular vibrations, respectively.[20] While solution studies with SWNTs are still a challenge because of their poor solubility, progress with synthetic nanotubes has been slow because of poor or unstable encapsulation complexes. For example, the first calixarene-derived nanotubes, designed as channels for small metal ions, showed only weak complexation abilities, as the calixarene tunnel did not bind metal cations.[57,59] However, the situation is different when calixarenes and NO^+ guests are employed. As mentioned in the previous chapter, simple calix[4]arenes reversibly interact with NO_2/N_2O_4 and entrap reactive NO^+ cation within their π-electron rich interiors. Stable nitrosonium complexes are formed upon addition of a Lewis acid ($SnCl_4$).[61]

We will show here how nanotubes **15**-**18** can be easily filled upon NO_2/N_2O_4 fixation, as each calixarene unit can accommodate one NO^+ guest.

3.1.1. Reactions with NO_2/N_2O_4

Addition of excess NO_2/N_2O_4 to nanotubes **15**-**18** in $(CHCl_2)_2$ in the presence of $SnCl_4$ or BF_3•Et_2O resulted in the formation of nitrosonium complexes **33**-**36** (Scheme 14). Complexes **33**-**36** were characterized by UV-vis, FTIR and ^{1}H NMR spectroscopy, which display typical features of simple calix[4]arene-NO^+ species.[60,61]

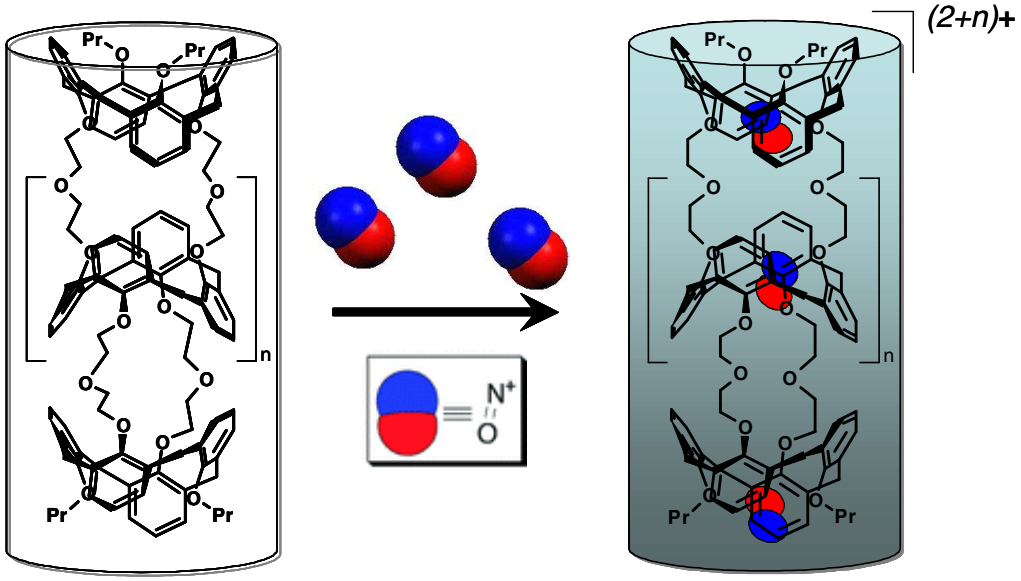

15: n = 0 **33**: n = 0

16: n = 1 **34**: n = 1

17: n = 2 **35**: n = 2

18: n = 3 **36**: n = 3

Scheme 14. Schematic diagram for filling calix[4]arene nanotubes.

The complexes exhibit a characteristic, deep purple color. Broad charge-transfer bands[62,63] are observed at λ_{max} ~520 nm in the absorption spectra of all these nanotubes (Figure 21). The charge-transfer only occurs when NO^+ guests are tightly entrapped

inside the calixarene cavities.[60] Similar experiments conducted with wider and more flexible calix[5]-, calix[6]-, and calix[8]arenes did not lead to NO^+ entrapment, and consequently, did not produce the characteristic color change.[74]

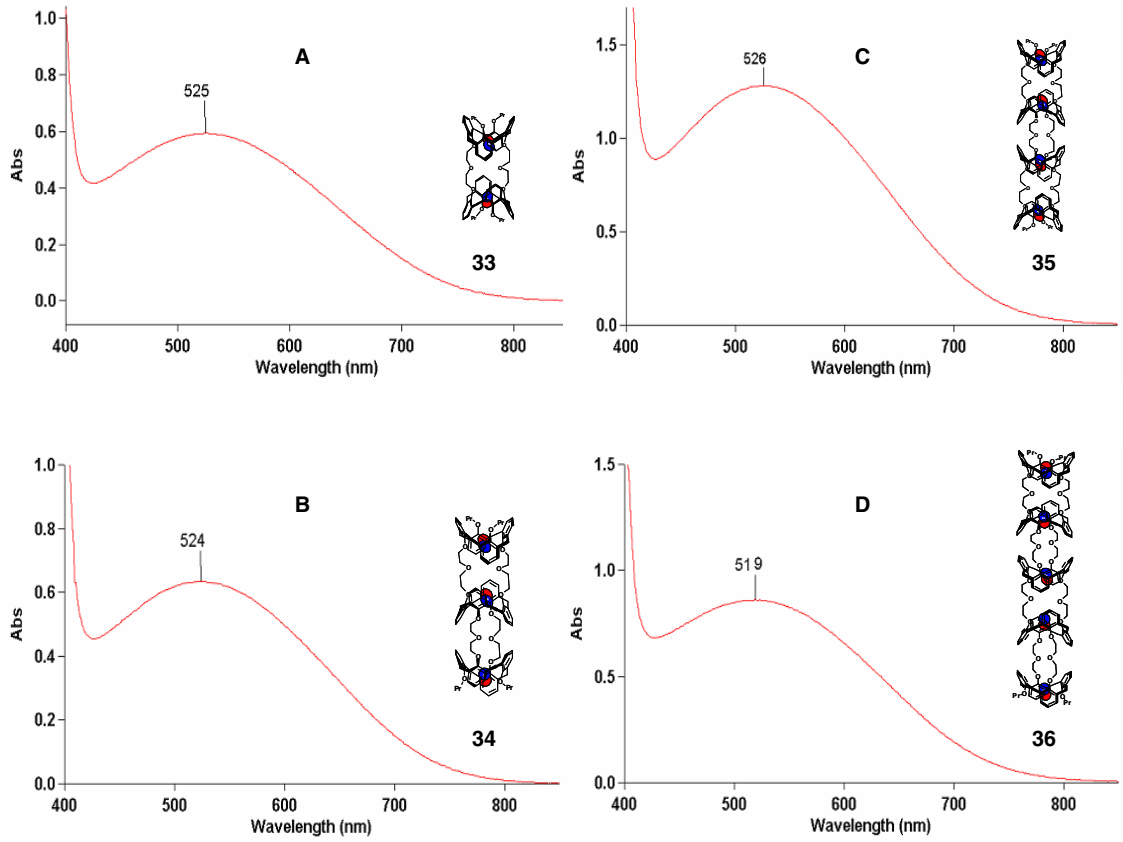

Figure 21. UV-vis absorption spectra ($(CHCl_2)_2$, 298 K) of nitrosonium complexes **33**-**36** (A to D).

Further evidence of the guests' presence and location inside nanotubes **15**-**18** can be deduced from ^{1}H NMR analysis (Figures 22 and 23).

All three groups of the propyl Ar-O-Pr protons in **33**-**36** were observed significantly downfield ($\Delta\delta$ ~ 1 ppm) compared to empty tubes **15**-**18**. For example, the

OCH_2 protons of empty tubes **15**-**18** appears as a triplet at 3.3 ppm shifted to 3.9 ppm in complexes **33**-**36**. This observation is similar to simple calixarenes where the OCH_2 protons of calixarene **13** shifted downfield from 3.54 ppm to 3.87 ppm in complex **14** (see Figure 15, page 31). This implies that there are NO^+ cations located at both ends of the nanotubes, occupying the terminal calixarene compartments.

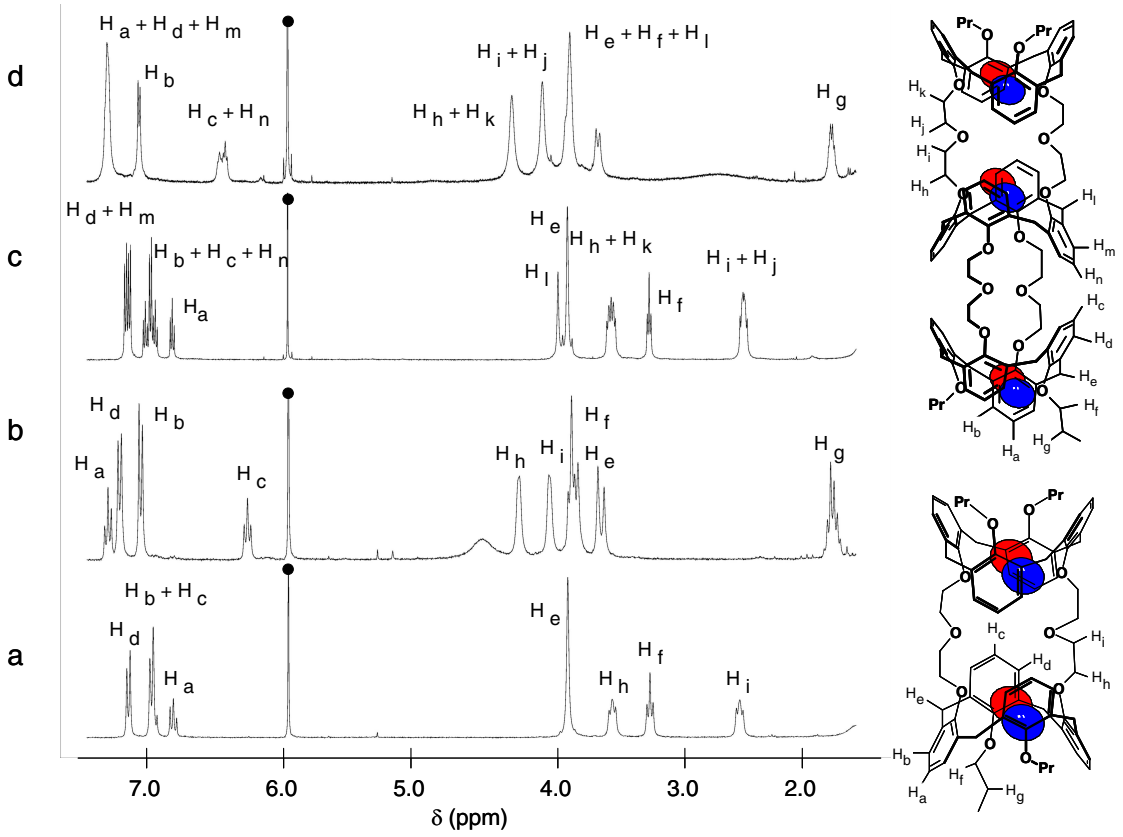

Figure 22. Partial ^{1}H NMR spectra (500 MHz, $(CDCl_2)_2$, 295 K) of nanotubes **15**-**16** and their complexes: (a) nanotube **15**, (b) filled nanotube **33**, (c) nanotube **16**, (d) filled nanotube **34**. The residual solvent signals are marked with (•).

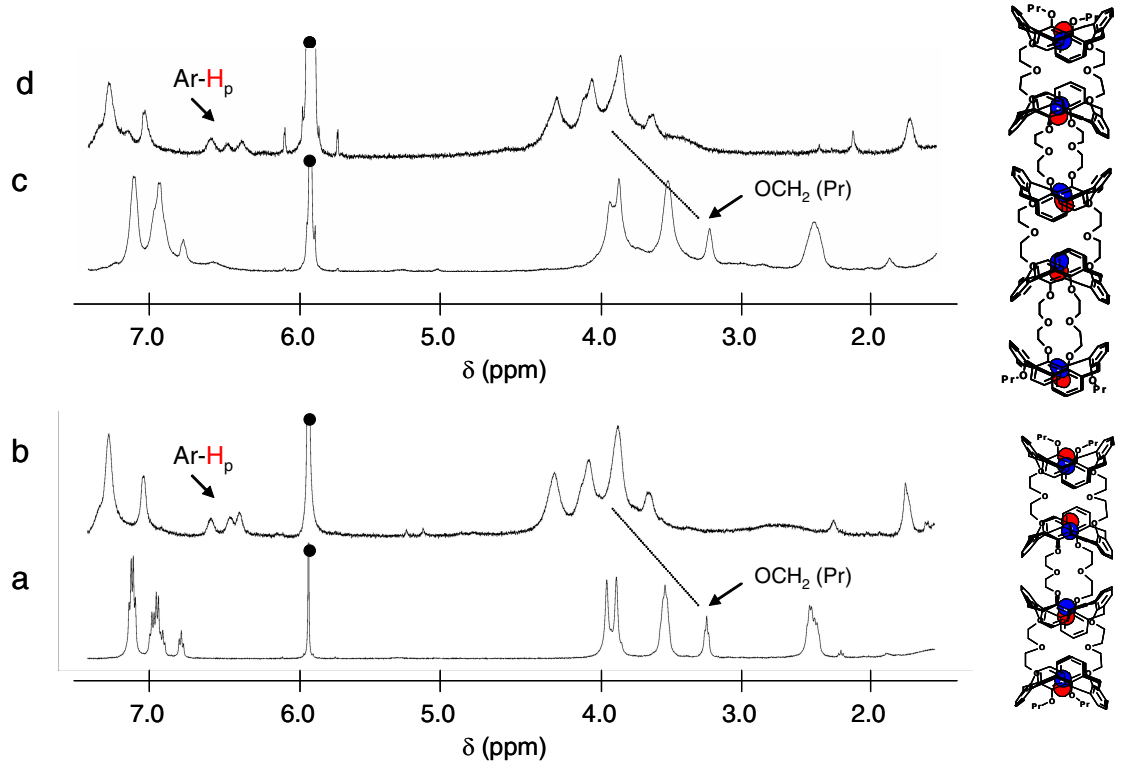

Figure 23. Partial ^{1}H NMR spectra (500 MHz, $(CDCl_2)_2$, 295 K) of nanotubes **17**-**18** and their complexes: (a) nanotube **17**, (b) filled nanotube **35**, (c) nanotube **18**, (d) filled nanotube **36**. The residual solvent signals are marked with (•).

Downfield shifts ($\Delta\delta > 1$ ppm) of the glycol Ar-O-CH_2 and CH_2-O-CH_2 protons situated in the middle of the tubular structures, were also observed. In empty tubes **15**-**18**, the Ar-O-CH_2 protons situated at around 3.6 ppm shifted to 4.3 ppm upon complexation. For the CH_2-O-CH_2 protons, their signals at 2.6 ppm in tubes **15**-**18** were seen at around 4.1 ppm in complexes **33**-**36**. These observations indicated that the middle calixarene(s) in the tubes are filled with NO^+ as well. It also suggests that in addition to the charge-transfer, strong cation-dipole interactions between the calixarene oxygen atoms and the entrapped NO^+ take place.

A surprising behavior was observed for the aromatic protons. Upon complexation, all of the aromatic protons in empty tube **15** shifted downfield except for a triplet which shifted upfield at 6.3 ppm. This behavior was also observed for longer tubes **16**-**18**, but with increasing sets of triplets found at 6.4-6.7 ppm in complexes **34**-**36**. This signal was assigned to the *para*-aromatic CH protons positioned in the middle of the tube (highlighted in red in Figure 22, right), based on the COSY and NOESY spectrum of complex **33**. This assignment was confirmed by NOESY spectrum for the nitrosonium-filled nonsymmetrical *O*,*O'*-dimethylated derivative of **27** (designated as **27b**).[74] As expected for the nonsymmetrical dimeric tube **27b**, two sets of triplets (1:1) were observed at 6.3 and 6.2 ppm upon complexation of NO^+. The triplet at 6.3 ppm belongs to the set of proton signals similar to the dimeric tube-NO^+ complex **33**. A possible explanation for the upfield shift of the aromatic *para*-protons is presented in Section 3.1.3 (page 53).

3.1.2. Stoichiometry of Nitrosonium Complexes

Using NO_2/N_2O_4 gases, we have demonstrated the ability of nanotubes **15**-**18** to encapsulate multiple NO^+ guests. However, we encountered some difficulties in handling small and precise quantities of NO_2/N_2O_4. Moreover, NO_2/N_2O_4 is so aggressive that it reacts with nanotubes upon standing by nitrosating/nitrating the aromatic rings. This has also been observed with simple calixarenes.[61] These aspects complicate the determination of the stoichiometry.

Molecular modeling and analogies with simpler calixarene-NO^+ complexes suggest that one calixarene fragment in the nanotubes can accommodate only one NO^+

guest. Therefore, nanotubes **33**-**36** should have two, three, four and five NO^+ species, respectively. Higher stoichiometries of NO^+ were ruled out because there is simply no room to accept larger number of repulsive cations.

Recently, we found alkyl nitrites (AlkO-N=O) to be more reliable sources of NO^+ for determining stoichiometry of the complexes.[75] Alkyl nitrites are known to be effective NO donors in medicine, and act as nitrosating reagents.[76,77] Alkyl nitrites are much easier to handle than NO_2/N_2O_4 gases. They are stable, nonvolatile liquids. They are easy to transfer by conventional laboratory pipettes. Thus, we can precisely determine the concentration of NO^+ being reacted with the nanotubes, and the stoichiometry of the complexes by titration.

Addition of one equivalent *t*-butyl nitrite to the $CDCl_3$ solution of calix[4]arene **37** in the presence of 4 equivalents of $SnCl_4$ resulted in a rapid formation of a deep purple solution. The UV-vis spectrum showed a broad charge-transfer band at λ_{max} ~580 nm, which is characteristic for arene-NO^+ complexes.[61,78]

^{1}H NMR spectrum of the complex also revealed similar features with simple calix[4]arenes-NO^+ complexes.[60,61] The spectrum revealed new sets of calixarene signals which are clearly distinguished from free calixarene **37** (Figure 24). The aromatic protons of free **37** were recorded as a singlet at 7.00 ppm. In the nitrosonium complex **38**, it was transformed into a singlet at 7.02 ppm. The methylene bridge CH_2 protons of **37** were seen as a singlet at 3.74 ppm, while in complex **38**, this was observed at 3.61 ppm. The OCH_2 protons in **37** were recorded at 3.39 ppm, and they shifted to 3.77 ppm in complex **38**.

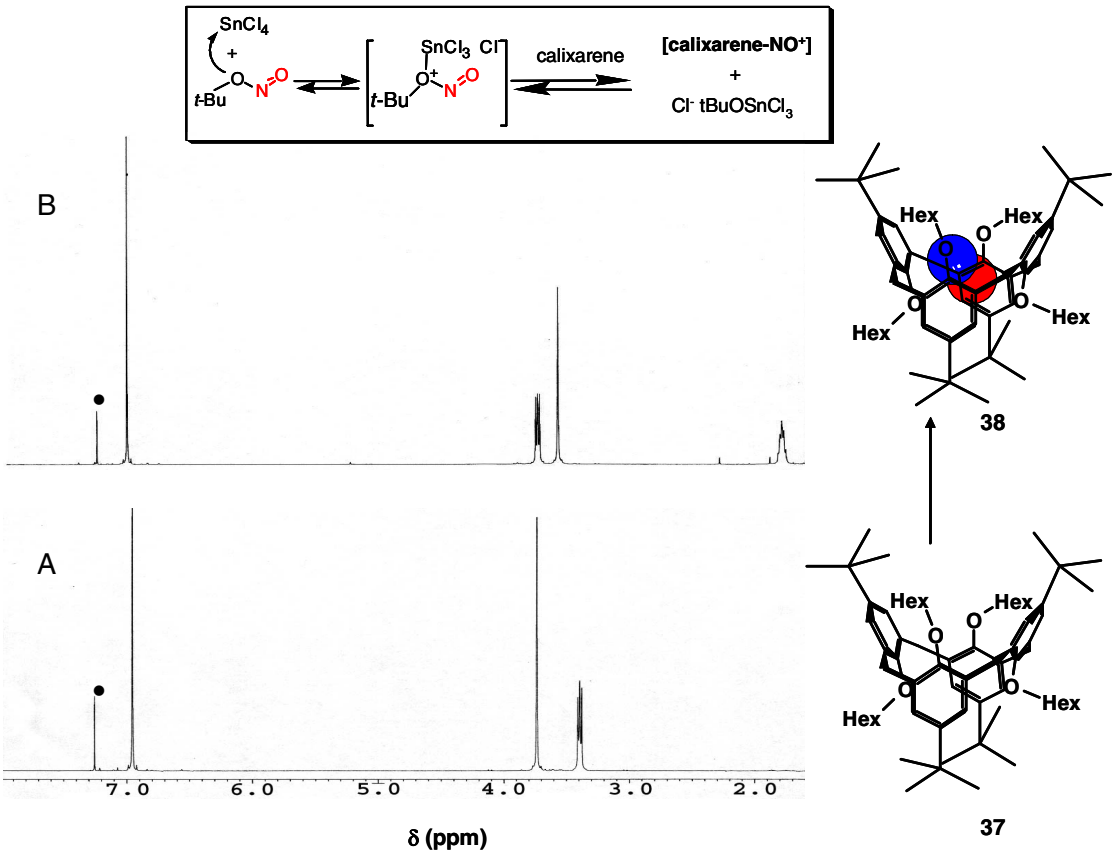

Figure 24. Portions of the ^{1}H NMR spectra (500 MHz, $CDCl_3$, 295 K) of (A) calixarene **37** and 4 equiv of $SnCl_4$, (B) calix[4]arene-NO^+ complex **38**. Residual $CDCl_3$ signals are marked with "•".[75]

We observed that the NO^+ transfer only occurs in the presence of $SnCl_4$. The Lewis acid most probably interacts with the nitrite C-O-N oxygen atom and facilitates the cleavage of the O-N bond (Figure 24, top).[79] It may also stabilize the complexes by coordinating to the counter ion, similar to known arene-nitrosonium nitrate complexes.[80]

Addition of *t*-butyl nitrite to nanotubes **15-18** in $(CDCl_2)_2$ in the presence of excess $SnCl_4$ or tetrafluoroacetic acid (TFA) also led to the rapid formation of the corresponding calixarene-NO^+ complexes. These were identified by NMR, FTIR and

UV-vis spectroscopy, and show similar features with the previously described complexes formed using NO_2/N_2O_4 (See Section 3.1.1, pages 43-47).

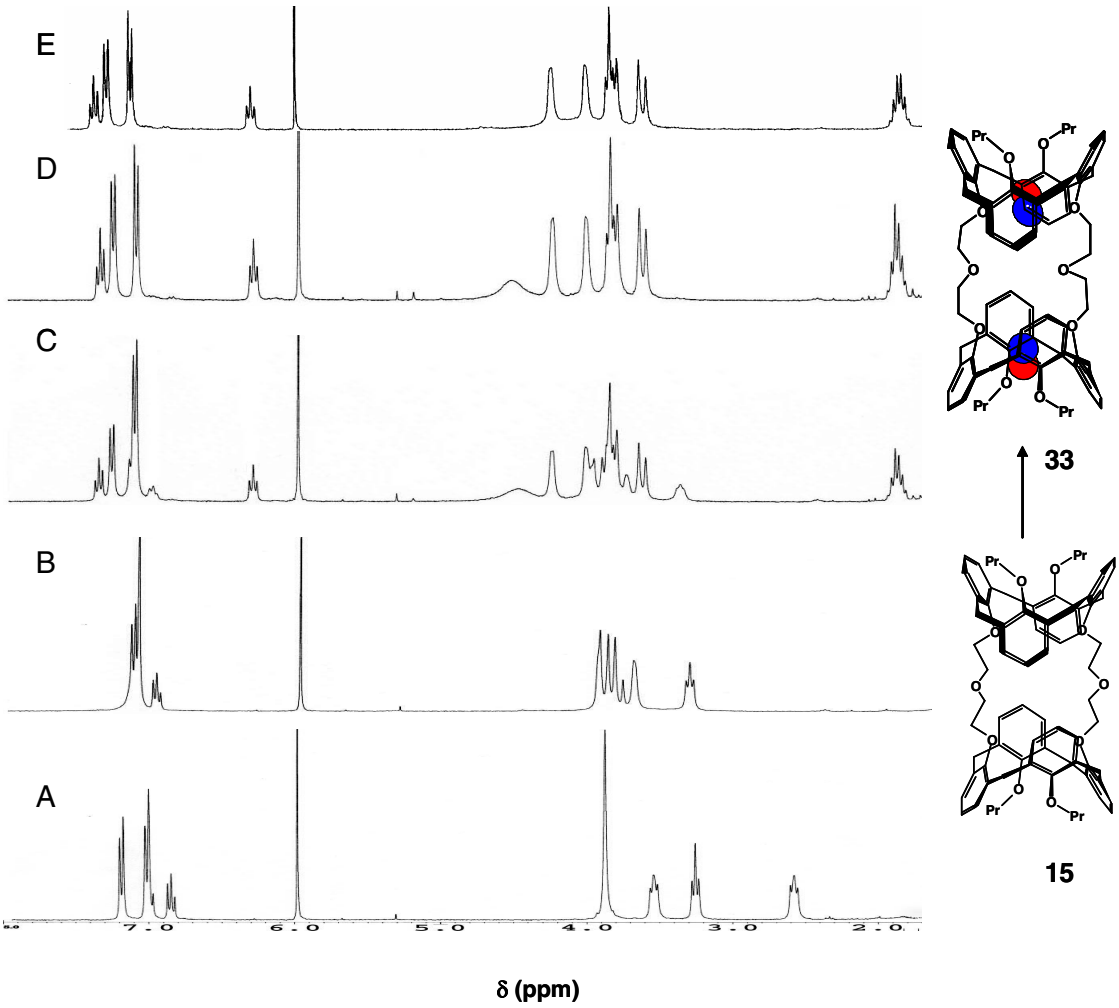

Figure 25. Titration of nanotube **15** with *t*-butyl nitrite. Portions of the ^{1}H NMR (500 MHz, $(CDCl_2)_2$, 295 K) of (A) empty tube **15**, (B) **15** + 4 equiv $SnCl_4$, (C) addition of 1 equiv tBuONO, (D) addition of 2 equiv tBuONO, (E) **33** prepared from NO_2/N_2O_4.

Upon stepwise addition of t-butyl nitrite, the ^{1}H NMR signals of empty tubes **15**-**18** and complexes **33**-**36** can be seen separately and in slow exchange. This is typical for host-guest complexes with high exchange $\Delta G^{\ddagger}$ barriers (>15 kcal/mol) and/or high

association constants ($K_{assoc} > 10^6$ M^{-1}).[63,81] Titration experiments also show that two equivalents of t-butyl nitrite were needed to fill dimeric tube **15** (Figure 25), and adding three equivalents of the nitrite completely filled trimeric nanotube **16** (Figure 26).

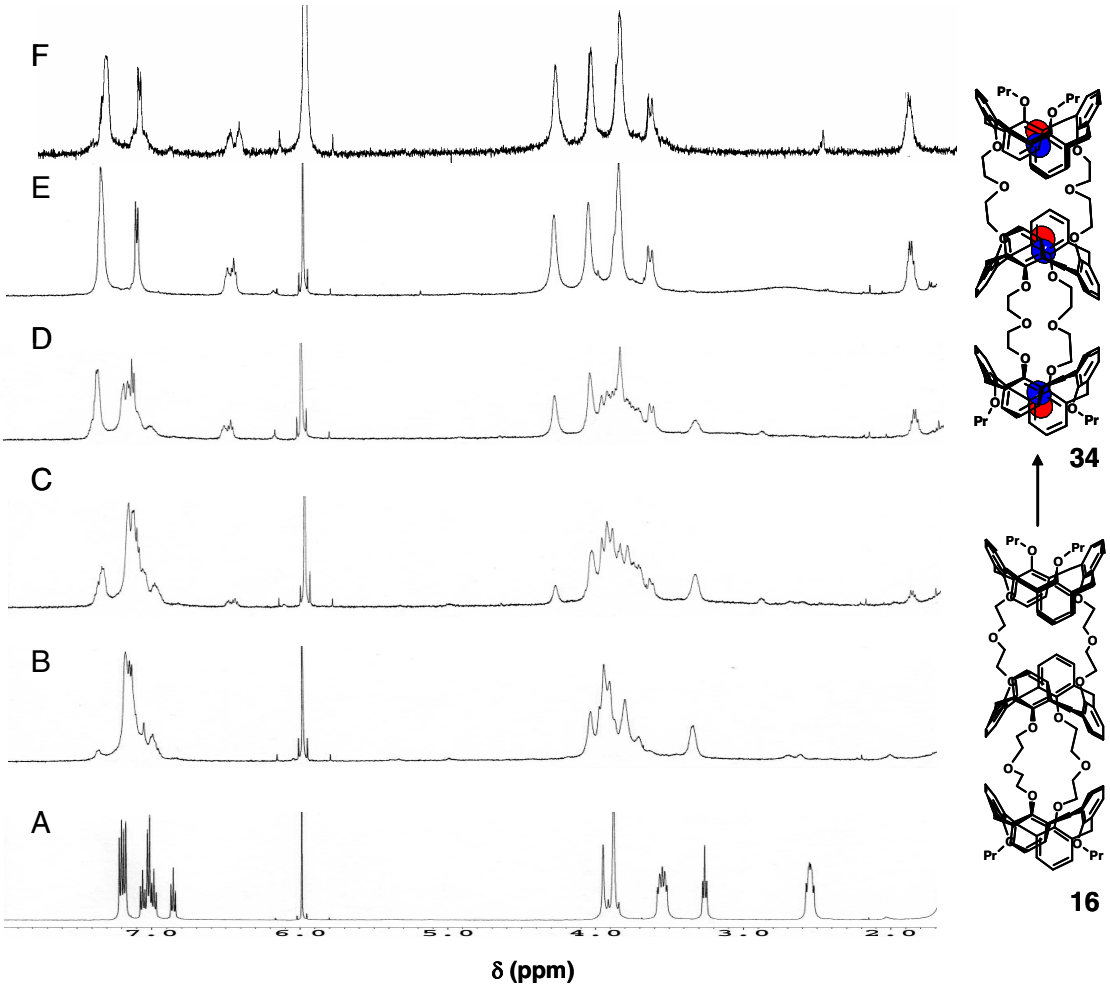

Figure 26. Titration of nanotube **16** with *t*-butyl nitrite. Portions of the ^{1}H NMR (500 MHz, $(CDCl_2)_2$, 295 K) of (A) empty tube **16**, (B) **16** + 6 equiv $SnCl_4$, (C) addition of 1 equiv tBuONO, (D) addition of 2 equiv tBuONO, (E) addition of 3 equiv tBuONO, (F) **34** prepared from NO_2/N_2O_4.

Analogously, a 1:4 tube-NO^+ ratio was established for longer tube **17**, possessing four calixarene units (Figure 27). Further addition of the nitrite did not

change the NMR spectra. This confirms the stoichiometry of the nanotube complexes, which possess one NO^+ per calixarene unit. A similar trend is expected for tube **18**, although the titrations in this case are less accurate due to the broadening of signals and low solubility of the complex.

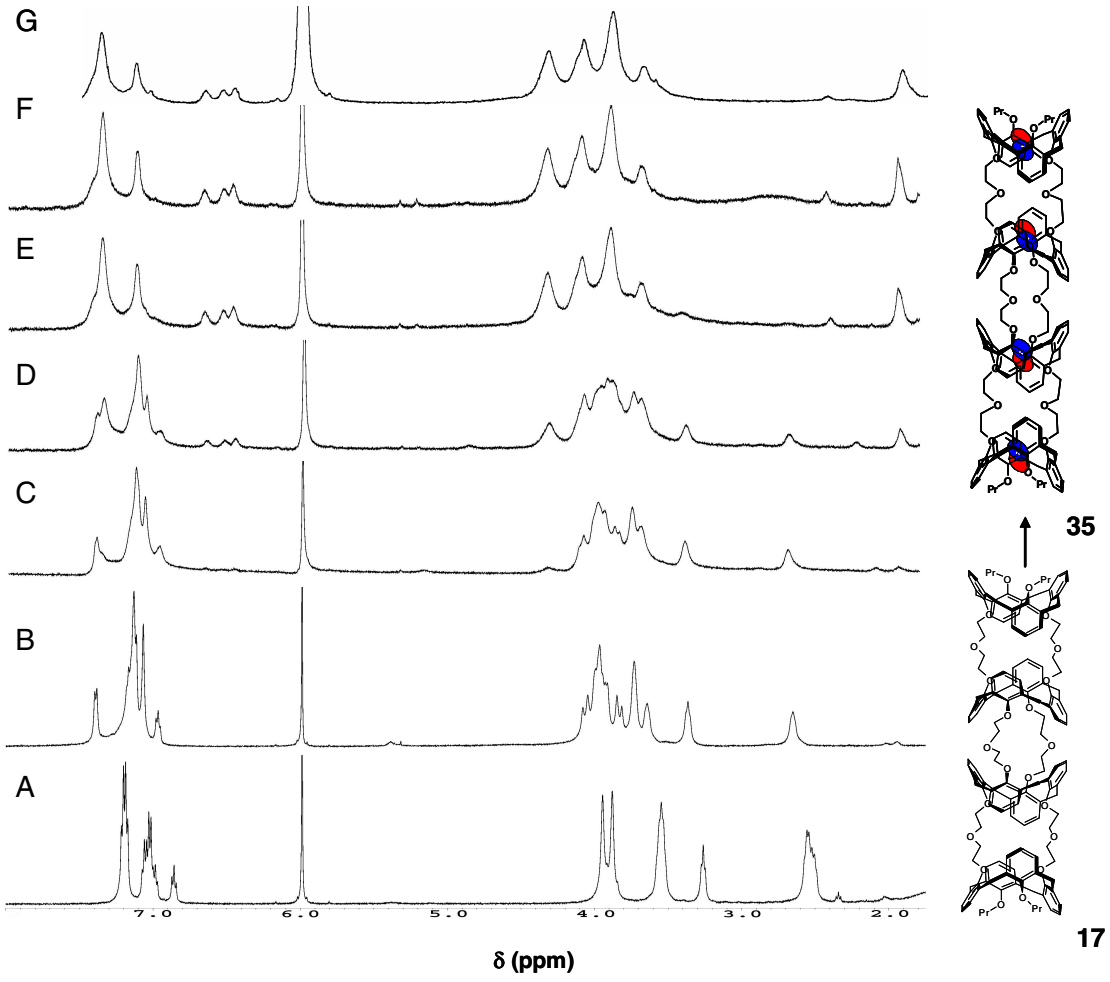

Figure 27. Titration of nanotube **17** with *t*-butyl nitrite. Portions of the ^{1}H NMR (500 MHz, $(CDCl_2)_2$, 295 K) of (A) empty tube **17**, (B) **17** + 8 equiv $SnCl_4$, (C) addition of 1 equiv tBuONO, (D) addition of 2 equiv tBuONO, (E) addition of 3 equiv tBuONO (F) addition of 4 equiv tBuONO, (G) **35** prepared from NO_2/N_2O_4.

3.1.3. FTIR Analysis

Based on molecular modeling, the NO^+ filled nanotubes **33**-**36** adopt a somewhat shrunken structure, with all *gauche* conformations about the glycol C-C bonds. On the other hand, empty tubes **15**-**18** possess all *anti* C-C conformation, which was also evident from the X-ray structures of tubes **15** and **16** (see Fig.18, p. 38). The experimental proof came from FTIR studies in $(CHCl_2)_2$. In empty tubes **15**-**18** the band corresponding to the *anti* C-C conformation at ν = 1340 cm^{-1} was observed. In complexes **33**-**36** this band disappeared and a new band at ν = 1355 cm^{-1} appeared, which is characteristic for the gauche C-C conformer (Figure 28). In the literature, these absorptions are attributed to the CH_2 wagging.[82,83]

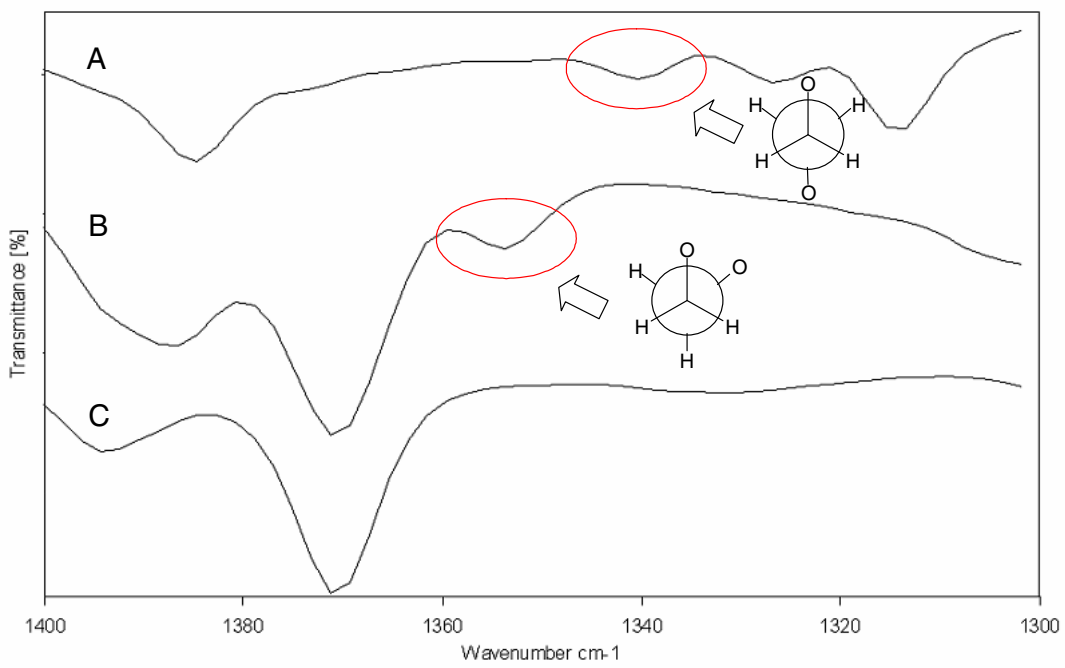

Figure 28. Portions of the IR spectra ($(CDCl_2)_2$, 295 K) of (A) nanotube **15**, (B) filled tube **33**, and (C) *t*-butyl nitrite. The band corresponding to the *anti* and *gauche* C-C conformations are marked. The band at ν = 1370 cm^{-1} belongs to *t*-butyl nitrite.

One reasonable explanation for such conformational change might be a participation of the basic glycol CH_2OCH_2 oxygens in NO^+ complexation. To bring in close proximity and thus contribute to dipole-cation interactions with the entrapped NO^+, the glycol chains should adopt the more compact *gauche* C-C conformation (Figure 29). As a result, the filled nanotubes are shorter. The shrinking also brings the aromatic rings from the neighboring calixarene units closer to each other. Thus, the para-aromatic CH protons of tubes **33**-**36** that face each other appear shielded and are seen upfield at 6.2 – 6.4 ppm in the ^{1}H NMR spectra. These signals can be used as a characteristic signature for the complex formation.

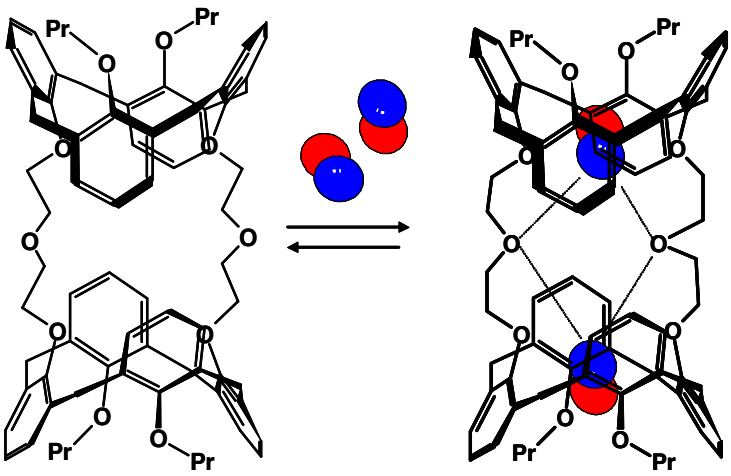

15 **33**

Figure 29. Conformational transition about the glycol C-C bonds.

Vibrational spectra also allowed us to obtain unique information on the bonding of multiple NO^+ species inside tubes **15**-**18** in solution. From the literature, the nitrosonium salts NO^+Y^- (Y^- = BF_4^-, PF_6^-, AsF_6^-) exhibit a single stretching band at

$\nu(NO^+)$ = 2270 cm^{-1} in CH_3NO_2 solutions,[84] and the stretching frequency of the neutral diatomic NO gas is $\nu(NO)$ = 1876 cm^{-1}.[84,85]

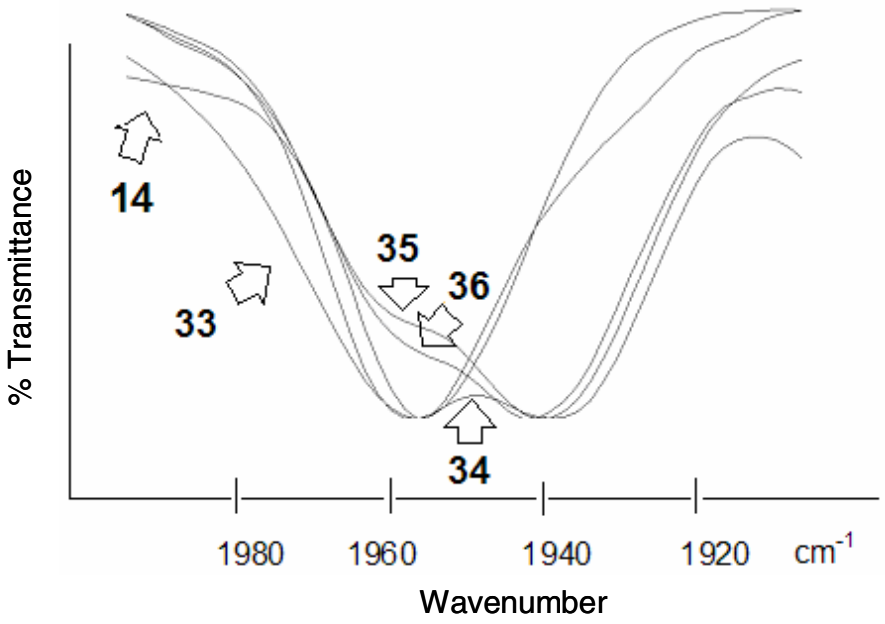

Figure 30. Portions of the IR spectra ($(CDCl_2)_2$, 295 K) of calix[4]arene-NO^+ complex **14** and completely filled nanotubes **33**-**36**.

In calixarene-NO^+ complex **14**, the NO^+ band significantly shifted ($\Delta\nu$ = 312 cm^{-1}) to lower energies compared to free NO^+ cation, and appeared at $\nu(NO^+)$ = 1958 cm^{-1} in $(CHCl_2)_2$ (Figure 30). This is due to strong electron donor-acceptor interactions between the encapsulated NO^+ and π-electron rich aromatic walls of the calixarene.[64,78] Dimeric complex **33** also exhibited similar shifts for the NO^+ guests at $\nu(NO^+)$ = 1958 cm^{-1}. Interestingly, for longer tubes **34**-**36** two absorption bands at $\nu(NO^+)$ = 1958 cm^{-1} and 1940 cm^{-1} were observed in $(CHCl_2)_2$. For trimeric tube **34**, these two bands have comparable intensities, while in longer tubes **35** and **36** the band at $\nu(NO^+)$ = 1940 cm^{-1}

dominates. This band was assigned to the NO^+ guest(s) which are situated in the middle of the tubes. Apparently, they are somewhat more strongly bound to the nanotubes walls. One possible explanation might be the participation of the glycol CH_2OCH_2 oxygens (Figure 29). As discussed earlier for the *anti-gauche* conformational transition upon complexation, these oxygens appear in close proximity and thus contribute to dipole-cation interactions with the entrapped NO^+. Accordingly, FTIR spectroscopy can be used to monitor multiple entrapped NO^+ guests inside nanotubes tubes **33**-**36** and even distinguish among them.

3.2 Conclusions

Nanotubes **15**-**18** can be filled with multiple NO^+ guests, producing deep colored solutions. They exhibit typical calix[4]arene-NO^+ complexes as evidenced by UV-vis, ^1H NMR and FTIR spectroscopy. The stoichiometry of the complexes reveals the encapsulation of one NO^+ guest per calixarene cavity. The filling process is cooperative and causes conformational changes within the nanotubes. NO^+ guests entrapped deep inside the nanotube experience stronger electron donor-acceptor interactions compared to guests near the ends of the nanotube.

CHAPTER 4

HOST-GUEST DYNAMICS OF FILLED NANOTUBES

4.1 Introduction

Aside from synthetic nanotubes, there are a number of designs and syntheses of nanoscale molecular containers that has emerged over the last decade. These include cavitands, carcerands, hemicarcerands, and capsules (Figure 31).[86] Cavitands are synthetic host molecules with open-ended cavities large enough to bind complementary organic molecules and ions. The concave inner surfaces of cavitands can be modified to have various shapes, with either integrated or appended binding sites. Carcerands are closed-surface structures but with enforced inner cavities large enough to incarcerate smaller organic molecules. The portals of carcerands are too narrow to allow the guest to escape without breaking covalent bonds. Thus, carcerands hold guests permanently. Hemicarcerands, on the other hand, have larger portals which allow the entrapped guest to escape at high temperature. Self-assembling capsules are receptors with enclosed cavities formed through reversible noncovalent interactions between two or more subunits. They can trap guests but may release them without breaking covalent bonds and under milder conditions.

Synthetic nanotubes, on the hand, possess a different topology, are open from both ends, and therefore, may feature different guest dynamics upon encapsulation.

Synthetic nanotubes can also be filled with multiple guests in a one-dimensional morphology inside its hollow structure, unlike cavitands, carcerands, hemicarcerands and capsules.

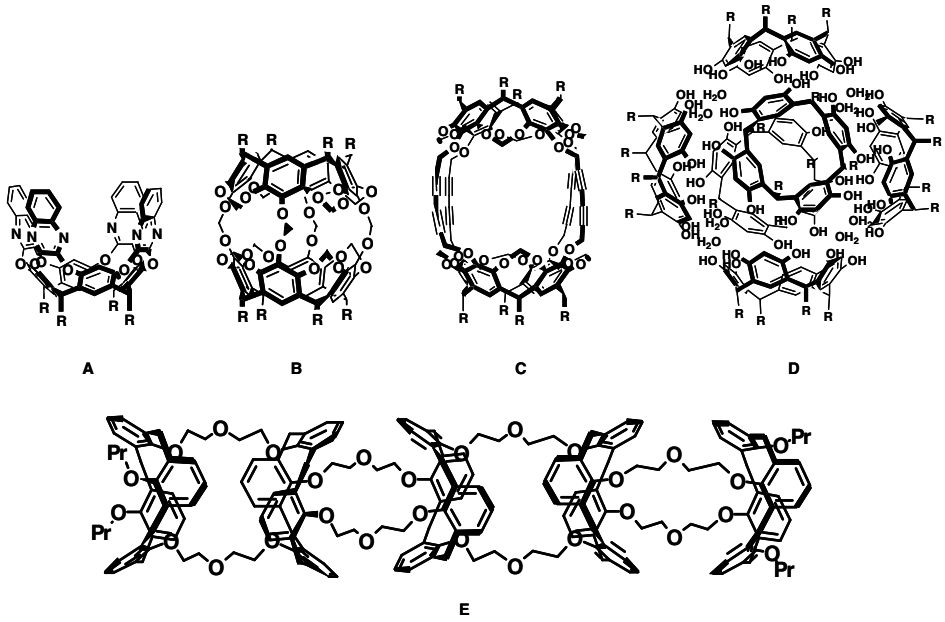

Figure 31. Nanoscale molecular containers: (A) cavitand, (B) carcerand, (C) hemicarcerand, (D) capsule, (E) nanotube.[86]

4.2 Guest Exchange and Dynamics

It is evident from ^{1}H NMR studies that the NO^+ exchange in and out of the nanotubes **15**-**18** is slow on the NMR time scale. Upon stepwise addition of *t*-butyl nitrite, the ^{1}H NMR signals of empty tubes **15**-**18** and complexes **33**-**36** can be seen separately. Moreover, the NO^+ complexation does not influence the symmetry of nanotubes **15**-**18** at 295 K. The number of the propyl OCH_2, the glycol CH_2OCH_2 and $ArOCH_2$, and the aromatic proton signals for **33**-**36** does not change. This implies that the NO^+ guests, with the van der Waals dimensions of ~2 Å, freely rotate along the N-O

axis and also tumble within the cavity at room temperature. Similar dynamics were also noticed for simple calixarene-NO^+ complexes.[61]

We also found that complexes **33**-**36** form even when less than stoichiometric amounts of *t*-butyl nitrite are added. From the integration, it was possible to quantitatively estimate the concentration of complexes **33** and **34**. For example, addition of 1 equivalent of *t*-butyl nitrite to dimeric tube **15** produces 50±5% of fully occupied complex **33**, and addition of 2 equivalents of *t*-butyl nitrite to trimeric tube **16** produces 55±5% of fully occupied complex **34**, which is much higher than simple statistical distribution, when partially filled tubes are considered. This may suggest that the strong binding allowed each calixarene unit in the tube to complex NO^+ independently from the others. This behavior may also reflect a cooperative effect[87] on nitrosonium binding with the tube, in which the binding of one NO^+ enhances the affinity of the tube towards another NO^+ guest. As discussed in the previous chapter, the encapsulation of NO^+ guests leads to conformational changes about the glycol bridges (see Fig. 29, p. 54). This conformational change may bring the glycol oxygen lone pairs in close proximity with adjacent oxygen lone pairs. The lone pair-lone pair repulsion can contribute to the thermodynamic instability[88] of the incompletely filled nanotube. This enthalpic gain, however, is compensated by further binding of NO^+ guests, resulting in positive cooperativity. This may be the reason behind the observed high formation of fully occupied complexes in the titration experiments.

Cooperativity is well known to take place in biological systems, for example in the oxygenation of hemoglobin.[89] This tetrameric protein binds four individual oxygen

molecules with increasing affinity until all four binding sites are occupied in a positive cooperative manner. The observed cooperativity is attributed to conformational changes in the quaternary structure of the protein, although a structural explanation for the low affinity quaternary state (unbounded protein) remains debatable.

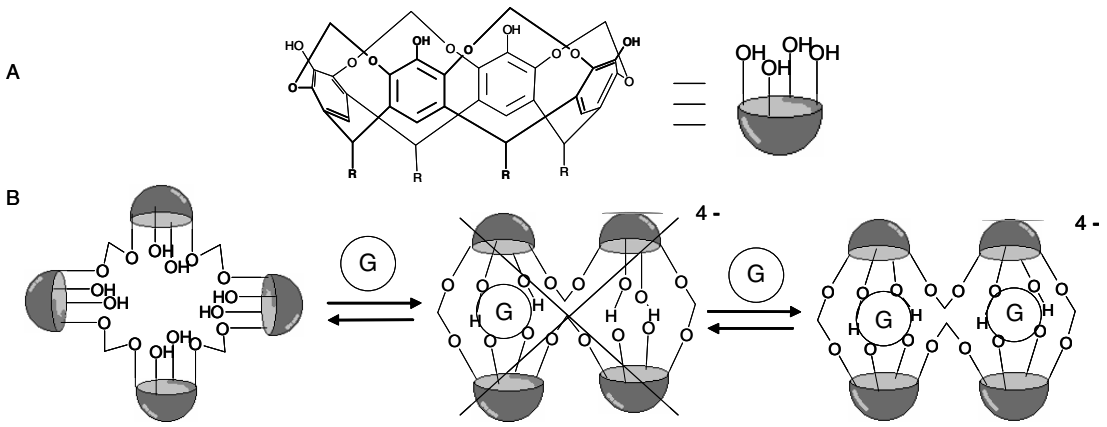

Figure 32. Cooperative reversible encapsulation of two pyrazine guests (G) in bis-capsules. (A) Schematic representation of a carceplex. (B) Formation of bis-capsules by encapsulation of guests.[90]

Cooperativity is also observed by Sherman in a biscarceplex, where two carceplexes are covalently linked such that one guest molecule is entrapped in each of the two adjacent but physically separate chambers.[90] The biscarceplex encapsulates one pyrazine molecule in each chamber. The binding of one guest causes two adjacent bowls to clamp down and form a filled capsule (Figure 32). This also forces the remaining two bowls to clamp down as well, forming an empty cavity which is thermodynamically unstable. Thus, a 1:1 ratio of host to guest is not formed in significant quantities at equilibrium.

The filled nanotubes **33**-**36** are stable in dry solution at room temperature within 24 hours, but can readily dissociate upon addition of H_2O, producing empty nanotubes **15**-**18**. The process however is not reversible. The released NO^+ species are converted to nitrous acid and complexes **33**-**36** cannot be regenerated.

We found that 18-crown-6 can reversibly remove the encapsulated NO^+ species. It is known that crown ethers form stable complexes with NO^+.[91-93] For example, the reaction of 18-crown-6 with $NOBF_4$ afforded a 1:1 complex. In the ^1H NMR spectrum, the OCH_2CH_2O protons, seen as a singlet at 3.67 ppm for 18-crown-6 is shifted downfield to 3.7 ppm for the complex. It also indicates a rapid exchange in the NMR time scale between the free crown molecule and the complex. From the IR spectrum, new absorption bands for the N-O stretching frequency at ν = 2250 cm^{-1} appeared in CH_2Cl_2.[94] The complexation constant was estimated at $K > 10^4$ M^{-1} based on the oxidation and reduction potentials of the complex in MeCN.[93]

When 4 equiv of 18-crown-6 was added to the $CDCl_3$ solution of complex **14**, free calixarene **13** was obtained. The deep purple colored solution disappeared, and the ^1H NMR spectrum changed (Figure 33). The aromatic proton signals for the nitrosonium complex **14** seen as a triplet and a doublet at 7.2 and 7.1 ppm were transformed into a doublet and a triplet at 6.9 and 6.7 ppm, which corresponds to free calixarene **13**. Likewise, the methylene bridge CH_2 and OCH_2 protons of **14** seen as a triplet and a singlet at 3.9 and 3.6 ppm were transformed into a singlet and a triplet at 3.6 and 3.5 ppm. Addition of excess $SnCl_4$ regenerated the complex, forming the deep purple colored solution, and restored the ^1H NMR signals corresponding to complex **14**.

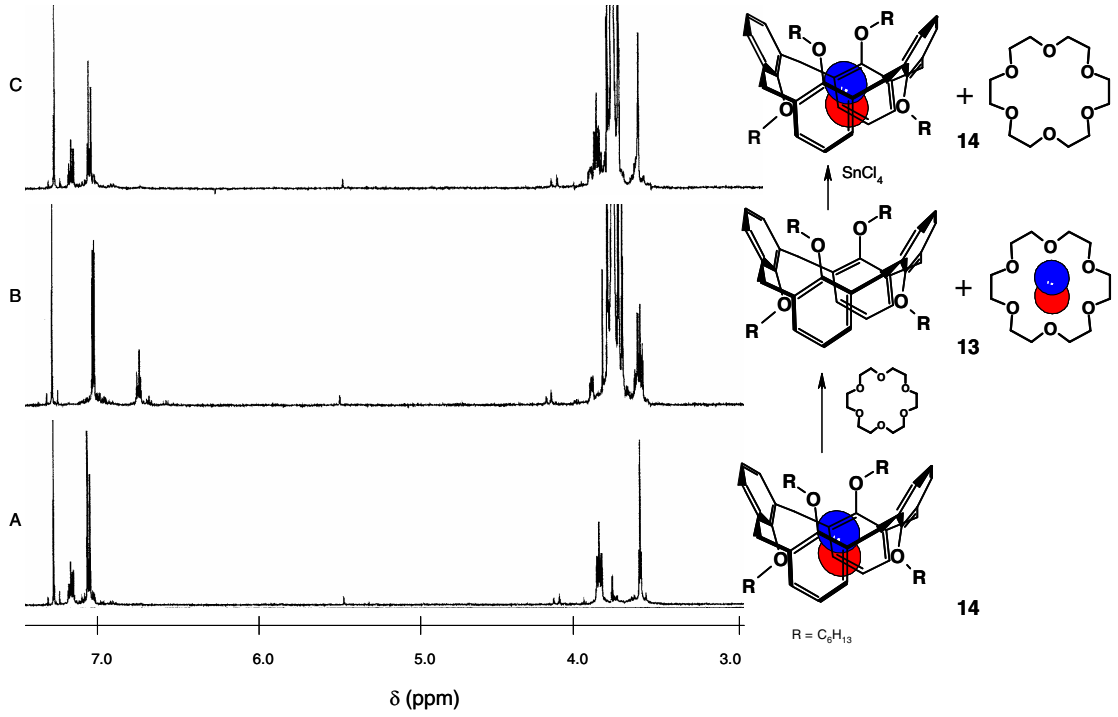

Figure 33. Nitrosonium exchange with simple calix[4]arene **13**. Selected portions of ^{1}H NMR (500 MHz, $CDCl_3$, 295 K) of: (A) nitrosonium complex **14**, (B) addition of 4 equiv 18-crown-6, (C) same as B with 4 equiv $SnCl_4$.

When 2 equiv of 18-crown-6 was added to $(CDCl_2)_2$ solutions of complex **33**, empty nanotube **15** was regenerated, and the deep purple color disappeared. The process can be followed by ^{1}H NMR spectroscopy (Figure 34). The NO^+ transfer process is slow in the NMR time scale as shown by the presence of both complex **33** and empty tube **15**.

Surprisingly, addition of 4 equiv of $SnCl_4$ to the same solution fully restores complex **33**. There have been reports in the literature showing that $SnCl_4$ form complexes with crown ethers.[95-97] X-ray analysis on a single crystal of $SnCl_4$ complexed to 18-crown-6 shows two adjacent oxygen atoms of the crown ether coordinated to Sn (IV).[97] In our hands, the addition of 4 equiv of $SnCl_4$ to a $(CDCl_2)_2$ solution containing

only 18-crown-6 resulted in the shift of the OCH_2CH_2O proton signal of 18-crown-6 seen as a singlet from 3.6 ppm to 3.7 ppm. This indicates an interaction between $SnCl_4$ and 18-crown-6 in solution. In the system under investigation, the OCH_2CH_2O proton signal of 18-crown-6 is also observed as a singlet at 3.7 ppm upon addition of $SnCl_4$. This indicates the $SnCl_4$ complexation and its competitive role in replacing NO^+ from the 18-crown-6-NO^+ complex (Figure 35). This observation is important, since in this case, foreign species can be replaced and returned back without decomposition or changing the solution polarity.

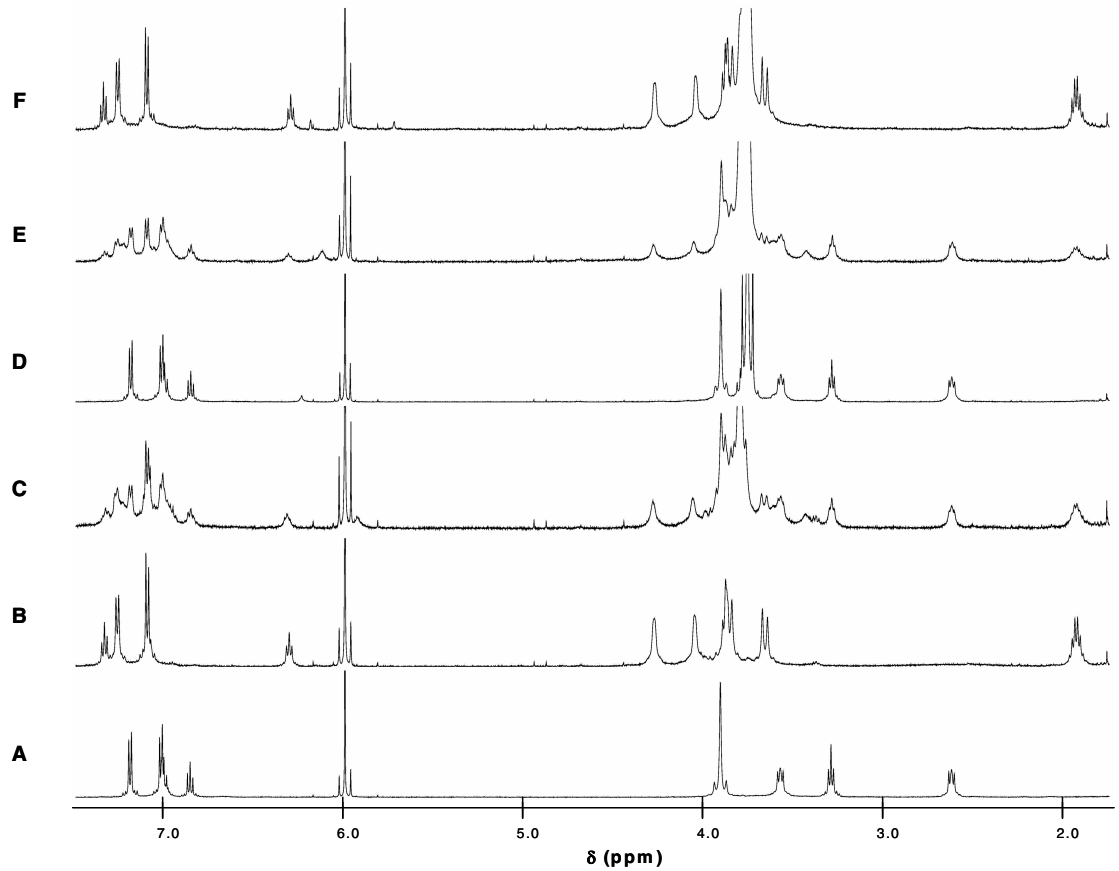

Figure 34. Nitrosonium exchange with nanotube **15**. Selected portions of the ^1H NMR spectra (500 MHz, $(CDCl_2)_2$, 295 K), of: A. nanotube **15**. B. filled nanotube **33**. C. same as B with 1 equiv of 18-crown-6. D. same as B with 2 equiv of 18-crown-6. E. same as D with 2 equiv of $SnCl_4$. F. same as D with 4 equiv of $SnCl_4$.

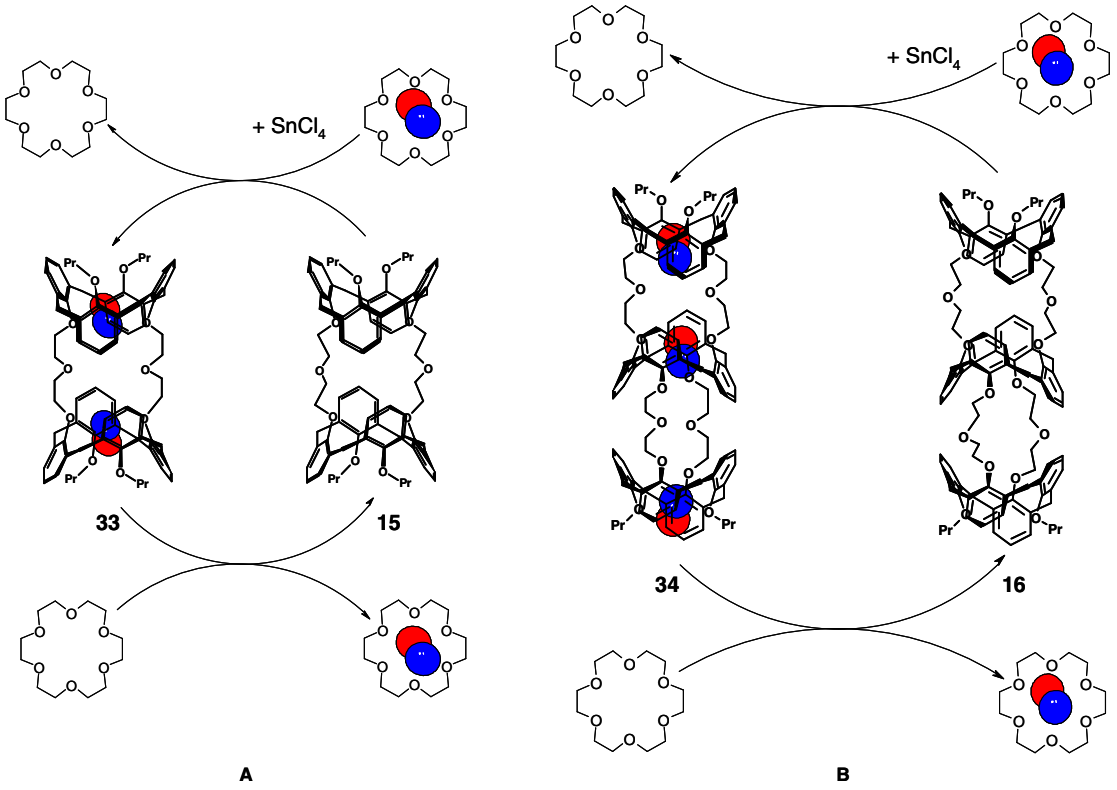

Figure 35. Reversible nitrosonium exchange with 18-crown-6 and calixarene nanotubes **15** (A) and **16** (B).

Nitrosonium transfer can also be demonstrated with complex **34**. In this case, 3 equiv of 18-crown-6 are required to completely remove NO^+ species and regenerate nanotube **16**. Stepwise addition of 18-crown-6 slowly bleaches the deep purple solution of the complex **34**. Again, this process can be monitored by ^1H NMR (Figure 36). The transformation of complex **34** to empty tube **16** and *vice versa* is slow in the NMR time scale, as both **16** and **34** species are observed in the spectra. Addition of 6 equiv of $SnCl_4$ is enough to bring back the NO^+ guests into the nanotube.

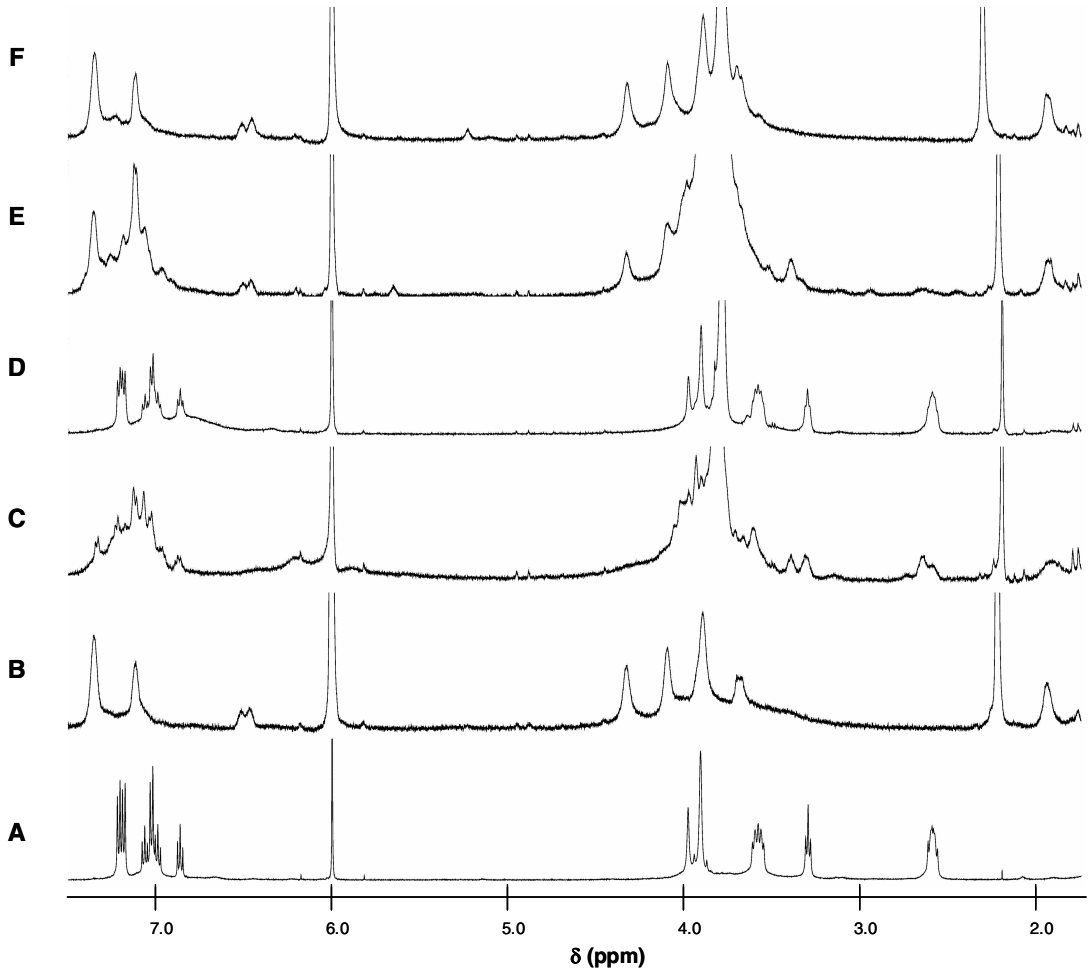

Figure 36. Nitrosonium exchange with nanotube **16**. Selected portions of the ^{1}H NMR spectra (500 MHz, $(CDCl_2)_2$, 295 K), of: A. nanotube **16**. B. filled nanotube **34**. C. same as B with 1.5 equiv of 18-crown-6. D. same as B with 3 equiv of 18-crown-6. E. same as D with 3 equiv of $SnCl_4$. F. same as D with 6 equiv of $SnCl_4$.

The NO^+ transfer between calixarene nanotube **16** and 18-crown-6 can also be observed by IR spectroscopy. Complex **34** shows two absorption bands at $\nu(NO^+)$ = 1955 cm^{-1} and 1940 cm^{-1}. Upon addition of 18-crown-6, these two bands diminished and a new absorption band at $\nu(NO^+)$ = 2248 cm^{-1} appeared (Figure 37). This new band

corresponds to the NO^+ encapsulated in 18-crown-6.[94] With the addition of excess $SnCl_4$ to the same solution, the two absorption bands at 1955 cm^{-1} and 1940 cm^{-1} reappears, and the band at 2248 cm^{-1} disappears.

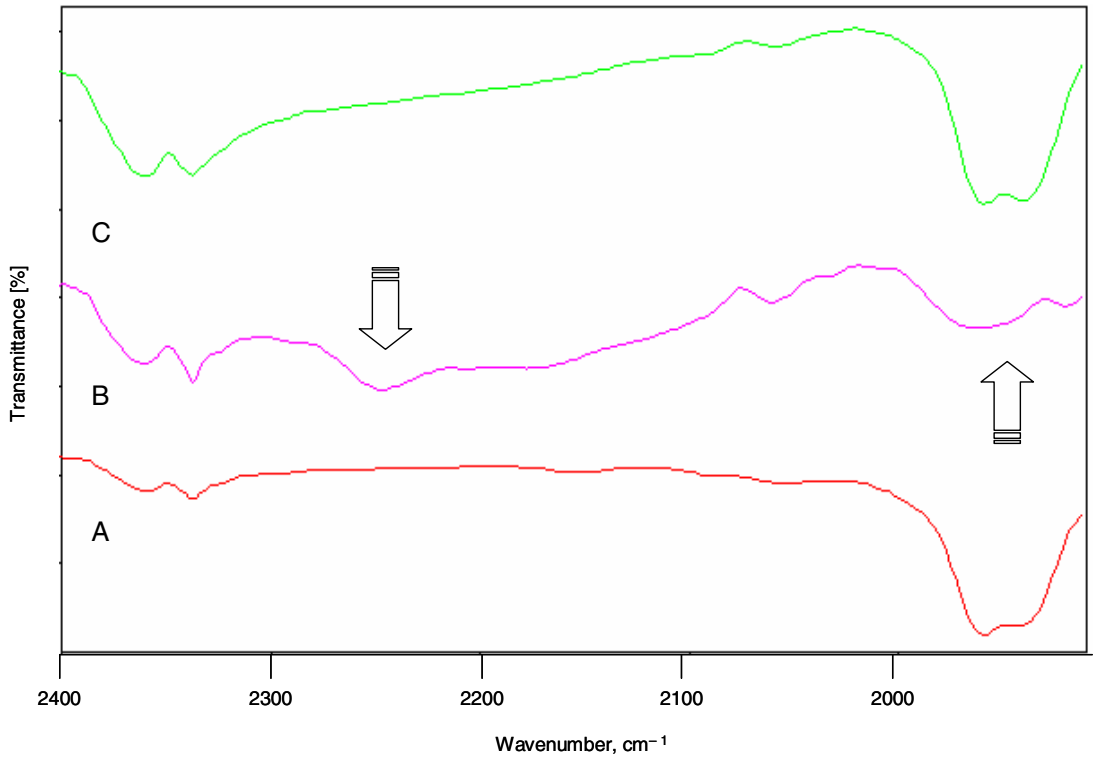

Figure 37. Selected portions of the IR spectra ($(CHCl_2)_2$, 295 K) of (A) complex **34**, (B) complex **34** + 3 equiv 18-crown-6, and (C) same as B + 6 equiv $SnCl_4$. Arrows indicate increase (arrow down) and decrease (arrow up) of bands.

Based on modeling, NO^+ species can enter and leave the nanotube either through its open ends (Route A, Figure 38) or the middle gates between the calixarene modules (Route B, Figure 38). The approach and exit through the ends of the tube is less hindered, and thus more favored. Besides, the middle gates between the calixarene units

become narrower due to the glycol conformational changes from *anti* to *gauche* upon complexation (see Figure 29). The encapsulated NO^+ species should also avoid electrostatic repulsions with each other. Most probably, the tube filling and release occurs through the guest tunneling along the interior.

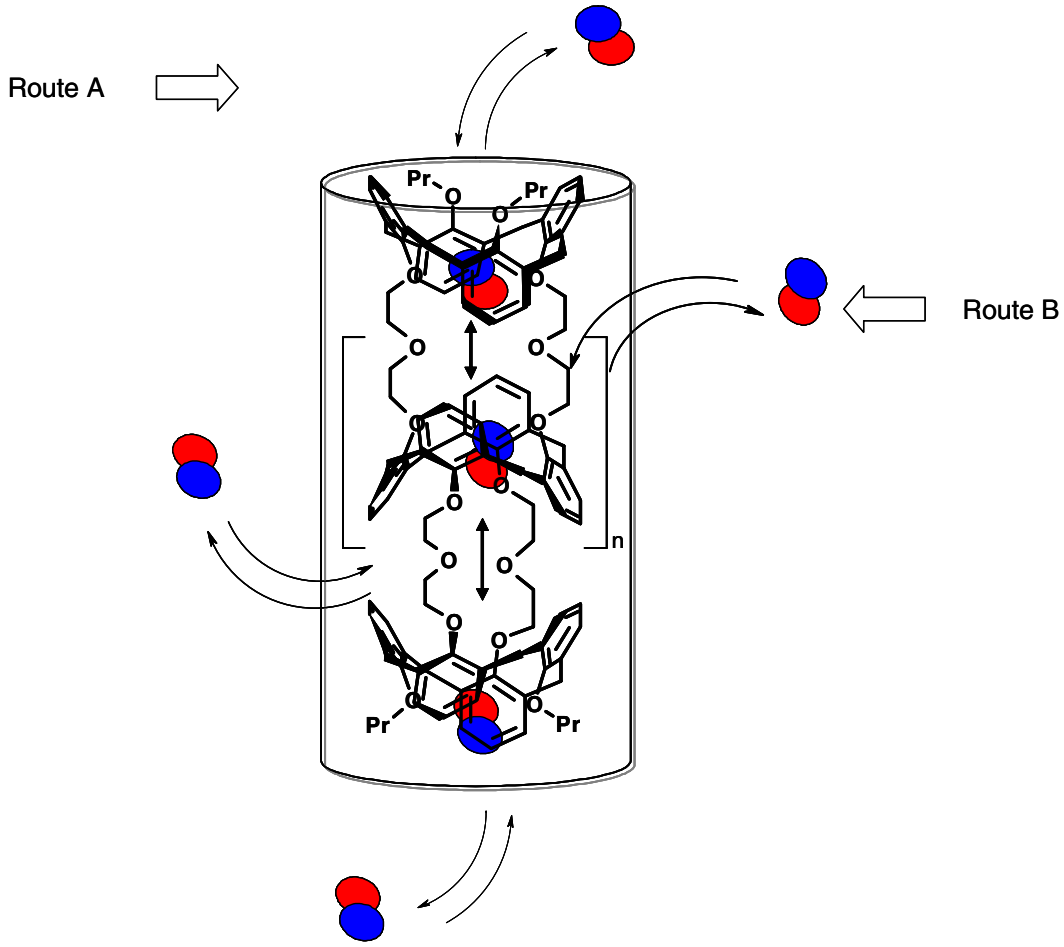

Figure 38. Potential routes for nanotube filling and release of NO^+ guests.

4.3 Conclusion and Outlook

Unlike other developed nanoscale molecular containers, synthetic nanotubes can be filled with multiple guests in one-dimensional morphology which leads to unique host-guest dynamics such as cooperativity. In the case of calix[4]arene-based nanotubes, NO^+ serves as the filling material. The tunnel of the nanotube allows the NO^+ guests to freely rotate along the N-O axis and also tumble within the cavity at room temperature. Though the filled nanotube is stable, it allows the release and re-entry of guests within its hollow structure. NO^+ can be transferred to and from another host such as 18-crown-6. The guest exchange and dynamics can be monitored by conventional spectroscopic techniques.

Potential applications of synthetic nanotubes such as nanowires, sensors, and molecular storage containers of reactive species can be explored. Generation of gas molecules inside the nanotubes such as NO can also be studied. Similar designs can be developed to fill synthetic nanotubes with other species.

CHAPTER 5

EXPERIMENTAL SECTION

5.1 General Information

All reagents and solvents were purchased from commercial suppliers (Aldrich, Acros Chemicals, Cambridge Isotope Laboratories, etc.) and were used without purification unless otherwise specified. Melting points were determined on a Mel-Temp apparatus (Laboratory Devices, Inc.) and are uncorrected. ^{1}H, ^{13}C NMR, COSY and NOESY spectra were recorded at 22 ± 1 ^{O}C on JEOL 300 and 500 MHz spectrometers. Chemical shifts were measured relative to residual non-deuterated solvent resonances. FTIR spectra were recorded on a Bruker Vector 22 FTIR spectrometer using KBr pressed pellet for solids or solution between NaCl plates and reported in cm^{-1}. UV-vis spectra were measured on a Varian Cary-50 spectrophotometer. Mass spectra were recorded at the Scripps Center for Mass Spectrometry (La Jolla, CA). High Resolution MALDI FT mass spectra were obtained on an IonSpec Ultima FTMS. ESI-TOF mass spectra were obtained on an Agilent ESI-TOF mass spectrometer. MALDI TOF mass spectra were obtained on an Applied Biosytems Voyager STR (2). Elemental analysis was performed on a Perkin-Elmer 2400 CHN analyzer. For column chromatography, Silica Gel 60 Å (Sorbent Technologies, Inc.; 200–425 mesh) was used. All experiments with moisture- and/or air-sensitive compounds were run under a dried nitrogen

atmosphere. Parent tetrahydroxycalix[4]arene **19**, and calix[4]arene derivatives **20** and **24** were prepared according to the published procedures.[70,71,73] NO_2/N_2O_4 was generated from copper and concentrated HNO_3. Molecular modeling was performed using commercial MacroModel 7.1 with Amber* Force Field.[98]

5.2 Experimental Procedures and Data

25,27-Bis(1-propyloxy)-26,28-bis(2-(*tert*-butyldimethylsiloxy)ethyloxy) calix[4]-arene, *1,3- alternate* (21): A suspension of 25,27-dihydroxy-26,28-bis(1-propyloxy)calix[4]arene **20**[70] (3.0 g, 6.0 mmol), 2-(*tert*-butyldimethylsiloxy)ethanol *p*-toluenesulfonate (3.9 g, 12.0 mmol), and Cs_2CO_3 (5.7 g, 18.0 mmol) in MeCN (100 mL) was refluxed for 24 h. The solvent was removed, and the reaction mixture was treated with 10% aq acetic acid (50 mL) and CH_2Cl_2 (50 mL). The organic layer was separated, washed with 10% aq $NaHCO_3$ (15 mL), brine (2 x 15 mL) and dried over $MgSO_4$. Evaporation of CH_2Cl_2 gave a light yellow solid, which was recrystallized from MeOH to give a white solid. Yield 2.7 g (55%); mp 140-142°C; ^{1}H NMR ($CDCl_3$): δ 7.08 (d, *J* = 7.7 Hz, 4 H), 6.99 (d, *J* = 7.3 Hz, 4 H), 6.65, 6.62 (2 x t, *J* = 7.7, 7.3 Hz, 4 H), 3.84 (t, *J* = 5.5 Hz, 4 H), 3.76 (t, *J* = 5.5 Hz, 4 H), 3.61 (t, *J* = 7.0 Hz, 4H), 3.60 (2 x d, *J* = 13.2 Hz, 8 H), 1.81 (m, 4 H), 1.02 (t, *J* = 7.3 Hz, 6 H), 0.96 (s, 18 H), 0.16 (s, 12 H); ^{13}C NMR ($CDCl_3$): δ 156.2, 155.9, 133.8, 133.5, 129.9, 129.7, 121.7, 121.5, 74.4, 73.6, 70.8, 62.5, 35.3, 26.1, 23.9, 18.5, 10.7, -5.1; FTIR ($CHCl_3$): ν 3069, 3030, 2932, 2859, 1453, 1250, 1198, 1093, 1044, 1008 cm^{-1}; Anal. calcd for $C_{50}H_{72}O_6Si_2$: C, 72.77; H, 8.79. Found: C, 72.70; H, 8.72.

25,27-Bis(2-hydroxyethyloxy)-26,28-bis(1-propyloxy)calix[4]arene, *1,3-alternate* (22): Acetyl chloride (0.20 mL, 2.9 mmol) was added dropwise to an ice-cold mixture of CH_2Cl_2/MeOH (10 mL, 9/1, v/v), and after 30 min a solution of calix[4]arene **21** (0.3 g, 4.1 mmol) in CH_2Cl_2 (5 mL) was added. After the starting material was consumed (TLC, Hex/AcOEt, 7/3, ~1h), the reaction mixture was washed with 10% aq $NaHCO_3$ (5 mL), brine (5 mL) and dried over $MgSO_4$, and evaporated in vacuo. The residue was treated with MeOH to give derivative **22** as a colorless solid. Yield 0.23 g (95%); mp = 262-264°C; ^{1}H NMR ($CDCl_3$): δ 7.07 (d, *J* = 7.5 Hz, 4H), 7.04 (d, *J* = 7.5 Hz, 4H), 6.89 (t, *J* = 7.0 Hz, 2H), 6.86 (t, *J* = 7.0 Hz, 2H), 3.91 (AB q, *J* = 16.5 Hz, 8H), 3.62 (m, 4H), 3.35 (t, *J* = 7.0, 4H), 3.28 (m, 4H) 2.33 (t, 2H), 1.01 (m, 4H), 0.63 (t, *J* = 7.2 Hz, 6H); FTIR (KBr): ν 3527, 3315, 3063, 3019, 2958, 2904, 2873, 1459, 1248, 1212, 1091, 1029 cm^{-1}. The spectral and analytical data are in agreement with previously published compound which was obtained from calix[4]arene **23**.[68]

25,27-Bis(2-*p*-toluenesulfonyloxyethyloxy)-26,28-bis(1-propyloxy) calix[4]arene, *1,3-alternate* (23): In a modified procedure, 25,27-Bis(2-hydroxyethyloxy)-26,28-bis(1-propyloxy)calix[4]arene **22** (0.65 g, 1.09 mmol), DMAP (0.025 g, 0.21 mmol), and *p*-toluenesulfonyl chloride (0.83 g, 4.35 mmol) were dissolved in CH_2Cl_2 (15 mL) and cooled at -5°C. Triethylamine (1.0 mL) was added, and the solution was stirred overnight at rt. The solution was evaporated to dryness, redissolved in CH_2Cl_2, then washed with 5% HCl, water, and brine. The organic layer was dried with Na_2SO_4 and evaporated to dryness. Treatment with MeOH produced

compound **23** as colorless solid. Yield 0.84 g (86%); mp 128-130°C; ^{1}H NMR ($CDCl_3$): δ 7.83 (d, *J* = 7.3 Hz, 4H), 7.40 (d, *J* = 7.3 Hz, 4H), 6.98 (d, *J* = 7.3 Hz, 4H), 6.89 (d, *J* = 7.3 Hz, 4H), 6.74 (t, *J* = 7.3 Hz, 2H), 6.54 (t, *J* = 7.3 Hz, 2H), 3.74 (t, *J* = 5.5 Hz, 4H), 3.70 (AB q, *J* = 15.4 Hz, 8H), 3.50 (t, *J* = 5.5 Hz, 4H), 3.43 (t, *J* = 5.5 Hz, 4H), 2.47 (s, 6H), 1.40 (m, 4H), 0.76 (t, *J* = 5.5 Hz, 6H); FTIR (KBr): ν 3063, 3017, 2960, 2932, 2876, 1457, 1360, 1248, 1210, 1177, 1095, 1011 cm^{-1}. The spectral and analytical data are in agreement with previously published data.[69]

25, 26, 27, 28-Tetrakis(2-hydroxyethoxy)calix[4]arene, *1,3-alternate* (25): Yield 0.60 g (77 %); mp > 250°C (decomp.); ^{1}H NMR ($CDCl_3$): 7.11 (d, *J* = 7.7 Hz, 8H), 6.97 (t, *J* = 7.7 Hz, 4 H), 3.97 (s, 8 H), 3.59 (t, *J* = 5.0 Hz, 8 H), 3.21 (t, *J* = 5.0 Hz, 8 H), 2.13 (s, 4 H); ^{13}C NMR ($CDCl_3$): δ 156.3, 133.6, 129.8, 123.9, 71.6, 61.1, 38.3. The spectral and analytical data are in agreement with previously published data.[71]

25,26,27,28-tetrakis(2-*p*-toluenesulfoxyethoxy)-calix[4]arene, *1,3-alternate* (26): In a modified procedure, 25, 26, 27, 28-Tetrakis(2-hydroxyethoxy)calix[4]arene **25** (0.10 g, 0.17 mmol), DMAP (8.5 mg, 0.070 mmol), and *p*-toluenesulfonyl chloride (0.27 g, 1.4 mmol) were dissolved in CH_2Cl_2 (15 mL) and cooled at -5°C. Triethylamine (1.0 mL) was added, and the solution was stirred overnight at rt. The solution was evaporated to dryness, redissolved in CH_2Cl_2, then washed with 5% HCl, water, and brine. The organic layer was dried with Na_2SO_4 and evaporated to dryness. Treatment with MeOH produced compound **26** as colorless solid. Yield 0.12 g (57%);

mp 216-218°C; ^{1}H NMR ($CDCl_3$): δ 7.80 (d, 8H), 7.39 (d, 8H), 6.90 (d, 8H), 6.61 (t, 4H), 3.64 (s, 8H), 3.48 (t, 8H), 2.47 (s, 12H); ^{13}C NMR ($CDCl_3$): δ 155.4, 145.1, 133.7, 133.0, 130.0, 129.7, 128.0, 123.2, 67.8, 67.6, 37.1, 21.7. The spectral and analytical data are in agreement with previously published data.[71]

25,27-Bis(2-benzyloxy)ethyloxy)-26,28-dihydroxycalix[4]arene (29): A suspension of parent calix[4]arene (1.0 g, 2.4 mmol), 2-(benzyloxy)ethanol *p*-toluene sulfonate (1.51 g, 4.9 mmol) and K_2CO_3 (0.67 g, 4.8 mmol) in MeCN (20 mL) was refluxed for 24 h. After cooling to rt, the solvent was removed under reduced pressure, and the residue was treated with 10% aq HCl (20 mL) and CH_2Cl_2 (40 mL). The organic layer was separated and washed with 10% aq $NaHCO_3$ (2 x 15 mL) and brine. The organic solution was dried over $MgSO_4$, filtered and evaporated in vacuo. The resulting pale yellow oil was solidified with MeOH (3 x 15 mL) to give product **29** as a white powder. Yield 1.03 g (62%); mp 138-140°C; ^{1}H NMR ($CDCl_3$): δ 7.87 (s, 2 H), 7.33 (m, 10 H), 7.06, 6.89 (2 x d, *J* = 7.5 Hz, 8 H), 6.72, 6.65 (2 x t, *J* = 7.5 Hz, 4 H), 4.65 (s, 4 H), 4.45, 3.37 (2 x d, *J* = 12.8 Hz, 8 H), 4.18 (t, *J* = 5.1 Hz, 4 H), 3.92 (t, *J* = 5.1 Hz, 4H); ^{13}C NMR ($CDCl_3$): δ 153.4, 152.0, 138.2, 133.4, 129.0, 128.6, 128.5, 128.2, 128.0, 127.7, 125.4, 118.9, 75.7, 73.7, 69.2, 31.4; FTIR (KBr): ν 3333, 3062, 3028, 2928, 2861, 1467, 1453, 1355, 1250, 1200, 1123, 1090, 1045 cm^{-1}; Anal. calcd for $C_{46}H_{46}O_6$: C, 79.51; H, 6.67. Found: C, 79.23; H, 6.41.

25,27-Bis(2-benzyloxy)ethyloxy)-26,28-bis(2-(*tert*-butyldimethylsiloxy) ethyloxy)calix[4]-arene, *1,3- alternate* (30): A suspension of 1,3-bis(2-benzyloxy)ethyloxy) calix[4]arene **29** (1.15 g, 1.65 mmol) and Cs_2CO_3 (2.7 g, 8.3 mmol) in DMF (50 mL) was heated at 90 °C for 1 h, then a solution of 2-(*tert*-butyldimethylsiloxy)ethanol *p*-toluenesulfonate (2.74 g, 8.29 mmol) in DMF (10 mL) was added. The reaction mixture was stirred at 90 °C for 24 h. DMF was completely removed in vacuo, and the reaction mixture was treated with 10% aq acetic acid (50 mL) and CH_2Cl_2 (50 mL). The organic layer was separated, washed with 10% aq $NaHCO_3$ (15 mL), brine (2 x 15 mL) and dried over $MgSO_4$. Evaporation of CH_2Cl_2 gave a light yellow solid, which was refluxed with KI (1 g) and Et_3N (1 mL) in MeCN (30 mL) for 1h. The solvent was evaporated *in vacuo*, and the residue was solidified with MeOH (3 x 15 mL). The resulting brownish-yellow solid was then refluxed with MeOH (25 mL) and filtered hot, washed with MeOH (3 x15 mL), giving product **30** as a white powder. Yield 1.12 g (67%); mp 116-120 °C; ^{1}H NMR ($CDCl_3$): δ 7.36 (m, 10 H), 7.07, 7.04 (2 x d, *J* = 7.3 Hz, 8 H), 6.62, 6.56 (2 x t, *J* = 7.3 Hz, 4 H), 4.66 (s, 4 H), 3.87 (m, 8 H), 3.77, 3.71 (2 x m, 8 H), 3.55 (s, 8 H), 0.96 (s, 18 H), 0.15 (s, 12 H); ^{13}C NMR ($CDCl_3$): δ 155.8, 155.6, 138.4, 133.6, 130.0, 129.8, 128.5, 127.8, 121.9, 74.0, 73.4, 71.6, 69.7, 62.7, 34.9, 26.2, 18.5, -5.1; FTIR ($CHCl_3$): ν 3068, 3032, 2931, 2714, 1452, 1361, 1250, 1198, 1098, 1029 cm^{-1}; Anal. calcd for $C_{62}H_{80}O_8Si_2$: C, 73.77; H, 7.99. Found: C, 73.52; H, 7.93.

25,27-Bis(2-benzyloxy)ethyloxy)-26,28-bis(2-(hydroxy)ethyloxy) calix[4]arene, *1,3-alternate* (31): Acetyl chloride (0.46 mL, 6.5 mmol) was added dropwise to the ice-cold mixture of CH_2Cl_2/MeOH (10 mL, 9/1, v/v), and after 30 min a solution of calix[4]arene **30** (1.1 g, 1.1 mmol) in CH_2Cl_2 (5 mL) was added. After the starting material was consumed (TLC, Hex/AcOEt, 7/3, ~1h), the reaction mixture was washed with 10% aq $NaHCO_3$ (5 mL), brine (5 mL) and dried over $MgSO_4$, and evaporated in vacuo. The residue was treated with hexane/CH_2Cl_2 (5:1) to give derivative **31** as a colorless solid. Yield 0.83g (95%); mp 174-176 °C; ^{1}H NMR ($CDCl_3$): δ 7.33 (m, 10 H), 7.07, 7.00 (2 x d, *J* = 7.3 Hz, 8 H), 6.91, 6.68 (2 x t, *J* = 7.3 Hz, 4 H), 4.38 (s, 4 H), 3.87 (AB q, *J* = 16.9 Hz, 8 H), 3.6 (m, 8 H), 3.30 (t, *J* = 6.0 Hz, 4 H), 2.91 (t, *J* = 6.0 Hz, 4 H), 1.68 (br s, 2 H); ^{13}C NMR ($CDCl_3$): δ 156.3, 156.1, 138.4, 133.8, 133.7, 129.5, 129.4, 128.5, 127.9, 127.8, 127.6, 123.2, 123.0, 73.2, 71.4, 68.1, 61.3, 38.0; FTIR ($CHCl_3$): ν 3529, 3421, 3066, 3033, 2927, 2872, 1468, 1365, 1324, 1247, 1215, 1092, 1037 cm^{-1}; Anal. calcd for $C_{50}H_{52}O_8$: C, 76.90; H, 6.71. Found: C, 76.82; H, 6.66.

Bis(1-propyloxy)-bis(2-benzyloxy(ethyloxy))calix[4]tube (32): 25,27-Bis(2-benzyloxy)-ethyloxy)-26,28-bis(2-(hydroxy)ethyloxy)calix[4]arene **31** (0.12 g, 0.153 mmol) was dissolved in dry THF (40 mL), and NaH (60% suspension in mineral oil, 0.61 g, 1.5 mmol) was added. The mixture was stirred at 45°C for 1 h, after which a solution of 25,27-bis(2-(*p*-toluenesulfonyloxy)ethyloxy)-26,28-bis(1-propyloxy) calix[4]arene **23**[69] (0.14 g, 0.153 mmol) in THF (20 mL) was added slowly over 4 h.

The reaction mixture was refluxed for 24 h. After cooling, the solvent was evaporated under reduced pressure and CH_2Cl_2 (30 mL) and 10% aq HCl (10 mL) were added. The organic layer was washed by 10% aq $NaHCO_3$ (10 mL), saturated solution of NaCl (2 x10 mL), dried over $MgSO_4$ and evaporated in vacuo. The residue was purified by column chromatography with CH_2Cl_2-MeOH, 99:1 (R_f = 0.3) as an eluent to afford product **32** as a colorless solid. Yield 0.12 g (56%); mp >270°C (decomp.); ^{1}H NMR ($CDCl_3$): δ 7.3 (m, 10 H), 7.17, 7.16 (2 x d, *J* = 7.5 Hz, 8 H), 7.02 (m, 12 H), 6.85, 6.72 (2 x t, *J* = 7.5 Hz, 4 H), 4.31 (s, 4 H), 3.90 (AB q, *J* = 16.5 Hz, 8 H), 3.88 (AB q, *J* = 16.5 Hz, 8 H), 3.56 (m, 8 H), 3.48, 3.31, 2.92 (3 x t, *J* = 6.5 Hz, 12 H), 2.57 (m, 8 H), 1.06 (m, 4 H), 0.56 (t, *J* = 7.3 Hz, 6 H); ^{13}C NMR ($CDCl_3$): δ 157.3, 156.6, 155.9, 155.8, 134.2, 134.1, 134.0, 129.1, 129.0, 128.9, 128.8, 128.5, 127.7, 127.6, 122.9, 122.8, 122.5, 122.0, 73.1, 71.5, 69.1, 68.5, 68.2, 66.1, 66.0, 38.3, 38.1, 22.7, 10.2; FTIR ($CHCl_3$): ν 3065, 3033, 2925, 2875, 1462, 1247, 1215, 1124, 1094, 1034, 1009 cm^{-1}; MALDI-FTMS: *m/z* ($M+Na^+$) 1363.6439, calcd for $C_{88}H_{92}O_{12}Na$ 1363.6486.

Bis(1-propyloxy)-bis(2-hydroxy(ethyloxy))calix[4]tube (27): A mixture of 10 wt % Pd/C (0.03 g), benzylated calix[4]tube **32** (0.06 g, 0.044 mmol) and AcOH (0.1 mL) in THF (5 mL) was stirred under H_2 atmosphere (1 atm) at rt until all starting material disappeared (TLC, CH_2Cl_2-MeOH, 99:1). The suspension was filtered through Celite and the clear solution was concentrated in vacuo. The residue was triturated with MeOH (3 x 2 mL) to afford product **7** as a white powder. Yield 82% (0.042 g, 0.036 mmol); mp >300°C (decomp.); ^{1}H NMR ($CDCl_3$): δ 7.21, 7.15 (2 x d, *J* = 7.6 Hz, 8 H),

7.05 (m, 12 H), 6.95, 6.86 (2 x t, J = 7.6 Hz, 4 H), 3.95 (AB q, J = 17.2 Hz, 8 H), 3.88 (AB q, J = 16.5 Hz, 8 H), 3.63 (t, J = 7.0 Hz, 4 H), 3.56 (m, 8 H), 3.31 (t, J = 7.0 Hz, 4 H), 3.21(m, 4 H), 2.56 (m, 8 H), 2.27 (br s, 2 H), 1.06 (m, 4 H), 0.56 (t, J = 7.6 Hz, 6 H); ^{13}C NMR ($CDCl_3$): δ 157.3, 156.4, 156.0, 155.8, 134.2, 134.0, 133.9, 133.5, 129.2, 129.1, 128.9, 128.8, 123.6, 123.0, 122.8, 121.9; FTIR (KBr): ν 3529, 3453, 3060, 3030, 3011, 2924, 2875, 1459, 1216, 1132, 1094, 1035, 1011 cm^{-1}; MALDI-FTMS: *m/z* ($M+Na^+$) 1183.5426, calcd for $C_{74}H_{80}O_{12}Na$ 1183.5547.

Bis(1-propyloxy)-bis(2-methyl(ethyloxy))calix[4]tube (27b): Sodium hydride (60% suspension in mineral oil, 0.034 mmol) was added to the THF (2 mL) solution of calix[4]tube **27** (0.010 g, 0.0086 mmol), and the mixture was stirred at rt for 1 h. MeI (0.0096 g, 0.068 mmol, 0.0040 mL) was added, and the reaction mixture was stirred overnight. The solvent was removed under reduced pressure, and the residue was dissolved in CH_2Cl_2 (5 mL). The organic solution was washed by 10% aq HCl (1 mL), 10% aq $NaHCO_3$ (1 mL) and dried over $MgSO_4$. Preparative TLC (SiO_2, Hexanes-AcOEt, 7:3) was then performed to obtain the dimethylated product. Yield 0.005 g (49%): ^{1}H NMR ($CDCl_3$): δ 7.19, 7.18 (2 x d, J = 7.3 Hz, 8 H), 7.05 (m, 12 H), 6.93, 6.84 (2 x t, J = 7.3 Hz, 4 H), 3.89 (m, 16 H), 3.57 (m, 12 H), 3.31 (t, J = 7.3 Hz, 4 H), 3.11 (s, 6 H), 2.95 (t, J = 6.0 Hz, 4 H), 2.58 (m, 8 H), 1.06 (m, 4 H), 0.57 (t, J = 7.3 Hz, 6 H); ESI-TOF: m/z ($M+Na^+$) 1211.5855, calcd for $C_{112}H_{120}O_{16}Na$ 1211.5838.

Bis(1-propyloxy)-bis(2-(p-toluenesulfonyloxy)ethyloxy)calix[4]tube (28): Bis(1-propyloxy)-bis(2-hydroxyethyloxy)calix[4]tube **7** (0.11 g, 0.095 mmol), DMAP (0.046 g, 0.38 mmol), and *p*-toluenesulfonyl chloride (0.070 g, 0.38 mmol) were dissolved in CH_2Cl_2 (15 mL) and cooled at -5°C. Triethylamine (0.20 mL) was added, and the solution was stirred overnight at rt. The solution was evaporated to dryness, redissolved in CH_2Cl_2, then washed with 5% HCl, water, and brine. The organic layer was dried with Na_2SO_4 and evaporated to dryness. Treatment with MeOH produced compound **28** as colorless solid. Yield 0.12 g (88%); mp 242-243 °C; ^{1}H NMR ($CDCl_3$): δ 7.79 (d, *J* = 8.4 Hz, 4H), 7.40 (d, *J* = 8.4 Hz, 4H), 7.17, 7.15 (2 x d, *J* = 1.7 Hz, 8H), 7.06-6.97 (t+d+t, *J* = 7.5 Hz, 8H), 6.94 (d, *J* = 7.3 Hz, 4H), 6.86 (t, *J* = 7.3 Hz, 2H), 6.69 (t, *J* = 7.3 Hz, 2H), 3.89-3.80 (m, 16H), 3.57 (m, 12H), 3.39 (m, 4H), 3.32 (t, *J* = 7.3 Hz, 4H), 2.57 (m, 8H), 2.48 (s, 6H), 1.10 (m, 4H), 0.58 (t, *J* = 7.3 Hz, 6H); ^{13}C ($CDCl_3$): δ 157.3, 155.9, 155.8, 155.6, 145.0, 134.2, 134.0, 133.9, 133.8, 133.2, 130.0, 129.1, 129.0, 128.8, 128.0, 123.3, 122.9, 122.8, 121.9, 71.5, 69.1, 68.9, 67.8, 66.8, 66.2, 66.0, 38.3, 38.0, 22.7, 21.7, 10.2; FTIR (KBr): ν 3061, 3031, 3014, 2959, 2918, 2874, 1459, 1214, 1177, 1095, 1033, 1011 cm^{-1}; Anal. calcd for $C_{88}H_{96}O_{16}S_2$: C, 71.71; H, 6.57. Found: C, 71.78; H, 6.46.

Dimeric Tube (15): A solution of 25, 27-bis(2-hydroxyethyloxy)-26, 28-bis(1-propyloxy)calix[4]arene **22**[68] (0.10 g, 0.16 mmol) and 25,27-bis(2-*p*-toluenesulfonyloxy-ethyloxy)-26,28-bis(1-propyloxy)calix[4]arene **23**[99] (0.14 g, 0.16 mmol) in THF (25 mL) were added dropwise to a suspension of NaH (60% in mineral

oil, 15 mg, 0.64 mmol) in THF (150 mL) at 70°C over 8 h. The mixture was further refluxed for 24 h, evaporated to dryness, suspended in CH_2Cl_2 (50 mL), and neutralized at 0°C with 5% aq HCl (50 mL). The organic layer was washed with water (3 x 5 mL), dried over Na_2SO_4, and then evaporated to dryness. The residue was treated with MeCN to produce nanotube **15** as a white solid. Yield 0.11 g (55%); mp > 300°C; ^{1}H NMR ($CDCl_3$): δ 7.18 (d, *J* = 7.5 Hz, 8 H), 7.03-6.99 (d + t, 12 H), 6.84 (t, *J* = 7.5 Hz, 4 H), 3.89 (2 x d, *J* = 17.0 Hz, 16 H), 3.57 (t, *J* = 7.0 Hz, 8 H), 3.31 (t, *J* = 7.0 Hz, 8 H), 2.58 (t, *J* = 7.5 Hz, 8 H), 1.09-1.05 (m, 8 H), 0.56 (t, *J* = 7.0 Hz, 12H); ^{13}C NMR ($C_2D_2Cl_4$): δ 157.2, 155.9, 134.2, 134.1, 129.2, 129.0, 122.8, 122.1, 71.7, 69.1, 66.5, 38.3, 22.8, 10.4; FTIR (CCl_4): ν 3063, 3034, 3016, 2961, 2961, 2922, 2875, 1459, 1216, 1128, 1094, 1034, 1011 cm^{-1}; MALDI-FTMS, *m*/*z* 1179.5939 [M + Na^+]; calcd for $C_{76}H_{84}O_{10}Na$, 1179.5956.

Trimeric Tube (16): A solution of 25,26,27,28-tetrakis(2-*p*-toluenesulfoxyethoxy)-calix[4]arene **26**[71] (100 mg, 0.08 mmol) and 25, 27-bis(2-hydroxyethyloxy)-26, 28-bis(1-propyloxy)calix[4]arene **22**[68] (98 mg, 0.16 mmol) in THF (25 mL) were added dropwise to a suspension of NaH (60% in mineral oil, 26 mg, 1.3 mmol) in THF (150 mL) at 70°C over 8 h. The mixture was further refluxed for 24 h, evaporated to dryness, suspended in CH_2Cl_2 (50 mL), and neutralized at 0°C with 5% aq HCl (50 mL). The organic layer was washed with water (3 x 5 mL), dried over Na_2SO_4, and then evaporated to dryness. The residue was treated with MeCN to produce nanotube **16** as a white solid. Yield 0.10g (70%); mp >300°C (decomp.); ^{1}H

NMR ($CDCl_3$): δ 7.20, 7.18 (2 x d, *J* = 7.3 Hz, 16 H), 7.08 (t, *J* = 7.3 Hz, 4 H), 7.02 (d, *J* = 7.3 Hz, 8 H), 6.98, 6.85 (2 x t, *J* = 7.3 Hz, 8 H), 3.94 (s, 8 H), 3.88 (AB q, *J* = 16.5 Hz, 16 H), 3.57 (m, 16 H), 3.30 (t, *J* = 7.3 Hz, 8 H), 2.55 (m, 16 H), 1.06 (m, 8 H), 0.56 (t, *J* = 7.3 Hz, 12 H); ^{13}C NMR ($C_2D_2Cl_4$): δ 157.2, 156.2, 155.9, 134.2, 134.1, 134.0, 129.3, 129.1, 128.8, 122.9, 122.7, 122.0, 71.8, 70.9, 69.2, 66.7, 66.5, 38.3, 38.1, 22.8, 10.4; FTIR (CCl_4): ν 3064, 3033, 3016, 2959, 2921, 2873, 1459, 1216, 1125, 1093, 1035, 1010 cm^{-1}; MALDI-FTMS: *m/z* [$M+Na^+$] 1743.8443, calcd for $C_{112}H_{120}O_{16}Na$ 1743.8473.

Tetrameric Nanotube (17): A solution of bis(1-propoxy)-bis(2-(*p*-toluene-sulfonyloxy)ethoxy)calix[4]tube **28** (57 mg, 0.039 mmol) and bis(1-propoxy)-bis(2-hydroxyethoxy)-calix[4]tube **27** (45 mg, 0.039 mmol) in THF (25 mL) was added dropwise over 1 hr into a mixture of NaH (60% suspension in mineral oil, 12 mg, 0.31 mmol) and K_2CO_3 (22 mg, 0.16 mmol) in THF (100 mL) at reflux temperature. The mixture was further refluxed for 24h, evaporated to dryness, suspended in CH_2Cl_2 (50 mL), and neutralized at 0°C with 5% HCl (25 mL). The organic layer was washed with water (2 x 5 mL), dried over Na_2SO_4, and then evaporated to dryness. The residue was treated with MeCN to produce tetracalix[4]tube as a colorless solid. Yield 56 mg (64%); mp >300 °C (decomp.); ^1H NMR $(CDCl_2)_2$: δ 7.22, 7.19 (2 x d, *J* = 7.3 Hz, 24 H), 7.07-6.97 (m, 20 H), 6.87 (t, *J* = 7.3 Hz, 4 H), 3.94 (s, 16 H), 3.88 (AB q, *J* = 17.5 Hz, 16 H), 3.58 (m, 24 H), 3.28 (t, *J* = 7.3 Hz, 8 H), 2.58 (m, 24 H), 1.09 (m, 8 H), 0.58 (t, *J* = 7.3 Hz, 12 H); FTIR (CCl_4): ν 3061, 3032, 3010, 2958, 2925, 2873, 1459, 1216, 1128,

1094, 1033, 1012 cm^{-1}; MALDI-TOF MS: *m/z* ($M+Na^+$) 2308, calcd for $C_{148}H_{156}O_{22}Na$ 2308. No high-resolution mass spectrum can be obtained due to high molecular weight. No good elemental analysis data can be obtained. Similar cases have been reported in literature.[100,101] There are two possible and widely accepted explanations presented: (1) inclusion of solvent or atmospheric molecules in cavity-possessing compounds, and (2) incomplete combustion of the high-melting compounds under standardized conditions of the elemental analysis.

Pentameric Nanotube (18): A solution of 25, 26, 27, 28-tetrakis(2-*p*-toluene-sulfoxyethoxy)-calix[4]arene **26**[71] (50 mg, 0.041 mmol) and bis(1-propoxy)-bis(2-hydroxyethoxy)calix[4]tube **27** (95 mg, 0.082 mmol) in THF (25 mL) was added dropwise over 1 hr into a mixture of NaH (60% suspension in mineral oil, 13 mg, 0.33 mmol) and K_2CO_3 (22 mg, 0.16 mmol) in THF (100 mL) at reflux temperature. The mixture was further refluxed for 24 h, evaporated to dryness, suspended in CH_2Cl_2 (50 mL), and neutralized at 0°C with 5% HCl (25 mL). The organic layer was washed with water (2 x 5 mL), dried over Na_2SO_4, and then evaporated to dryness. The residue was treated with MeCN to produce pentacalix[4]tube **18** as a colorless solid. Yield 96 mg (82%); mp >300 °C (decomp.); ^1H NMR ($CDCl_3$):δ 7.20, 7.17 (2 x d, *J* = 7.0 Hz, 32 H), 7.09-6.98 (m, 24 H), 6.87 (t, *J* = 7.3 Hz, 4 H), 3.94 (s, 24 H), 3.93 (AB q, *J* = 16.9 Hz, 16 H), 3.62 (m, 32 H), 3.33 (t, J = 7.3 Hz, 8 H), 2.58 (m, 32 H), 1.11 (m, *J* = 7.3 Hz, 8 H), 0.58 (t, *J* = 7.3 Hz, 12 H); FTIR (CCl_4): ν 3063, 3033, 3016, 2958, 2926, 2874, 1459, 1217, 1128, 1094, 1033, 1010 cm^{-1}; MALDI-TOF MS: *m/z* ($M+Na^+$) 2872, calcd

for $C_{184}H_{192}O_{28}Na$ 2872. No high-resolution mass spectrum can be obtained due to high molecular weight. No good elemental analysis data can be obtained. Two possible and widely accepted explanations have been presented in literature: (1) inclusion of solvent or atmospheric molecules in cavity-possessing compounds, and (2) incomplete combustion of the high-melting compounds under standardized conditions of the elemental analysis.[100,101]

X-ray Crystallography: X-ray quality crystals of **15**, **16** and **31** were obtained from $CHCl_3$-CH_3OH solutions at room temperature. A suitable crystal of **15**, **16** or **31** covered with a layer of hydrocarbon oil was selected and mounted with Paratone-N oil on a Cryo-Loop, and immediately placed in the low-temperature nitrogen stream. The X-ray intensity data were measured at 100(2) K on a Bruker SMART APEX CCD area detector system equipped with a Oxford Cryosystems 700 Series cooler, a graphite monochromator, and a Mo K(fine-focus sealed tube (λ = 0.710 73 Å). The detector was placed at a distance of 5.995 cm from the crystal. The data frames were integrated with the Bruker SAINT-Plus (version 6.45) software package. Data were corrected for absorption effects using the multi-scan technique (SADABS). Structures were solved and refined using Bruker SHELXTL (Version 6.14) software package. Compound **15** crystallizes with two $CHCl_3$ molecules for each **15** moiety. Solution and refinement proceeded smoothly. Compound **16** crystallizes with 4.5 $CHCl_3$ molecules in the asymmetric unit. The $CHCl_3$ molecules show severe disorder. The intensity of high angle data suffers due to this disorder. It also causes significant difficulties during the

refinement stage. Nevertheless, a good data set was collected, and the various disorders were modeled well to bring the overall ~R1 = 8%. More importantly, nanotube **16** behaves well during the refinement and shows no ill effects as a result of $CHCl_3$ disorder. One of the *n*-propyl groups of **16** displays minor disorder which was modeled successfully. All the hydrogen atoms were also included during the refinement. For the x-ray data, see pages 143, 148 and 155.

General Procedure for the Preparation of Nitrosonium Complexes from NO_2/N_2O_4: In the NMR tube, NO_2/N_2O_4 gas was bubbled for 20 s through a solution of calix[4]tubes (~ 4 mM) and 2 equiv $SnCl_4$ (from 2.8 M stock solution) per calixarene unit in $(CDCl_2)_2$, and after homogenization the spectrum was recorded.

General Procedure for Titration Experiments: An aliquot from the stock solution of *t*-butyl nitrite (2.8 M) in $(CDCl_2)_2$ was added to the NMR tube containing solution of calix[4]tubes (~ 4 mM) and 2 equiv of $SnCl_4$ (from 2.8 M stock solution) per calixarene unit in $(CDCl_2)_2$ and after homogenization the spectrum was recorded. Additional aliquots of the nitrite were added and the spectrum was recorded after each addition. The concentration of complexes **33** and **34** were determined by integration of the aromatic CH protons and/or the OCH_2 methylene protons *vs.* the corresponding signals of free tubes **15** and **16**, respectively.

FTIR Spectroscopy: In a general procedure, each compound was dissolved in $(CHCl_2)_2$ at 4 x 10^{-3} M, followed by the addition of 2 equiv of $SnCl_4$ and 2 equiv of *t*-BuONO per calixarene unit. The spectra were recorded in solution, using a NaCl amalgamated sealed cell (1.0 mm) by co-addition of 20 scans, back and forward, at a resolution 4 cm^{-1}. For each measurement, the solvent was used for background.

Biscalix[4]tube-NO^+ Complex (33). ^{1}H NMR $(CDCl_2)_2$: δ 7. 36 (t, *J* = 7.5 Hz, 4H), 7.26 (d, *J* = 7.5 Hz, 8 H), 7.10 (d, *J* = 7.5 Hz, 8 H), 6.31 (t, *J* = 7.5Hz, 4 H), 4.24 (m, 8 H), 4.02 (m, 8 H), 3.87 (t, *J* = 7.5 Hz, 8 H), 3.83, 3.64 (2 x d, *J* = 14 Hz, 16 H), 1.9-1.8 (m, 8H), 1.08 (t, *J* = 7.5 Hz, 12 H); UV-vis $(CDCl_2)_2$: λ_{max} 525.0 nm; FTIR $(CDCl_2)_2$: ν 1958 cm^{-1} (NO^+).

Triscalix[4]tube-NO^+ Complex (34). ^{1}H NMR $(CDCl_2)_2$: δ 7.35 (m, 20H), 7.11 (d, *J* = 7.3 Hz, 8H), 6.50 (t, *J* = 7.3 Hz, 4H), 6.47 (t, *J* = 7.3 Hz, 4H), 4.30 (m, 16H), 4.06 (m, 16H), 3.86 (m, 24H), 3.66 (d, *J* = 14, 8H), 1.92-1.86 (m, 8H), 1.08 (t, *J* = 7.3 Hz, 12H); UV-vis $(CDCl_2)_2$: λ_{max} 524.1 nm; FTIR $(CDCl_2)_2$: ν 1958, 1940 cm^{-1} (NO^+).

Tetracalix[4]tube-NO^+ Complex (35): ^{1}H NMR $(CDCl_2)_2$: δ 7.41-7.09 (m, 36H), 6.62-6.56 (m, 8H), 6.42 (t, *J* = 7.5 Hz, 4H), 4.27 (m, 24H), 4.05 (m, 24H), 3.87 (m, 34H), 3.67 (d, *J* = 15.4 Hz, 8H), 1.91 (m, *J* = 7.3 Hz, 8H), 1.08 (t, *J* = 7.3 Hz, 12H); UV-vis $(CDCl_2)_2$: λ_{max} 526.0 nm; FTIR $(CDCl_2)_2$: ν 1958, 1940 cm^{-1} (NO^+).

Pentacalix[4]tube-NO^+ Complex (36): ^1H NMR $(CDCl_2)_2$: δ 7.41-7.08 (m, 44H), 6.67-6.55 (m, 12H), 6.43 (t, *J* = 7.5 Hz, 4H), 4.27-3.63 (m, 112H), 1.94 (m, *J* = 7.5 Hz, 8H), 1.08 (t, *J* = 7.5 Hz, 12H); UV-vis $(CDCl_2)_2$: λ_{max} 518.9 nm; FTIR $(CDCl_2)_2$: ν 1958, 1940 cm^{-1} (NO^+).

APPENDIX 1

^{1}H and ^{13}C NMR SPECTRA OF 25,27-BIS(1-PROPYLOXY)-26,28-BIS(2-*TERT*-BUTYLDIMETHYLSILOXY)ETHYLOXY)CALIX[4]ARENE, *1,3-ALTERNATE* (21)

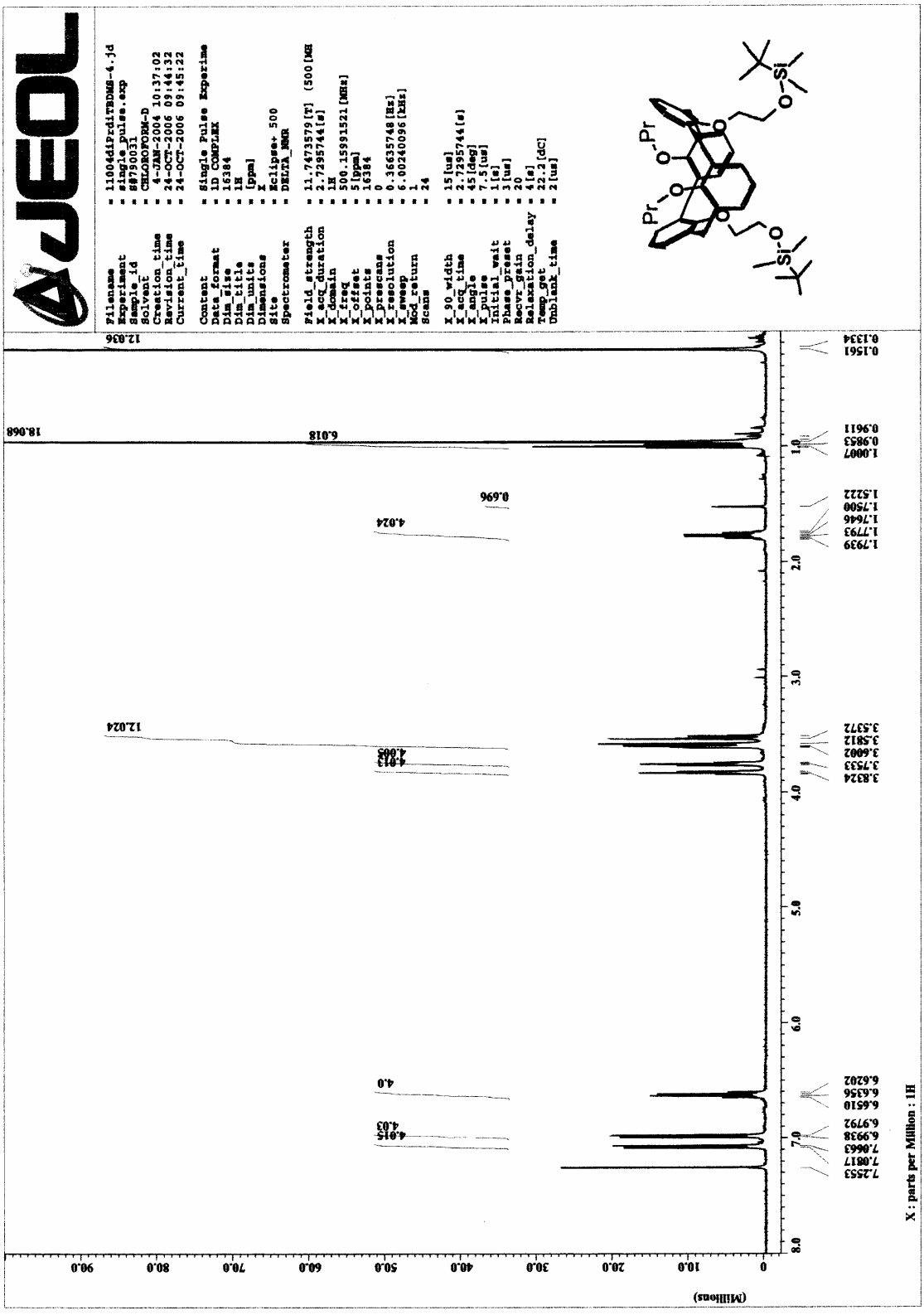
JEOL
Filename = 110044iPrdiTBDMS-4.jd
Experiment = single_pulse.exp
Sample_id = #8790037
Solvent = CHLOROFORM-D
Creation_time = 4-JAN-2006 10:37:02
Revision_time = 24-OCT-2006 09:44:32
Current_time = 24-OCT-2006 09:45:22
Content = Single Pulse Experime
Data_format = 1D COMPLEX
Dim_size = 16384
Dim_title = 1H
Dim_units = [ppm]
Dimensions = X
Site = Eclipse+ 500
Spectrometer = DELTA_NMR
Field_strength = 11.7473579[T] (500[MH
X_acq_duration = 2.7295744[s]
X_domain = 1H
X_freq = 500.15991521[MHz]
X_offset = 5[ppm]
X_points = 16384
X_prescans = 0
X_resolution = 0.36635748[Hz]
X_sweep = 6.00240096[kHz]
Mod_return = 1
Scans = 24
X_90_width = 15[us]
X_acq_time = 2.7295744[s]
X_angle = 45[deg]
X_pulse = 7.5[us]
Initial_wait = 1[s]
Phase_preset = 3[us]
Recvr_gain = 20
Relaxation_delay = 4[s]
Temp_get = 22.2[dC]
Unblank_time = 2[us]
Pr
O
Si
12.036
18.068
6.018
0.696
4.024
12.024
4.0
4.03
7.2553
7.0817
7.0663
6.9938
6.9792
6.6510
6.6356
6.6202
3.8324
3.7533
3.6002
3.5812
3.5372
1.7939
1.7793
1.7646
1.7500
1.5222
1.0007
0.9853
0.9611
0.1561
0.1334
(Millions)
X : parts per Million : 1H

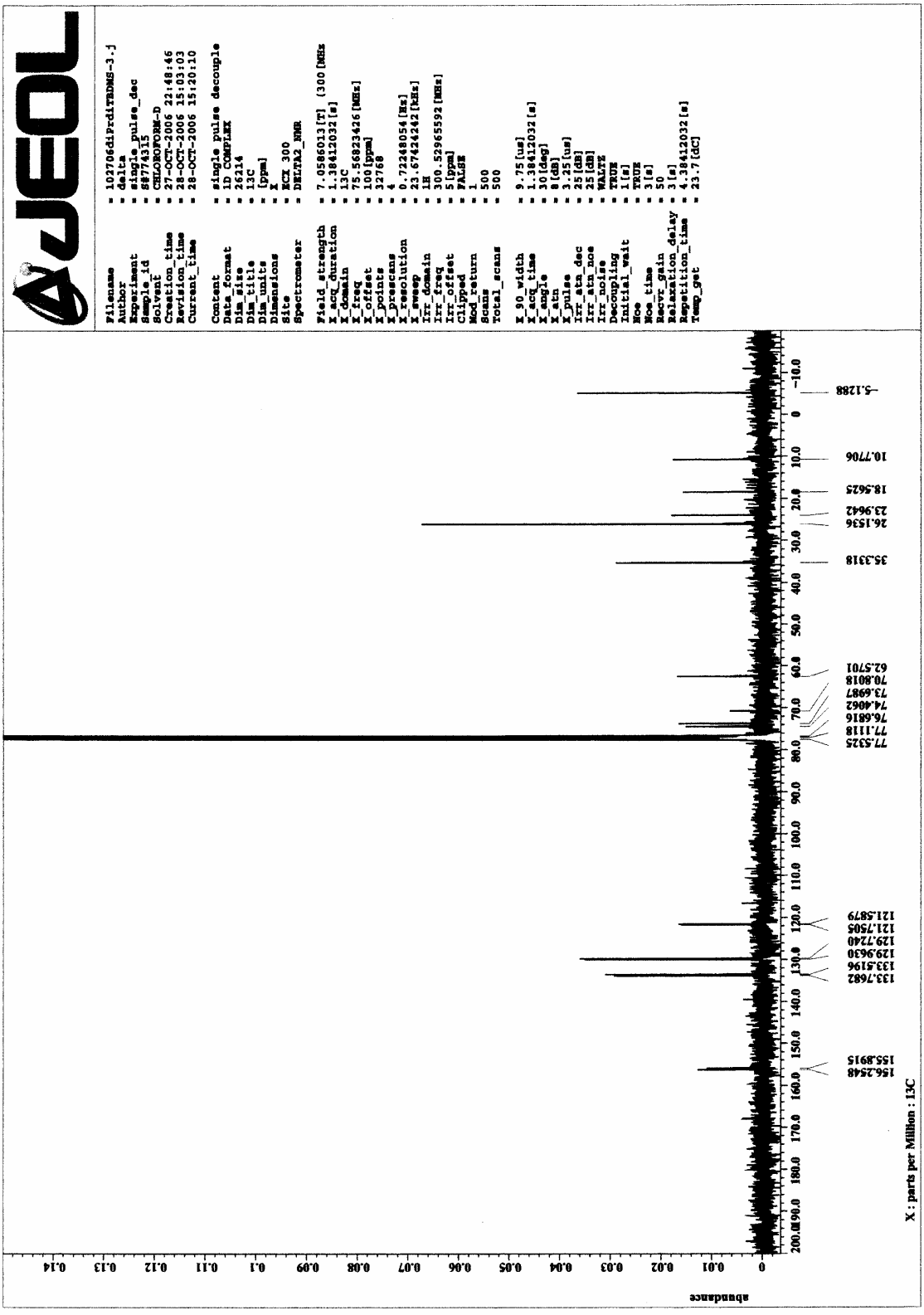
JEOL
Filename = 102706d1PrdiTBDMS-3.j
Author = delta
Experiment = single_pulse_dec
Sample_id = SH774315
Solvent = CHLOROFORM-D
Creation_time = 27-OCT-2006 22:48:46
Revision_time = 28-OCT-2006 15:03:03
Current_time = 28-OCT-2006 15:20:10
Content = single pulse decouple
Data_format = 1D COMPLEX
Dim_size = 26214
Dim_title = 13C
Dim_units = [ppm]
Dimensions = X
Site = ECX 300
Spectrometer = DELTA2_NMR
Field_strength = 7.0586013[T] (300[MHz
X_acq_duration = 1.38412032[s]
X_domain = 13C
X_freq = 75.56823426[MHz]
X_offset = 100[ppm]
X_points = 32768
X_prescans = 4
X_resolution = 0.72248054[Hz]
X_sweep = 23.67424242[kHz]
Irr_domain = 1H
Irr_freq = 300.52965592[MHz]
Irr_offset = 5[ppm]
Clipped = FALSE
Mod_return = 1
Scans = 500
Total_scans = 500
X_90_width = 9.75[us]
X_acq_time = 1.38412032[s]
X_angle = 30[deg]
X_atn = 0[dB]
X_pulse = 3.25[us]
Irr_atn_dec = 25[dB]
Irr_atn_noe = 25[dB]
Irr_noise = WALTZ
Decoupling = TRUE
Initial_wait = 1[s]
Noe = TRUE
Noe_time = 3[s]
Recvr_gain = 50
Relaxation_delay = 3[s]
Repetition_time = 4.38412032[s]
Temp_get = 23.7[dC]
abundance
X : parts per Million : 13C
-5.1288
10.7706
18.5625
23.9642
26.1536
35.3318
62.5701
70.8018
73.6987
74.4062
76.6816
77.1118
77.5325
121.5879
121.7505
129.7240
129.9630
133.5196
133.7682
155.8915
156.2548

APPENDIX 2

^{1}H NMR SPECTRUM OF 25,27-BIS(2-HYDROXYETHYLOXY)-26,28-BIS(1-PROPYLOXY)CALIX[4]ARENE, *1,3-ALTERNATE* (22)

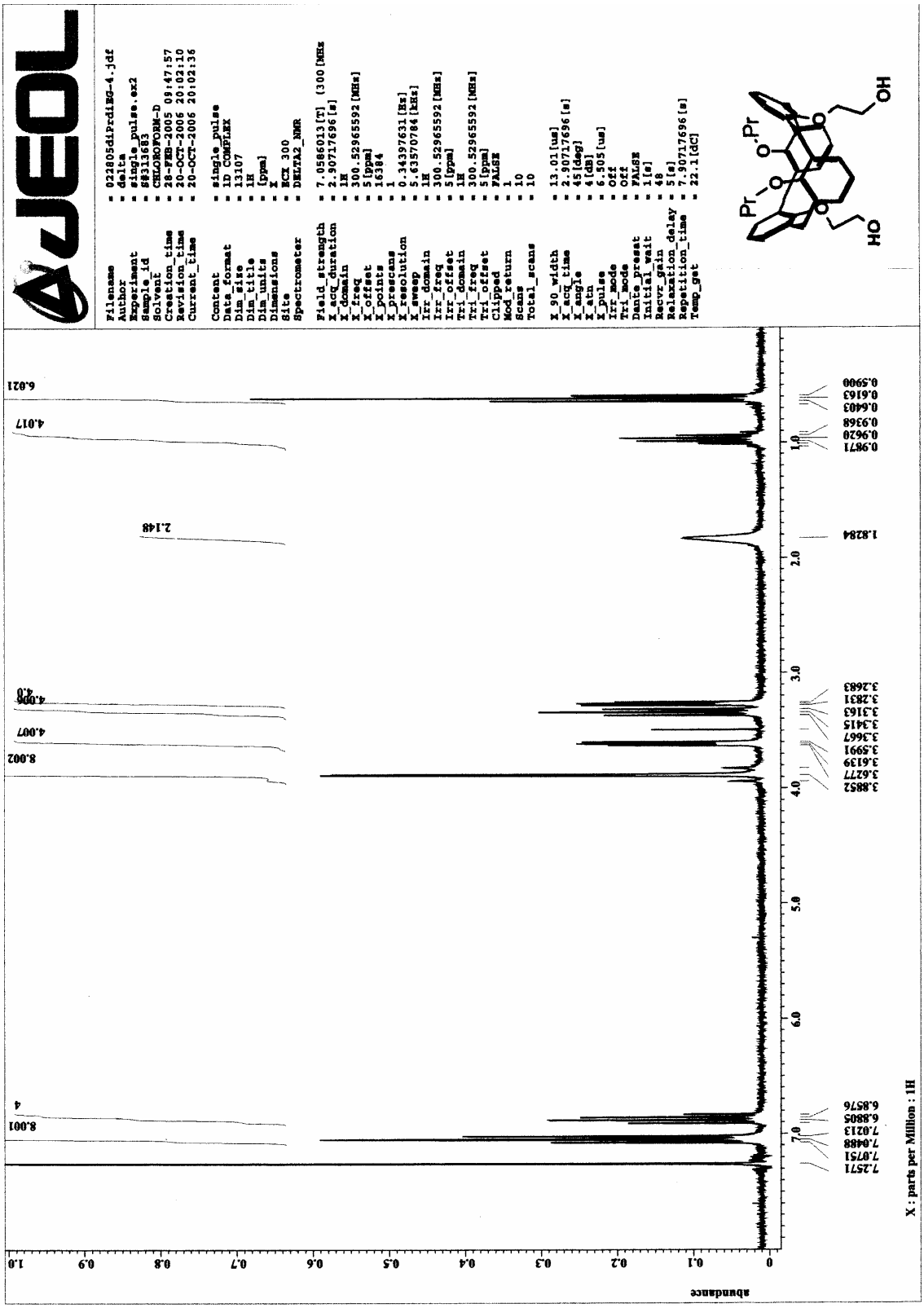
JEOL
Filename = 022805diPrdiEG-4.jdf
Author = delta
Experiment = single_pulse.ex2
Sample_id = #8313683
Solvent = CHLOROFORM-D
Creation_time = 28-FEB-2005 09:47:57
Revision_time = 20-OCT-2006 20:02:10
Current_time = 20-OCT-2006 20:02:36
Content = single_pulse
Data_format = 1D COMPLEX
Dim_size = 13107
Dim_title = 1H
Dim_units = [ppm]
Dimensions = X
Site = NCH 300
Spectrometer = DELTA2_NMR
Field_strength = 7.0566013[T] (300[MHz
X_acq_duration = 2.90717696[s]
X_domain = 1H
X_freq = 300.52965592[MHz]
X_offset = 5[ppm]
X_points = 16384
X_prescans = 1
X_resolution = 0.34397631[Hz]
X_sweep = 5.63570784[kHz]
Irr_domain = 1H
Irr_freq = 300.52965592[MHz]
Irr_offset = 5[ppm]
Tri_domain = 1H
Tri_freq = 300.52965592[MHz]
Tri_offset = 5[ppm]
Clipped = FALSE
Mod_return = 1
Scans = 10
Total_scans = 10
X_90_width = 13.01[us]
X_acq_time = 2.90717696[s]
X_angle = 45[deg]
X_atn = 4[dB]
X_pulse = 6.505[us]
Irr_mode = Off
Tri_mode = Off
Dante_presat = FALSE
Initial_wait = 1[s]
Recvr_gain = 48
Relaxation_delay = 5[s]
Repetition_time = 7.90717696[s]
Temp_get = 22.1[dC]
OH
HO
Pr
Pr
O
O
O
O
8.001
4
8.002
4.007
4.005
4.0
4.017
6.021
2.148
7.2571
7.0751
7.0488
7.0213
6.8805
6.8576
3.8852
3.6277
3.6139
3.5991
3.3667
3.3415
3.3163
3.2831
3.2683
1.8284
0.9871
0.9620
0.9368
0.6403
0.6163
0.5900
abundance
X : parts per Million : 1H

APPENDIX 3

^{1}H NMR SPECTRUM OF 25,27-BIS(2-*P*-TOLUENESULFONYLOXYETHYLOXY)-26,28-BIS(1-PROPYLOXY)CALIX[4]ARENE, *1,3-ALTERNATE* (23)

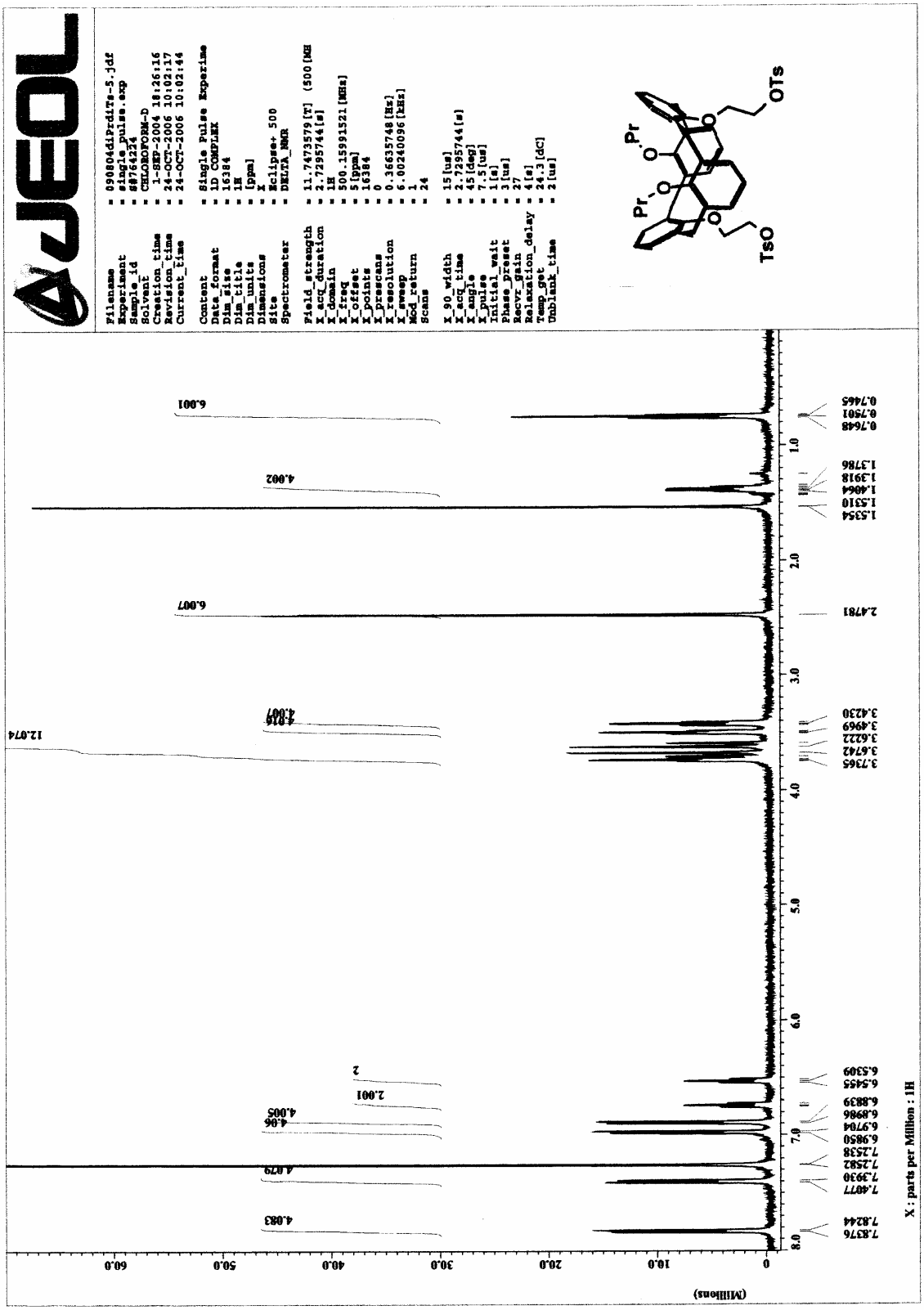
JEOL
Filename = 090804diPrdiTs-5.jdf
Experiment = #single_pulse.exp
Sample_id = ##764224
Solvent = CHLOROFORM-D
Creation_time = 1--SEP-2004 18:26:16
Revision_time = 24-OCT-2006 10:02:17
Current_time = 24-OCT-2006 10:02:44
Content = #Single Pulse Experime
Date_format = 1D COMPLEX
Dim_size = 16384
Dim_title = 1H
Dim_units = [ppm]
Site = X
Spectrometer = Eclipse+ 500
DELTA_NMR
Field_strength = 11.74733579[T] (500[MH
X_acq_duration = 2.72955744[s]
X_domain = 1H
X_freq = 500.15991521[MHz]
X_offset = 5[ppm]
X_points = 16384
X_prescans = 0
X_resolution = 0.36635748[Hz]
X_sweep = 6.00240096[kHz]
Mod_return = 1
Scans = 24
X_90_width = 15[us]
X_acq_time = 2.72955744[s]
X_angle = 45[deg]
X_pulse = 7.5[us]
Initial_wait = 1[s]
Phase_preset = 3[us]
Recvr_gain = 27
Relaxation_delay = 4[s]
Temp_get = 24.3[dC]
Unblank_time = 2[us]
Pr
Pr
OTs
TsO
12.074
6.001
4.002
6.007
4.010
4.007
2.001
2
4.083
4.079
4.06
4.005
7.8376
7.8244
7.4077
7.3930
7.2582
7.2538
6.9850
6.9704
6.8986
6.8839
6.5455
6.5309
0.7648
0.7501
0.7465
1.5354
1.5310
1.4064
1.3918
1.3786
2.4781
3.7365
3.6742
3.6222
3.4969
3.4230
(Million)
X : parts per Million : 1H

APPENDIX 4

^{1}H NMR SPECTRUM OF 25,26,27,28-TETRAKIS[(ETHOXYCARBONYL)METHOXY]CALIX[4]ARENE, *1,3-ALTERNATE* (24)

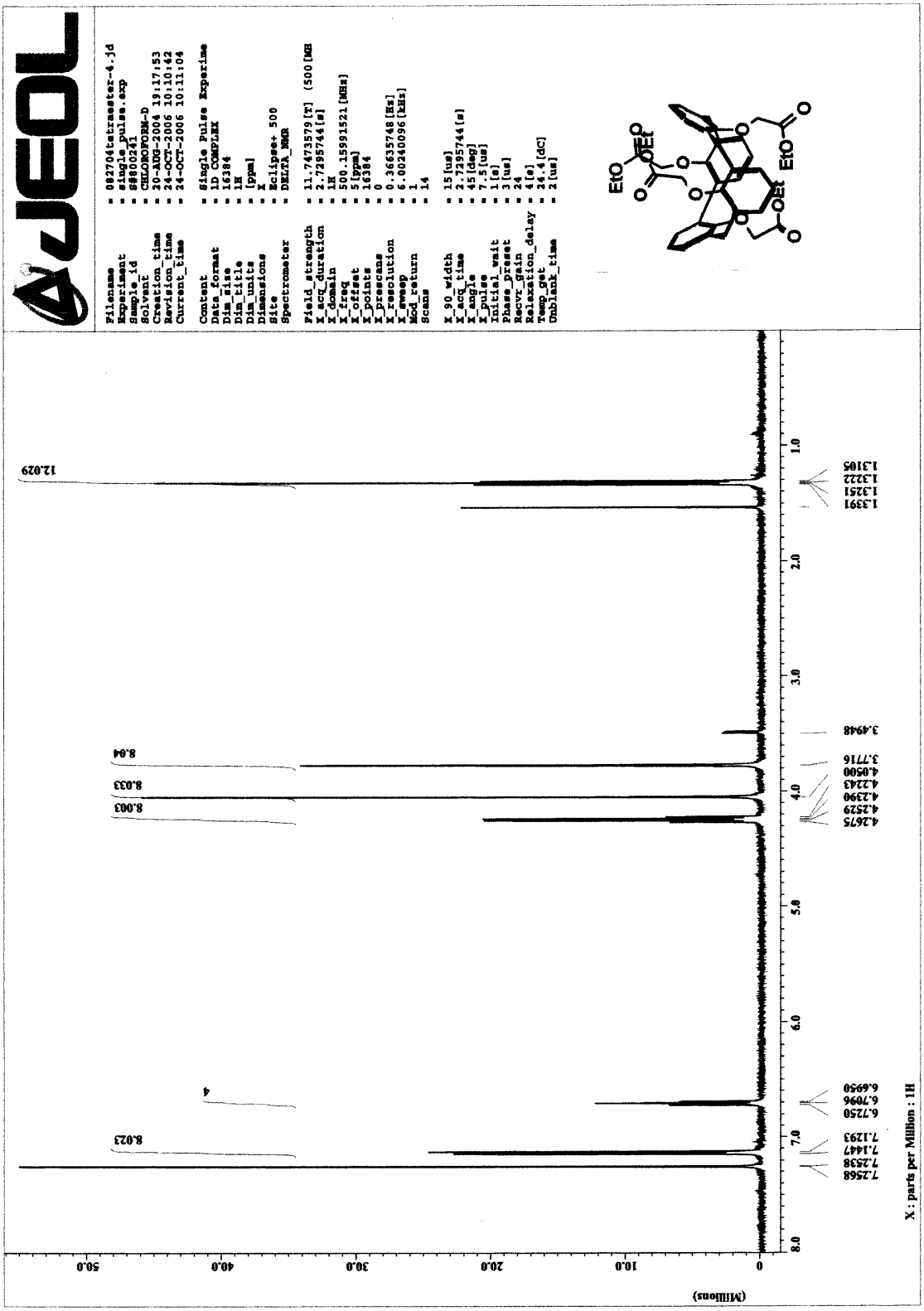
JEOL
Filename = 082704tetraester-4.jd
Experiment = single_pulse.exp
Sample_id = ##800241
Solvent = CHLOROFORM-D
Creation_time = 20-AUG-2004 13:17:53
Revision_time = 24-OCT-2006 10:10:42
Current_time = 24-OCT-2006 10:11:04
Content = Single Pulse Experime
Data_format = 1D COMPLEX
Dim_size = 16384
Dim_title = 1H
Dim_units = [ppm]
Dimensions = X
Site = Eclipse+ 500
Spectrometer = DELTA_NMR
Field_strength = 11.7473579[T] (500[MH
X_acq_duration = 2.7295744[s]
X_domain = 1H
X_freq = 500.15991521[MHz]
X_offset = 5[ppm]
X_points = 16384
X_prescans = 0
X_resolution = 0.36635748[Hz]
X_sweep = 6.00240096[kHz]
Mod_return = 1
Scans = 14
X_90_width = 15[us]
X_acq_time = 2.7295744[s]
X_angle = 45[deg]
X_pulse = 7.5[us]
Initial_wait = 1[s]
Phase_preset = 3[us]
Recvr_gain = 24
Relaxation_delay = 4[s]
Temp_get = 24.4[dC]
Unblank_time = 2[us]
EtO
OEt
EtO
OEt
12.029
8.023
8.003
8.033
8.04
4
7.2568
7.2538
7.1447
7.1293
6.7250
6.7096
6.6950
4.2675
4.2529
4.2390
4.2243
4.0500
3.7716
3.4948
1.3391
1.3251
1.3222
1.3105
(Millions)
X : parts per Million : 1H

APPENDIX 5

^{1}H AND ^{13}C NMR SPECTRA OF 25,26,27,28-TETRAKIS(2-HYDROXYETHYLOXY)CALIX[4]ARENE, *1,3-ALTERNATE* (25)

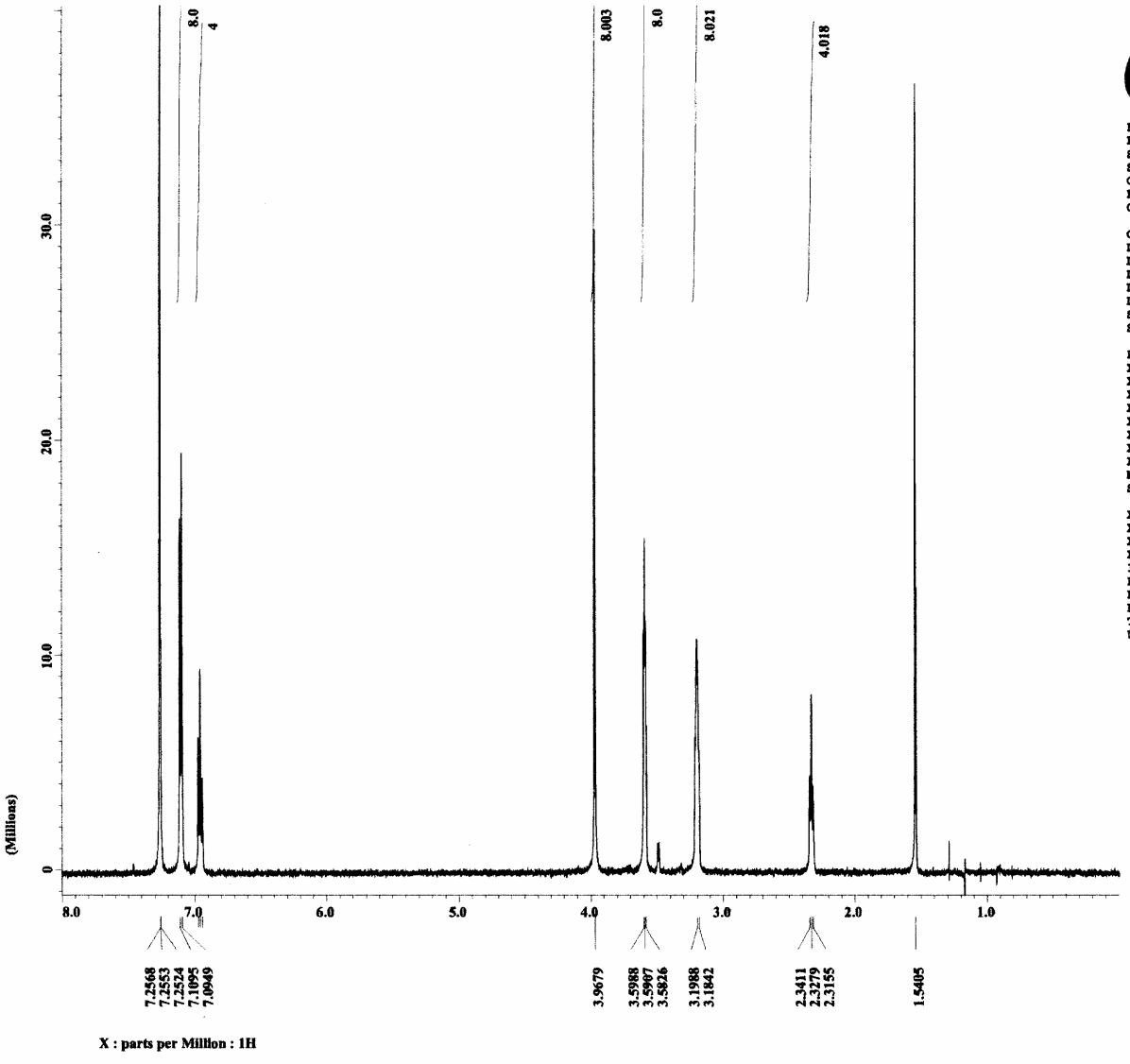

JEOL

Filename	= 082404tetraEG-4.jdf
Experiment	= single_pulse.exp
Sample_id	= S#164839
Solvent	= CHLOROFORM-D
Creation_time	= 18-AUG-2004 01:36:59
Revision_time	= 19-OCT-2006 14:01:30
Current_time	= 19-OCT-2006 14:01:47
Content	= Single Pulse Experime
Data_format	= 1D COMPLEX
Dim_size	= 16384
Dim_title	= 1H
Dim_units	= [ppm]
Dimensions	= X
Site	= Eclipse+ 500
Spectrometer	= DELTA_NMR
Field_strength	= 11.7473579[T] (500[MH
X_acq_duration	= 2.7295744[s]
X_domain	= 1H
X_freq	= 500.15991521[MHz]
X_offset	= 5[ppm]
X_points	= 16384
X_prescans	= 0
X_resolution	= 0.36635748[Hz]
X_sweep	= 6.00240096[kHz]
Mod_return	= 1
Scans	= 13
X_90_width	= 15[us]
X_acq_time	= 2.7295744[s]
X_angle	= 45[deg]
X_pulse	= 7.5[us]
Initial_wait	= 1[s]
Phase_preset	= 3[us]
Recvr_gain	= 27
Relaxation_delay	= 4[s]
Temp_get	= 23.9[dC]
Unblank_time	= 2[us]

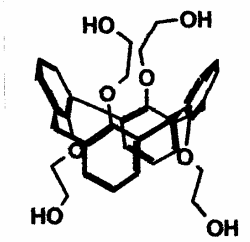

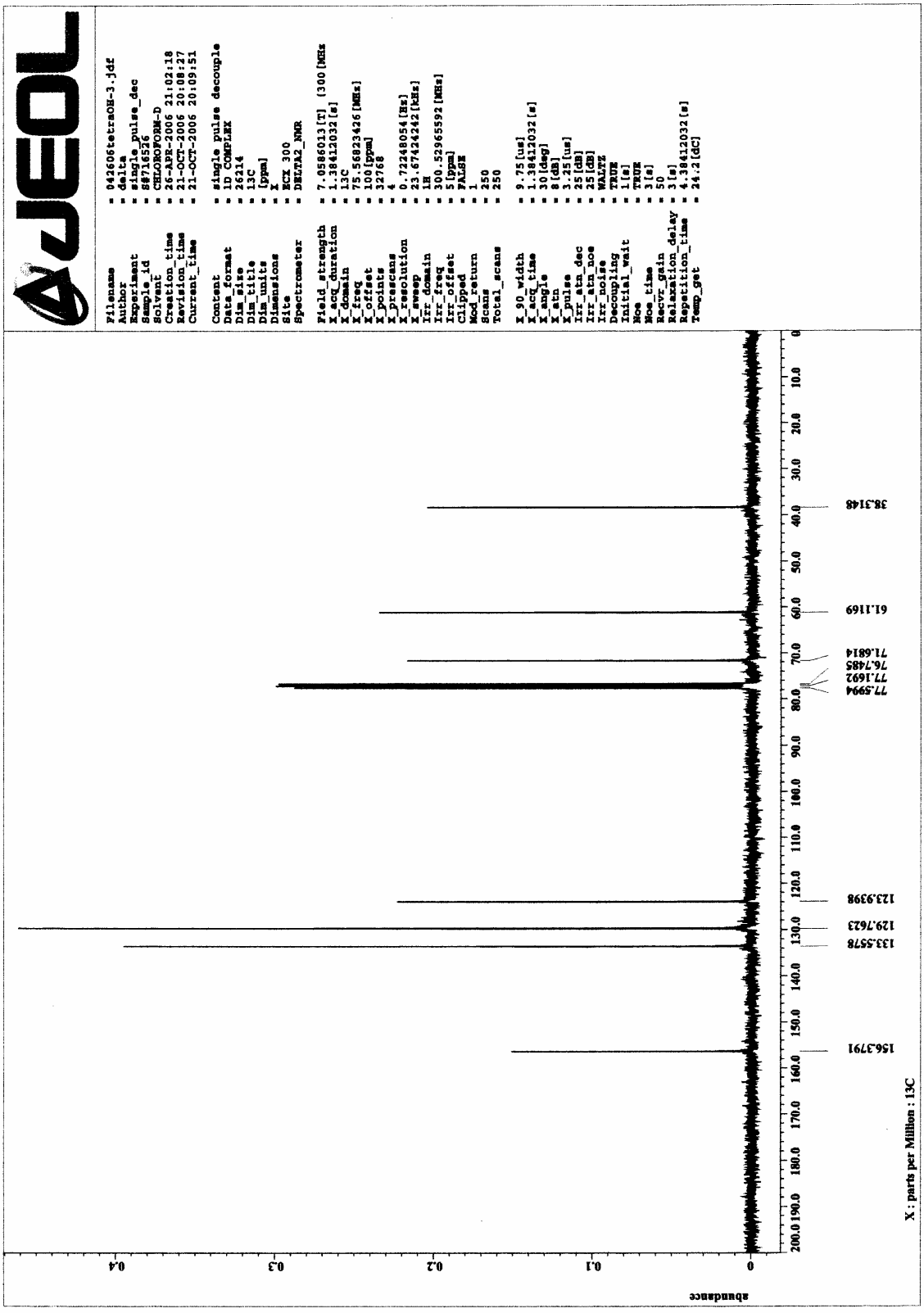
JEOL
Filename = 042606tetraOH-3.jdf
Author = delta
Experiment = single_pulse_dec
Sample_id = S#716526
Solvent = CHLOROFORM-D
Creation_time = 26-APR-2006 21:02:18
Revision_time = 21-OCT-2006 20:08:27
Current_time = 21-OCT-2006 20:09:51
Content = single pulse decouple
Data_format = 1D COMPLEX
Dim_size = 26214
Dim_title = 13C
Dim_units = [ppm]
Dimensions = X
Site = ECX 300
Spectrometer = DELTA2_NMR
Field_strength = 7.0586013[T] (300[MHz
X_acq_duration = 1.38412032[s]
X_domain = 13C
X_freq = 75.56823426[MHz]
X_offset = 100[ppm]
X_points = 32768
X_prescans = 4
X_resolution = 0.72248054[Hz]
X_sweep = 23.67424242[kHz]
Irr_domain = H
Irr_freq = 300.52965592[MHz]
Irr_offset = 5[ppm]
Clipped = FALSE
Mod_return = 1
Scans = 250
Total_scans = 250
X_90_width = 9.75[us]
X_acq_time = 1.38412032[s]
X_angle = 30[deg]
X_atn = 8[dB]
X_pulse = 3.25[us]
Irr_atn_dec = 25[dB]
Irr_atn_noe = 25[dB]
Irr_noise = WALTZ
Decoupling = TRUE
Initial_wait = 1[s]
Noe = TRUE
Noe_time = 3[s]
Recvr_gain = 50
Relaxation_delay = 3[s]
Repetition_time = 4.38412032[s]
Temp_get = 24.2[dC]
abundance
X : parts per Million : 13C
156.3791
133.5578
129.7623
123.9398
77.5994
77.1692
76.7485
71.6814
61.1169
38.3148

APPENDIX 6

^{1}H AND ^{13}C NMR SPECTRA OF 25,26,27,28-TETRAKIS(2-*P*-TOLUENESULFOXYETHOXY)CALIX[4]ARENE, *1,3-ALTERNATE* (26)

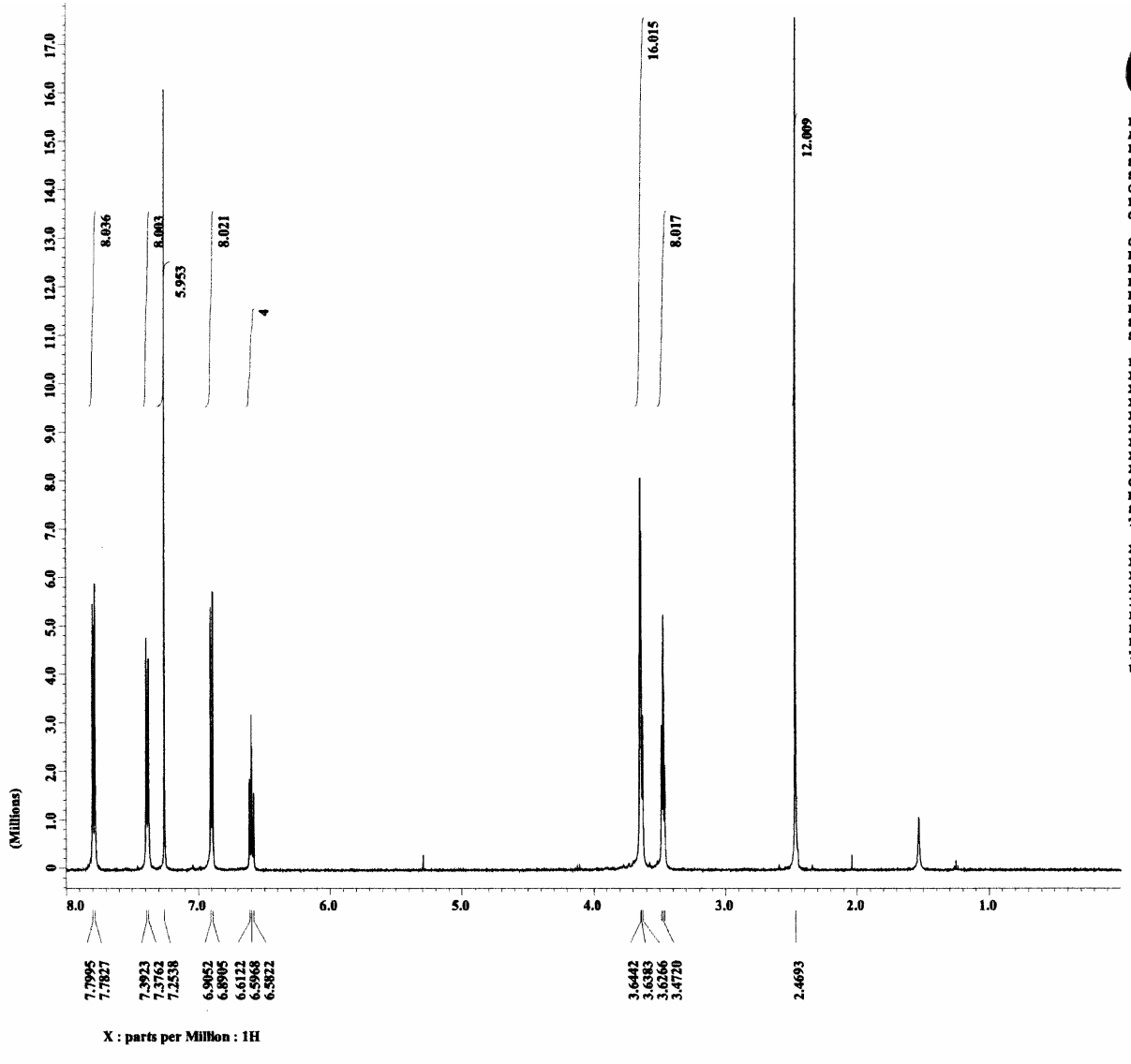

JEOL

```
Filename          = 021005tetraTs-4.jdf
Author            = delta
Experiment        = single_pulse.exp
Sample_id         = S#579331
Solvent           = CHLOROFORM-D
Creation_time     = 26-DEC-2004 22:28:01
Revision_time     = 19-OCT-2006 22:58:07
Current_time      = 19-OCT-2006 22:58:36

Content           = Single Pulse Experime
Data_format       = 1D COMPLEX
Dim_size          = 16384
Dim_title         = 1H
Dim_units         = [ppm]
Dimensions        = X
Site              = Eclipse+ 500
Spectrometer      = DELTA_NMR

Field_strength    = 11.7473579[T]  (500[MH
X_acq_duration    = 2.7295744[s]
X_domain          = 1H
X_freq            = 500.15991521[MHz]
X_offset          = 5[ppm]
X_points          = 16384
X_prescans        = 0
X_resolution      = 0.36635748[Hz]
X_sweep           = 6.00240096[kHz]
Clipped           = FALSE
Mod_return        = 1
Scans             = 16
Total_scans       = 16

X_90_width        = 18.5[us]
X_acq_time        = 2.7295744[s]
X_angle           = 45[deg]
X_pulse           = 9.25[us]
Initial_wait      = 1[s]
Phase_preset      = 3[us]
Recvr_gain        = 23
Relaxation_delay  = 4[s]
Temp_get          = 25.6[dC]
Unblank_time      = 2[us]
```

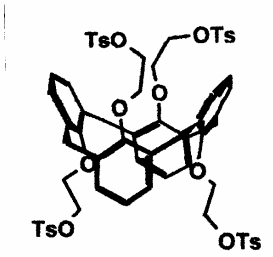

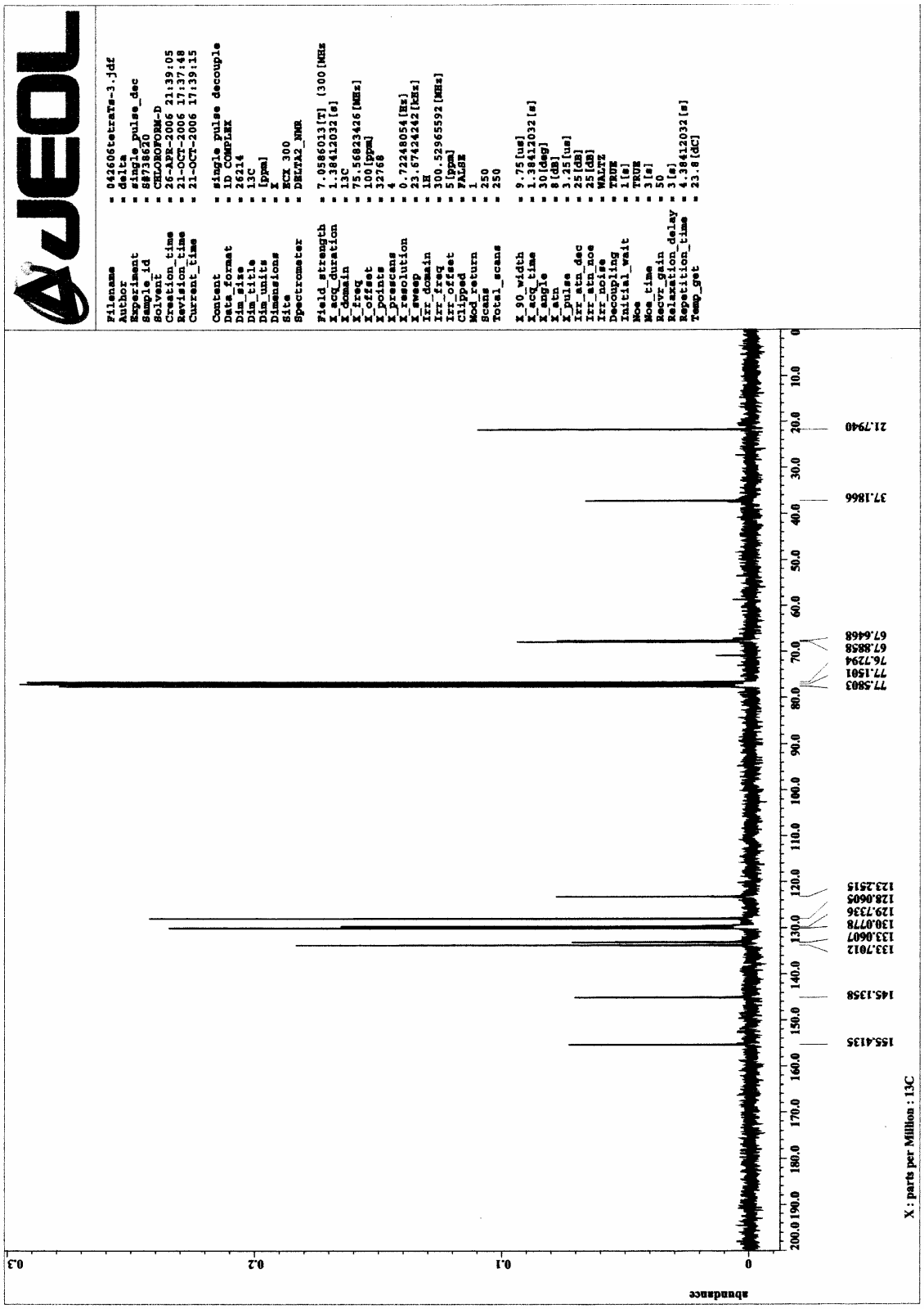
JEOL
Filename = 042606tetraTs-3.jdf
Author = delta
Experiment = single_pulse_dec
Sample_id = $#738620
Solvent = CHLOROFORM-D
Creation_time = 26-APR-2006 21:39:05
Revision_time = 21-OCT-2006 17:37:48
Current_time = 21-OCT-2006 17:39:15
Content = single pulse decouple
Data_format = 1D COMPLEX
Dim_size = 26214
Dim_title = 13C
Dim_units = [ppm]
Dimensions = X
Site = ECX 300
Spectrometer = DELTA2_NMR
Field_strength = 7.05860131[T] (300[MHz
X_acq_duration = 1.38412032[s]
X_domain = 13C
X_freq = 75.56823426[MHz]
X_offset = 100[ppm]
X_points = 32768
X_prescans = 4
X_resolution = 0.72248054[Hz]
X_sweep = 23.67424242[kHz]
Irr_domain = 1H
Irr_freq = 300.52965592[MHz]
Irr_offset = 5[ppm]
Clipped = FALSE
Mod_return = 1
Scans = 250
Total_scans = 250
X_90_width = 9.75[us]
X_acq_time = 1.38412032[s]
X_angle = 30[deg]
X_atn = 8[dB]
X_pulse = 3.25[us]
Irr_atn_dec = 25[dB]
Irr_atn_noe = 25[dB]
Irr_noise = WALTZ
Decoupling = TRUE
Initial_wait = 1[s]
Noe = TRUE
Noe_time = 3[s]
Recvr_gain = 50
Relaxation_delay = 3[s]
Repetition_time = 4.38412032[s]
Temp_get = 23.8[dC]
abundance
X : parts per Million : 13C
155.4135
145.1358
133.7012
133.0607
130.0778
129.7336
128.0605
123.2515
77.5803
77.1501
76.7294
67.8858
67.6468
37.1866
21.7940

APPENDIX 7

^{1}H AND ^{13}C NMR SPECTRA OF
25,27-BIS[(2-BENZYLOXY)ETHYLOXY]-26,28-DIHYDROXYCALIX[4]ARENE,
CONE (29)

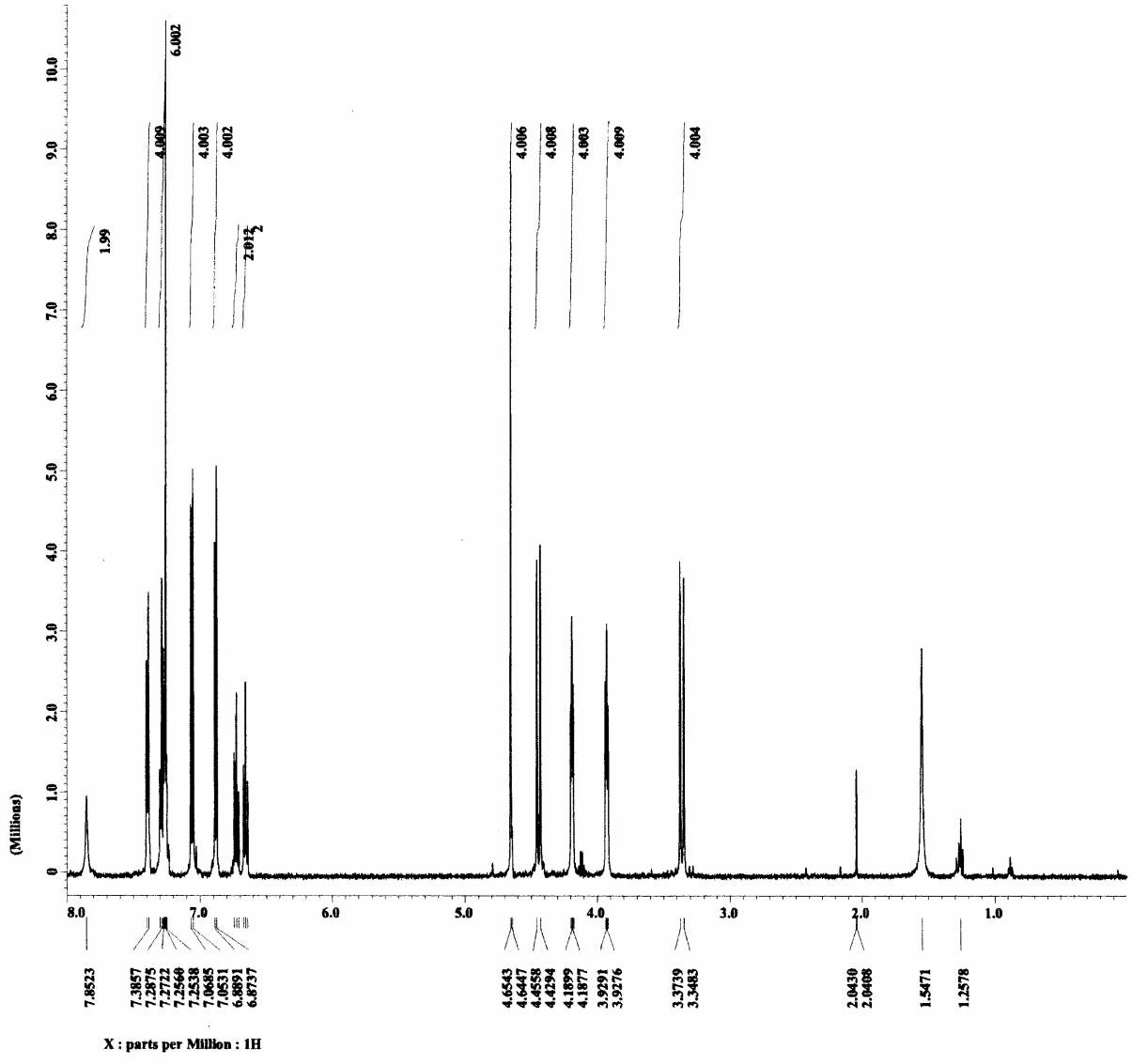

JEOL

```
Filename          = 051805spleA-2.jdf
Author            = delta
Experiment        = single_pulse.exp
Sample_id         = S@538033
Solvent           = CHLOROFORM-D
Creation_time     =  2-APR-2005 21:11:40
Revision_time     = 19-OCT-2006 23:16:55
Current_time      = 19-OCT-2006 23:17:13

Content           = Single Pulse Experime
Data_format       = 1D COMPLEX
Dim_size          = 16384
Dim_title         = 1H
Dim_units         = [ppm]
Dimensions        = X
Site              = Eclipse+ 500
Spectrometer      = DELTA_NMR

Field_strength    = 11.7473579[T]  (500[MH
X_acq_duration    = 2.7295744[s]
X_domain          = 1H
X_freq            = 500.15991521[MHz]
X_offset          = 5[ppm]
X_points          = 16384
X_prescans        = 0
X_resolution      = 0.36635748[Hz]
X_sweep           = 6.00240096[kHz]
Clipped           = FALSE
Mod_return        = 1
Scans             = 6
Total_scans       = 6

X_90_width        = 18.5[us]
X_acq_time        = 2.7295744[s]
X_angle           = 45[deg]
X_pulse           = 9.25[us]
Initial_wait      = 1[s]
Phase_preset      = 3[us]
Recvr_gain        = 22
Relaxation_delay  = 4[s]
Temp_get          = 26.2[dC]
Unblank_time      = 2[us]
```

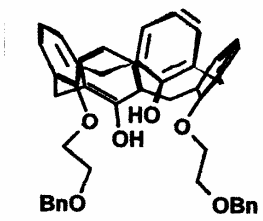

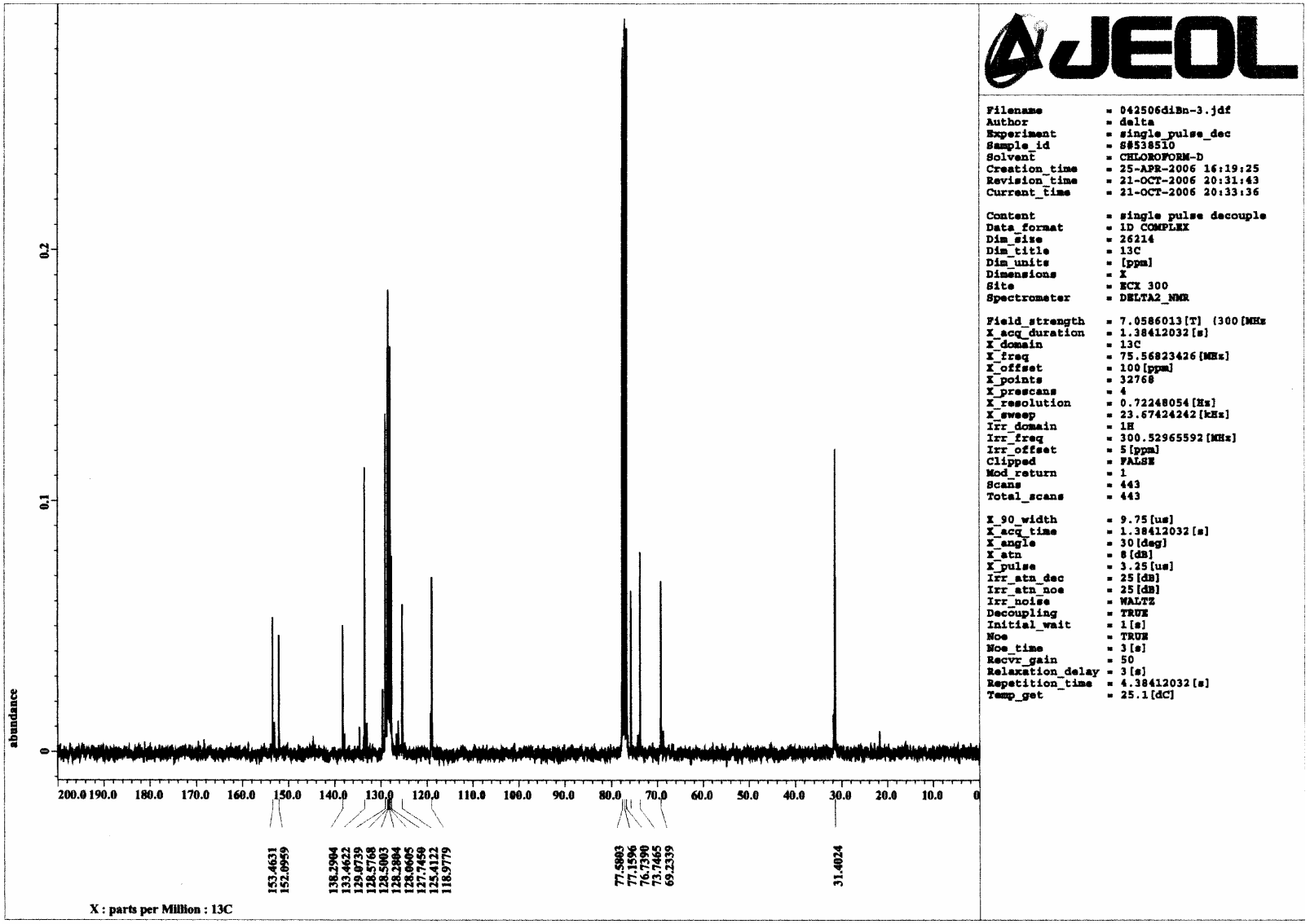

JEOL

Filename	= 042506diBn-3.jdf
Author	= delta
Experiment	= single_pulse_dec
Sample_id	= S#538510
Solvent	= CHLOROFORM-D
Creation_time	= 25-APR-2006 16:19:25
Revision_time	= 21-OCT-2006 20:31:43
Current_time	= 21-OCT-2006 20:33:36
Content	= single pulse decouple
Data_format	= 1D COMPLEX
Dim_size	= 26214
Dim_title	= 13C
Dim_units	= [ppm]
Dimensions	= X
Site	= ECX 300
Spectrometer	= DELTA2_NMR
Field_strength	= 7.0586013[T] (300[MHz
X_acq_duration	= 1.38412032[s]
X_domain	= 13C
X_freq	= 75.56823426[MHz]
X_offset	= 100[ppm]
X_points	= 32768
X_prescans	= 4
X_resolution	= 0.72248054[Hz]
X_sweep	= 23.67424242[kHz]
Irr_domain	= 1H
Irr_freq	= 300.52965592[MHz]
Irr_offset	= 5[ppm]
Clipped	= FALSE
Mod_return	= 1
Scans	= 443
Total_scans	= 443
X_90_width	= 9.75[us]
X_acq_time	= 1.38412032[s]
X_angle	= 30[deg]
X_atn	= 8[dB]
X_pulse	= 3.25[us]
Irr_atn_dec	= 25[dB]
Irr_atn_noe	= 25[dB]
Irr_noise	= WALTZ
Decoupling	= TRUE
Initial_wait	= 1[s]
Noe	= TRUE
Noe_time	= 3[s]
Recvr_gain	= 50
Relaxation_delay	= 3[s]
Repetition_time	= 4.38412032[s]
Temp_get	= 25.1[dC]

APPENDIX 8

^{1}H and ^{13}C NMR SPECTRA OF
25,27-BIS[(2-BENZYLOXY)ETHYLOXY]-26,28-BIS(2-*TERT*-BUTYLDIMETHYLSILOXY)ETHYLOXY)CALIX[4]ARENE,
1,3-ALTERNATE (30)

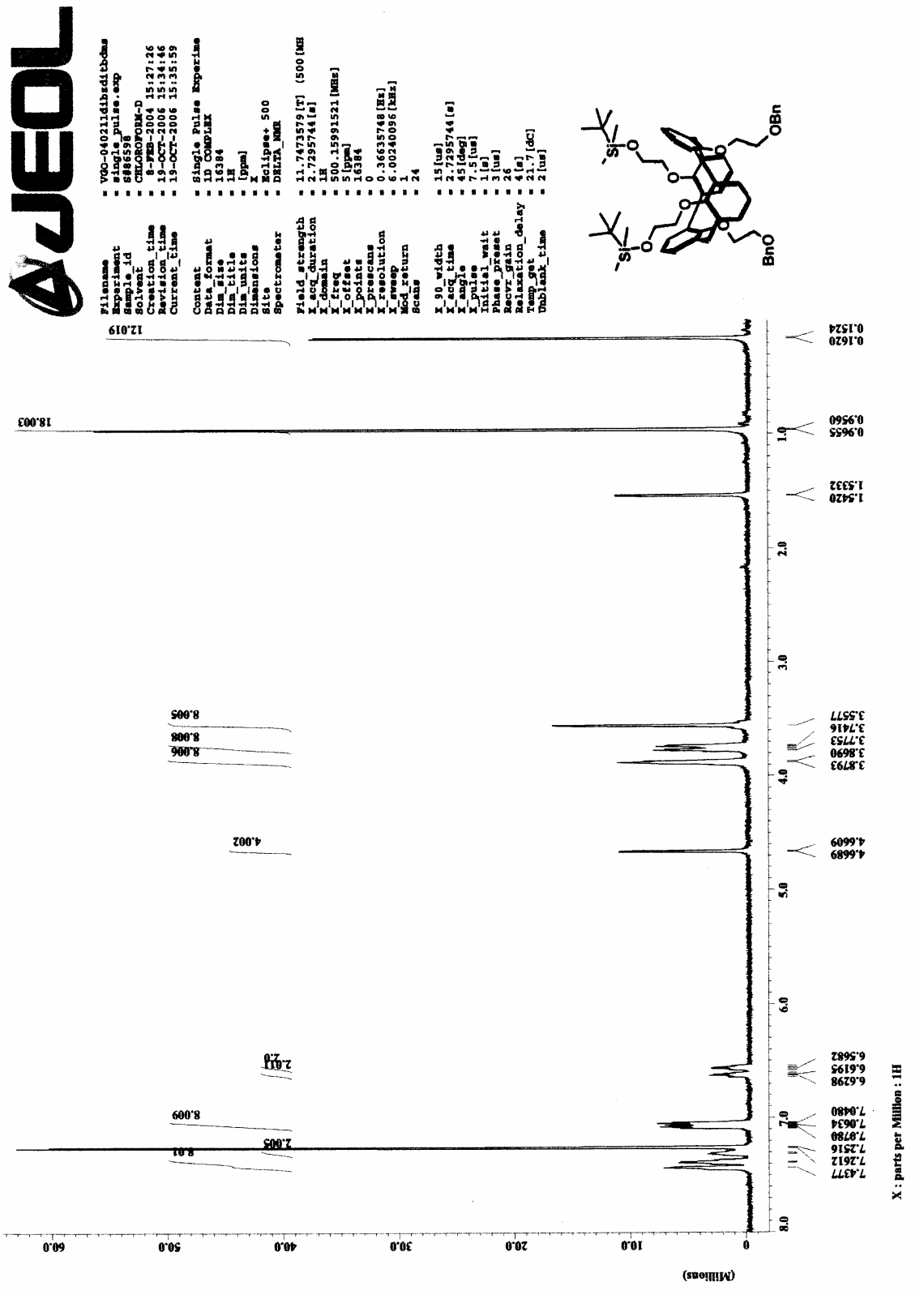
JEOL
Filename = VGO-040211dibzd1tcbms
Experiment = single_pulse.exp
Sample_id = s886598
Solvent = CHLOROFORM-D
Creation_time = 8-FEB-2004 15:27:26
Revision_time = 19-OCT-2006 15:34:46
Current_time = 19-OCT-2006 15:35:59
Content = Single Pulse Experime
Data_format = 1D COMPLEX
Dim_size = 16384
Dim_title = 1H
Dim_units = [ppm]
Dimensions = X
Site = Eclipse+ 500
Spectrometer = DELTA_NMR
Field_strength = 11.7473579[T] (500[MH
X_acq_duration = 2.7295744[s]
X_domain = 1H
X_freq = 500.15991521[MHz]
X_offset = 5[ppm]
X_points = 16384
X_prescans = 0
X_resolution = 0.36635748[Hz]
X_sweep = 6.00240096[kHz]
Mod_return = 1
Scans = 24
X_90_width = 15[us]
X_acq_time = 2.7295744[s]
X_angle = 45[deg]
X_pulse = 7.5[us]
Initial_wait = 1[s]
Phase_preset = 3[us]
Recvr_gain = 26
Relaxation_delay = 4[s]
Temp_get = 21.7[dC]
Unblank_time = 2[us]
OBn
BnO
Si
Si
12.019
18.003
8.005
8.008
8.006
4.002
2.011
2.0
8.009
2.005
8.01
7.4377
7.2612
7.2516
7.8780
7.0634
7.0480
6.6298
6.6195
6.5682
4.6689
4.6609
3.8793
3.8690
3.7753
3.7416
3.5577
1.5420
1.5332
0.9655
0.9560
0.1620
0.1524
(Milliohms)
X : parts per Million : 1H

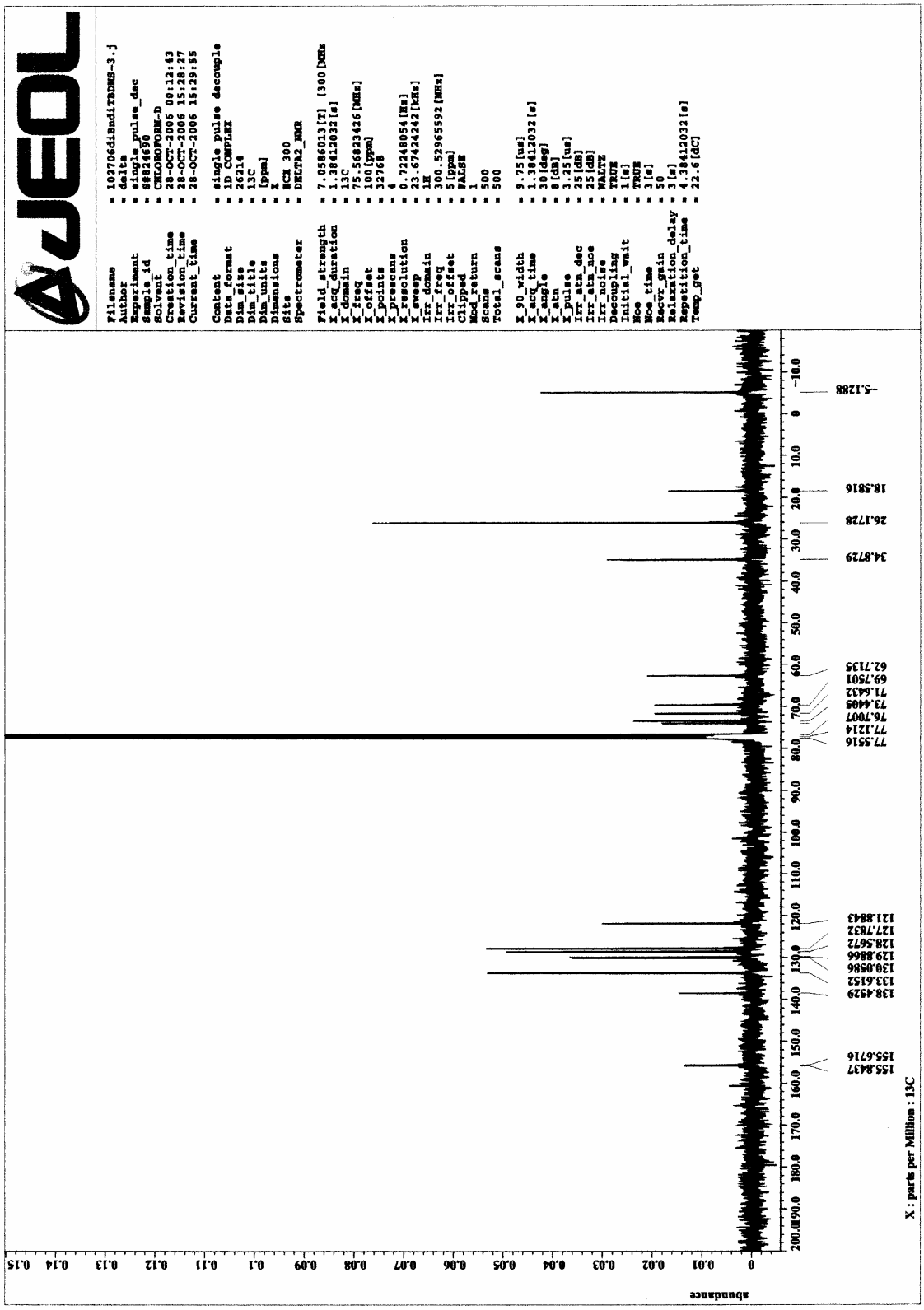
JEOL
Filename = 102706diBndiTBDMS-3.j
Author = delta
Experiment = single_pulse_dec
Sample_id = 88824690
Solvent = CHLOROFORM-D
Creation_time = 28-OCT-2006 00:12:43
Revision_time = 28-OCT-2006 15:28:27
Current_time = 28-OCT-2006 15:29:55
Content = single pulse decouple
Data_format = 1D COMPLEX
Dim_size = 26214
Dim_title = 13C
Dim_units = [ppm]
Dimensions = X
Site = ECX 300
Spectrometer = DELTA2_NMR
Field_strength = 7.05860213[T] (300[MHz
X_acq_duration = 1.38412032[s]
X_domain = 13C
X_freq = 75.36823426[MHz]
X_offset = 100[ppm]
X_points = 32768
X_prescans = 4
X_resolution = 0.72248054[Hz]
X_sweep = 23.67424242[kHz]
Irr_domain = 1H
Irr_freq = 300.52965592[MHz]
Irr_offset = 5[ppm]
Clipped = FALSE
Mod_return = 1
Scans = 500
Total_scans = 500
X_90_width = 9.75[us]
X_acq_time = 1.38412032[s]
X_angle = 30[deg]
X_atn = 8[dB]
X_pulse = 3.25[us]
Irr_atn_dec = 25[dB]
Irr_atn_noe = 25[dB]
Irr_noise = WALTZ
Decoupling = TRUE
Initial_wait = 1[s]
Noe = TRUE
Noe_time = 3[s]
Recvr_gain = 50
Relaxation_delay = 3[s]
Repetition_time = 4.38412032[s]
Temp_get = 22.6[dC]
abundance
X : parts per Million : 13C
-5.1288
18.5816
26.1728
34.8729
62.7135
69.7501
71.6432
73.4485
76.7007
77.1214
77.5516
121.8843
127.7832
128.5672
129.8866
130.0586
133.6152
138.4529
155.8437
155.6716

APPENDIX 9

^{1}H AND ^{13}C NMR SPECTRA OF
25,27-BIS[(2-BENZYLOXY)ETHYLOXY]-26,28-BIS(2-HYDROXYETHYLOXY)CALIX[4]ARENE, *1,3-ALTERNATE* (31)

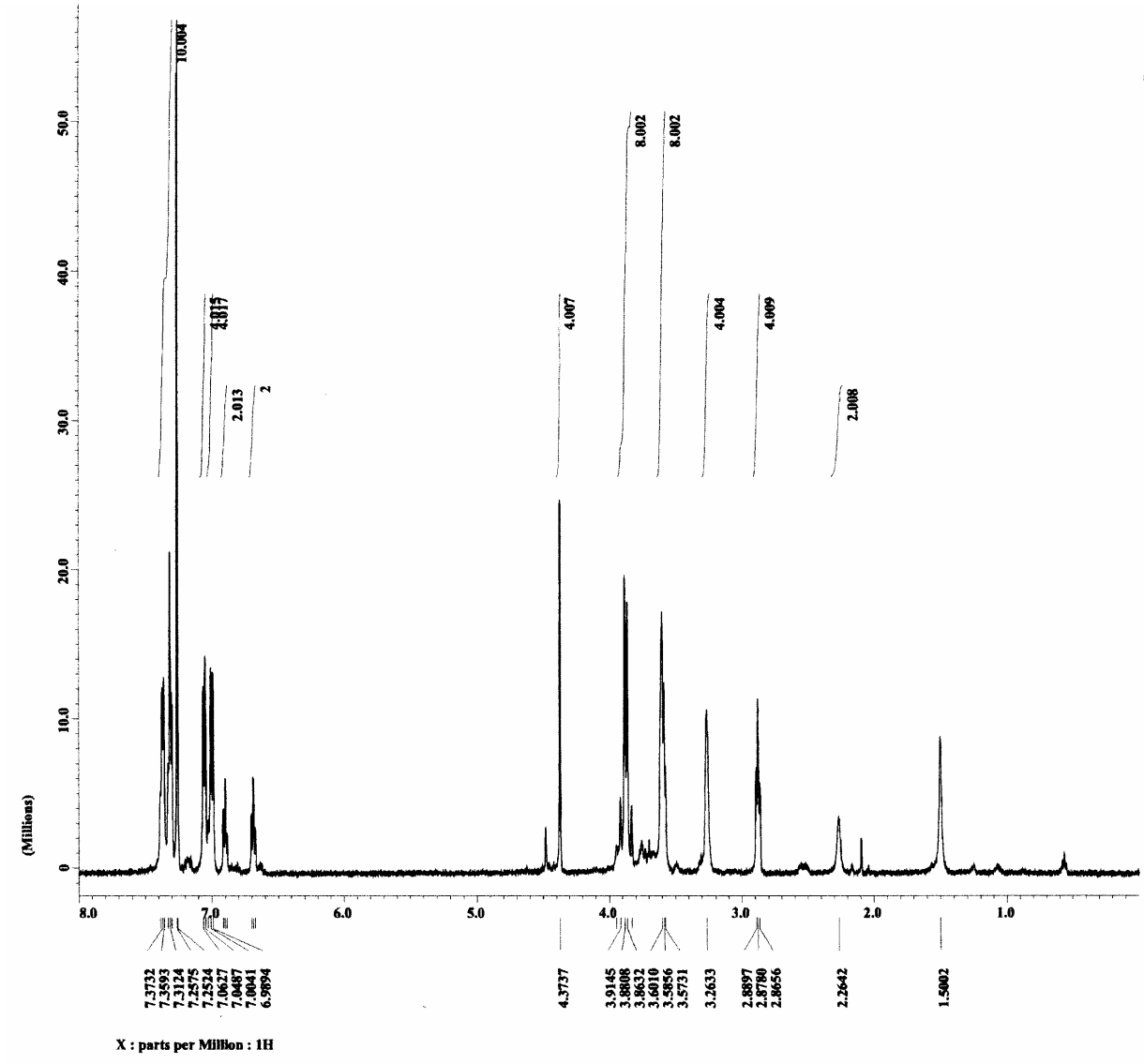

JEOL

```
Filename          = VGO-040219diBzdiEG-5.
Experiment        = single_pulse.exp
Sample_id         = S#21441
Solvent           = CHLOROFORM-D
Creation_time     = 25-FEB-2004 13:48:45
Revision_time     = 19-OCT-2006 15:23:51
Current_time      = 19-OCT-2006 15:24:11

Content           = Single Pulse Experime
Data_format       = 1D COMPLEX
Dim_size          = 16384
Dim_title         = 1H
Dim_units         = [ppm]
Dimensions        = X
Site              = Eclipse+ 500
Spectrometer      = DELTA_NMR

Field_strength    = 11.7473579[T]  (500[MH
X_acq_duration    = 2.7295744[s]
X_domain          = 1H
X_freq            = 500.15991521[MHz]
X_offset          = 5[ppm]
X_points          = 16384
X_prescans        = 0
X_resolution      = 0.36635748[Hz]
X_sweep           = 6.00240096[kHz]
Mod_return        = 1
Scans             = 24

X_90_width        = 15[us]
X_acq_time        = 2.7295744[s]
X_angle           = 45[deg]
X_pulse           = 7.5[us]
Initial_wait      = 1[s]
Phase_preset      = 3[us]
Recvr_gain        = 25
Relaxation_delay  = 4[s]
Temp_get          = 22.8[dC]
Unblank_time      = 2[us]
```

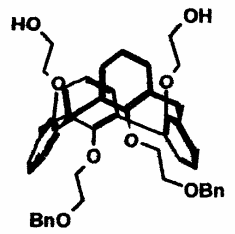

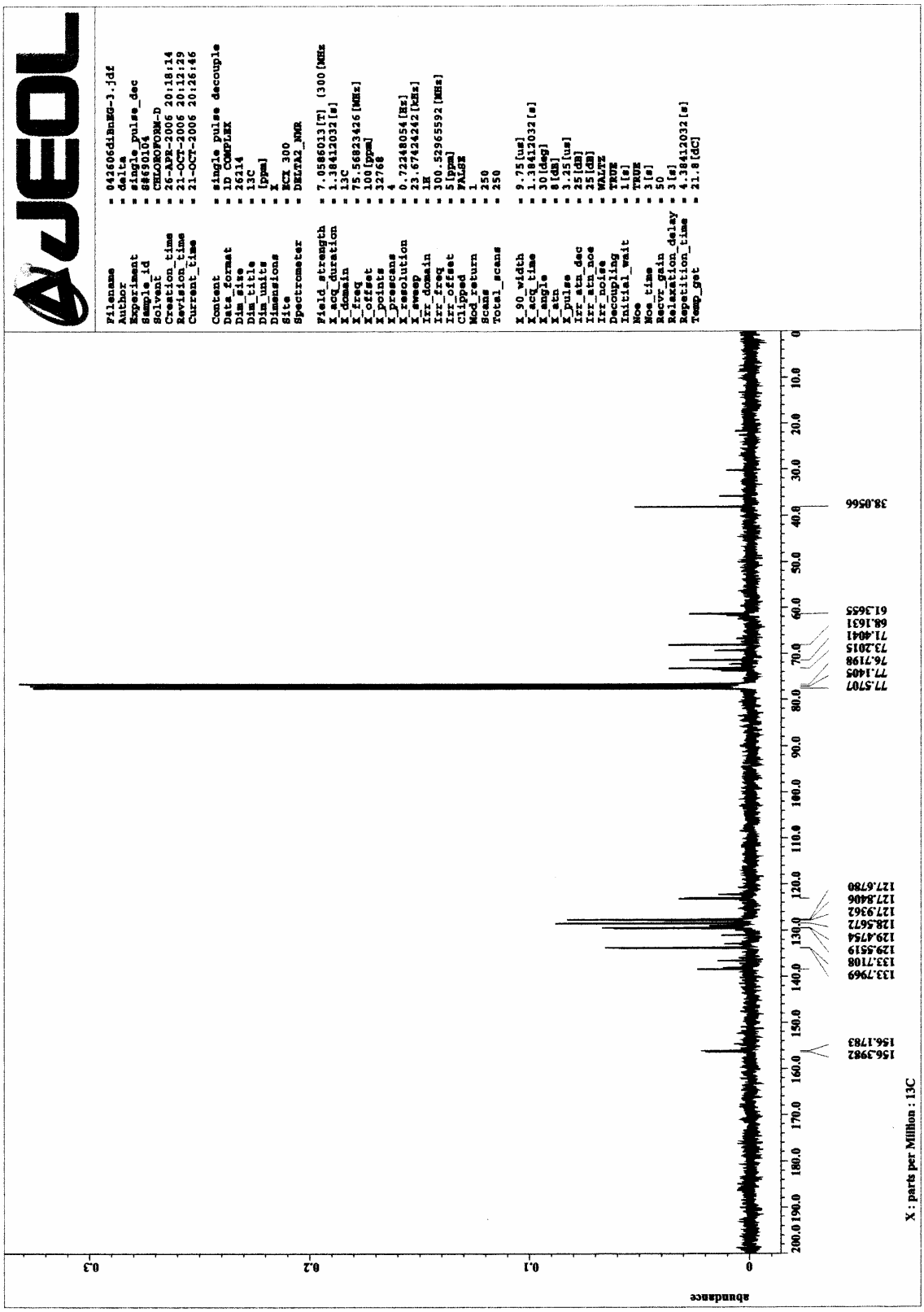
JEOL
Filename = 042606diBnEG-3.jdf
Author = delta
Experiment = single_pulse_dec
Sample_id = ##690104
Solvent = CHLOROFORM-D
Creation_time = 26-APR-2006 20:18:14
Revision_time = 21-OCT-2006 20:12:29
Current_time = 21-OCT-2006 20:26:46
Content = single pulse decouple
Data_format = 1D COMPLEX
Dim_size = 26114
Dim_title = 13C
Dim_units = [ppm]
Dimensions = X
Site = NCX 300
Spectrometer = DELTA2_NMR
Field_strength = 7.0586013[T] (300[MHz
X_acq_duration = 1.38412032[s]
X_domain = 13C
X_freq = 75.56823426[MHz]
X_offset = 100[ppm]
X_points = 32768
X_prescans = 4
X_resolution = 0.72248054[Hz]
X_sweep = 23.67424242[kHz]
X_window = LB
Irr_domain = 300.52965592[MHz]
Irr_freq = 5[ppm]
Irr_offset = FALSE
Clipped = FALSE
Mod_return = 1
Scans = 250
Total_scans = 250
X_90_width = 9.75[us]
X_acq_time = 1.38412032[s]
X_angle = 30[deg]
X_atn = 8[dB]
X_pulse = 3.25[us]
Irr_atn_dec = 25[dB]
Irr_atn_noe = 25[dB]
Irr_noise = WALTZ
Decoupling = TRUE
Initial_wait = 1[s]
Noe = TRUE
Noe_time = 3[s]
Recvr_gain = 50
Relaxation_delay = 3[s]
Repetition_time = 4.38412032[s]
Temp_get = 21.8[dC]
abundance
0.3
0.2
0.1
0
X : parts per Million : 13C
200.0 190.0 180.0 170.0 160.0 150.0 140.0 130.0 120.0 110.0 100.0 90.0 80.0 70.0 60.0 50.0 40.0 30.0 20.0 10.0 0
156.3982
156.1783
133.7969
133.7108
129.9519
129.4754
128.5672
127.9362
127.8406
127.6780
77.5707
77.1405
76.7198
73.2015
71.4041
68.1631
61.3655
38.0566

APPENDIX 10

^{1}H and ^{13}C NMR SPECTRA OF
BIS(1-PROPYLOXY)-BIS(2-BENZYLOXYETHYLOXY)CALIX[4]TUBE (32)

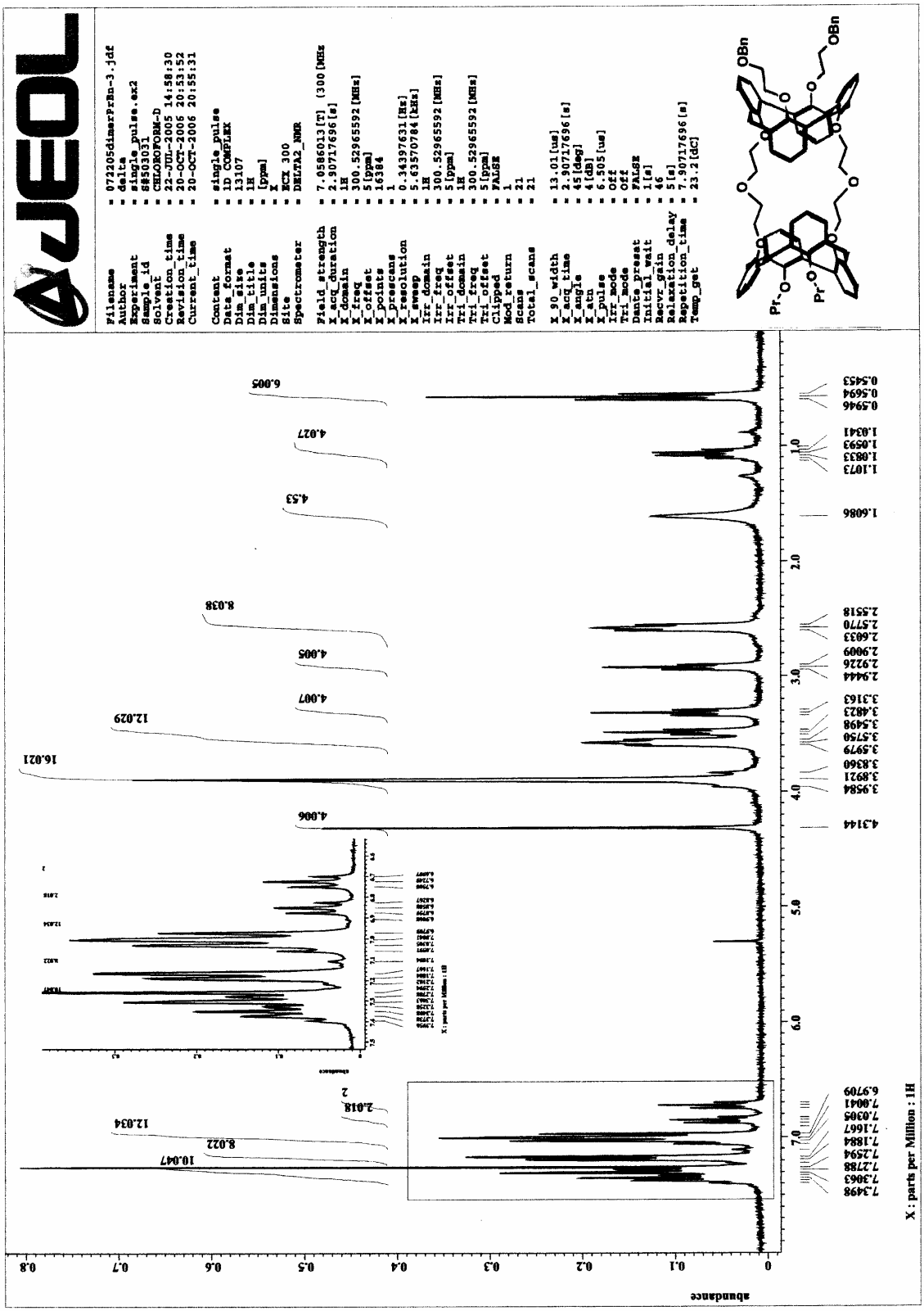
JEOL
Filename = 072205dimerPrRn-3.jdf
Author = delta
Experiment = single_pulse.ex2
Sample_id = s#503031
Solvent = CHLOROFORM-D
Creation_time = 22-JUL-2005 14:58:30
Revision_time = 20-OCT-2006 20:53:52
Current_time = 20-OCT-2006 20:55:31
Content = single_pulse
Data_format = 1D COMPLEX
Dim_size = 13107
Dim_title = 1H
Dim_units = [ppm]
Dimensions = X
Site = ECX 300
Spectrometer = DELTA2_NMR
Field_strength = 7.05860131[T] (300[MHz
X_acq_duration = 2.90717696[s]
X_domain = 1H
X_freq = 300.52965592[MHz]
X_offset = 5[ppm]
X_points = 16384
X_prescans = 1
X_resolution = 0.34397631[Hz]
X_sweep = 5.43570784[kHz]
Irr_domain = 1H
Irr_freq = 300.52965592[MHz]
Irr_offset = 5[ppm]
Tri_domain = 1H
Tri_freq = 300.52965592[MHz]
Tri_offset = 5[ppm]
Clipped = FALSE
Mod_return = 1
Scans = 21
Total_scans = 21
X_90_width = 13.01[us]
X_acq_time = 2.90717696[s]
X_angle = 45[deg]
X_atn = 4[dB]
X_pulse = 6.505[us]
Irr_mode = Off
Tri_mode = Off
Dante_presat = FALSE
Initial_wait = 1[s]
Recvr_gain = 46
Relaxation_delay = 5[s]
Repetition_time = 7.90717696[s]
Temp_get = 23.2[dC]
OBn
OBn
Pr
Pr
abundance
X : parts per Million : 1H
16.021
12.034
12.029
10.047
8.038
8.022
6.005
4.53
4.027
4.007
4.006
4.005
2.018
1.6086
7.3498
7.3063
7.2788
7.2594
7.1884
7.1667
7.0305
7.0041
6.9709
4.3144
3.9584
3.8921
3.8360
3.5979
3.5750
3.5498
3.4823
3.3163
2.9444
2.9226
2.9009
2.6033
2.5770
2.5518
1.1073
1.0833
1.0593
1.0341
0.5946
0.5694
0.5453

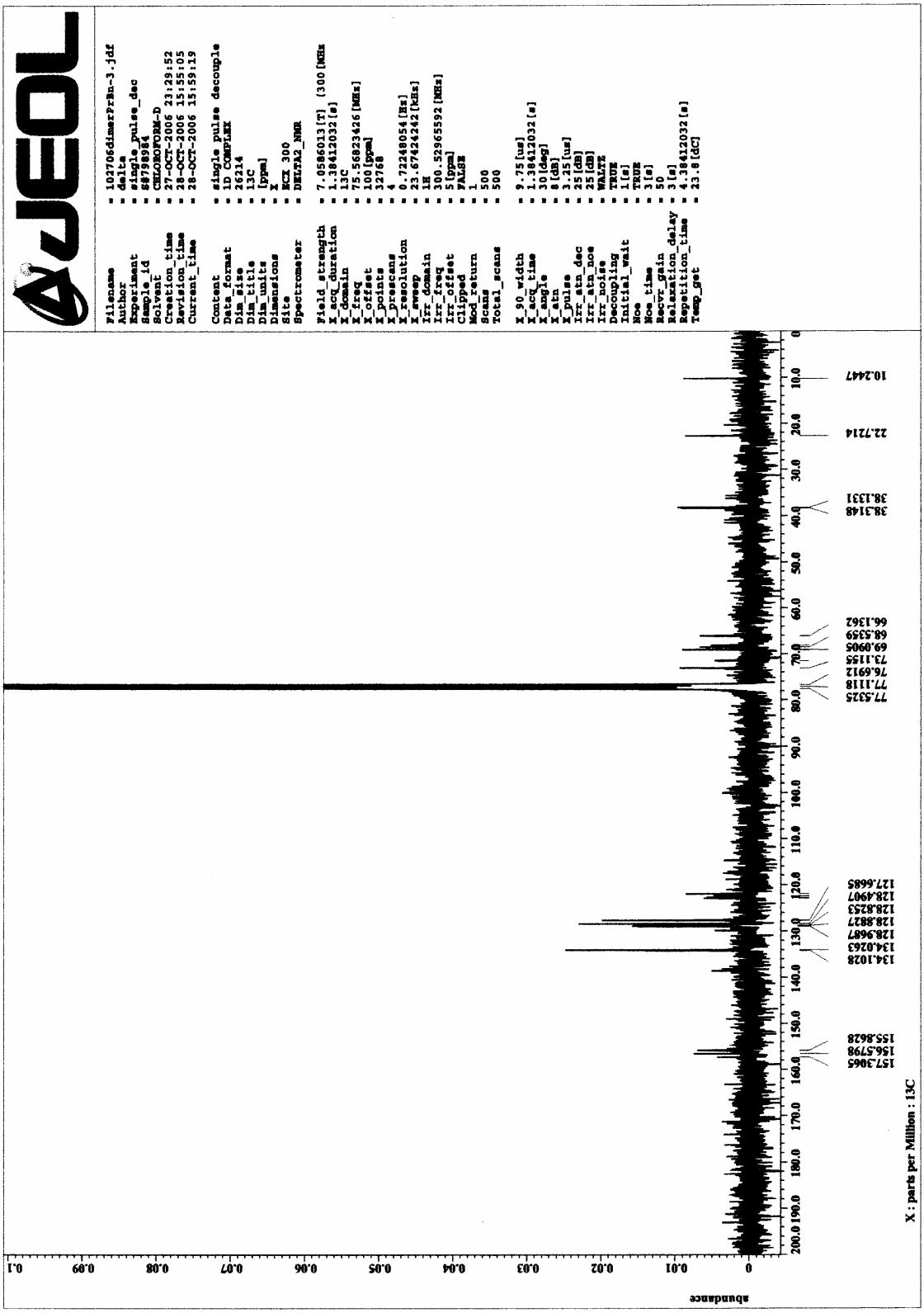
JEOL
Filename = 102706dimerPrRn-3.jdf
Author = delta
Experiment = single_pulse_dec
Sample_id = #8738564
Solvent = CHLOROFORM-D
Creation_time = 27-OCT-2006 23:29:52
Revision_time = 28-OCT-2006 15:55:05
Current_time = 28-OCT-2006 15:59:19
Content = single pulse decouple
Data_format = 1D COMPLEX
Dim_size = 16214
Dim_title = 13C
Dim_units = [ppm]
Dimensions = X
Site = NCH 300
Spectrometer = DEF2A2_NMR
Field_strength = 7.05860113[T] (300[MHz
X_acq_duration = 1.38412032[s]
X_domain = 13C
X_freq = 75.56823426[MHz]
X_offset = 100[ppm]
X_points = 32768
X_prescans = 4
X_resolution = 0.72248054[Hz]
X_sweep = 23.67424242[kHz]
Irr_domain = 1H
Irr_freq = 300.52965592[MHz]
Irr_offset = 5[ppm]
Clipped = FALSE
Mod_return = 1
Scans = 500
Total_scans = 500
X_90_width = 9.75[us]
X_acq_time = 1.38412032[s]
X_angle = 30[deg]
X_atn = 0[dB]
X_pulse = 3.25[us]
Irr_atn_dec = 25[dB]
Irr_atn_noe = 25[dB]
Irr_noise = WALTZ
Decoupling = TRUE
Initial_wait = 1[s]
Noe = TRUE
Noe_time = 3[s]
Recvr_gain = 50
Relaxation_delay = 3[s]
Repetition_time = 4.38412032[s]
Temp_get = 23.8[dC]
abundance
X : parts per Million : 13C
10.2447
22.7214
38.3148
38.1331
66.1362
68.3359
69.0905
73.1155
76.6912
77.1118
77.5325
127.6685
128.4907
128.8253
128.8827
128.9687
134.0263
134.1028
155.8628
156.5798
157.3065

APPENDIX 11

^{1}H AND ^{13}C NMR SPECTRA OF BIS(1-PROPYLOXY)-BIS(2-HYDROXYETHYLOXY)CALIX[4]TUBE (27)

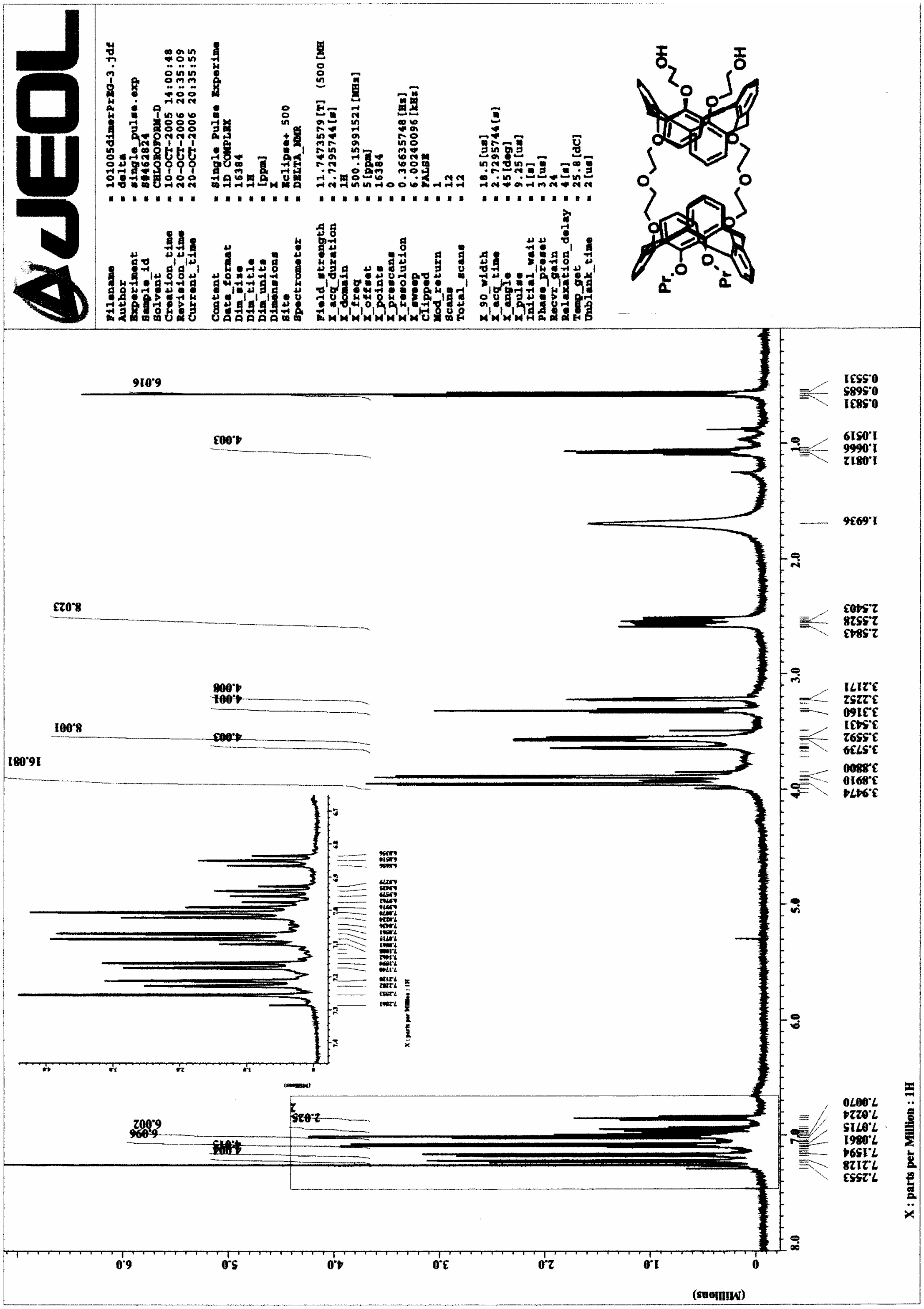
Filename = 101005dimerPrEG-3.jdf
Author = delta
Experiment = single_pulse.exp
Sample_id = S#462824
Solvent = CHLOROFORM-D
Creation_time = 10-OCT-2005 14:00:48
Revision_time = 20-OCT-2006 20:35:09
Current_time = 20-OCT-2006 20:35:55
Content = Single Pulse Experime
Data_format = 1D COMPLEX
Dim_size = 16384
Dim_title = 1H
Dim_units = [ppm]
Dimensions = X
Site = Eclipse+ 500
Spectrometer = DELTA_NMR
Field_strength = 11.7473579[T] (500[MH
X_acq_duration = 2.7295744[s]
X_domain = 1H
X_freq = 500.15991521[MHz]
X_offset = 5[ppm]
X_points = 16384
X_prescans = 0
X_resolution = 0.36635748[Hz]
X_sweep = 6.00240096[kHz]
Clipped = FALSE
Mod_return = 1
Scans = 12
Total_scans = 12
X_90_width = 18.5[us]
X_acq_time = 2.7295744[s]
X_angle = 45[deg]
X_pulse = 9.25[us]
Initial_wait = 1[s]
Phase_preset = 3[us]
Recvr_gain = 24
Relaxation_delay = 4[s]
Temp_get = 25.8[dC]
Unblank_time = 2[us]
Pr
Pr
O
OH
OH
(Millions)
X : parts per Million : 1H
16.081
8.001
8.023
6.016
6.096
6.002
4.003
4.001
4.008
4.003
2.025
7.2553
7.2128
7.1594
7.0861
7.0715
7.0224
7.0070
3.9474
3.8910
3.8800
3.5739
3.5592
3.5431
3.3160
3.2252
3.2171
2.5843
2.5528
2.5403
1.6936
1.0812
1.0666
1.0519
0.5831
0.5685
0.5531

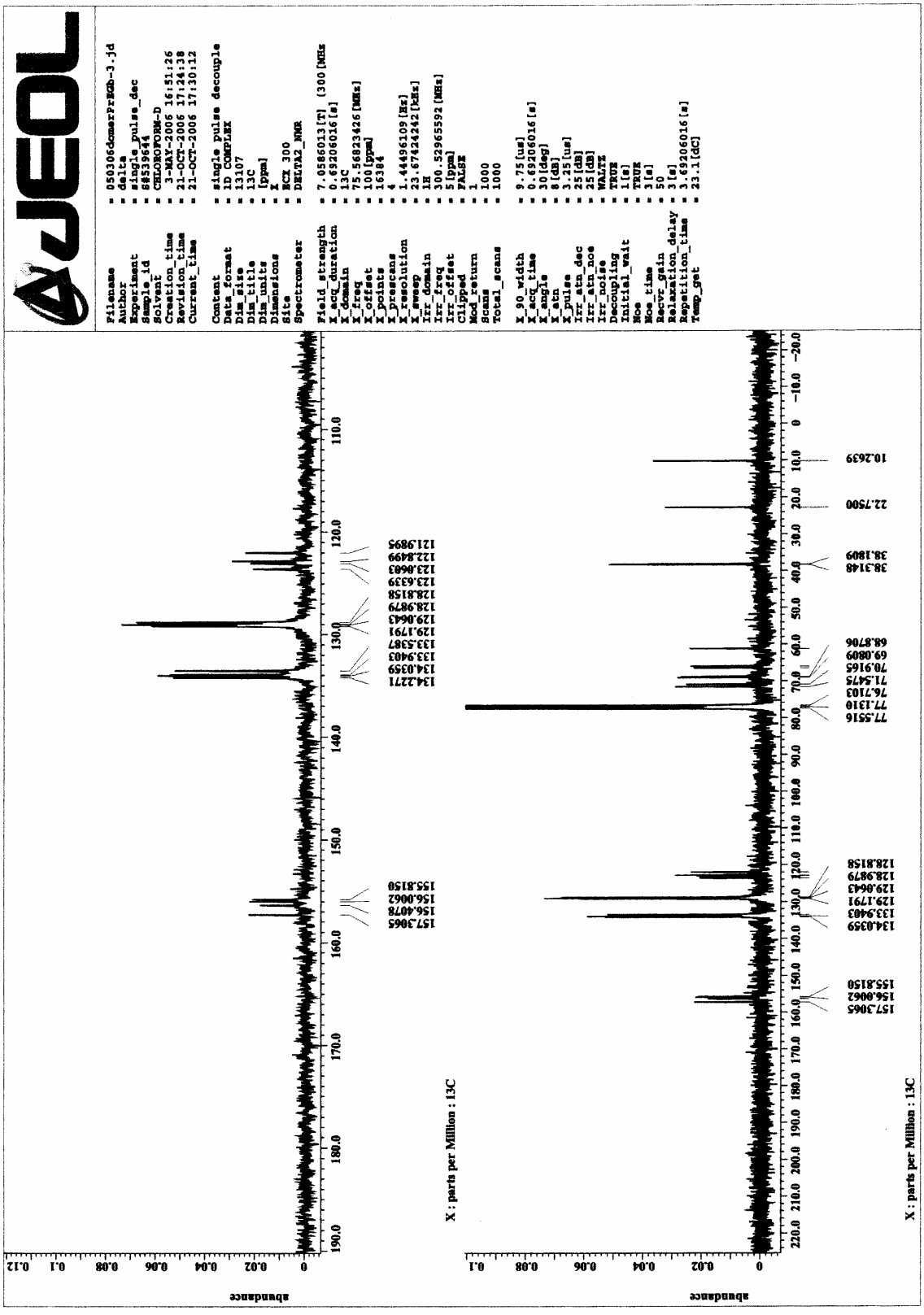
JEOL
Filename = 050306dcmszPrBZh-3.jd
Author = delta
Experiment = #single_pulse_dec
Sample_id = #$539644
Solvent = CHLOROFORM-D
Creation_time = 3-MAY-2006 16:51:26
Revision_time = 21-OCT-2006 17:24:38
Current_time = 21-OCT-2006 17:30:12
Content = #single pulse decouple
Data_format = 1D COMPLEX
Dim_size = 13107
Dim_title = 13C
Dim_units = [ppm]
Dimensions = X
Site = NCX 300
Spectrometer = DELTA2_NMR
Field_strength = 7.05860213[T] (300[MHz
X_acq_duration = 0.69206016[s]
X_domain = 13C
X_freq = 75.56823426[MHz]
X_offset = 100[ppm]
X_points = 16384
X_prescans = 4
X_resolution = 1.44496109[Hz]
X_sweep = 23.67424242[kHz]
Irr_domain = 1H
Irr_freq = 300.52965592[MHz]
Irr_offset = 5[ppm]
Clipped = FALSE
Mod_return = 1
Scans = 1000
Total_scans = 1000
X_90_width = 9.75[us]
X_acq_time = 0.69206016[s]
X_angle = 30[deg]
X_atn = 8[dB]
X_pulse = 3.25[us]
Irr_atn_dec = 25[dB]
Irr_atn_noe = 25[dB]
Irr_noise = WALTZ%
Decoupling = TRUE
Initial_wait = 1[s]
Noe = TRUE
Noe_time = 3[s]
Recvr_gain = 50
Relaxation_delay = 3[s]
Repetition_time = 3.69206016[s]
Temp_get = 23.1[dC]
abundance
X : parts per Million : 13C
157.3065
156.4078
156.0062
155.8150
134.4271
134.0359
133.9403
133.5387
129.1791
129.0643
128.9879
128.8158
123.6339
123.0683
122.8499
121.9895
10.2639
22.7500
38.3148
38.1809
68.8706
69.0809
70.9165
71.5475
76.7103
77.1310
77.5516

APPENDIX 12

^{1}H NMR SPECTRUM OF
BIS(1-PROPYLOXY)-BIS(2-METHYLETHYLOXY)CALIX[4]TUBE (27B)

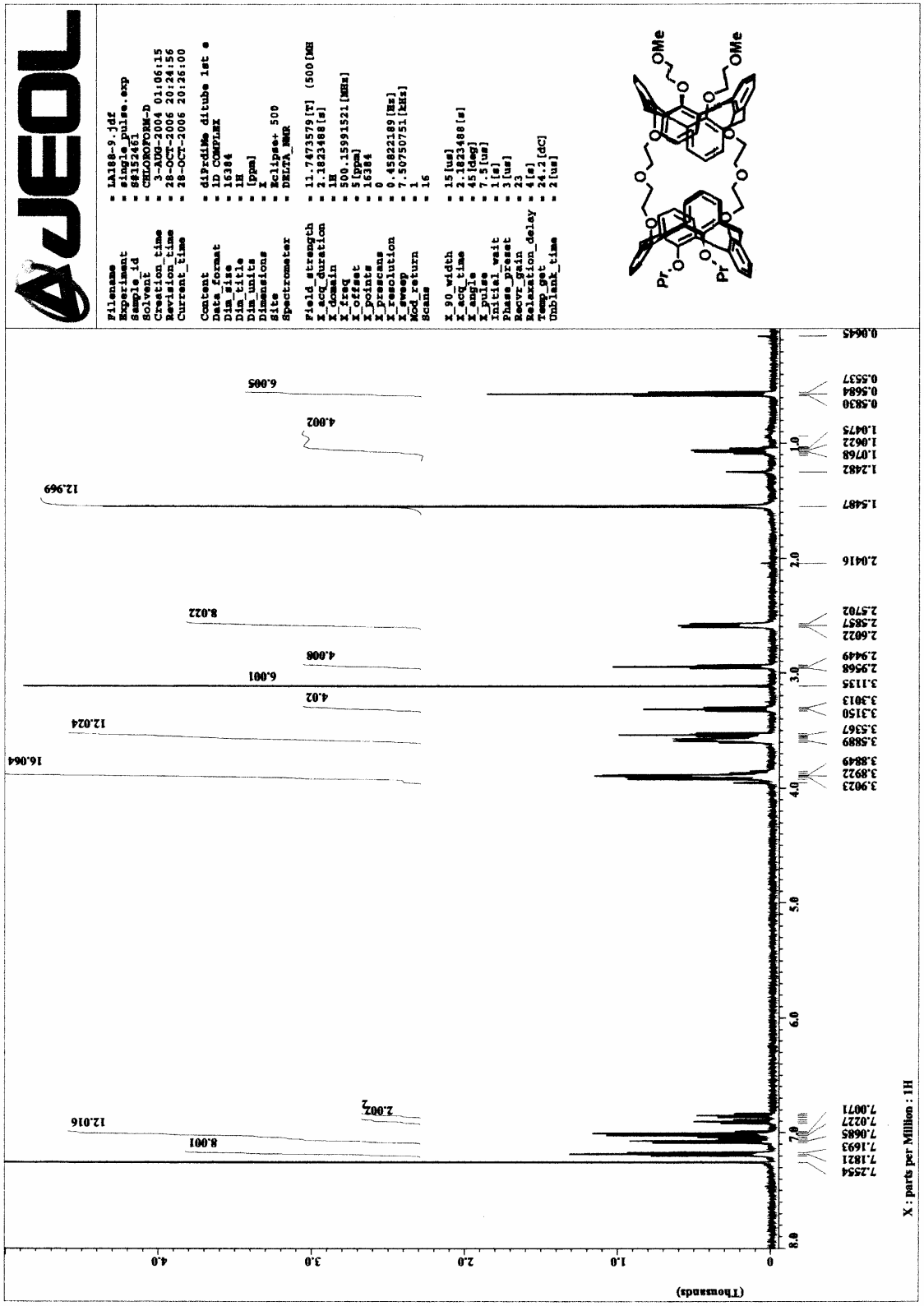
JEOL
Filename = LA188-9.jdf
Experiment = single_pulse.exp
Sample_id = #8152461
Solvent = CHLOROFORM-D
Creation_time = 3-AUG-2004 01:06:15
Revision_time = 28-OCT-2006 20:24:56
Current_time = 28-OCT-2006 20:26:00
Content = diPrdiMe ditube 1st e
Data_format = 1D COMPLEX
Dim_size = 16384
Dim_title = 1H
Dim_units = [ppm]
Dimensions = X
Site = Eclipse+ 500
Spectrometer = DELTA_NMR
Field_strength = 11.7473579[T] (500[MH
X_acq_duration = 2.18233488[s]
X_domain = 1H
X_freq = 500.159991521[MHz]
X_offset = 5[ppm]
X_points = 16384
X_prescans = 0
X_resolution = 0.45822189[Hz]
X_sweep = 7.50750751[kHz]
Rcd_return = 1
Scans = 16
X_90_width = 15[us]
X_acq_time = 2.1823488[s]
X_angle = 45[deg]
X_pulse = 7.5[us]
Initial_wait = 1[s]
Phase_preset = 3[us]
Recvr_gain = 23
Relaxation_delay = 4[s]
Temp_get = 24.2[dC]
Unblank_time = 2[us]
OMe
OMe
Pr
Pr
12.969
8.022
6.005
6.001
4.008
4.002
4.02
12.024
16.064
12.016
8.001
2.002
(Thousands)
X : parts per Million : 1H

APPENDIX 13

^{1}H and ^{13}C NMR SPECTRA OF
BIS(1-PROPYLOXY)-BIS(2-(*P*-
TOLUENESULFONYLOXY)ETHYLOXY)CALIX[4]TUBE (28)

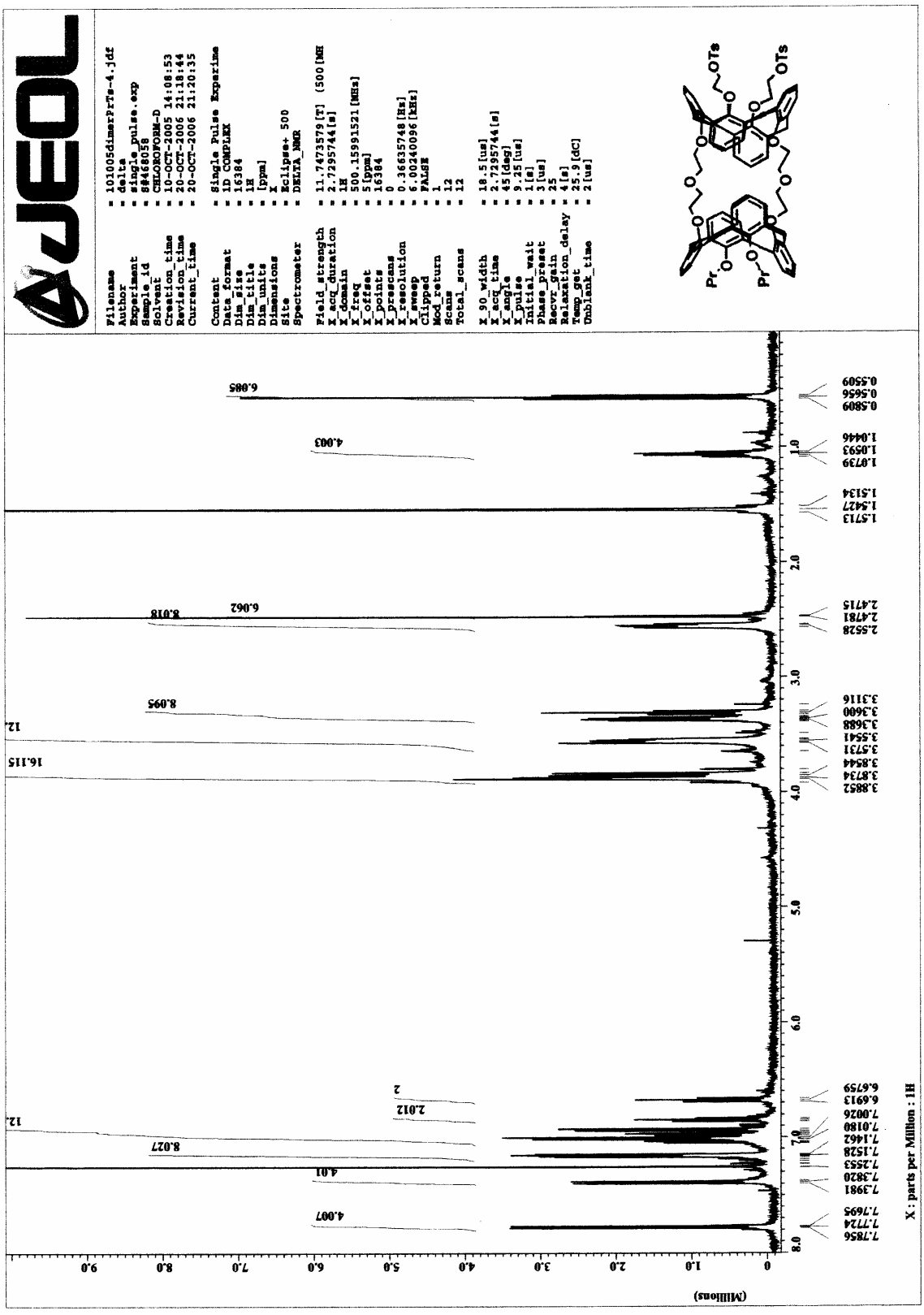
JEOL
Filename = 101005dimerPrTs-4.jdf
Author = delta
Experiment = single_pulse.exp
Sample_id = #4468058
Solvent = CHLOROFORM-D
Creation_time = 10-OCT-2005 14:08:53
Revision_time = 20-OCT-2006 21:18:44
Current_time = 20-OCT-2006 21:20:35
Content = Single Pulse Experime
Data_format = 1D COMPLEX
Dim_size = 16384
Dim_title = 1H
Dim_units = [ppm]
Dimensions = X
Site = Eclipse+ 500
Spectrometer = DELTA_NMR
Field_strength = 11.74733579[T] (500[MH
X_acq_duration = 2.72955744[s]
X_domain = 1H
X_freq = 500.15991521[MHz]
X_offset = 5[ppm]
X_points = 16384
X_prescans = 0.36635748[Hz]
X_resolution = 6.00240096[kHz]
X_sweep = FALSE
Clipped = 1
Mod_return = 12
Scans = 12
Total_scans = 1
X_90_width = 18.5[us]
X_acq_time = 2.72955744[s]
X_angle = 45[deg]
X_pulse = 9.25[us]
Initial_wait = 1[s]
Phase_preset = 3[us]
Recvr_gain = 25
Relaxation_delay = 4[s]
Temp_get = 25.9[dC]
Xblank_time = 2[us]
OTs
OTs
Pr
Pr
X : parts per Million : 1H
(Millions)

JEOL
Filename = 110206dimerPrTs-4.jdf
Author = delta
Experiment = single_pulse_dec
Sample_id = s#621341
Solvent = CHLOROFORM-D
Creation_time = 2-NOV-2006 18:59:27
Revision_time = 3-NOV-2006 12:10:22
Current_time = 3-NOV-2006 12:12:03
Content = single pulse decouple
Data_format = 1D COMPLEX
Dim_size = 13107
Dim_title = 13C
Dim_units = [ppm]
Dimensions = X
Site = ECX 300
Spectrometer = DELTA2_NMR
Field_strength = 7.05860131[T] (300[MHz
X_acq_duration = 0.69206016[s]
X_domain = 13C
X_freq = 75.56823426[MHz]
X_offset = 100[ppm]
X_points = 16384
X_prescans = 4
X_resolution = 1.44496109[Hz]
X_sweep = 23.67424242[kHz]
Irr_domain = 1H
Irr_freq = 300.52965592[MHz]
Irr_offset = 5[ppm]
Clipped = FALSE
Mod_return = 1
Scans = 1000
Total_scans = 1000
X_90_width = 9.75[us]
X_acq_time = 0.69206016[s]
X_angle = 30[deg]
X_atn = 8[dB]
X_pulse = 3.25[us]
Irr_atn_dec = 25[dB]
Irr_atn_noe = 25[dB]
Irr_noise = WALTZ
Decoupling = TRUE
Initial_wait = 1[s]
Noe = TRUE
Noe_time = 3[s]
Recvr_gain = 50
Relaxation_delay = 3[s]
Repetition_time = 3.69206016[s]
Temp_get = 23.5[dC]
(thousandths)
X : parts per Million : 13C
157.3256
155.9680
155.8341
145.0115
134.2080
134.0359
133.9976
130.0204
129.1026
129.0452
129.0070
128.7966
128.0700
122.8308
10.2447
21.7940
22.7118
38.0088
38.3148
67.8189
68.9662
69.1000
71.5475
76.6912
77.1118
77.5325

APPENDIX 14

^{1}H and ^{13}C NMR SPECTRA OF
DIMERIC CALIX[4]TUBE (15)

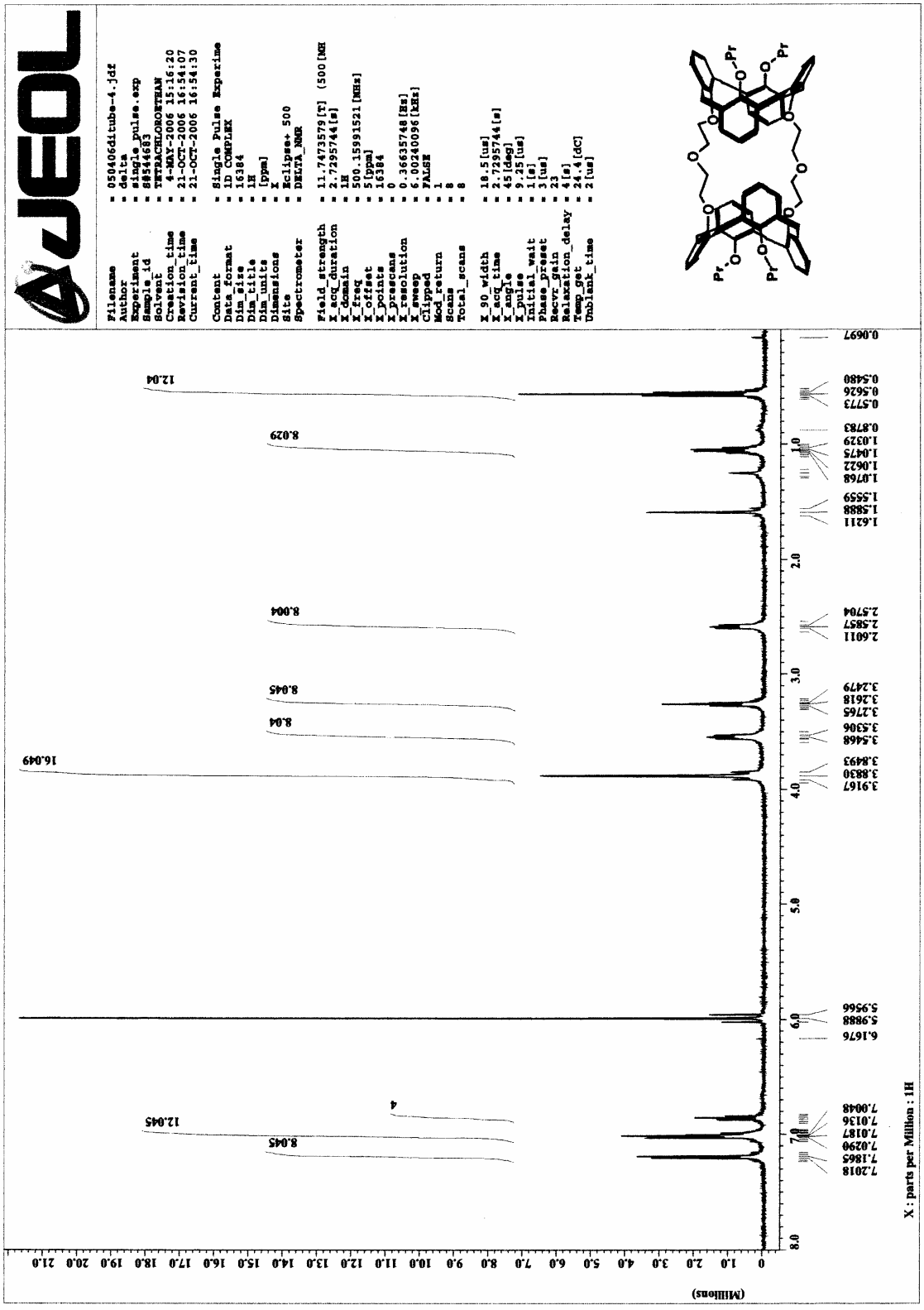
JEOL
Filename = 050406dtube-4.jdf
Author = delta
Experiment = single_pulse.exp
Sample_id = #8544683
Solvent = TETRACHLOROETHAN
Creation_time = 4-MAY-2006 15:16:20
Revision_time = 21-OCT-2006 16:54:07
Current_time = 21-OCT-2006 16:54:30
Content = Single Pulse Experime
Data_format = 1D COMPLEX
Dim_size = 16384
Dim_title = 1H
Dim_units = [ppm]
Dimensions = X
Site = Eclipse+ 500
Spectrometer = DELTA_NMR
Field_strength = 11.74735795[T] (500[MH
X_acq_duration = 2.72955744[s]
X_domain = 1H
X_freq = 500.15991521[MHz]
X_offset = 5[ppm]
X_points = 16384
X_prescans = 0
X_resolution = 0.36635748[Hz]
X_sweep = 6.00240096[kHz]
Clipped = FALSE
Mod_return = 1
Scans = 8
Total_scans = 8
X_90_width = 18.5[us]
X_acq_time = 2.72955744[s]
X_angle = 45[deg]
X_pulse = 9.25[us]
Initial_wait = 1[s]
Phase_preset = 3[us]
Recvr_gain = 23
Relaxation_delay = 4[s]
Temp_get = 24.4[dC]
Unblank_time = 2[us]
Pr
Pr
Pr
Pr
12.04
8.029
8.004
8.045
8.04
16.049
12.045
8.045
4
(Millions)
X : parts per Million : 1H

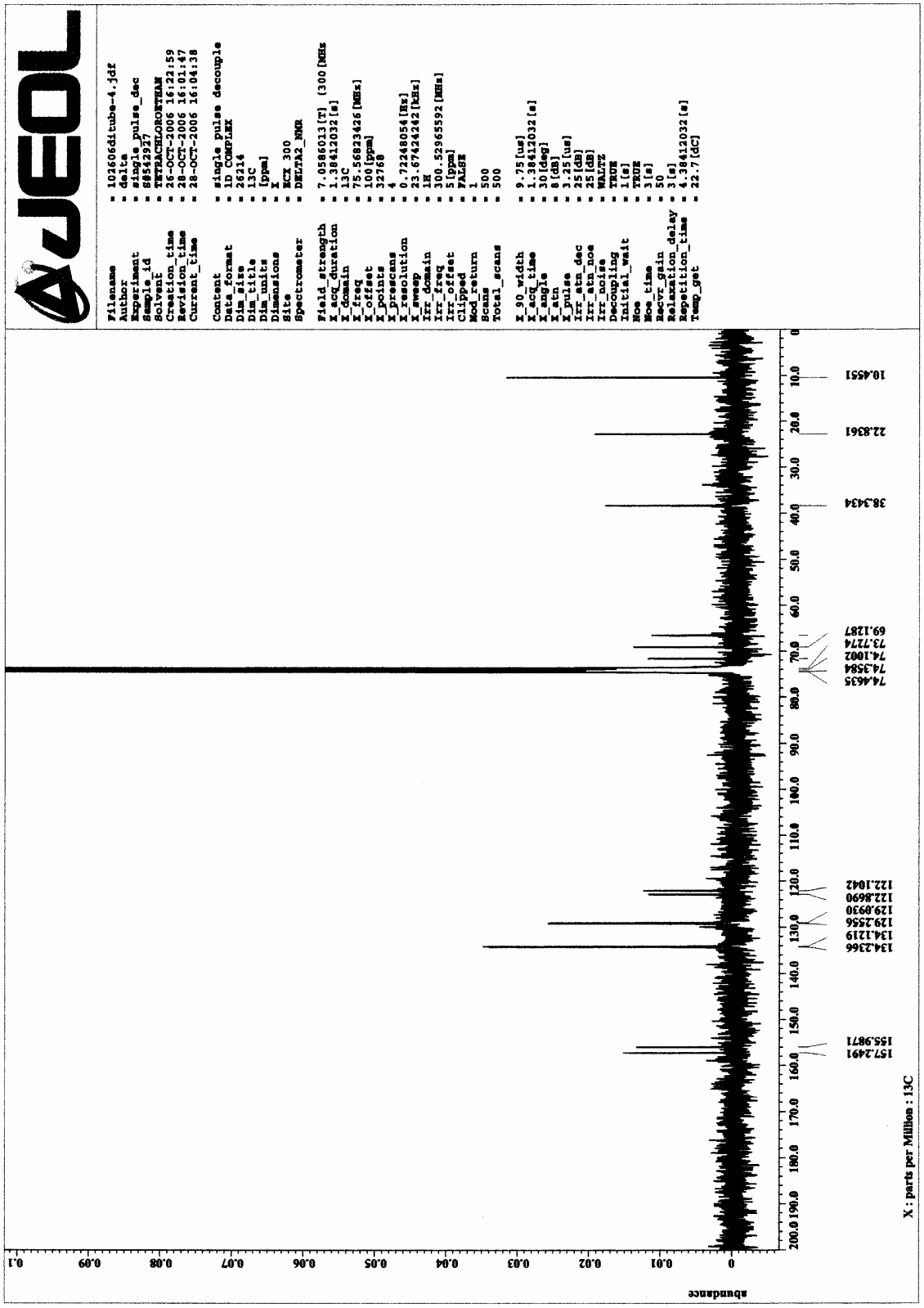
JEOL
Filename = 102606dtube-4.jdf
Author = delta
Experiment = single_pulse_dec
Sample_id = #$542927
Solvent = TETRACHLOROETHAN
Creation_time = 26-OCT-2006 16:22:59
Revision_time = 28-OCT-2006 16:01:47
Current_time = 28-OCT-2006 16:04:38
Content = single pulse decouple
Date_format = 1D COMPLEX
Dim_size = 26214
Dim_title = 13C
Dim_units = [ppm]
Dimensions = X
Site = ECX 300
Spectrometer = DELTA2_NMR
Field_strength = 7.05866113[T] (300[MHz
X_acq_duration = 1.38412032[s]
X_domain = 13C
X_freq = 75.56823426[MHz]
X_offset = 100[ppm]
X_points = 32768
X_prescans = 4
X_resolution = 0.72248054[Hz]
X_sweep = 23.67424242[kHz]
Irr_domain = 1H
Irr_freq = 300.52965592[MHz]
Irr_offset = 5[ppm]
Clipped = FALSE
Mod_return = 1
Scans = 500
Total_scans = 500
X_90_width = 9.75[us]
X_acq_time = 1.38412032[s]
X_angle = 30[deg]
X_atn = 8[dB]
X_pulse = 3.25[us]
Irr_atn_dec = 25[dB]
Irr_atn_noe = 25[dB]
Irr_noise = WALTZ
Decoupling = TRUE
Initial_wait = 1[s]
Noe = TRUE
Noe_time = 3[s]
Recvr_gain = 50
Relaxation_delay = 3[s]
Repetition_time = 4.38412032[s]
Temp_get = 22.7[dC]
abundance
X : parts per Million : 13C
157.2491
155.9871
134.2366
134.1219
129.2556
129.0930
122.8690
122.1042
74.4635
74.3584
74.1002
73.7274
69.1287
38.3434
22.8361
10.4551

APPENDIX 15

^{1}H and ^{13}C NMR SPECTRA OF
TRIMERIC CALIX[4]TUBE (16)

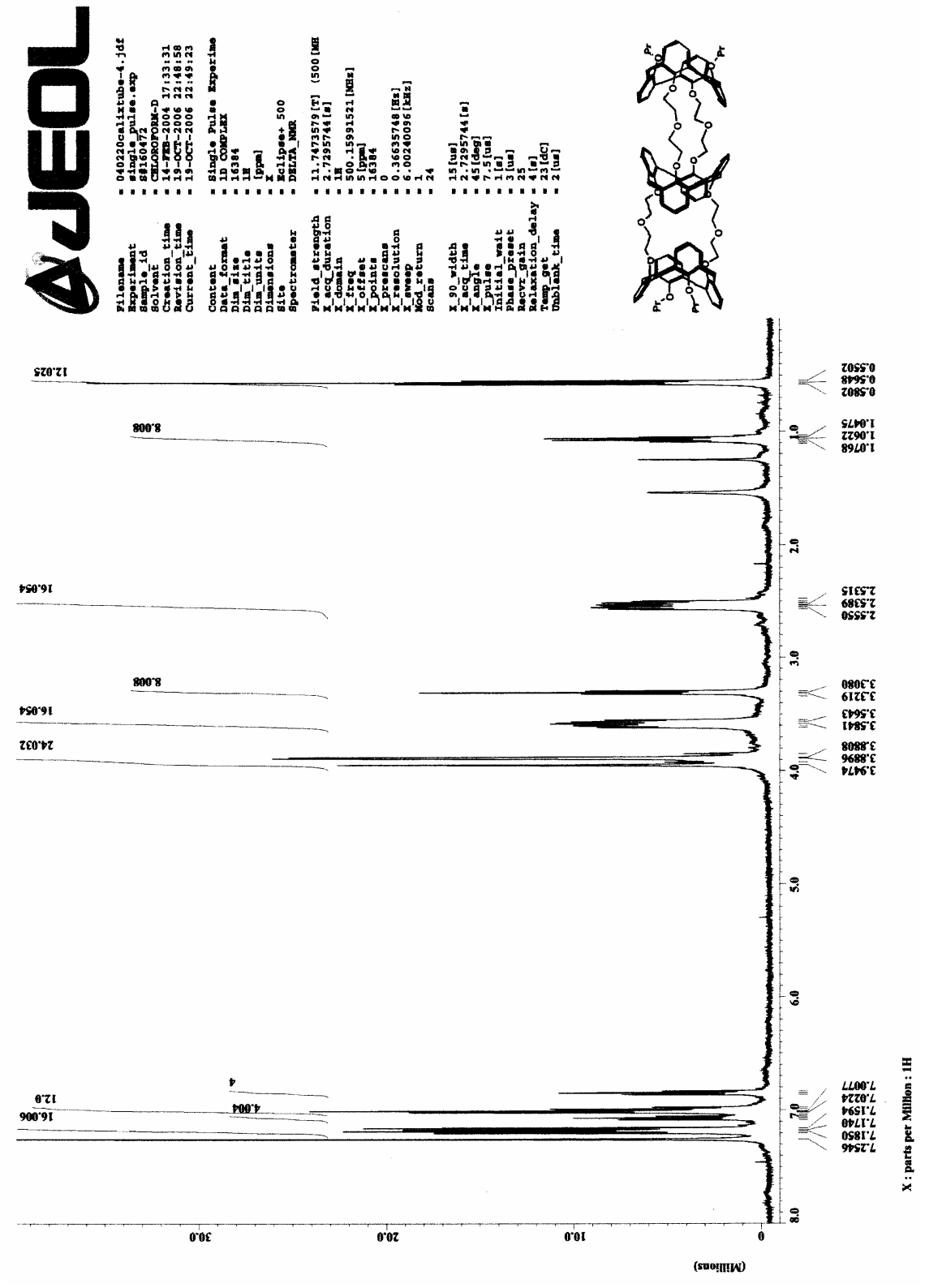
JEOL
Filename = 040220calixtube-4.jdf
Experiment = #single_pulse.exp
Sample_id = SH160472
Solvent = CHLOROFORM-D
Creation_time = 14-FEB-2004 17:33:31
Revision_time = 19-OCT-2006 22:48:58
Current_Time = 19-OCT-2006 22:49:23
Content = Single Pulse Experime
Data_format = 1D COMPLEX
Dim_size = 16384
Dim_title = 1H
Dim_units = [ppm]
Dimensions = X
Site = Eclipse+ 500
Spectrometer = DELTA_NMR
Field_strength = 11.74735579[T] (500[MH
X_acq_duration = 2.72957744[s]
X_domain = 1H
X_freq = 500.15991521[MHz]
X_offset = 5[ppm]
X_points = 16384
X_prescans = 0
X_resolution = 0.36635748[Hz]
X_sweep = 6.00240096[kHz]
Mod_return = 1
Scans = 24
X_90_width = 15[us]
X_acq_time = 2.72957744[s]
X_angle = 45[deg]
X_pulse = 7.5[us]
Initial_wait = 1[s]
Phase_preset = 3[us]
Recvr_gain = 25
Relaxation_delay = 4[s]
Temp_get = 23[dC]
Unblank_time = 2[us]
Pr
Pr
Pr
Pr
12.025
8.008
16.054
8.008
16.054
24.032
4
4.004
16.006
12.0
7.2546
7.1850
7.1740
7.1594
7.0224
7.0077
3.9474
3.8896
3.8808
3.5841
3.5643
3.3219
3.3080
2.5550
2.5389
2.5315
1.0768
1.0622
1.0475
0.5802
0.5648
0.5502
(Millions)
X : parts per Million : 1H

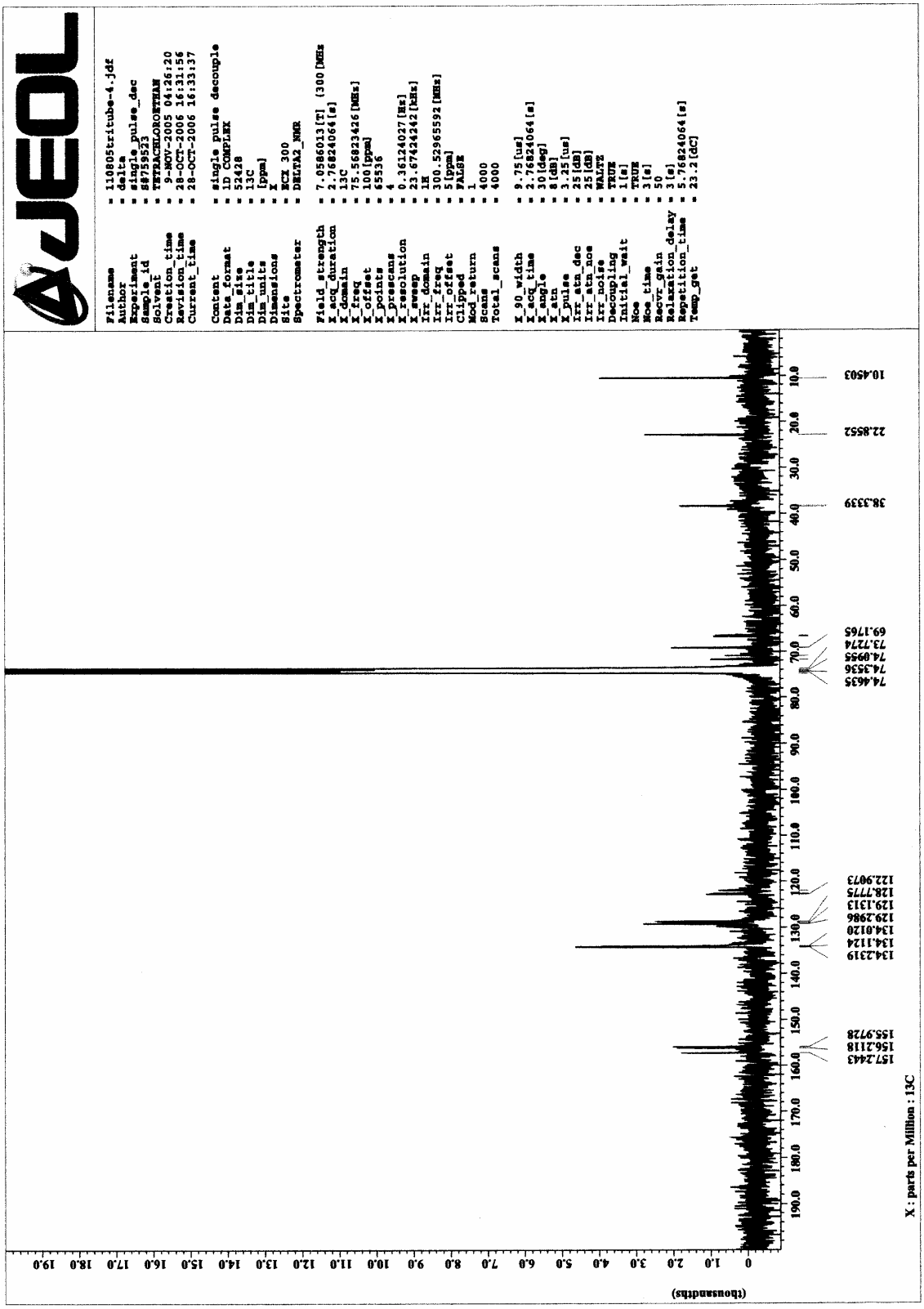
JEOL
Filename = 110805tritube-4.jdf
Author = delta
Experiment = single_pulse_dec
Sample_id = S#759523
Solvent = TETRACHLOROETHAN
Creation_time = 9-NOV-2005 04:26:20
Revision_time = 28-OCT-2006 16:31:56
Current_time = 28-OCT-2006 16:33:37
Content = single pulse decouple
Data_format = 1D COMPLEX
Dim_size = 52428
Dim_title = 13C
Dim_units = [ppm]
Dimensions = X
Site = ECX 300
Spectrometer = DELTA2_NMR
Field_strength = 7.05860131[T] (300[MHz
X_acq_duration = 2.76824064[s]
X_domain = 13C
X_freq = 75.56823426[MHz]
X_offset = 100[ppm]
X_points = 65536
X_prescans = 4
X_resolution = 0.36124027[Hz]
X_sweep = 23.67424242[kHz]
X_window = EM
Irr_domain = 1H
Irr_freq = 300.52965592[MHz]
Irr_offset = 5[ppm]
Clipped = FALSE
Mod_return = 1
Scans = 4000
Total_scans = 4000
X_90_width = 9.75[us]
X_acq_time = 2.76824064[s]
X_angle = 30[deg]
X_atn = 6[dB]
X_pulse = 3.25[us]
Irr_atn_dec = 25[dB]
Irr_atn_noe = 25[dB]
Irr_noise = WALTZ
Decoupling = TRUE
Initial_wait = 1[s]
Noe = TRUE
Noe_time = 3[s]
Recvr_gain = 50
Relaxation_delay = 3[s]
Repetition_time = 5.76824064[s]
Temp_get = 23.2[dC]
(thousands)
X : parts per Million : 13C
157.2443
156.2118
155.9728
134.2319
134.1124
134.0120
129.2986
129.1513
128.7775
122.9073
74.4635
74.3536
74.0955
73.7274
69.1765
38.3339
22.8552
10.4503

APPENDIX 16

^{1}H NMR SPECTRUM OF
TETRAMERIC CALIX[4]TUBE (17)

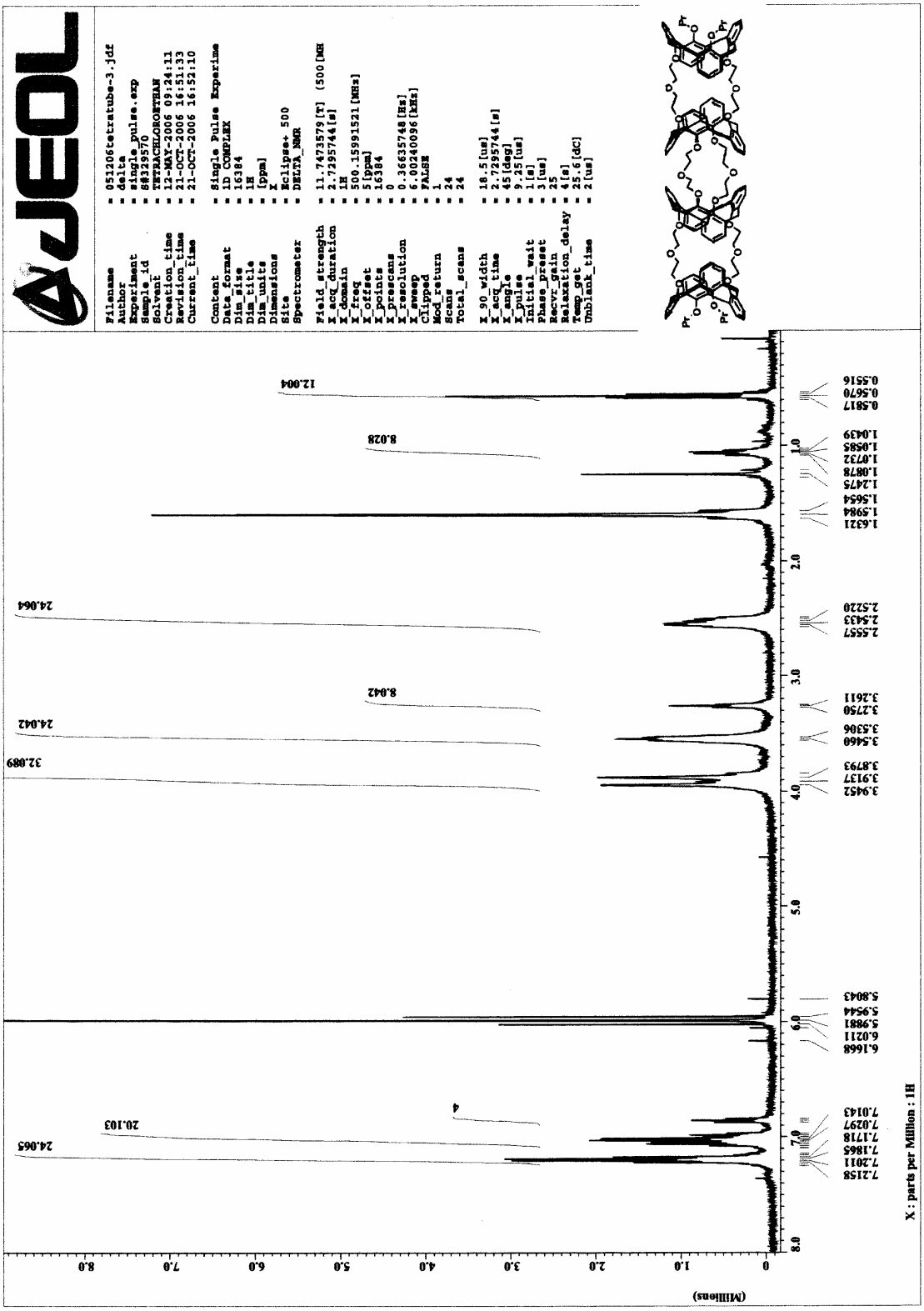
JEOL
Filename = 051206tetratube-3.jdf
Author = delta
Experiment = single_pulse.exp
Sample_id = 8#329570
Solvent = TETRACHLOROETHAN
Creation_time = 12-MAY-2006 09:24:11
Revision_time = 21-OCT-2006 16:51:33
Current_time = 21-OCT-2006 16:52:10
Content = Single Pulse Experime
Data_format = 1D COMPLEX
Dim_size = 16384
Dim_title = 1H
Dim_units = [ppm]
Dimensions = X
Site = Eclipse+ 500
Spectrometer = DELTA_NMR
Field_strength = 11.74731579[T] (500[MH
X_acq_duration = 2.72957444[s]
X_domain = 1H
X_freq = 500.15991521[MHz]
X_offset = 5[ppm]
X_points = 16384
X_prescans = 0
X_resolution = 0.36635748[Hz]
X_sweep = 6.00240096[kHz]
Clipped = FALSE
Mod_return = 1
Scans = 24
Total_scans = 24
X_90_width = 18.5[us]
X_acq_time = 2.72957444[s]
X_angle = 45[deg]
X_pulse = 9.25[us]
Initial_wait = 1[s]
Phase_preset = 3[us]
Recvr_gain = 25
Relaxation_delay = 4[s]
Temp_get = 25.6[dC]
Unblank_time = 2[us]
12.004
8.028
24.064
8.042
24.042
32.089
24.065
20.103
4
7.2158
7.2011
7.1718
7.1865
7.0297
7.0143
6.1668
6.0211
5.9881
5.9544
5.8043
3.9452
3.9137
3.8793
3.5460
3.5306
3.2750
3.2611
2.5557
2.5433
2.5220
1.6321
1.5984
1.5654
1.2475
1.0878
1.0732
1.0585
1.0439
0.5817
0.5670
0.5516
X : parts per Million : 1H
(Millions)

APPENDIX 17

^{1}H NMR SPECTRUM OF
PENTAMERIC CALIX[4]TUBE (18)

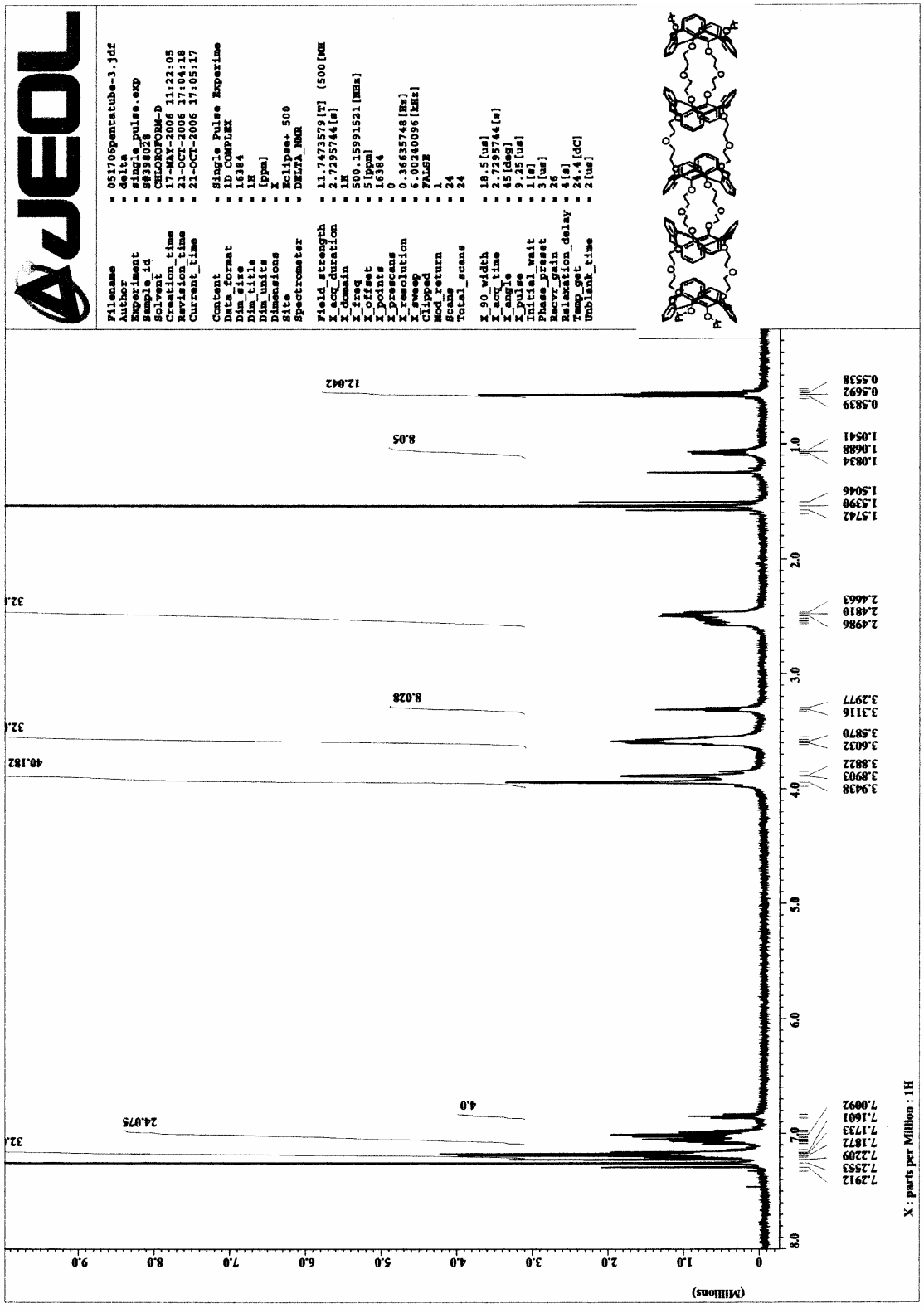
JEOL
Filename = 051706pentatube-3.jdf
Author = delta
Experiment = single_pulse.exp
Sample_id = 88398028
Solvent = CHLOROFORM-D
Creation_time = 17-MAY-2006 11:22:05
Revision_time = 21-OCT-2006 17:04:18
Current_time = 21-OCT-2006 17:05:17
Content = Single Pulse Experime
Data_format = 1D COMPLEX
Dim_size = 16384
Dim_title = 1H
Dim_units = [ppm]
Dimensions = X
Site = Eclipse+ 500
Spectrometer = DELTA_NMR
Field_strength = 11.7473579[T] (500[MH
X_acq_duration = 2.7295744[s]
X_domain = 1H
X_freq = 500.15991521[MHz]
X_offset = 5[ppm]
X_points = 16384
X_prescans = 0
X_resolution = 0.36635748[Hz]
X_sweep = 6.00240096[kHz]
Clipped = FALSE
Mod_return = 1
Scans = 24
Total_scans = 24
X_90_width = 18.5[us]
X_acq_time = 2.7295744[s]
X_angle = 45[deg]
X_pulse = 9.25[us]
Initial_wait = 1[s]
Phase_preset = 3[us]
Recvr_gain = 26
Relaxation_delay = 4[s]
Temp_get = 24.4[dC]
Unblank_time = 2[us]
12.042
8.05
8.028
4.0
24.075
40.182
7.2912
7.2553
7.2209
7.1872
7.1733
7.1601
7.0092
3.9438
3.8903
3.8822
3.5870
3.6032
3.3116
3.2977
2.4986
2.4810
2.4663
1.5742
1.5390
1.5046
1.0834
1.0688
1.0541
0.5839
0.5692
0.5538
(Millions)
X : parts per Million : 1H

APPENDIX 18

^{1}H NMR SPECTRA OF
BISCALIX[4]TUBE-NO^{+} COMPLEX (33)

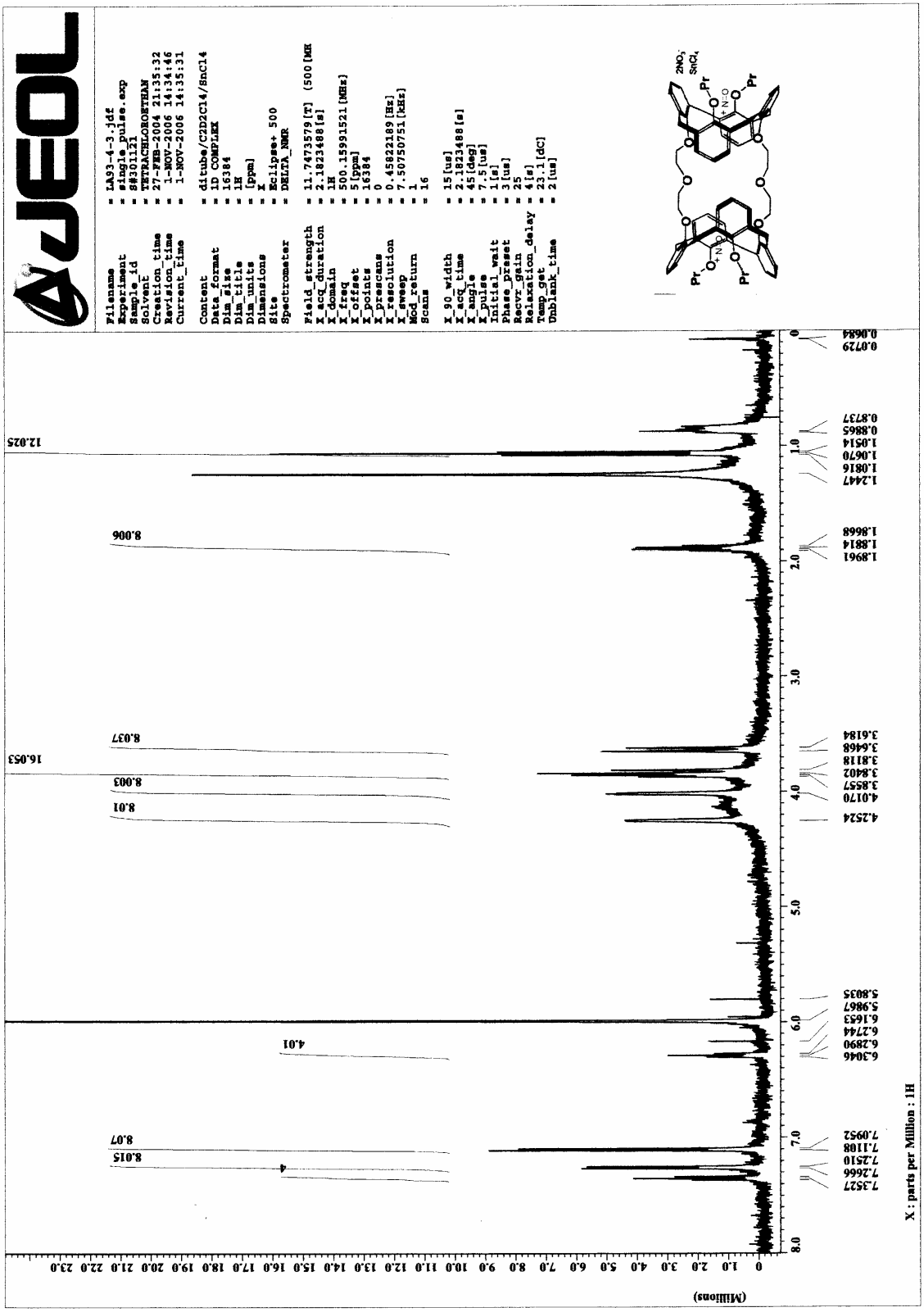
JEOL
Filename = LA93-4-3.jdf
Experiment = single_pulse.exp
Sample_id = S#3011121
Solvent = TETRACHLOROETHAN
Creation_time = 27-FEB-2004 21:35:32
Revision_time = 1-NOV-2006 14:34:46
Current_time = 1-NOV-2006 14:35:31
Content = ditube/C2D2Cl4/SnCl4
Data_format = 1D COMPLEX
Dim_size = 16384
Dim_title = 1H
Dim_units = [ppm]
Dimensions = X
Site = Eclipse+ 500
Spectrometer = DELTA_NMR
Field_strength = 11.74735791[T] (500[MH
X_acq_duration = 2.18234881[s]
X_domain = 1H
X_freq = 500.15991521[MHz]
X_offset = 5[ppm]
X_points = 16384
X_prescans = 0
X_resolution = 0.45822189[Hz]
X_sweep = 7.50750751[kHz]
Mod_return = 1
Scans = 16
X_90_width = 15[us]
X_acq_time = 2.18234881[s]
X_angle = 45[deg]
X_pulse = 7.5[us]
X_Initial_wait = 3[us]
Phase_preset = 25
Recvr_gain = 45[s]
Relaxation_delay = 4[s]
Temp_get = 23.1[dC]
Unblank_time = 2[us]
2NO2
SnCl4
Pr
Pr
Pr
Pr
12.025
8.006
16.053
8.037
8.003
8.01
4.01
8.07
8.015
4
0.0729
0.0684
0.8737
0.8865
1.0514
1.0670
1.0816
1.2447
1.8961
1.8814
1.8668
4.0170
3.8557
3.8402
3.8118
3.6468
3.6184
4.2524
6.3046
6.2890
6.2744
6.1653
5.9867
5.8035
7.3527
7.2666
7.2510
7.1108
7.0952
(Millions)
X : parts per Million : 1H

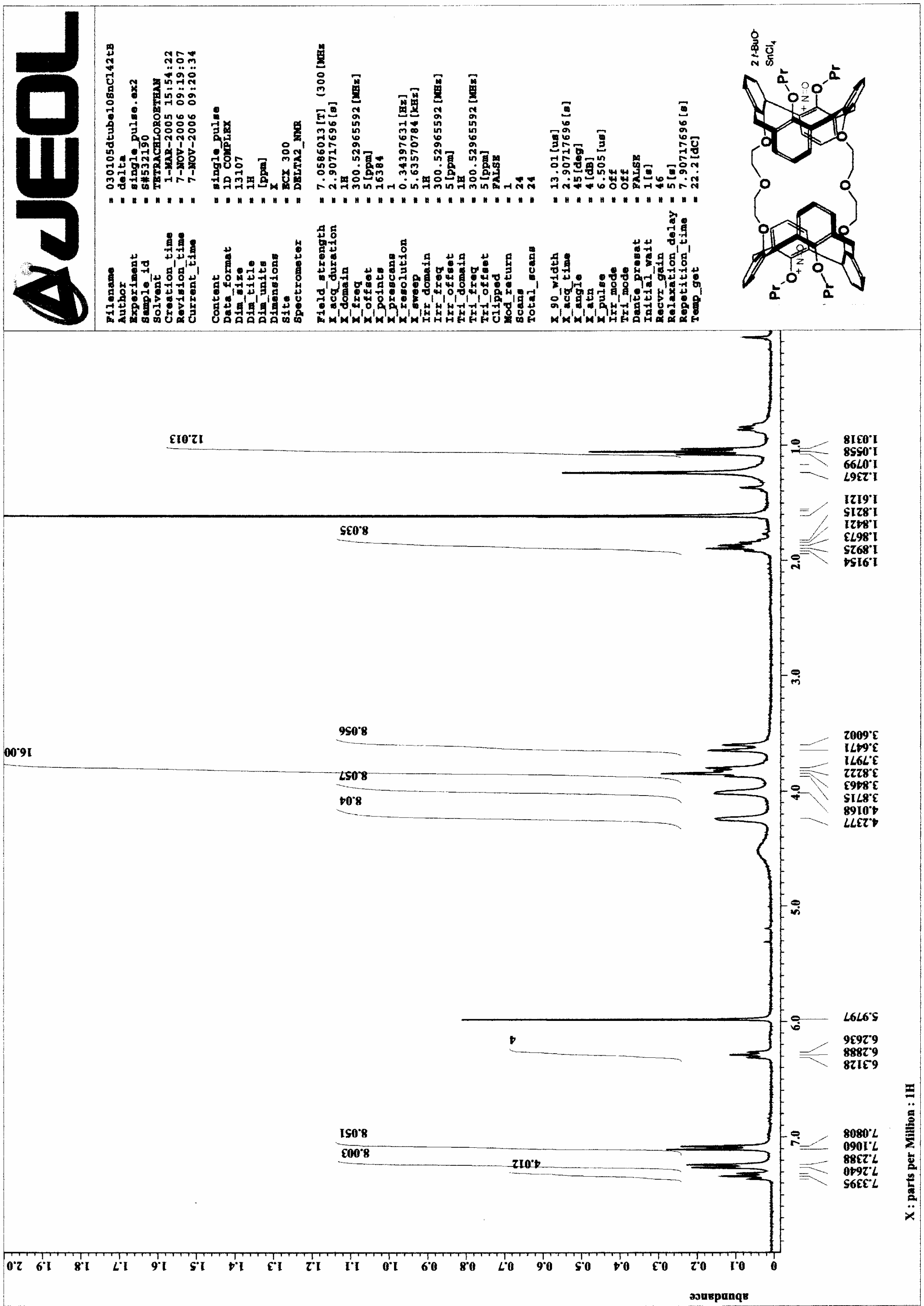
JEOL
Filename = 030105dtube108SnCl42tB
Author = delta
Experiment = single_pulse.ex2
Sample_id = S#532190
Solvent = TETRACHLOROETHAN
Creation_time = 1-MAR-2005 15:54:22
Revision_time = 7-NOV-2006 09:19:07
Current_time = 7-NOV-2006 09:20:34
Content = single_pulse
Data_format = 1D COMPLEX
Dim_size = 13107
Dim_title = 1H
Dim_units = [ppm]
Dimensions = X
Site = ECX 300
Spectrometer = DELTA2_NMR
Field_strength = 7.0586013[T] (300[MHz
X_acq_duration = 2.90717696[s]
X_domain = 1H
X_freq = 300.52965592[MHz]
X_offset = 5[ppm]
X_points = 16384
X_prescans = 1
X_resolution = 0.34397631[Hz]
X_sweep = 5.63570784[kHz]
Irr_domain = 1H
Irr_freq = 300.52965592[MHz]
Irr_offset = 5[ppm]
Tri_domain = 1H
Tri_freq = 300.52965592[MHz]
Tri_offset = 5[ppm]
Clipped = FALSE
Mod_return = 1
Scans = 24
Total_scans = 24
X_90_width = 13.01[us]
X_acq_time = 2.90717696[s]
X_angle = 45[deg]
X_atn = 4[dB]
X_pulse = 6.505[us]
Irr_mode = Off
Tri_mode = Off
Dante_presat = FALSE
Initial_wait = 1[s]
Recvr_gain = 46
Relaxation_delay = 5[s]
Repetition_time = 7.90717696[s]
Temp_get = 22.2[dC]
2 t-BuO⁻
SnCl4
Pr
Pr
N
O
abundance
X : parts per Million : 1H
16.00
12.013
8.035
8.056
8.057
8.04
4
8.051
8.003
4.012
1.0318
1.0558
1.0799
1.2367
1.6121
1.8215
1.8421
1.8673
1.8925
1.9154
3.6002
3.6471
3.7971
3.8222
3.8463
3.8715
4.0168
4.2377
5.9797
6.2636
6.2888
6.3128
7.0808
7.1060
7.2388
7.2640
7.3395

APPENDIX 19

^{1}H NMR SPECTRA OF
TRISCALIX[4]TUBE-NO^{+} COMPLEX (34)

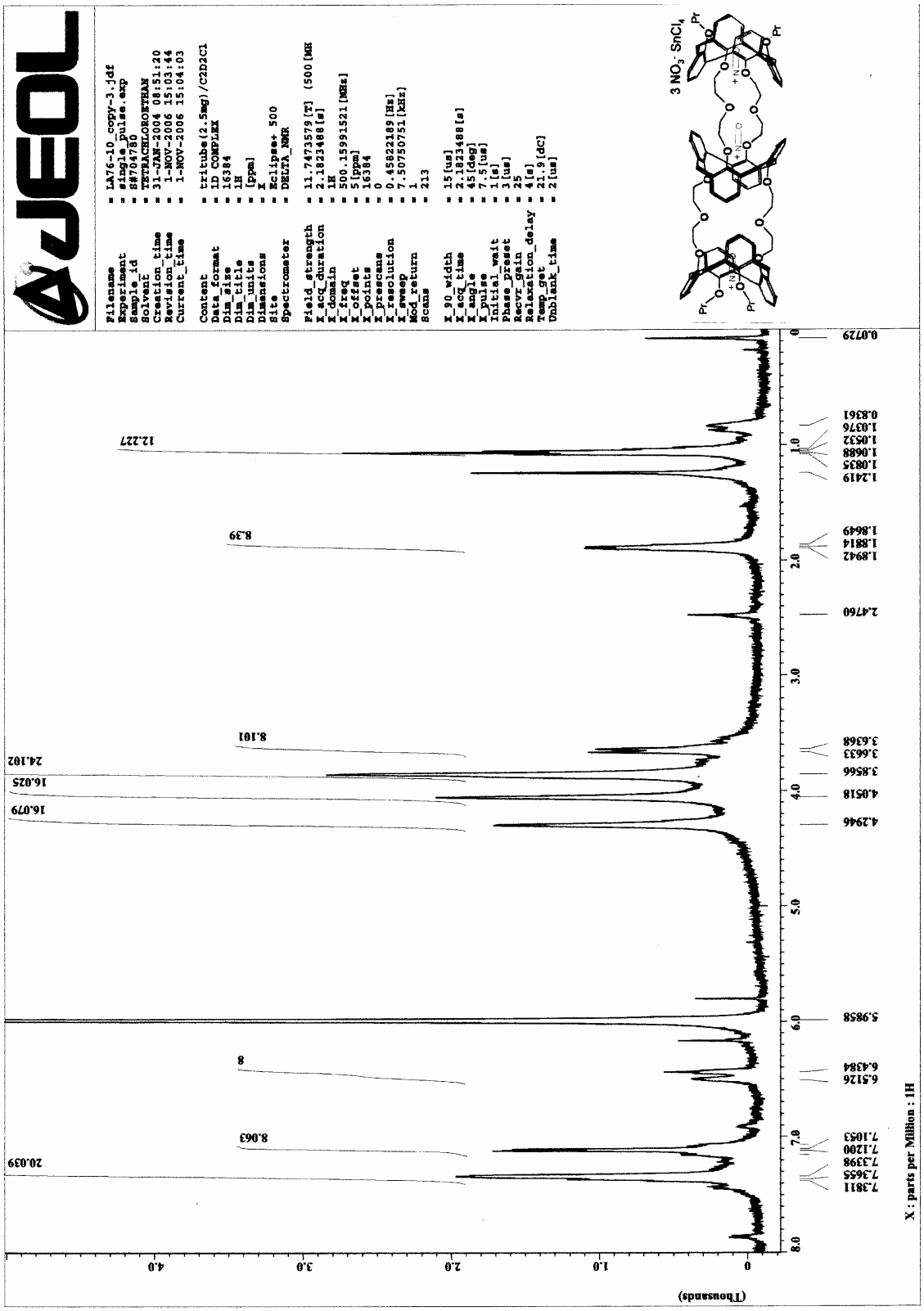
JEOL
Filename = LA76-10_copy-3.jdf
Experiment = single_pulse.exp
Sample_id = S#704780
Solvent = TETRACHLOROETHAN
Creation_time = 31-JAN-2004 08:51:20
Revision_time = 1-NOV-2006 15:03:44
Current_Time = 1-NOV-2006 15:04:03
Content = tritube(2.5mg)/C2D2Cl
Data_format = 1D COMPLEX
Dim_size = 16384
Dim_title = 1H
Dim_units = [ppm]
Dimensions = X
Site = Eclipse+ 500
Spectrometer = DELTA_NMR
Field_strength = 11.7473579[T] (500[MH
X_acq_duration = 2.1823488[s]
X_domain = 1H
X_freq = 500.15991521[MHz]
X_offset = 5[ppm]
X_points = 16384
X_prescans = 0
X_resolution = 0.45822189[Hz]
X_sweep = 7.50750751[kHz]
Mod_return = 1
Scans = 213
X_90_width = 15[us]
X_acq_time = 2.1823488[s]
X_angle = 45[deg]
X_pulse = 7.5[us]
Initial_wait = 1[s]
Phase_preset = 3[us]
Recvr_gain = 25
Relaxation_delay = 4[s]
Temp_get = 21.9[dC]
Unblank_time = 2[us]
3 NO3- SnCl4
Pr
Pr
Pr
Pr
20.039
8.063
8
12.227
8.39
8.101
24.102
16.025
16.079
0.0729
0.8361
1.0376
1.0532
1.0688
1.0835
1.2419
1.8649
1.8814
1.8942
2.4760
3.6368
3.6633
3.8566
4.0518
4.2946
5.9858
6.4384
6.5126
7.1053
7.1200
7.3398
7.3655
7.3811
(Thousands)
X : parts per Million : 1H

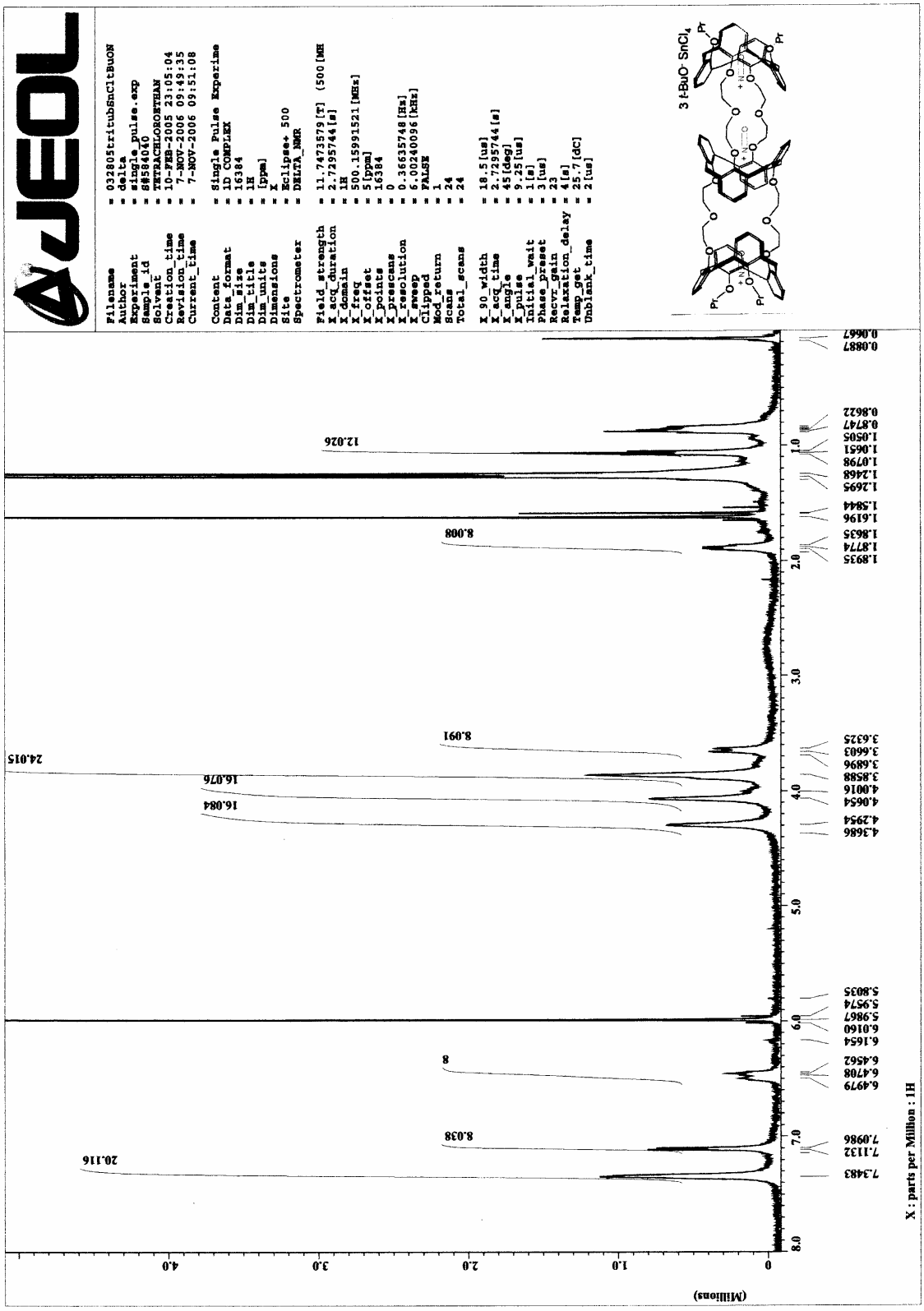
JEOL
Filename = 032805tritubSnCltBuON
Author = delta
Experiment = single_pulse.exp
Sample_id = #4584040
Solvent = TETRACHLOROETHAN
Creation_time = 10-FEB-2005 23:05:04
Revision_time = 7-NOV-2006 09:49:35
Current_Time = 7-NOV-2006 09:51:08
Content = Single Pulse Experime
Data_format = 1D COMPLEX
Dim_size = 16384
Dim_title = 1H
Dim_units = [ppm]
Dimensions = X
Site = Eclipse+ 500
Spectrometer = DELTA_NMR
Field_strength = 11.7473579[T] (500[MH
X_acq_duration = 2.7295744[s]
X_domain = 1H
X_freq = 500.15991521[MHz]
X_offset = 5[ppm]
X_points = 16384
X_prescans = 0
X_resolution = 0.36635748[Hz]
X_sweep = 6.00240096[kHz]
Clipped = FALSE
Mod_return = 1
Scans = 24
Total_scans = 24
X_90_width = 18.5[us]
X_acq_time = 2.7295744[s]
X_angle = 45[deg]
X_pulse = 9.25[us]
Initial_wait = 1[s]
Phase_preset = 3[us]
Recvr_gain = 23
Relaxation_delay = 4[s]
Temp_get = 25.7[dC]
Unblank_time = 2[us]
3 t-BuO⁻ SnCl4
Pr
Pr
Pr
Pr
20.116
8.038
8
8.008
8.091
24.015
16.076
16.084
12.026
X : parts per Million : 1H
(Millions)
0.0667
0.0887
0.8622
0.8747
1.0505
1.0651
1.0798
1.2468
1.2695
1.5844
1.6196
1.8635
1.8774
1.8935
3.6325
3.6603
3.6896
3.8588
4.0016
4.0654
4.2954
4.3686
5.8035
5.9574
5.9867
6.0160
6.1654
6.4562
6.4708
6.4979
7.0986
7.1132
7.3483

APPENDIX 20

^{1}H NMR SPECTRA OF
TETRACALIX[4]TUBE-NO^{+} COMPLEX (35)

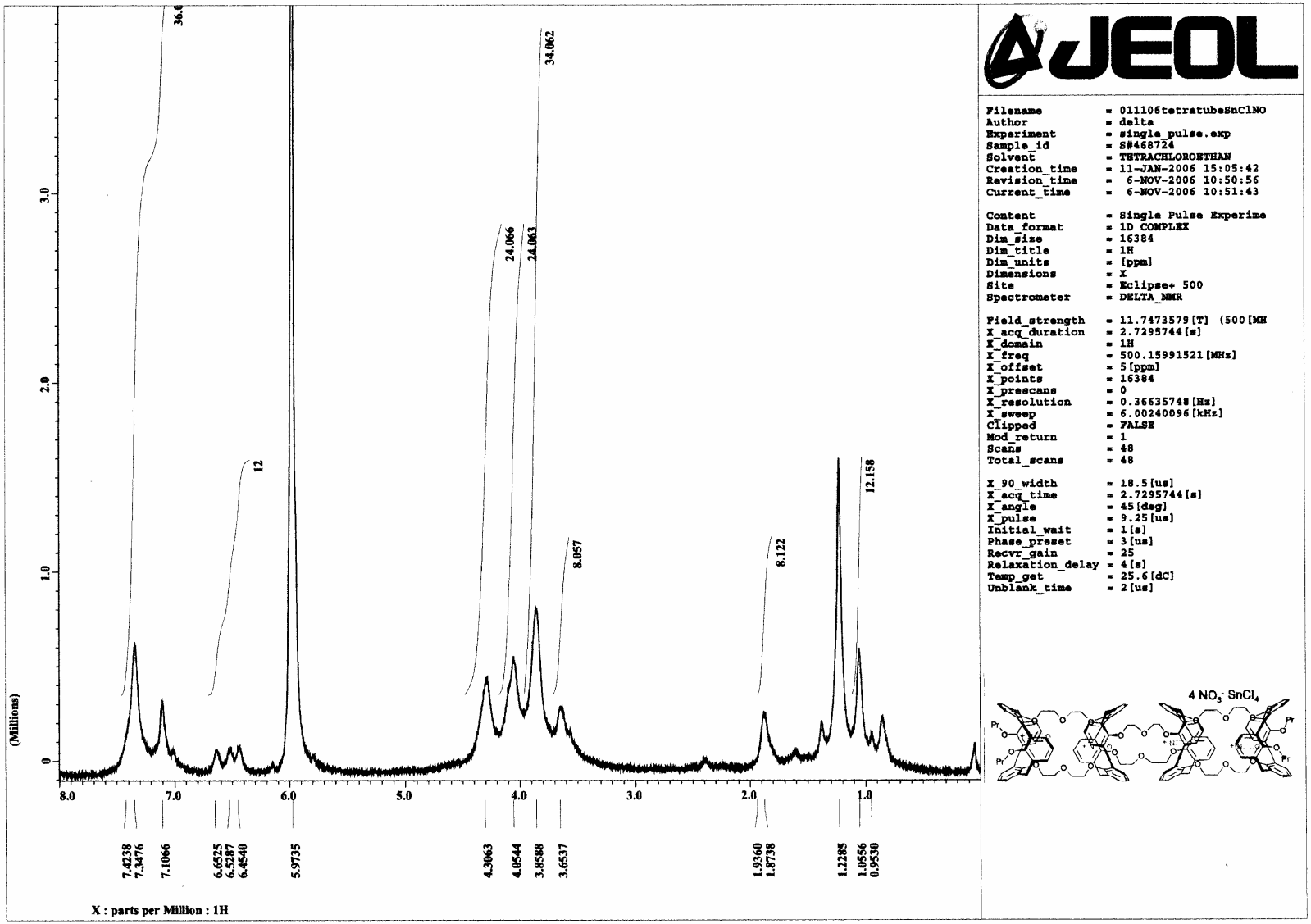
36.0
34.062
24.066
24.063
12
8.057
8.122
12.158
(Millions)
3.0
2.0
1.0
0
8.0
7.0
6.0
5.0
4.0
3.0
2.0
1.0
7.4238
7.3476
7.1066
6.6525
6.5287
6.4540
5.9735
4.3063
4.0544
3.8588
3.6537
1.9360
1.8738
1.2285
1.0556
0.9530
X : parts per Million : 1H
JEOL
Filename = 011106tetratubeSnClNO
Author = delta
Experiment = single_pulse.exp
Sample_id = S#468724
Solvent = TETRACHLOROETHAN
Creation_time = 11-JAN-2006 15:05:42
Revision_time = 6-NOV-2006 10:50:56
Current_time = 6-NOV-2006 10:51:43
Content = Single Pulse Experime
Data_format = 1D COMPLEX
Dim_size = 16384
Dim_title = 1H
Dim_units = [ppm]
Dimensions = X
Site = Eclipse+ 500
Spectrometer = DELTA_NMR
Field_strength = 11.7473579[T] (500[MH
X_acq_duration = 2.7295744[s]
X_domain = 1H
X_freq = 500.15991521[MHz]
X_offset = 5[ppm]
X_points = 16384
X_prescans = 0
X_resolution = 0.36635748[Hz]
X_sweep = 6.00240096[kHz]
Clipped = FALSE
Mod_return = 1
Scans = 48
Total_scans = 48
X_90_width = 18.5[us]
X_acq_time = 2.7295744[s]
X_angle = 45[deg]
X_pulse = 9.25[us]
Initial_wait = 1[s]
Phase_preset = 3[us]
Recvr_gain = 25
Relaxation_delay = 4[s]
Temp_get = 25.6[dC]
Unblank_time = 2[us]
4 NO3- SnCl4


JEOL
Filename = 033106tetratubeTFAtBu
Author = delta
Experiment = single_pulse.exp
Sample_id = 8437595
Solvent = TETRACHLOROETHAN
Creation_time = 31-MAR-2006 13:11:37
Revision_time = 7-NOV-2006 10:27:18
Current_time = 7-NOV-2006 10:27:38
Content = Single Pulse Experime
Data_format = 1D COMPLEX
Dim_size = 16384
Dim_title = 1H
Dim_units = [ppm]
Dimensions = X
Site = Eclipse+ 500
Spectrometer = DELTA_NMR
Field_strength = 11.7473579[T] (500[MH
X_acq_duration = 2.7295744[s]
X_domain = 1H
X_freq = 500.15991521[MHz]
X_offset = 5[ppm]
X_points = 16384
X_prescans = 0
X_resolution = 0.36635748[Hz]
X_sweep = 6.00240096[kHz]
Clipped = FALSE
Mod_return = 1
Scans = 12
Total_scans = 12
X_90_width = 18.5[us]
X_acq_time = 2.7295744[s]
X_angle = 45[deg]
X_pulse = 9.25[us]
Initial_wait = 1[s]
Phase_preset = 3[us]
Recvr_gain = 18
Relaxation_delay = 4[s]
Temp_get = 24.6[dC]
Dnblank_time = 2[us]
4 t-BuO-TFA
12.002
8.191
8.073
8.049
4
36.142
34.086
24.125
24.017
10.4431
10.4094
10.3742
7.3608
7.3461
7.1410
7.1257
6.6107
6.5726
6.4078
6.3932
6.0211
5.9867
5.9522
4.2748
4.0199
3.8698
3.8559
3.8419
1.7192
1.5603
1.4321
1.4152
1.3808
1.3464
1.2504
1.0629
1.0483
(Millions)
X : parts per Million : 1H

APPENDIX 21

^{1}H NMR SPECTRA OF
PENTACALIX[4]TUBE-NO^{+} COMPLEX (36)

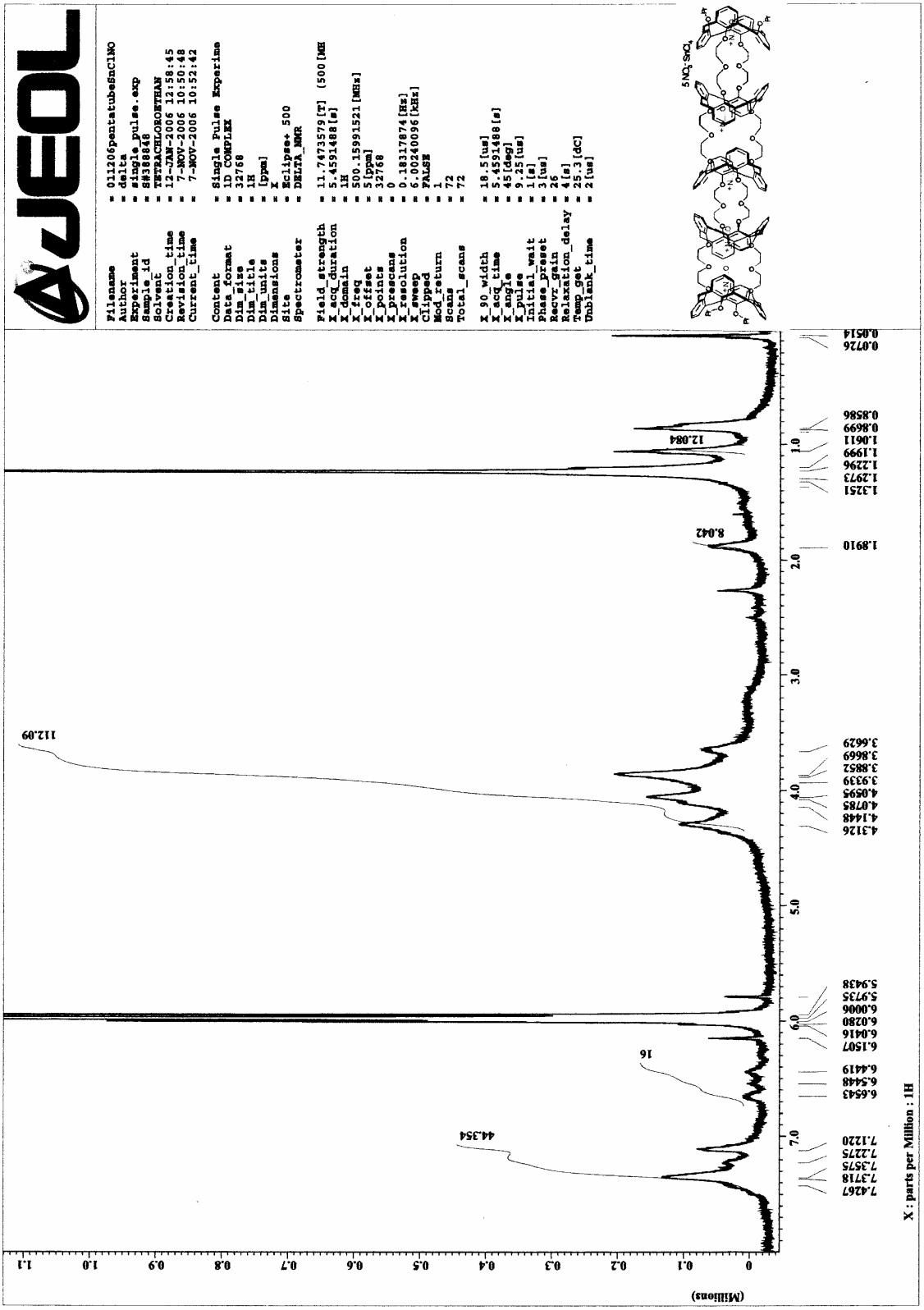
JEOL
Filename = 011206pentatubeSnClNO
Author = delta
Experiment = single_pulse.exp
Sample_id = s#3188848
Solvent = TETRACHLOROETHAN
Creation_time = 12-JAN-2006 12:58:45
Revision_time = 7-NOV-2006 10:50:48
Current_time = 7-NOV-2006 10:52:42
Content = Single Pulse Experime
Data_format = 1D COMPLEX
Dim_size = 32768
Dim_title = 1H
Dim_units = [ppm]
Dimensions = X
Site = Eclipse+ 500
Spectrometer = DELTA_NMR
Field_strength = 11.7473579[T] (500[MH
X_acq_duration = 5.45914080[s]
X_domain = 1H
X_freq = 500.15991521[MHz]
X_offset = 5[ppm]
X_points = 32768
X_prescans = 0
X_resolution = 0.18317874[Hz]
X_sweep = 6.00240096[kHz]
Clipped = FALSE
Mod_return = 1
Scans = 72
Total_scans = 72
X_90_width = 18.5[us]
X_acq_time = 5.45914080[s]
X_angle = 45[deg]
X_pulse = 9.25[us]
Initial_wait = 1[s]
Phase_preset = 3[us]
Recvr_gain = 26
Relaxation_delay = 4[s]
Temp_get = 25.3[dC]
Unblank_time = 2[us]
5NQ:SnCl4
112.09
44.354
16
12.084
8.042
1.8910
X : parts per Million : 1H
(Millions)

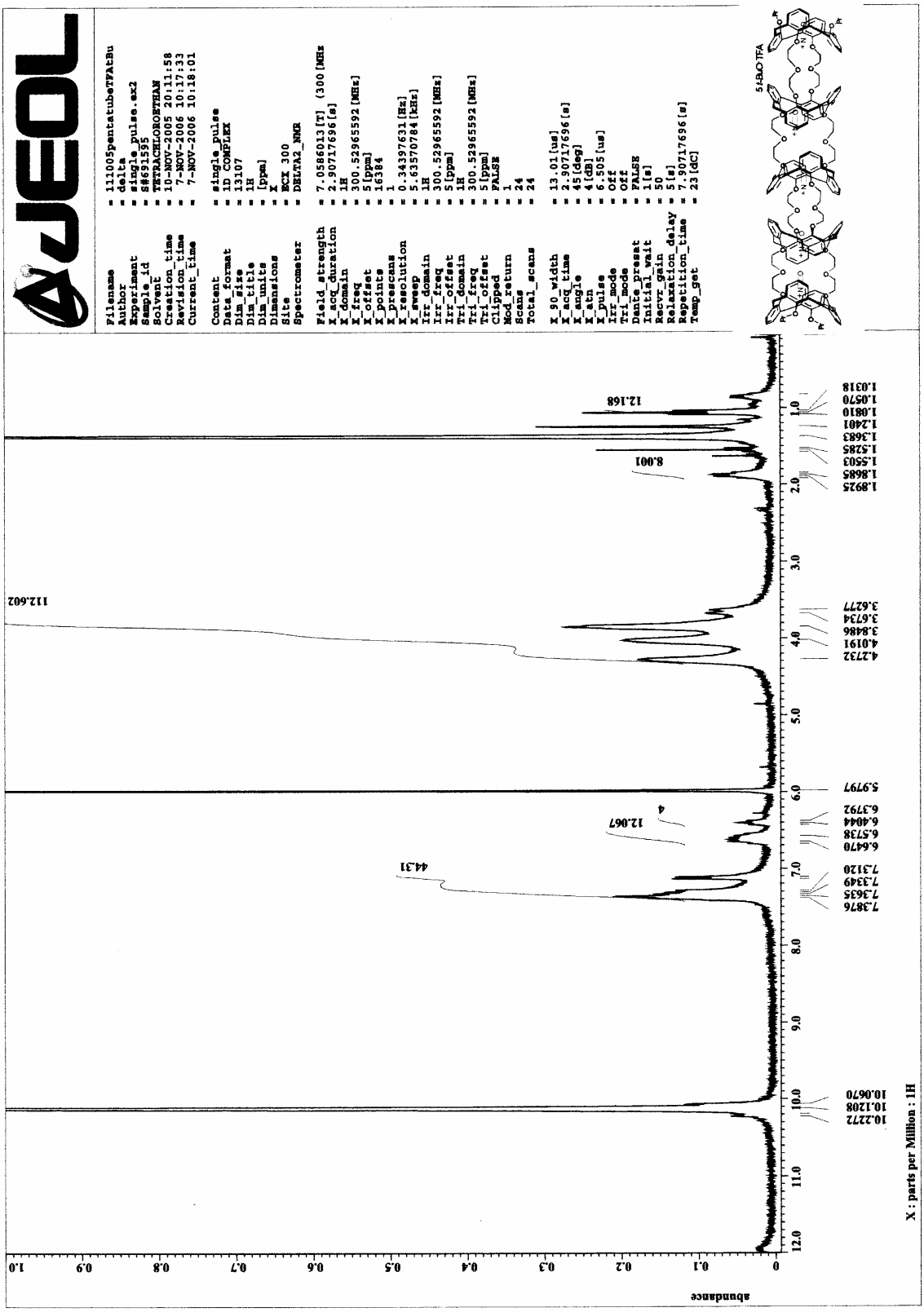
JEOL
Filename = 111005pentatubeTFAtBu
Author = delta
Experiment = single_pulse.ex2
Sample_id = S#691595
Solvent = TETRACHLOROETHAN
Creation_time = 10-NOV-2005 20:11:58
Revision_time = 7-NOV-2006 10:17:33
Current_time = 7-NOV-2006 10:18:01
Content = single_pulse
Data_format = 1D COMPLEX
Dim_size = 13107
Dim_title = 1H
Dim_units = [ppm]
Dimensions = X
Site = ECX 300
Spectrometer = DELTA2_NMR
Field_strength = 7.0586013[T] (300[MHz
X_acq_duration = 2.90717696[s]
X_domain = 1H
X_freq = 300.52965592[MHz]
X_offset = 5[ppm]
X_points = 16384
X_prescans = 1
X_resolution = 0.34397631[Hz]
X_sweep = 5.63570784[kHz]
Irr_domain = 1H
Irr_freq = 300.52965592[MHz]
Irr_offset = 5[ppm]
Tri_domain = 1H
Tri_freq = 300.52965592[MHz]
Tri_offset = 5[ppm]
Clipped = FALSE
Mod_return = 1
Scans = 24
Total_scans = 24
X_90_width = 13.01[us]
X_acq_time = 2.90717696[s]
X_angle = 45[deg]
X_atn = 4[dB]
X_pulse = 6.505[us]
Irr_mode = Off
Tri_mode = Off
Dante_presat = FALSE
Initial_wait = 1[s]
Recvr_gain = 50
Relaxation_delay = 5[s]
Repetition_time = 7.90717696[s]
Temp_get = 23[dC]
5+BAOTFA
abundance
X : parts per Million : 1H
112.602
44.31
12.067
8.001
12.168
10.2272
10.1208
10.0670
7.3876
7.3635
7.3349
7.3120
6.6470
6.5738
6.4044
6.3792
5.9797
4.2732
4.0191
3.8486
3.6734
3.6277
1.8925
1.8685
1.5503
1.5285
1.3683
1.2401
1.0810
1.0570
1.0318

APPENDIX 22

X-RAY CRYSTAL DATA FOR
DIMERIC CALIX[4]TUBE 15• 2 $CHCl_3$

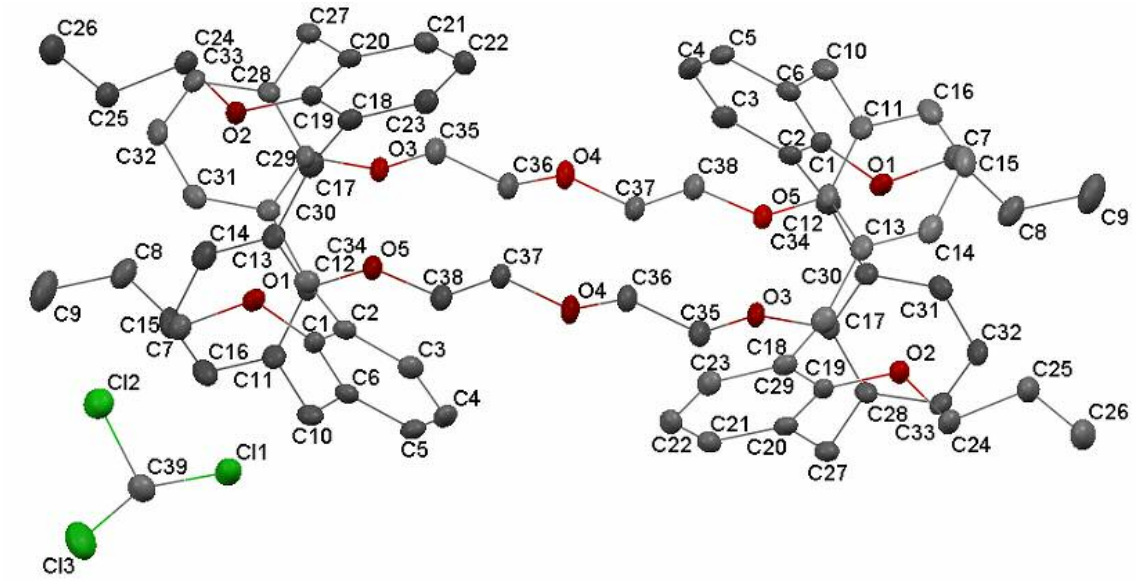

Formula	$C_{78}H_{86}Cl_6O_{10}$
Crystal System	Monoclinic
Space Group	P $2_1/n$
Cell Lengths	a = 17.9825(7) Å, b = 10.6205(4) Å, c = 19.8479(7) Å
Cell Angles	α = 90.00°, β = 111.7390(10)°, γ = 90.00°
Cell Volume	3521.0(2) $Å^3$
Z	2
Density (calculated)	1.317 Mg/m^3
Crystal size	0.36 x 0.17 x 0.02 mm^3
Goodness-of-fit on F^2	1.040
Final R indices [I>2σ(I)]	R1 = 0.0397, wR2 = 0.1024
R indices (all data)	R1 = 0.0465, wR2 = 0.1077

Bond Lengths for **15•2CHCl$_3$**:

Atom 1	Atom 2	Distance (Å)	Atom 1	Atom 2	Distance (Å)
Cl1	C39	1.7629(19)	Cl2	C39	1.772(2)
Cl3	C39	1.7566(19)	O1	C1	1.3857(19)
O1	C7	1.431(2)	O5	C12	1.3829(19)
O5	C38	1.4201(19)	O4	C36	1.421(2)
O4	C37	1.4262(19)	O3	C29	1.3905(18)
O3	C35	1.429(2)	O2	C19	1.3865(19)
O2	C24	1.438(2)	C1	C2	1.401(2)
C1	C6	1.401(2)	C2	C3	1.396(2)
C2	C34	1.517(2)	C3	C4	1.385(3)
C3	H3	0.9500	C4	C5	1.386(3)
C4	H4	0.9500	C5	C6	1.397(2)

C5	H5	0.9500	C6	C10	1.514(2)
C7	C8	1.515(2)	C7	H7A	0.9900
C7	H7B	0.9900	C8	C9	1.524(3)
C8	H8A	0.9900	C8	H8B	0.9900
C9	H9A	0.9800	C9	H9B	0.9800
C9	H9C	0 .9800	C10	C11	1.515(2)
C10	H10A	0.9900	C10	H10B	0.9900
C11	C16	1.393(2)	C11	C12	1.399(2)
C12	O5	1.3828(19)	C12	C13	1.401(2)
C13	C14	1.394(2)	C13	C17	1.516(2)
C14	C15	1.385(3)	C14	H14	0.9500
C15	C16	1.382(3)	C15	H15	0.9500
C16	H16	0.9500	C17	C18	1.514(2)
C17	H17A	0.9900	C17	H17B	0.9900
C38	C37	1.507(2)	C38	H38A	0.9900
C38	H38B	0.9900	C37	H37A	0.9900
C37	H37B	0.9900	C36	C35	1.512(2)
C36	H36A	0.9900	C36	H36B	0.9900
C35	H35A	0.9900	C35	H35B	0.9900
C29	C28	1.395(2)	C29	C30	1.397(2)
C28	C33	1.398(2)	C28	C27	1.513(2)
C33	C32	1.384(2)	C33	H33	0.9500
C32	C31	1.385(2)	C32	H32	0.9500
C31	C30	1.392(2)	C31	H31	0.9500
C30	C34	1.515(2)	C34	H34A	0.9900
C34	H34B	0.9900	C27	C20	1.516(2)
C27	H27A	0.9900	C27	H27B	0.9900
C20	C21	1.393(2)	C20	C19	1.395(2)
C19	C18	1.399(2)	C18	C23	1.391(2)
C23	C22	1.387(2)	C23	H23	0.9500
C22	C21	1.388(2)	C22	H22	0.9500
C21	H21	0.9500	C24	C25	1.515(2)
C24	H24A	0.9900	C24	H24B	0.9900
C25	C26	1.527(3)	C25	H25A	0.9900
C25	H25B	0.9900	C26	H26A	0.9800
C26	H26B	0.9800	C26	H26C	0.9800
C39	H39	1.0000			

Bond Angles for **15•2CHCl$_3$**:

Atom 1	Atom 2	Atom 3	Angle (°)	Atom 1	Atom 2	Atom 3	Angle (°)
C1	O1	C7	116.85(12)	C12	O5	C38	116.34(12)
C36	O4	C37	111.50(13)	C29	O3	C35	114.49(12)

C19	O2	C24	113.74(12)	O1	C1	C2	120.07(14)
O1	C1	C6	118.59(14)	C2	C1	C6	121.18(15)
C3	C2	C1	118.42(15)	C3	C2	C34	118.06(15)
C1	C2	C34	123.33(14)	C4	C3	C2	121.09(16)
C4	C3	H3	119.5	C2	C3	H3	119.5
C3	C4	C5	119.80(16)	C3	C4	H4	120.1
C5	C4	H4	120.1	C4	C5	C6	120.88(16)
C4	C5	H5	119.6	C6	C5	H5	119.6
C5	C6	C1	118.55(16)	C5	C6	C10	118.71(15)
C1	C6	C10	122.61(15)	O1	C7	C8	107.25(14)
O1	C7	H7A	110.3	C8	C7	H7A	110.3
O1	C7	H7B	110.3	C8	C7	H7B	110.3
H7A	C7	H7B	108.5	C7	C8	C9	110.71(17)
C7	C8	H8A	109.5	C9	C8	H8A	109.5
C7	C8	H8B	109.5	C9	C8	H8B	109.5
H8A	C8	H8B	108.1	C8	C9	H9A	109.5
C8	C9	H9B	109.5	H9A	C9	H9B	109.5
C8	C9	H9C	109.5	H9A	C9	H9C	109.5
H9B	C9	H9C	109.5	C6	C10	C11	120.45(14)
C6	C10	H10A	107.2	C11	C10	H10A	107.2
C6	C10	H10B	107.2	C11	C10	H10B	107.2
H10A	C10	H10B	106.8	C16	C11	C12	117.71(16)
C16	C11	C10	118.89(15)	C12	C11	C10	123.35(15)
O5	C12	C11	119.57(15)	O5	C12	C13	118.21(15)
C11	C12	C13	122.01(15)	C14	C13	C12	117.90(16)
C14	C13	C17	119.34(15)	C12	C13	C17	122.63(15)
C15	C14	C13	121.24(17)	C15	C14	H14	119.4
C13	C14	H14	119.4	C16	C15	C14	119.52(16)
C16	C15	H15	120.2	C14	C15	H15	120.2
C15	C16	C11	121.62(17)	C15	C16	H16	119.2
C11	C16	H16	119.2	C18	C17	C13	118.56(14)
C18	C17	H17A	107.7	C13	C17	H17A	107.7
C18	C17	H17B	107.7	C13	C17	H17B	107.7
H17A	C17	H17B	107.1	O5	C38	C37	105.20(13)
O5	C38	H38A	110.7	C37	C38	H38A	110.7
O5	C38	H38B	110.7	C37	C38	H38B	110.7
H38A	C38	H38B	108.8	O4	C37	C38	108.04(13)
O4	C37	H37A	110.1	C38	C37	H37A	110.1
O4	C37	H37B	110.1	C38	C37	H37B	110.1
H37A	C37	H37B	108.4	O4	C36	C35	108.32(14)
O4	C36	H36A	110.0	C35	C36	H36A	110.0
O4	C36	H36B	110.0	C35	C36	H36B	110.0
H36A	C36	H36B	108.4	O3	C35	C36	105.62(13)
O3	C35	H35A	110.6	C36	C35	H35A	110.6

O3	C35	H35B	110.6	C36	C35	H35B	110.6
H35A	C35	H35B	108.7	O3	C29	C28	119.08(14)
O3	C29	C30	118.77(14)	C28	C29	C30	122.06(14)
C29	C28	C33	117.93(15)	C29	C28	C27	122.43(14)
C33	C28	C27	119.59(15)	C32	C33	C28	121.09(16)
C32	C33	H33	119.5	C28	C33	H33	119.5
C33	C32	C31	119.62(15)	C33	C32	H32	120.2
C31	C32	H32	120.2	C32	C31	C30	121.27(16)
C32	C31	H31	119.4	C30	C31	H31	119.4
C31	C30	C29	117.94(15)	C31	C30	C34	119.65(15)
C29	C30	C34	122.39(14)	C30	C34	C2	119.43(14)
C30	C34	H34A	107.5	C2	C34	H34A	107.5
C30	C34	H34B	107.5	C2	C34	H34B	107.5
H34A	C34	H34B	107.0	C28	C27	C20	117.12(13)
C28	C27	H27A	108.0	C20	C27	H27A	108.0
C28	C27	H27B	108.0	C20	C27	H27B	108.0
H27A	C27	H27B	107.3	C21	C20	C19	118.64(15)
C21	C20	C27	119.97(15)	C19	C20	C27	121.36(14)
O2	C19	C20	119.26(14)	O2	C19	C18	119.41(14)
C20	C19	C18	121.24(15)	C23	C18	C19	118.35(15)
C23	C18	C17	119.52(15)	C19	C18	C17	122.13(15)
C22	C23	C18	121.34(15)	C22	C23	H23	119.3
C18	C23	H23	119.3	C23	C22	C21	119.29(15)
C23	C22	H22	120.4	C21	C22	H22	120.4
C22	C21	C20	121.01(16)	C22	C21	H21	119.5
C20	C21	H21	119.5	O2	C24	C25	108.01(14)
O2	C24	H24A	110.1	C25	C24	H24A	110.1
O2	C24	H24B	110.1	C25	C24	H24B	110.1
H24A	C24	H24B	108.4	C24	C25	C26	111.20(15)
C24	C25	H25A	109.4	C26	C25	H25A	109.4
C24	C25	H25B	109.4	C26	C25	H25B	109.4
H25A	C25	H25B	108.0	C25	C26	H26A	109.5
C25	C26	H26B	109.5	H26A	C26	H26B	109.5
C25	C26	H26C	109.5	H26A	C26	H26C	109.5
H26B	C26	H26C	109.5	Cl3	C39	Cl1	110.95(11)
Cl3	C39	Cl2	110.64(10)	Cl1	C39	Cl2	110.77(10)
Cl3	C39	H39	108.1	Cl1	C39	H39	108.1
Cl2	C39	H39	108.1				

APPENDIX 23

X-RAY CRYSTAL DATA FOR
TRIMERIC CALIX[4]TUBE 16•4.5 $CHCl_3$

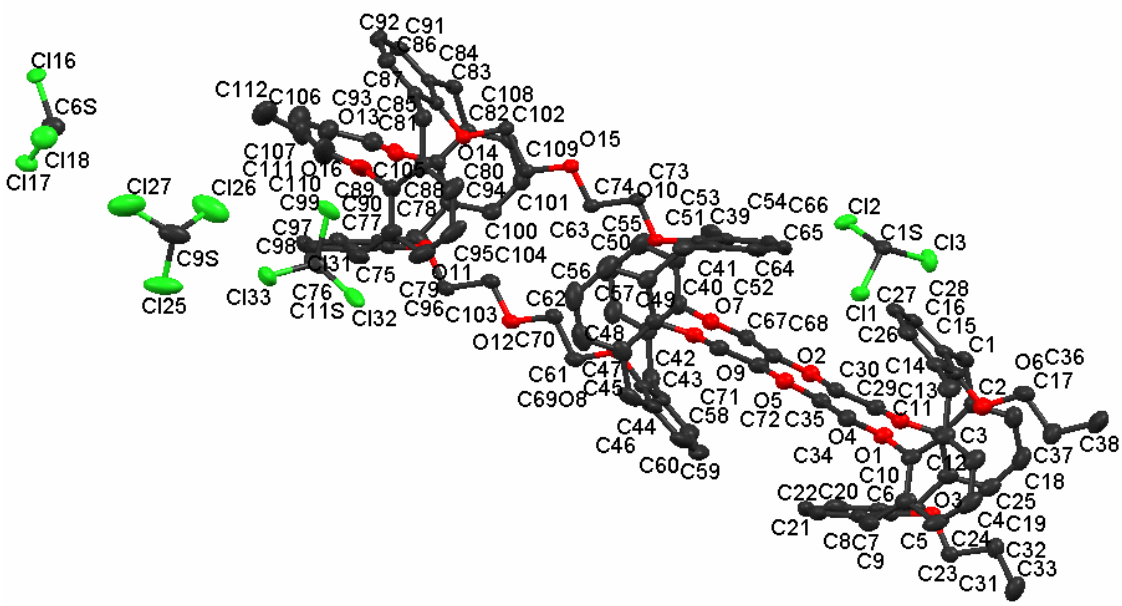

Formula	$C_{116.5}H_{124.5}C_{113.5}O_{16}$
Crystal System	Triclinic
Space Group	P – 1
Cell Lengths	a = 14.7634(6) Å, b = 15.2376(6) Å, c = 26.4844(11) Å
Cell Angles	α = 75.9360(10)°, β = 78.0270(10)°, γ = 80.0890(10)°
Cell Volume	5606.9(4) $Å^3$
Z	2
Density (calculated)	1.338 Mg/m^3
Crystal size	0.31 x 0.27 x 0.07 mm^3
Goodness-of-fit on F^2	1.105
Final R indices [I>2σ(I)]	R1 = 0.0828, wR2 = 0.1667
R indices (all data)	R1 = 0.1100, wR2 = 0.1783

Bond Lengths for **16•4.5CHCl$_3$**:

Atom 1	Atom 2	Distance (Å)	Atom 1	Atom 2	Distance (Å)
C1	C2	1.511(5)	C1	C16	1.520(6)
C2	C17	1.390(5)	C2	C3	1.399(5)
C3	C4	1.385(5)	C3	O1	1.388(4)
C4	C19	1.402(5)	C4	C5	1.512(5)
C5	C6	1.508(5)	C6	C20	1.395(6)
C6	C7	1.401(5)	C7	O3	1.381(4)
C7	C8	1.404(5)	C8	C22	1.386(6)

C8	C9	1.519(6)	C9	C10	1.501(6)
C10	C23	1.395(6)	C10	C11	1.410(5)
C11	C12	1.380(6)	C11	O4	1.384(4)
C12	C25	1.402(5)	C12	C13	1.524(5)
C13	C14	1.517(5)	C14	C26	1.373(5)
C14	C15	1.401(6)	C15	O6	1.370(4)
C15	C16	1.405(5)	C16	C28	1.393(5)
C17	C18	1.392(6)	C18	C19	1.372(6)
C20	C21	1.375(7)	C21	C22	1.376(7)
C23	C24	1.367(7)	C24	C25	1.387(6)
C26	C27	1.401(6)	C27	C28	1.375(6)
O1	C29	1.434(4)	C29	C30	1.507(5)
C30	O2	1.436(4)	O2	C68	1.428(4)
O3	C31	1.430(4)	C31	C32	1.504(5)
C32	C33	1.530(6)	O4	C34	1.431(4)
C34	C35	1.502(5)	C35	O5	1.421(4)
O5	C72	1.414(4)	O6	C36	1.386(5)
C36	C37	1.568(6)	C37	C38	1.514(6)
C39	C54	1.504(6)	C39	C40	1.509(6)
C40	C55	1.392(6)	C40	C41	1.413(5)
C41	C42	1.387(5)	C41	O7	1.391(4)
C42	C57	1.417(5)	C42	C43	1.510(5)
C43	C44	1.508(6)	C44	C58	1.391(5)
C44	C45	1.406(6)	C45	O8	1.388(4)
C45	C46	1.399(5)	C46	C60	1.415(6)
C46	C47	1.514(6)	C47	C48	1.520(6)
C48	C61	1.385(6)	C48	C49	1.392(5)
C49	O9	1.383(4)	C49	C50	1.395(5)
C50	C63	1.388(6)	C50	C51	1.521(6)
C51	C52	1.523(6)	C52	C64	1.381(6)
C52	C53	1.398(6)	C53	O10	1.388(4)
C53	C54	1.393(5)	C54	C66	1.397(6)
C55	C56	1.364(7)	C56	C57	1.367(6)
C58	C59	1.362(7)	C59	C60	1.382(7)
C61	C62	1.372(7)	C62	C63	1.397(7)
C64	C65	1.398(8)	C65	C66	1.362(8)
O7	C67	1.424(4)	C67	C68	1.513(5)
O8	C69	1.420(4)	C69	C70	1.513(5)
C70	O12	1.423(4)	O9	C71	1.427(4)
C71	C72	1.510(5)	O10	C73	1.430(4)
C73	C74	1.503(5)	C74	O15	1.419(4)
C75	C90	1.503(7)	C75	C76	1.515(7)
C76	C97	1.399(6)	C76	C77	1.407(5)
C77	C78	1.383(6)	C77	O11	1.390(5)

C78	C99	1.397(6)	C78	C79	1.512(6)
C79	C80	1.529(5)	C80	C100	1.391(5)
C80	C81	1.400(5)	C81	O13	1.388(4)
C81	C82	1.394(5)	C82	C102	1.385(5)
C82	C83	1.514(5)	C83	C84	1.526(5)
C84	C91	1.396(5)	C84	C85	1.398(5)
C85	O14	1.390(4)	C85	C86	1.393(5)
C86	C93	1.399(5)	C86	C87	1.519(5)
C87	C88	1.521(5)	C88	C94	1.386(5)
C88	C89	1.398(6)	C89	O16	1.379(5)
C89	C90	1.406(5)	C90	C96	1.385(6)
C91	C92	1.369(5)	C92	C93	1.387(5)
C94	C95	1.385(6)	C95	C96	1.393(7)
C97	C98	1.385(7)	C98	C99	1.379(7)
C100	C101	1.379(5)	C101	C102	1.383(5)
O11	C103	1.435(4)	C103	C104	1.498(5)
C104	O12	1.433(4)	O13	C105	1.412(5)
C105	C106	1.527(6)	C106	C107	1.495(7)
O14	C108	1.430(4)	C108	C109	1.508(4)
C109	O15	1.432(4)	O16	C110	1.350(12)
O16	C113	1.448(14)	C110	C111	1.483(12)
C111	C112	1.463(11)	C113	C114	1.468(13)
C114	C115	1.427(14)	C1S	Cl1	1.761(5)
C1S	Cl3	1.762(5)	C1S	Cl2	1.775(5)
C2S	Cl6	1.761(14)	C2S	Cl5	1.764(14)
C2S	Cl4	1.763(14)	C3S	Cl7	1.759(11)
C3S	Cl8	1.766(11)	C3S	Cl9	1.766(11)
C4S	Cl10	1.753(7)	C4S	Cl12	1.771(7)
C4S	Cl11	1.774(6)	C5S	Cl14	1.757(14)
C5S	Cl15	1.768(14)	C5S	Cl13	1.775(14)
C6S	Cl18	1.755(12)	C6S	Cl16	1.757(12)
C6S	Cl17	1.766(12)	C7S	Cl19	1.753(11)
C7S	Cl20	1.756(10)	C7S	Cl21	1.761(10)
C8S	Cl24	1.742(10)	C8S	Cl22	1.750(10)
C8S	Cl23	1.756(10)	C9S	Cl25	1.754(10)
C9S	Cl27	1.772(9)	C9S	Cl26	1.781(9)
C10S	Cl30	1.767(11)	C10S	Cl28	1.777(12)
C10S	Cl29	1.783(12)	C11S	Cl32	1.742(10)
C11S	Cl33	1.748(9)	C11S	Cl31	1.769(9)
C12S	Cl34	1.756(14)	C12S	Cl36	1.761(14)
C12S	Cl35	1.765(14)			

Bond Angles for **16•4.5CHCl$_3$**:

Atom 1	Atom 2	Atom 3	Angle (°)	Atom 1	Atom 2	Atom 3	Angle (°)
C2	C1	C16	117.5(3)	C17	C2	C3	118.3(4)
C17	C2	C1	120.4(4)	C3	C2	C1	121.3(3)
C4	C3	O1	119.8(3)	C4	C3	C2	122.5(3)
O1	C3	C2	117.6(3)	C3	C4	C19	117.1(4)
C3	C4	C5	123.2(4)	C19	C4	C5	119.6(3)
C6	C5	C4	118.6(3)	C20	C6	C7	117.8(4)
C20	C6	C5	121.1(4)	C7	C6	C5	121.1(3)
O3	C7	C6	117.2(3)	O3	C7	C8	120.9(3)
C6	C7	C8	121.7(3)	C22	C8	C7	117.2(4)
C22	C8	C9	118.9(4)	C7	C8	C9	123.8(3)
C10	C9	C8	118.3(3)	C23	C10	C11	117.2(4)
C23	C10	C9	121.0(4)	C11	C10	C9	121.8(4)
C12	C11	O4	119.6(3)	C12	C11	C10	122.7(4)
O4	C11	C10	117.5(3)	C11	C12	C25	117.6(4)
C11	C12	C13	123.4(4)	C25	C12	C13	118.9(4)
C14	C13	C12	119.1(3)	C26	C14	C15	118.2(4)
C26	C14	C13	121.0(4)	C15	C14	C13	120.7(4)
O6	C15	C14	116.1(3)	O6	C15	C16	121.6(4)
C14	C15	C16	122.1(4)	C28	C16	C15	117.4(4)
C28	C16	C1	118.7(3)	C15	C16	C1	123.8(4)
C2	C17	C18	120.3(4)	C19	C18	C17	119.9(4)
C18	C19	C4	121.8(4)	C21	C20	C6	121.5(4)
C20	C21	C22	119.2(4)	C21	C22	C8	122.4(4)
C24	C23	C10	121.4(4)	C23	C24	C25	120.1(4)
C24	C25	C12	121.0(4)	C14	C26	C27	121.0(4)
C28	C27	C26	119.8(4)	C27	C28	C16	121.4(4)
C3	O1	C29	114.4(3)	O1	C29	C30	105.0(3)
O2	C30	C29	108.7(3)	C68	O2	C30	110.1(3)
C7	O3	C31	115.0(3)	O3	C31	C32	107.8(3)
C31	C32	C33	111.3(3)	C11	O4	C34	116.7(3)
O4	C34	C35	104.5(3)	O5	C35	C34	109.0(3)
C72	O5	C35	110.3(3)	C15	O6	C36	112.4(3)
O6	C36	C37	108.2(3)	C38	C37	C36	110.3(4)
C54	C39	C40	117.6(3)	C55	C40	C41	117.8(4)
C55	C40	C39	121.0(4)	C41	C40	C39	121.2(4)
C42	C41	O7	120.1(3)	C42	C41	C40	121.3(4)
O7	C41	C40	118.3(3)	C41	C42	C57	117.9(4)
C41	C42	C43	121.6(3)	C57	C42	C43	120.4(4)
C44	C43	C42	119.6(3)	C58	C44	C45	117.9(4)
C58	C44	C43	118.6(4)	C45	C44	C43	123.5(3)

O8	C45	C46	118.6(3)	O8	C45	C44	118.1(3)
C46	C45	C44	123.1(4)	C45	C46	C60	116.0(4)
C45	C46	C47	123.2(4)	C60	C46	C47	120.6(4)
C46	C47	C48	118.9(3)	C61	C48	C49	118.2(4)
C61	C48	C47	120.2(4)	C49	C48	C47	121.6(4)
O9	C49	C48	118.0(3)	O9	C49	C50	119.4(3)
C48	C49	C50	122.5(4)	C63	C50	C49	117.6(4)
C63	C50	C51	120.8(4)	C49	C50	C51	121.5(3)
C50	C51	C52	117.9(3)	C64	C52	C53	118.5(4)
C64	C52	C51	119.9(4)	C53	C52	C51	121.6(3)
O10	C53	C54	119.2(4)	O10	C53	C52	118.6(3)
C54	C53	C52	122.1(4)	C53	C54	C66	117.1(4)
C53	C54	C39	122.8(4)	C66	C54	C39	120.1(4)
C56	C55	C40	121.9(4)	C55	C56	C57	120.0(4)
C56	C57	C42	121.2(4)	C59	C58	C44	120.4(5)
C58	C59	C60	121.6(4)	C59	C60	C46	120.9(4)
C62	C61	C48	120.6(4)	C61	C62	C63	120.5(4)
C50	C63	C62	120.4(4)	C52	C64	C65	120.4(5)
C66	C65	C64	119.9(4)	C65	C66	C54	122.0(5)
C41	O7	C67	117.9(3)	O7	C67	C68	103.0(3)
O2	C68	C67	109.7(3)	C45	O8	C69	115.3(3)
O8	C69	C70	105.2(3)	O12	C70	C69	108.5(3)
C49	O9	C71	114.3(3)	O9	C71	C72	105.4(3)
O5	C72	C71	109.1(3)	C53	O10	C73	115.1(2)
O10	C73	C74	106.0(3)	O15	C74	C73	108.7(3)
C90	C75	C76	119.8(3)	C97	C76	C77	116.0(5)
C97	C76	C75	121.2(4)	C77	C76	C75	122.8(4)
C78	C77	O11	118.3(3)	C78	C77	C76	122.0(4)
O11	C77	C76	119.6(4)	C77	C78	C99	119.4(4)
C77	C78	C79	121.0(4)	C99	C78	C79	119.7(4)
C78	C79	C80	117.6(3)	C100	C80	C81	117.9(3)
C100	C80	C79	118.6(3)	C81	C80	C79	123.5(4)
O13	C81	C82	117.9(3)	O13	C81	C80	120.3(3)
C82	C81	C80	121.7(3)	C102	C82	C81	118.2(3)
C102	C82	C83	120.9(3)	C81	C82	C83	120.9(3)
C82	C83	C84	119.5(3)	C91	C84	C85	117.4(3)
C91	C84	C83	118.5(3)	C85	C84	C83	124.0(3)
O14	C85	C86	118.4(3)	O14	C85	C84	119.2(3)
C86	C85	C84	122.3(3)	C85	C86	C93	117.9(3)
C85	C86	C87	122.6(3)	C93	C86	C87	119.5(3)
C86	C87	C88	117.9(3)	C94	C88	C89	117.4(4)
C94	C88	C87	119.8(4)	C89	C88	C87	122.7(3)
O16	C89	C88	120.2(3)	O16	C89	C90	117.6(4)
C88	C89	C90	122.1(4)	C96	C90	C89	118.1(4)

C96	C90	C75	120.6(4)	C89	C90	C75	121.2(4)
C92	C91	C84	121.7(3)	C91	C92	C 93	120.0(3)
C92	C93	C86	120.7(3)	C88	C94	C95	122.1(5)
C94	C95	C96	119.2(4)	C90	C96	C95	121.0(4)
C98	C97	C76	123.4(4)	C99	C98	C97	118.6(4)
C98	C99	C78	120.6(5)	C101	C100	C80	121.2(4)
C100	C101	C102	119.6(4)	C101	C102	C82	121.3(3)
C77	O11	C103	114.9(3)	O11	C103	C104	105.8(3)
O12	C104	C103	108.2(3)	C70	O12	C104	110.2(3)
C81	O13	C105	115.5(3)	O13	C105	C106	106.6(4)
C107	C106	C105	112.7(4)	C85	O14	C108	115.9(2)
O14	C108	C109	104.3(3)	O15	C109	C108	109.4(3)
C74	O15	C109	110.2(2)	C110	O16	C89	129.0(7)
C110	O16	C113	122.0(7)	C89	O16	C113	107.2(7)
O16	C110	C111	108.6(11)	C112	C111	C110	103.9(9)
O16	C113	C114	122.0(13)	C115	C114	C113	108.8(14)
Cl1	C1S	Cl3	109.9(3)	Cl1	C1S	Cl2	109.6(3)
Cl3	C1S	Cl2	111.0(3)	Cl6	C2S	Cl5	109.0(11)
Cl6	C2S	Cl4	110.1(11)	Cl5	C2S	Cl4	110.6(12)
Cl7	C3S	Cl8	111.3(7)	Cl7	C3S	Cl9	108.8(8)
Cl8	C3S	Cl9	109.7(7)	Cl10	C4S	Cl12	110.2(4)
Cl10	C4S	Cl11	109.5(4)	Cl12	C4S	Cl11	110.0(4)
Cl14	C5S	Cl15	111.1(11)	Cl14	C5S	Cl13	109.4(11)
Cl15	C5S	Cl13	108.9(11)	Cl18	C6S	Cl16	110.8(9)
Cl18	C6S	Cl17	110.2(8)	Cl16	C6S	Cl17	109.9(9)
Cl19	C7S	Cl20	110.5(6)	Cl19	C7S	Cl21	109.7(7)
Cl20	C7S	Cl21	111.4(7)	Cl24	C8S	Cl22	110.1(7)
Cl24	C8S	Cl23	111.4(8)	Cl22	C8S	Cl23	109.0(6)
Cl25	C9S	Cl27	109.5(6)	Cl25	C9S	Cl26	111.6(7)
Cl27	C9S	Cl26	111.5(5)	Cl30	C10S	Cl28	110.0(8)
Cl30	C10S	Cl29	114.2(8)	Cl28	C10S	Cl29	106.0(8)
Cl32	C11S	Cl33	110.0(5)	Cl32	C11S	Cl31	112.2(6)
Cl33	C11S	Cl31	110.5(6)	Cl34	C12S	Cl36	111.2(12)
Cl34	C12S	Cl35	110.4(11)	Cl36	C12S	Cl35	110.0(12)

APPENDIX 24

X-RAY CRYSTAL DATA FOR
25,27-BIS(2-BENZYLOXYETHYLOXY)-26,28-BIS(2-HYDROXYETHYLOXY)CALIX[4]ARENE, *1,3-ALTERNATE* (31)

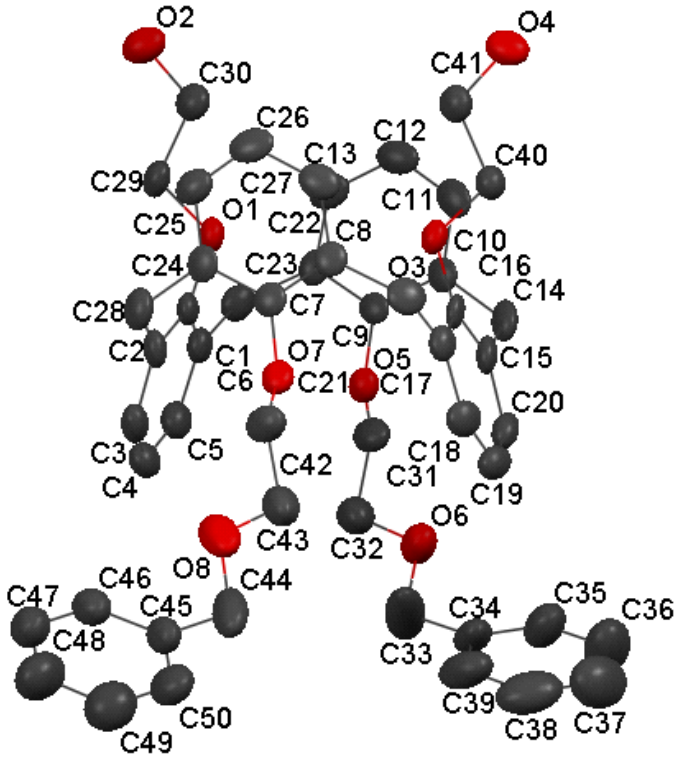

Formula	$C_{50}H_{52}O_8$
Crystal System	Triclinic
Space Group	P – 1
Cell Lengths	a = 9.9059(14) Å, b = 17.173(2) Å, c = 25.001(4) Å
Cell Angles	α = 81.553(2)°, β = 87.810(2)°, γ = 89.952(2)°
Cell Volume	4203.76 $Å^3$
Z	4
Density (calculated)	1.244 Mg/m^3
Goodness-of-fit on F^2	1.028
Final R indices [I>2σ(I)]	R1 = 0.0844, wR2 = 0.2185
R indices (all data)	R1 = 0.1323, wR2 = 0.2522

Bond Lengths for **31**:

Atom 1	Atom 2	Distance (Å)	Atom 1	Atom 2	Distance (Å)
O1	C1	1.376(6)	O1	C29	1.430(6)
O2	C30	1.425(6)	O3	C16	1.385(6)
O3	C40	1.422(6)	O4	C41	1.436(6)
O5	C9	1.395(6)	O5	C31	1.440(6)
O6	C32	1.389(7)	O6	C33	1.396(8)
O7	C23	1.392(6)	O7	C42	1.437(7)

O8	C43	1.327(8)	O8	C44	1.435(8)
C1	C2	1.410(7)	C1	C6	1.413(7)
C2	C3	1.374(7)	C2	C28	1.534(7)
C3	C4	1.384(8)	C4	C5	1.382(8)
C5	C6	1.386(7)	C6	C7	1.514(7)
C7	C8	1.517(7)	C8	C13	1.392(7)
C8	C9	1.404(7)	C9	C10	1.376(7)
C10	C11	1.392(7)	C10	C14	1.517(7)
C11	C12	1.379(8)	C12	C13	1.378(8)
C14	C15	1.519(7)	C15	C20	1.396(7)
C15	C16	1.410(7)	C16	C17	1.409(7)
C17	C18	1.389(7)	C17	C21	1.520(7)
C18	C19	1.394(8)	C19	C20	1.382(8)
C21	C22	1.510(7)	C22	C27	1.400(7)
C22	C23	1.400(7)	C23	C24	1.392(7)
C24	C25	1.387(7)	C24	C28	1.514(7)
C25	C26	1.377(8)	C26	C27	1.385(8)
C29	C30	1.494(7)	C31	C32	1.502(8)
C33	C34	1.504(11)	C34	C39	1.360(11)
C34	C35	1.386(9)	C35	C36	1.369(10)
C36	C37	1.385(12)	C37	C38	1.334(12)
C38	C39	1.396(12)	C40	C41	1.514(7)
C42	C43	1.493(8)	C44	C45	1.479(10)
C45	C46	1.387(8)	C45	C50	1.392(9)
C46	C47	1.381(9)	C47	C48	1.375(10)
C48	C49	1.370(11)	C49	C50	1.375(10)

Bond Angles for **31**:

Atom 1	Atom 2	Atom 3	Angle (°)	Atom 1	Atom 2	Atom 3	Angle (°)
C1	O1	C29	114.2(4)	C16	O3	C40	113.8(3)
C9	O5	C31	114.3(4)	C32	O6	C33	112.8(5)
C23	O7	C42	114.1(4)	C43	O8	C44	113.7(5)
O1	C1	C2	120.2(4)	O1	C1	C6	119.0(4)
C2	C1	C6	120.7(5)	C3	C2	C1	118.3(5)
C3	C2	C28	120.2(5)	C1	C2	C28	121.4(5)
C2	C3	C4	122.0(5)	C5	C4	C3	119.2(5)
C4	C5	C6	121.5(5)	C5	C6	C1	118.1(5)
C5	C6	C7	121.5(5)	C1	C6	C7	120.4(4)
C6	C7	C8	116.9(4)	C13	C8	C9	116.7(5)
C13	C8	C7	121.1(5)	C9	C8	C7	122.3(5)
C10	C9	O5	118.7(4)	C10	C9	C8	122.2(5)
O5	C9	C8	119.1(4)	C9	C10	C11	119.0(5)

C9	C10	C14	120.6(5)	C11	C10	C14	120.4(5)
C12	C11	C10	120.3(5)	C13	C12	C11	119.7(5)
C12	C13	C8	122.0(5)	C10	C14	C15	117.4(4)
C20	C15	C16	117.6(5)	C20	C15	C14	120.0(4)
C16	C15	C14	122.3(5)	O3	C16	C17	119.0(4)
O3	C16	C15	119.1(4)	C17	C16	C15	121.8(5)
C18	C17	C16	117.9(5)	C18	C17	C21	121.2(5)
C16	C17	C21	120.9(5)	C17	C18	C19	121.5(5)
C20	C19	C18	119.4(5)	C19	C20	C15	121.8(5)
C22	C21	C17	116.8(4)	C 27	C22	C23	117.1(5)
C27	C22	C21	120.8(5)	C23	C22	C21	122.0(4)
C24	C23	O7	118.5(4)	C24	C23	C22	121.9(5)
O7	C23	C22	119.6(4)	C25	C24	C23	118.8(5)
C25	C24	C28	120.6(5)	C23	C24	C28	120.5(5)
C26	C25	C24	120.8(5)	C25	C26	C27	119.8(5)
C26	C27	C22	121.5(5)	C24	C28	C2	117.5(4)
O1	C29	C30	108.8(4)	O2	C30	C29	111.2(4)
O5	C31	C32	109.7(5)	O6	C32	C31	108.5(5)
O6	C33	C34	110.1(6)	C39	C34	C35	118.9(7)
C39	C34	C33	122.9(7)	C35	C34	C33	118.1(7)
C36	C35	C34	119.1(7)	C35	C36	C37	120.5(8)
C38	C37	C36	121.2(9)	C37	C38	C39	118.2(9)
C34	C39	C38	122.1(8)	O3	C40	C41	108.0(4)
O4	C41	C40	109.8(4)	O7	C42	C43	111.4(6)
O8	C43	C42	108.9(6)	O8	C44	C45	108.9(6)
C46	C45	C50	118.2(6)	C46	C45	C44	121.1(6)
C50	C45	C44	120.7(6)	C47	C46	C45	120.5(7)
C48	C47	C46	120.3(7)	C49	C48	C47	119.8(8)
C48	C49	C50	120.2(7)	C49	C50	C45	120.9(7)

REFERENCES

(1) The National Nanotechnology Initiative Home Page. http://www.nano.gov/html/res/smallwonder.html (accessed Mar 2006).

(2) Brydson, R. M.; Hammind, C. In *Nanoscale Science and Technology*; Kelsall, R. W., Hamley, I. W., Geoghegan, M., Eds.; John Wiley & Sons, Ltd.: Hoboken, NJ, 2005, p 1.

(3) Allen, N. S.; Edge, M.; Sandoval, G.; Verran, J.; Stratton, J.; Maltby, J. *Photochem. Photobiol.* **2005**, *81*, 279-290.

(4) Vlasov, Y. A.; O'Boyle, M.; Hamann, H. F.; McNab, S. J. *Nature* **2005**, *438*, 65-69.

(5) Cuenca, A. G.; Jiang, H. B.; Hochwald, S. N.; Delano, M.; Cance, W. G.; Grobmyer, S. R. *Cancer* **2006**, *107*, 459-466.

(6) Chang, J. S.; Jhung, S. H.; Hwang, Y. K.; Park, S. E.; Hwang, J. S. *Int. J. Nanotech.* **2006**, *3*, 150-180.

(7) Kolmakov, A.; Moskovits, M. *Annu. Rev. Mater. Res.* **2004**, *34*, 151-180.

(8) Derkacs, D.; Lim, S. H.; Matheu, P.; Mar, W.; Yu, E. T. *Appl. Phys. Lett.* **2006**, *89*, 1-3.

(9) Malchesky, P. S. *Artif Organs* **2004**, *28*, 969-970.

(10) Bong, D. T.; Clark, T. D.; Granja, J. R.; Ghadiri, M. R. *Angew. Chem. Int. Ed.* **2001**, *40*, 988-1011.

(11) Baudry, Y.; Bollot, G.; Gorteau, V.; Litvinchuk, S.; Mareda, J.; Nishihara, M.; Pasini, D.; Perret, F.; Ronan, D.; Sakai, N.; Shah, M. R.; Som, A.; Sorde, N.; Talukdar, P.; Tran, D.-H.; Matile, S. *Adv. Funct. Mater.* **2006**, *16*, 169-179.

(12) Kohli, P.; Martin, C. R. *Curr. Pharm. Biotechnol.* **2005**, *6*, 35-47.

(13) Matranga, C.; Chen, L.; Smith, M.; Bittner, E.; Johnson, J. K.; Bockrath, B. *J. Phys. Chem. B* **2003**, *107*, 12930-12941.

(14) Iijima, S.; Ichihashi, T. *Nature* **1993**, *363*, 603-605.

(15) Bethune, D. S.; Klang, C. H.; Vries, M. S. D.; Gorman, G.; Savoy, R.; Vazquez, J.; Beyers, R. *Nature* **1993**, *363*, 605-607.

(16) Fujiwara, A.; Ishii, K.; Suematsu, H.; Kataura, H.; Maniwa, Y.; Suzuki, S.; Achiba, Y. *Chem. Phys. Lett.* **2001**, *336*, 205-211.

(17) Ajayan, P. M.; Stephan, O.; Redlich, P.; Colliex, C. *Nature* **1995**, *375*, 564-567.

(18) Dillon, A. C.; Jones, K. M.; Bekkedahl, T. A.; Kiang, C. H.; Bethune, D. S.; Heben, M. J. *Nature* **1997**, *386*, 377-379.

(19) Smith, B. W.; Monthioux, M.; Luzzi, D. E. *Nature* **1998**, *396*, 323-324.

(20) Khlobystov, A. N.; Britz, D. A.; Briggs, G. A. D. *Acc. Chem. Res.* **2005**, *38*, 901-909.

(21) Khlobystov, A. N.; Porfyrakis, K.; Kanai, M.; Britz, D. A.; Ardavan, A.; Shinohara, H.; Dennis, T. J. S.; Briggs, G. A. D. *Angew. Chem. Int. Ed.* **2004**, *43*, 1386-1389.

(22) Wang, J.; Kuimova, M. K.; Poliakoff, M.; Briggs, G. A. D.; Khlobystov, A. N. *Angew. Chem. Int. Ed.* **2006**, *45*, 5188-5191.

(23) Britz, D. A.; Khlobystov, A. N.; Porfyrakis, K.; Ardavan, A.; Briggs, G. A. D. *Chem. Comm.* **2005**, 37-39.

(24) Byl, O.; Liu, J.-C.; Wang, Y.; Yim, W.-L.; Johnson, J. K.; John T. Yates, J. *J. Am. Chem. Soc.* **2006**, *128*, 12090-12097.

(25) Niyogi, S.; Hamon, M. A.; Hu, H.; Zhao, B.; Bhowmik, P.; Sen, R.; Itkis, M. E.; Haddon, R. C. *Acc. Chem. Res.* **2002**, *35*, 1105-1113.

(26) Ajayan, P. M. *Chem. Rev.* **1999**, *99*, 1787-1799.

(27) Byl, O.; Kondratyuk, P.; Forth, S. T.; Fitzgerald, S. A.; Chen, L.; Johnson, J. K.; John T. Yates, J. *J. Am. Chem. Soc.* **2003**, *125*, 5889-5896.

(28) Fu, K.; Sun, Y.-P. *J. Nanosci. Nanotech.* **2003**, *3*, 351-364.

(29) Tasis, D.; Tagmatarchis, N.; Bianco, A.; Prato, M. *Chem. Rev.* **2006**, *106*, 1105-1136.

(30) Sloan, J.; Kirkland, A. I.; Hutchison, J. L.; Green, M. L. H. *Acc. Chem. Res.* **2002**, *35*, 1054-1062.

(31) Ugarte, D.; Stockli, T.; Bonard, J. M.; Heer, W. A. d. *Appl. Phys. A* **1998**, *67*, 101-105.

(32) Monthioux, M. *Carbon* **2002**, *40*, 1809-1823.

(33) Fenniri, H.; Deng, B.-L.; Ribbe, A. E.; Hallenga, K.; Jacob, J.; Thiyagarajan, P. *Proc. Natl. Acad. Sci. USA* **2002**, *99*, 6487-6492.

(34) Reches, M.; Gazit, E. *Science* **2003**, *300*, 625-627.

(35) Moralez, J. G.; Raez, J.; Yamazaki, T.; Motkuri, R. K.; Kovalenko, A.; Fenniri, H. *J. Am. Chem. Soc.* **2005**, *127*, 8307-8309.

(36) Fenniri, H.; Mathivanan, P.; Vidale, K. L.; Sherman, D. M.; Hallenga, K.; Wood, K. V.; Stowell, J. G. *J. Am. Chem. Soc.* **2001**, *123*, 3854-3855.

(37) Sakai, N.; Mareda, J.; Matile, S. *Acc. Chem. Res.* **2005**, *38*, 79-87.

(38) Aoyagi, M.; Biradha, K.; Fujita, M. *J. Am. Chem. Soc.* **1999**, *121*, 7457-7458.

(39) Yamaguchi, T.; Tashiro, S.; Tominaga, M.; Kawano, M.; Ozeki, T.; Fujita, M. *J. Am. Chem. Soc.* **2004**, *126*, 10818-10819.

(40) Gao, X.; Matsui, H. *Adv. Mater.* **2005**, *17*, 2037-2050.

(41) Harada, A.; Li, J.; Kamachi, M. *Nature* **1993**, *364*, 516-518.

(42) Couet, J.; Samuel, J. D. J. S.; Kopyshev, A.; Santer, S.; Biesalski, M. *Angew. Chem. Int. Ed.* **2005**, *44*, 3297-3301.

(43) Hecht, S.; Khan, A. *Angew. Chem. Int. Ed.* **2003**, *42*, 6021-6024.

(44) Khan, A.; Hecht, S. *Synth. Met.* **2004**, *147*, 37-42.

(45) Kim, Y.; Mayer, M. F.; Zimmerman, S. C. *Angew. Chem. Int. Ed.* **2003**, *42*, 1121-1126.

(46) Gutsche, C. D. *Calixarenes Revisited*; The Royal Society of Chemistry: Cambridge, UK, 1998.

(47) Pochini, A.; Arduini, A. In *Calixarenes In Action*; Mandolini, L., Ungaro, R., Eds.; Imperial College Press: Covent Garden, 2000.

(48) Beer, P. D.; Gale, P. A.; Smith, D. K. *Supramolecular Chemistry*; Oxford University Press: Oxford, 1999.

(49) *Calixarenes 2001*; Asfari, Z.; Bohmer, V.; Harrowfield, J.; Vicens, J., Eds.; Kluwer Academic Publishers: Dordrecht, 2001.

(50) Ungaro, R. In *Calixarenes In Action*; Mandolini, L., Ungaro, R., Eds.; Imperial College Press: Covent Garden, London, 2000.

(51) Jaime, C.; Mendoza, J. d.; Prados, P.; Nieto, P. M.; Sanchez, C. *J. Org. Chem.* **1991**, *56*, 3372-3376.

(52) Fujimoto, K.; Nishiyama, N.; Tsuzuki, H.; Shinkai, s. *J. Chem. Soc., Perkin Trans. 2* **1992**, 643-648.

(53) Beer, P. D.; Drew, M. G. B.; Gale, P. A.; Leeson, P. B.; Ogden, M. I. *J. Chem. Soc., Dalton Trans.* **1994**, 3479-3485.

(54) Ikeda, A.; Shinkai, S. *Tetrahedron Lett.* **1992**, *33*, 7385-7388.

(55) Ikeda, A.; Tsudera, T.; Shinkai, S. *J. Org. Chem.* **1997**, *62*, 3568-3574.

(56) Ikeda, A.; Shinkai, S. *J. Chem. Soc., Chem. Commun.* **1994**, 2375-2376.

(57) Ikeda, A.; Kawaguchi, M.; Shinkai, S. *An. Quim. Int.* **1997**, *93*, 408-414.

(58) Kim, S. K.; Sim, W.; Vicens, J.; Kim, J. S. *Tetrahedron Lett.* **2003**, *44*, 805-809.

(59) Kim, S. K.; Vicens, J.; Park, K.-M.; Lee, S. S.; Kim, J. S. *Tetrahedron Lett.* **2003**, *44*, 993-997.

(60) Zyryanov, G.; Kang, Y.; Stampp, S.; Rudkevich, D. M. *Chem. Comm.* **2002**, 2792-2793.

(61) Zyryanov, G. V.; Kang, Y.; Rudkevich, D. M. *J. Am. Chem. Soc.* **2003**, *125*, 2997-3007.

(62) Rosokha, S. V.; Lindeman, S. V.; Kochi, J. K. *J. Chem. Soc., Perkin Trans. 2* **2002**, 1468-1474.

(63) Rosokha, S. V.; Lindeman, S. V.; Rathore, R.; Kochi, J. K. *J. Org. Chem.* **2003**, *68*, 3947-3957.

(64) Rathore, R.; Lindeman, S. V.; Rao, K. S. S. P.; Sun, D.; Kochi, J. K. *Angew. Chem. Int. Ed.* **2000**, *39*, 2123-2127.

(65) Iwamoto, K.; Araki, K.; Shinkai, S. *J. Org. Chem.* **1991**, *56*, 4955-4962.

(66) Iwamoto, K.; Araki, K.; Shinkai, S. *Tetrahedron* **1991**, *41*, 4325-4342.

(67) Verboom, W.; Datta, S.; Asfari, Z.; Harkema, S.; Reinhoudt, D. N. *J. Org. Chem.* **1992**, *57*, 5394-5398.

(68) Zyryanov, G. V.; Rudkevich, D. M. *J. Am. Chem. Soc.* **2004**, *126*, 4264-4270.

(69) Kim, J. S.; Shon, O. J.; Ko, J. W.; Cho, M. H.; Yu, I. Y.; Vicens, J. *J. Org. Chem.* **2000**, *65*, 2386-2392.

(70) Casnati, A.; Pochini, A.; Ungaro, R.; Ugozzoli, F.; Arnaud, F.; Fanni, S.; Schwing, M. J.; Egberink, R. J. M.; Jong, F. d.; Reinhoudt, D. N. *J. Am. Chem. Soc.* **1995**, *117*, 2767-2777.

(71) Kim, S.; Kim, J. S.; Kim, S. K.; Suh, I.-H.; Kang, S. O.; Ko, J. *Inorg. Chem.* **2005**, *44*, 1846-1851.

(72) Iwamoto, K.; Shinkai, S. *J. Org. Chem.* **1992**, *57*, 7066-7073.

(73) Kwang, H. N.; Gutsche, C. D. *J. Org. Chem.* **1982**, *47*, 2713-2719.

(74) Organo, V. G.; Leontiev, A. V.; Sgarlata, V.; Dias, H. V. R.; Rudkevich, D. M. *Angew. Chem. Int. Ed.* **2005**, *44*, 3043 –3047.

(75) Sgarlata, V.; Organo, V. G.; Rudkevich, D. M. *Chem. Comm.* **2005**, 5630-5632.

(76) Iglesias, E.; Casado, J. *Int. Rev. Phys. Chem.* **2002**, *21*, 37-74.

(77) Wang, P. G.; Xian, M.; Tang, X.; Wu, X.; Wen, Z.; Cai, T.; Janczuk, A. J. *Chem. Rev.* **2002**, *102*, 1091-1134.

(78) Borodkin, G. I.; Shubin, V. G. *Russ. Chem. Rev.* **2001**, *70*, 211-230.

(79) Bosch, E. *Spectrosc. Lett.* **2001**, *34*, 35-42.

(80) Bosch, E.; Kochi, J. K. *J. Org. Chem.* **1994**, *59*, 3314-3325.

(81) Rathore, R.; Lindeman, S. V.; Kochi, J. K. *Angew. Chem. Int. Ed.* **1998**, *37*, 1585-1587.

(82) Begum, R.; Sagawa, T.; Masatoki, S.; Matsuura, H. *J. Mol. Struct.* **1998**, *442*, 243-250.

(83) Hofacker, A. L.; Parquette, J. R. *Angew. Chem. Int. Ed.* **2005**, *44*, 1053-1057.

(84) Kim, E. K.; Kochi, J. K. *J. Am. Chem. Soc.* **1991**, *113*, 4962-4974.

(85) Keck, D. B.; Hause, C. D. *J. Mol. Spectr.* **1968**, *26*, 163-174.

(86) Rudkevich, D. M. *Bull. Chem. Soc. Jpn.* **2002**, *75*, 393-413.

(87) Badjic, J. D.; Nelson, A.; Cantrill, S. J.; Turnbull, W. B.; Stoddart, J. F. *Acc. Chem. Res.* **2005**, *38*, 723-732.

(88) Steed, J. W.; Atwood, J. L. In *Supramolecular Chemistry*; John Wiley & Sons, Ltd: West Sussex, England, 2000.

(89) Eaton, W. A.; Henry, E. R.; Hofrichter, J.; Mozzarelli, A. *Nat. Struct. Biol.* **1999**, *6*, 351-358.

(90) Chopra, N.; Naumann, C.; Sherman, J. C. *Angew. Chem. Int. Ed.* **2000**, *39*, 194-196.

(91) Ricard, S.; Audet, P.; Savoie, R. *J. Mol. Struct.* **1988**, *178*, 135-140.

(92) Heo, G. S.; Hillman, P. E.; Bartsch, R. A. *J. Heterocyclic Chem.* **1982**, *19*, 1099-1103.

(93) Lee, K. Y.; Kuchynka, D. J.; Kochi, J. K. *Inorg. Chem.* **1990**, *29*, 4196-4204.

(94) Elsenbaumer, R. *J. Org. Chem.* **1988**, *53*, 437-439.

(95) Russo, U.; Cassol, A.; Silvestri, A. *J. Organomet. Chem.* **1984**, *260*, 69-72.

(96) Cusack, P. A.; Patel, B. N.; Smith, P. J.; Allen, D. W.; Nowell, I. W. *J. Chem. Soc., Dalton Trans.* **1984**, 1239-1243.

(97) Bott, S. G.; Prinz, H.; Alvanipour, A.; Atwood, J. L. *J. Coord. Chem.* **1987**, *16*, 303-309.

(98) Mohamadi, F.; Richards, N. G.; Guida, W. C.; Liskamp, R.; Lipton, M.; Caufield, C.; Chang, G.; Hendrickson, T.; Still, W. C. *J. Comput. Chem.* **1990**, *11*, 440-467.

(99) Kim, J. S.; Shon, O. J.; Ko, J. W.; Cho, M. H.; Yu, I. Y.; Vicens, J. *J. Org. Chem.* **2000**, *65*, 2386-2392.

(100) Bohmer, V.; Jung, K.; Schon, M.; Wolff, A. *J. Org. Chem.* **1992**, *57*, 790-792.

(101) Gutsche, C. D.; See, K. A. *J. Org. Chem.* **1992**, *57*, 4527-4539.

BIOGRAPHICAL INFORMATION

Voltaire Guanlao Organo was born in the city of Manila, Philippines. He obtained his Bachelor's Degree in Chemistry from Adamson University, Manila in 1994. After working in the industry and academe for six years, he pursued his doctoral study at the University of Texas at Arlington in the United States in 2002. He worked with Professor Dmitry M. Rudkevich on calix[4]arene-based synthetic nanotubes. In the summer of 2006, he went to Maryland at the National Cancer Institute of the National Institutes of Health and worked with Dr. Martin W. Brechbiel on monoclonal antibody immunoconjugates for cancer treatment. In December of 2006, he received his doctorate degree in chemistry. He will be moving to Medford, Massachusetts to begin his research career as a postdoctoral associate in the laboratory of Professor Elena Rybak-Akimova at the Chemistry Department in Tufts University. His research interests include supramolecular chemistry and molecular recognition.